SYNOPSIS

Ph.D. Thesis

MECHANICAL BEHAVIOUR OF ULTRAFINE GRAINED 5083 Al ALLOY PROCESSED BY CRYO ROLLING

Submitted By

DHARMENDRA SINGH

(Enrollment No. 10924003)

Under the Supervision of

Dr. R. JAYAGANTHAN

Associate Professor

DEPARTMENT OF METLLURGICAL & MATATERIALS ENGINEERING

INDIAN INSTITUTE OF TECHNOLOGY ROORKEE

ROORKEE- 247667 (UTTRAKHAND), [INDIA]

Aluminium 5083 alloy (Al-4.4Mg-0.7Mn-0.08Cr) is a medium strength, non-heat treatable alloy known for its excellent corrosion resistance. The unique mechanical properties of the alloys, greater design efficiency, better welding characteristics, good formability, excellent resistance to corrosion, and relatively high strength-to-weight ratio coupled with low cost makes it suitable for structural applications. Specifically, aluminium 5083 alloy is attractive for ships and marine applications due to the above mentioned properties. With the development of super plastic and quick plastic forming techniques, its application is extended to automobile and aerospace structural components. The extensive use of the alloy demands for the improvement in strength and formability of the alloy for ensuring long term performance of the alloy. In spite of enormous efforts over the decade, maintaining high strength with reasonable ductility is a challenging task. Strengthening in polycrystalline materials is related to refining the grain structure to ultrafine regime (100nm-1000 nm) through severe plastic deformation processing of the materials. Several plastic deformation techniques have been explored to develop homogeneous and equiaxed material with ultrafine grain sizes (UFG) in the bulk materials. It requires exceptionally high strain to induce high dislocation density for the formation of ultrafine grain structures in the alloy

UFG materials possess superior properties such as high strength, excellent fatigue life, high toughness and low temperature super plasticity, improved corrosion resistance, enhanced electrical conductivity, wear characteristics, higher specific heat, enhanced thermal coefficient, and superior magnetic properties. The stringent demand of exceptional material properties requirements have led to a considerable interest in the development of ultrafine-grained/nanomaterials worldwide.

Non-heat treatable aluminum alloys found their application in the form of rolled products (thin sheets and foils). Therefore, there is increasing demand to develop rolling technologies to fabricate sheets ensuring its long time performance. It is identified that cold rolling can result in significant refinement in microstructure from its bulk alloys at very low temperature (Liquid nitrogen temperature) called as cryorolling. It is widely used to produce UFG structure in different metals and their alloys. However, it produces cellular type substructure consisting of boundaries with low angle misorientation. Cryorolling followed by warm rolling and asymmetric cryorolling is also gaining popularity to produce ultrafine grained aluminium alloys. The effect of cryorolling on microstructural evolution and mechanical behavior of pure metals and heat treatable aluminium alloys (6XXX, 7XXX) has been reported in literature. On the other hand, there is scarcity of literature on non-heat

treatable alloys, especially ultrafine grained 5XXX (AA 5083) alloys, where the prime mechanism of strengthening is solid solution strengthening and work hardening. Therefore, the present work has been envisaged to develop high strength aluminium 5083 alloy by grain refinement processed through cryorolling and cryorolling followed by warm rolling. The microstructure of deformed Al alloys was characterized by Optical microscopy, TEM, and FE-SEM/EBSD to substantiate their influence on mechanical properties. Optimization of annealing conditions for the deformed Al alloy so as to achieve best combination of strength and ductility with impact strength has been carried out in the present work.

The objectives of present research work are: (i) To investigate the mechanical and microstructural behaviour of Al 5083 alloy deformed through cryorolling; (ii) To study microstructures and impact toughness behavior of Al 5083 alloy processed by cryorolling and annealing; (iii) To study the effect of deformation temperature on mechanical properties of ultrafine grained Al-Mg alloys processed by rolling; (iv) To study the corrosion behavior of ultrafine grained Al 5083 aluminium alloy developed by cryorolling; (v) To study the high cycle fatigue behaviour of ultrafine grained Al-Mg alloy processed by cryorolling and warm rolling.

A detailed description of the present work is presented in six chapters and it is briefly discussed below.

Chapter 1 gives an overview of aluminium alloys, their applications, worldwide production and consumption in different sectors. Explanation for non heat treatable aluminium alloys and their applications are also discussed.

Chapter 2 presents the details of aluminium and their alloys, their classification, and different strengthening mechanisms. Development of ultrafine grained aluminium alloys through different techniques and their characteristics are included. Literature review pertaining to different severe plastic deformation techniques and cryorolling used for producing ultrafine grain microstructure in aluminium and other materials are also discussed. Based on literature review, the formulation of problem for the present research work has been made. The scope, objectives, and outline of the dissertation work are discussed in this chapter.

Chapter 3 describes the selection of material and its sampling for different experimental technique adopted for development of ultrafine grained materials. The methodology of various characterization techniques and mechanical testing employed in dissertation work has been discussed.

Chapter 4 describes the results and discussion of different experimental investigations performed on Al 5083 alloy processed through cryorolling, and cryorolling followed by warm rolling. **Section 4.1** investigates the effect of rolling at very low temperature on microstructure and mechanical behaviour of Al 5083 alloy. The alloy was subjected to rolling up to different strain levels at room temperature and immediate quenching at liquid nitrogen temperature. The effect of second phase particles in the alloy was investigated, especially on the evolution of microstructure and grain refinement in terms of pinning and driving forces for recrystallization. It is observed that there is a significant improvement in yield strength (103%) and ultimate tensile strength (40.8%) with CR 90% sample. It is due to the effective suppression of dynamic recovery and accumulation of high dislocations density during low temperature deformation. A homogeneous ultrafine grained structure with an average grains size of 300 nm was achieved after short annealing treatment at 300 ºC for 6 min of CR 90 % thickness reduction sample. The volume fraction of high angle grain boundaries has increased after short annealing treatment due to formation of recrystallized grains, which is due to the combined effect of static recovery and recrystallization.

After investigating microstructure and mechanical behavior of cryorolled material, the energy absorption capability of cryorolled Al 5083 alloy and effect of subsequent annealing treatment on impact and tensile properties of Al 5083 alloy are reported in **Section 4.2**. The microstructure of the CR Al 5083 alloy and CR+ annealed Al 5083 alloy were characterized. The fractography of impact test samples were characterized by FE-SEM to reveal the mode of failure in the CR Al 5083 alloy. The Charpy impact test results have shown that cryorolling significantly decreases impact toughness of the alloy (ST - 32 J to CR 30% - 10 J) and that further decreases with increasing % of cryorolling (CR 30% - 10 J to CR 50% - 7.5 J). The loss in impact energy after cryorolling is due to lack of plastic deformation in the sample due to increase in yield strength, and brittle fracture as observed from SEM micrographs. Annealing at 350 °C, 1 hr of CR 50% sample shows an average grain size of 14 µm, whereas in CR 30%, the average grain size is 25 µm. The difference in the size is due to more nuclei generated during 50% CR resulting in smaller size of the grains. A comparative study of impact toughness behavior of starting solution treated material with 50% cryorolled sample after annealing shows that the loss in impact toughness due to cryorolling has been compensated by occurrence of recrystallization after annealing treatment.

Section 4.3 describes the effect of rolling performed at room temperature, cryogenic temperature and cryorolling followed by warm rolling for establishing the optimum rolling

condition. Rolling was carried out up to 90% reduction (~2.3 true strain) at room temperature, cryogenic temperature and warm rolled at different temperatures of 100, 145, 175, 200 ℃ on 50% cryorolled samples up to 90% reduction. On the basis of hardness values for different conditions, cryorolling followed by warm rolling at 175 °C was found to be optimum condition (Hv-146) for further investigation and compared with cryorolled alloy alone (Hv-127). Annealing was also performed to observe thermal stability of the material. The significant improvement in mechanical properties (UTS-539 MPa, YTS-522 MPa, and ductility 6.8 %) was observed in the samples processed by cryorolling followed by warm rolling. The increase in strength and ductility may be attributed to formation of fine precipitates and dynamic recovery effect. It was evident from microstructural characterization that CR and CR +WR samples exhibit high density of dislocations and substructures, high fraction of high angle grain boundaries.

An attempt has also been made to investigate the effect of rolling condition on high cycle fatigue behaviour in S**ection 4.4.** The Al 5083 alloy was rolled for different thickness reductions of 50% and 85% at cryogenic (liquid nitrogen) temperature. The 50% CR sample was subjected to 70% warm rolling (CR+ WR) up to 85% reduction. Their hardness, tensile strength, and fatigue life using constant amplitude stress controlled fatigue were investigated. The cryorolled Al alloy after 85% thickness reduction exhibits high dislocation density due to suppression of dynamic recovery. Whereas, CR+WR alloy has shown ultrafine grain (UFG) structure associated with dynamic recovery during rolling. The deformed Al 5083 alloy was cyclically deformed over a range of stress amplitude at ambient temperature and observed the significant enhancement in fatigue strength as compared to the coarse grained (CG) bulk alloy.

Apart from investigating mechanical properties of the ultrafine grained materials, understanding the corrosion behavior is essential for structural applications as discussed in S**ection 4.5**. Since Al 5083 alloy is potential material for marine applications, the corrosion behavior of UFG Al 5083 alloy in chloride environment is also investigated for cryorolled, cryorolling followed by short annealing and cryorolling followed by warm rolling and compared with starting material. It was observed from polarization test that cryorolled material has shown lower corrosion current density (I_{corr}-0.46 $\mu A/cm^2$) compared to ST material (Icorr- 4.4 $\mu A/cm^2$) with increased E_{pit} - E_{corr} value (194 mV), which indicates more resistance to pitting corrosion. It can be attributed to rapid formation of passive films due to

higher dislocation density and grain boundaries, fragmentation and distribution of coarse intermetallic particles in cryorolled sample.

Chapter 5 presents the summary and conclusion of entire work presented in this thesis as well as future scope of the work in Al 5083 alloy.

Research publications (Published/Under review)

1. **Dharmendra Singh,** P. Nageswara Rao, R. Jayaganthan, "Study of microstructural evolution and Mechanical properties of Al 5083 alloy processed by cryorolling**". Advanced Materials Research,** 2012, 585, 376-380.
2. **Dharmendra Singh,** P.Nageswara rao, R.Jayaganthan, "Study of microstructural evolution and impact toughness behavior of Al 5083 alloy processed by cryorolling". **International Journal of Minerals, Metallurgy, and Materials**, 2013, 20, 759-769.

3. **Dharmendra Singh,** P.Nageswara Rao, R. Jayaganthan, (2013), "Effect of deformation temperature on mechanical properties of ultrafine grained Al-Mg alloys processed by rolling", **Materials and Design**, 2013, 50, 646-655.
4. **Dharmendra Singh,** P.Nageswara Rao, R. Jayaganthan, "Corrosion behavior of Ultrafine grained Al 5083 aluminium alloy developed by Cryorolling", **Corrosion Science**, 2013, (Under review).
5. **Dharmendra Singh,** P.Nageswara Rao, R. Jayaganthan, (2013), "High cycle fatigue behavior of Ultrafine grained Al 5083 aluminium alloy developed by cryorolling and cryorolling followed by warm rolling", **Journal of Material Science and Technology**, 2013, (Under review).

International Conference Proceedings (Presented/published/accepted)

6. **Dharmendra Singh,** P.Nageswara Rao, R.Jayaganthan "Effect of second phase particles on strengthening behavior 0f Al 5083 and 6061 alloys processed by cryorolling" International conference on Recent Advances in Materials & Processing (RAMP -2011), **PSG Coimbatore,** 23-24 December, 2011.
7. **Dharmendra Singh,** P.Nageswara Rao, R.Jayaganthan "Study of microstructural evolution and mechanical properties of Al 5083 alloy processed by cryorolling", International conference on Advanced Materials Processing: Challenges and Opportunities- 2012, (AMPCO), **Indian Institute of Technology, Roorkee,** 2-4 November, 2012.
8. **Dharmendra Singh,** P.Nageswara Rao, R.Jayaganthan, "Effect of grain size and microstructure on corrosion resistance of Al-Mg Alloy processed through cryorolling", TMS Annual Meeting & Exhibition 2013, Symposium: Aluminum Processing, **Warrendale, Texas, USA,** 3-7 March, 2013.
9. **Dharmendra Singh,** P.Nageswara Rao, R.Jayaganthan, "Fatigue behavior of ultrafine grained of 5083-Al alloy produced by cryorolling", TMS Annual Meeting & Exhibition 2013, Symposium: Aluminum Alloys: Fabrication, Characterization and Applications, **Warrendale, Texas, USA,** 3-7 March, 2013.

INDIAN INSTITUTE OF TECHNOLOGY ROORKEE
ROORKEE

CANDIDATE'S DECLARATION

I hereby certify that the work which is being presented in the thesis entitled **"Mechanical Behaviour of Ultrafine Grained 5083 Al Alloy Processed by Cryorolling"** in partial fulfilment of the requirements for the award of the Degree of Doctor of Philosophy and submitted in the Department of Metallurgical and Materials Engineering of the Indian Institute of Technology Roorkee, Roorkee is an authentic record of my own work carried out during a period from July 2010 to August 2013 under the supervision of Dr. R. Jayaganthan, Associate Professor, Department of Metallurgical and Materials Engineering, Indian Institute of Technology Roorkee, Roorkee.

The matter presented in this thesis has not been submitted by me for the award of any other degree of this or any other Institute.

(DHARMENDRA SINGH)

This is to certify that the above statement made by the candidate is correct to the best of my knowledge.

(R. Jayaganthan)
Supervisor

Date:

The Ph.D. Viva-Voce Examination of **Mr. Dharmendra Singh**, Research Scholar, has been held on.....

Signature of Supervisor Chairman, SRC Signature of External Examiner

Head of the Department/ Chairman, ODC

ABSTRACT

Aluminium 5083 alloy (Al-4.4Mg-0.7Mn-0.08Cr) is a medium strength, non-heat treatable alloy known for its excellent corrosion resistance. The unique mechanical properties of the alloys, greater design efficiency, better welding characteristics, good formability, excellent resistance to corrosion, and relatively high strength-to-weight ratio coupled with low cost makes it suitable for structural applications. Specifically, 5083 Al alloy is attractive for ships and marine applications due to the above mentioned properties. With the development of super plastic and quick plastic forming techniques, its application is extended to automobile and aerospace structural components. The extensive use of the alloy demands for the improvement in strength and formability of the alloy for ensuring long term performance of the alloy. Strengthening in polycrystalline materials is related to refining the grain structure to ultrafine regime (100 nm-1000 nm) through severe plastic deformation processing of the materials. Several plastic deformation techniques have been explored to develop homogeneous and equiaxed material with ultrafine grain sizes (UFG) in the bulk materials. It requires exceptionally high strain to induce high dislocation density for the formation of ultrafine grain structures in the alloy. In spite of enormous efforts over the decade, maintaining high strength with reasonable ductility is a challenging task.

UFG materials possess superior properties such as high strength, excellent fatigue life, high toughness and low temperature super plasticity, improved corrosion resistance, enhanced electrical conductivity, wear characteristics, higher specific heat, enhanced thermal coefficient, and superior magnetic properties. The stringent demand of exceptional material properties requirements has led to a considerable interest in the development of ultrafine-grained/ nanomaterials worldwide.

Non-heat treatable aluminium alloys found their application in the form of rolled products (thin sheets and foils). Therefore, there is increasing demand to develop rolling technologies to fabricate sheets ensuring its long time performance. It is identified that cold rolling can result in significant refinement in microstructure from its bulk alloys at very low temperature (Liquid nitrogen temperature) called as cryorolling. It is widely used to produce UFG structure in different metals and their alloys. However, it produces cellular type substructure consisting of boundaries with low angle misorientation. Cryorolling followed by warm rolling and asymmetric cryorolling is also gaining popularity to produce ultrafine grained aluminium alloys. The effect of cryorolling on microstructural evolution and mechanical behaviour of pure metals and heat treatable

aluminium alloys (6xxx, 7xxx) has been reported in literature. On the other hand, there is scarcity of literature on non-heat treatable alloys, especially ultrafine grained 5xxx (5083 Al) alloys, where the prime mechanism of strengthening is solid solution strengthening and work hardening. Therefore, the present work has been envisaged to develop high strength 5083 Al alloy by grain refinement processed through cryorolling and cryorolling followed by warm rolling. The microstructure of deformed Al alloys was characterized by Optical microscopy, TEM, and FE-SEM/EBSD to substantiate their influence on mechanical properties. Optimization of annealing conditions for the deformed Al alloy so as to achieve best combination of strength and ductility with impact strength has been carried out in the present work.

The objectives of present research work are: (i) To investigate the mechanical and microstructural behaviour of 5083 Al alloy deformed through cryorolling; (ii) To study microstructures and impact toughness behaviour of 5083 Al alloy processed by cryorolling and annealing; (iii) To study the effect of deformation temperature on mechanical properties of ultrafine grained Al-Mg alloys processed by rolling; (iv) To study the high cycle fatigue of ultrafine grained Al-Mg alloy processed by cryorolling and warm rolling; (v) To study the corrosion behaviour of ultrafine grained 5083 Al aluminium alloy developed by cryorolling.

A detailed description of the present work is presented in five chapters and it is briefly discussed below.

Chapter 1 gives an overview of aluminium alloys, their applications, worldwide production and consumption in different sectors. Explanation for non heat treatable aluminium alloys and their applications are also discussed.

Chapter 2 presents the details of aluminium and their alloys, their classification, and different strengthening mechanisms. Development of ultrafine grained aluminium alloys through different techniques and their characteristics are included. Literature review pertaining to different severe plastic deformation techniques and cryorolling used for producing ultrafine grain microstructure in aluminium and other materials are also discussed. Based on literature review, the formulation of problem for the present research work has been made. The scope, objectives, and outline of the dissertation work are discussed in this chapter.

Chapter 3 describes the selection of material and its sampling for different experimental technique adopted for development of ultrafine grained materials. The methodology of various

characterization techniques and mechanical testing employed in dissertation work has been discussed.

Chapter 4 describes the results and discussion of different experimental investigations performed on 5083 Al alloy processed through cryorolling, and cryorolling followed by warm rolling. **Section 4.1** investigates the effect of rolling at very low temperature on microstructure and mechanical behaviour of 5083 Al alloy. The alloy was subjected to rolling up to different strain levels at room temperature and immediate quenching at liquid nitrogen temperature. The effect of second phase particles in the alloy was investigated, especially on the evolution of microstructure and grain refinement in terms of pinning and driving forces for recrystallization. It is observed that there is a significant improvement in yield strength (103%) and ultimate tensile strength (40.8%) with CR 90% sample. It is due to the effective suppression of dynamic recovery and accumulation of high dislocations density during low temperature deformation. A homogeneous ultrafine grained structure with an average grains size of 300 nm was achieved after short annealing treatment at 300 ºC for 6 min of CR 90 % thickness reduction sample. The volume fraction of high angle grain boundaries has increased after short annealing treatment due to formation of recrystallized grains, which is due to the combined effect of static recovery and recrystallization.

After investigating microstructure and mechanical behaviour of cryorolled material, the energy absorption capability of cryorolled 5083 Al alloy and effect of subsequent annealing treatment on impact and tensile properties of 5083 Al alloy are reported in **Section 4.2**. The microstructure of the CR 5083 Al alloy and CR and annealed 5083 Al alloy were characterized. The fractography of impact test samples were characterized by FE-SEM to reveal the mode of failure in the CR 5083 Al alloy. The Charpy impact test results have shown that cryorolling significantly decreases impact toughness of the alloy (ST - 32 J to CR 30% - 10 J) and that further decreases with increasing % of cryorolling (CR 30% - 10 J to CR 50% - 7.5 J). The loss in impact energy after cryorolling is due to lack of plastic deformation in the sample due to increase in yield strength, and brittle fracture as observed from SEM micrographs. Annealing at 350 °C for 1 hr, CR 50% sample shows an average grain size of 14 µm, whereas in CR 30%, the average grain size is 25 µm. The difference in the size is due to more nuclei generated during 50% CR resulting in smaller size of the grains. A comparative study of impact toughness behaviour of starting solution treated material with 50% cryorolled sample after annealing shows that the loss in impact

toughness due to cryorolling has been compensated by occurrence of recrystallization after annealing treatment.

Section 4.3 describes the effect of rolling performed at room temperature, cryogenic temperature and cryorolling followed by warm rolling for establishing the optimum rolling condition. Rolling was carried out up to 90% reduction (~2.3 true strain) at room temperature, cryogenic temperature and warm rolled at different temperatures of 100, 145, 175, 200 °C on 50% cryorolled samples up to 90% reduction. On the basis of hardness values for different conditions, cryorolling followed by warm rolling at 175 °C was found to be optimum condition (HV-146) for further investigation and compared with cryorolled alloy alone (HV-127). Annealing was also performed to observe thermal stability of the material. The significant improvement in mechanical properties (UTS-539 MPa, YTS-522 MPa, and ductility 6.8 %) was observed in the samples processed by cryorolling followed by warm rolling. The increase in strength and ductility may be attributed to formation of fine precipitates and dynamic recovery effect. It was evident from microstructural characterization that cryorolling and cryorolling followed by warm rolling samples exhibit high density of dislocations and substructures, high fraction of high angle grain boundaries.

An attempt has also been made to investigate the effect of rolling condition on high cycle fatigue (HCF) in S**ection 4.4.** The 5083 Al alloy was rolled for different thickness reductions of 50% and 85% at cryogenic (liquid nitrogen) temperature. The CR 50% sample was subjected to warm rolling upto 85% total reduction. Their hardness, tensile strength, and fatigue life using constant amplitude stress controlled fatigue were investigated. The cryorolled Al alloy after 85% thickness reduction exhibits high dislocation density due to suppression of dynamic recovery. Whereas, cryorolling followed by warm rolling material has shown ultrafine grain (UFG) structure associated with dynamic recovery during rolling. The deformed 5083 Al alloy was cyclically deformed over a range of stress amplitude at ambient temperature and observed the significant enhancement in fatigue strength as compared to the coarse grained (CG) bulk alloy. Cryorolling followed by warm rolling sample has shown subgrain structure with high angle grain boundaries. It shows occurrence of both high angle and low angle grain boundaries, and very fine grains of 100-200nm were observed, which contributes for HCF life of the material.

Apart from investigating mechanical properties of the ultrafine grained materials, understanding the corrosion behaviour is essential for structural applications as discussed in S**ection 4.5**. Since 5083 Al alloy is potential material for marine applications, the corrosion

behaviour of UFG 5083 Al alloy in chloride environment is also investigated for cryorolling, cryorolling followed by warm rolling and compared with as received and solution treated material. It was observed from polarization test that cryorolling followed by warm rolling samples has shown corrosion current density (I_{corr}- 2.37 μA/cm^2) compared to cryorolled alone (I_{corr}-2.05 μA/cm^2) and ST material (I_{corr}-1.82 μA/cm^2), but showing higher E_{pit} - E_{corr} value (119 mV), which indicates more resistance to pitting corrosion. Solution treated material has undergone pitting corrosion as observed in immersion test and SEM microscopy. Whereas, cryorolling and cryorolling followed by warm rolling (WR) materials has shown resistance to pitting corrosion. These samples have also shown high resistance to IGC, attributed to the combination of various effects, which reduced the presence of active precipitates at the grain boundaries. In cryorolling followed by warm rolling material processing temperature did not sensitize the material and formation of low angle grain boundaries which are less prone to intergranular corrosion, leads to increased IGC resistance.

Chapter 5 presents the summary and conclusion of entire work presented in this thesis as well as future scope of the work in 5083 Al alloys.

ACKNOWLEDGEMENT

First and foremost, I would like to express my deep sense of gratitude to my supervisor Dr. R. Jayaganthan, Associate Professor, Department of Metallurgical and Materials Engineering, Indian Institute of Technology Roorkee, for the inspiration, encouragement and expert guidance that have directed me towards my research goals. I am thankful and gratified for having me in his research group, and all of his help, assistance, and guidance on the all aspects directing the research work. This thesis could not have been completed without his tireless support and encouragement, and I could not have reached to this stage of my academic career.

I am thankful to Prof. S. K. Nath, Head, MMED, IIT Roorkee and faculty members of the department for their help and support throughout the course of my research work. I am highly grateful to the members of my Student Research Committee, Prof. Surendra Singh (Chairman), Dr. I. V. Singh (External member) and Prof. Anjan Sil (Internal member) for their invaluable suggestions, encouragement and motivation to improve the quality of my research work. My sincere thank to Head, Institute Instrument Center (IIC) IIT Roorkee for extending characterization facilities required for my work. I would also like to thank Prof. A.K Singh (IIT Roorkee, Saharanpur Campus) for his cooperation in providing the corrosion testing facilities.

A special thanks to all technical staff of MMED and IIC for their assistance in preparation, testing and characterization of my samples. I would like to thank Mr. T. K. Sharma, Mr. R. K. Sharma, Mr. Rajendra Sharma, Mr. Shakti Gupta, Mr. S. M. Giri, Mr. H.K. Ahuja, Mr. Narendra Kumar, Mr. Dinesh Kumar, Mr. Pradeep Kumar, Mr. Dhan Prakash, and Mr. S. D Sharma for their technical support, and office staff of the department, who have rendered all their help during my work.

I am thankful to The Principal, Government Engineering College Bikaner Rajasthan, for giving me a permission to pursue the Ph.D. at Indian Institute of Technology Roorkee. I personally thanks to Head, Mechanical Engineering Department and other faculty members of the department for their everlasting support. I would like to thank QIP centre, IIT Roorkee and All India Council for Technical Education, New Delhi for providing me the opportunity to pursue Ph.D. work at IIT Roorkee.

I express my heartiest thanks to Mr. P. Nageswara Rao for his valuable suggestions and constant support during testing and characterization of my samples. Sincere thanks to my friend and colleagues for their moral support, encouragement and memorable stay at IIT Roorkee. I greatly enjoyed working with my friends Mr. Sunkulp Goel, Mr. Abhishek Kumar, Mr. Rajeev Sehrawat, Mr. V. N. Shukla, Mrs. Nidhi Rana, Ms. Devasri Fuloria, Mr. Vinod Jeenegar, Ms. Deepa Mudgal, and all other colleagues in the department.

Finally, I express heartiest gratitude to my family members for their unflagging love and support throughout my life and their worships for the betterment of my future. This work would not have been possible without their support, sacrifice and constant encouragement. I am indebted to my father Shri Shanker Singh Aveliya, my sister Priti and her husband Mr. Vinod Barodia, my younger sister Kamini and her husband Mr. Sudheer Kumar, my younger brother Mr. Uttam Singh and his wife Usha for his valuable advices, care, and support that make me free from my social responsibilities.

I would like to extend my reverence and gratitude to my wife, Mrs. Chandrani Aveliya for her support, sacrifice, and providing me constant encouragement, her patience and belief in me enabled this thesis to be completed. I am thankful to my daughter Ekta and son Bhavya, their innocent face and smile has always relieved the stress of my research work.

I express my sincere thanks to my father in law Shri Om Prakash Shakya, mother in law Smt. Malti Shakya, brother in law Mr. Bhupendra Shakya and sister in law Mitali Shakya for providing moral support and encouragement during this period of my research work.

I would like to thank everyone who was directly or indirectly involved to the successful completion of my thesis as well as expressing my apology, if I could not mention everyone personally.

Above all, I am highly indebted to the almighty GOD from the core of my heart for his blessings with spiritual support, strength and patience at each and every stage to accomplish my research work.

The present research work is dedicated to my beloved mother Late Smt. Sushma Devi.

(Dharmendra Singh)

CONTENTS

LIST OF FIGURES

LIST OF TABLES

LIST OF PUBLICATIONS

Research publications (Published/Under review)

1. **DharmendraSingh,** P. Nageswara Rao, R. Jayaganthan, "Study of microstructural evolution and mechanical properties of 5083 Al alloy processed by cryorolling**", Advanced Materials Research,** 2012, 585, 376-380.
2. **Dharmendra Singh,** P. Nageswara Rao, R.Jayaganthan, "Study of microstructural evolution and impact toughness behaviour of 5083 Al alloy processed by cryorolling", **International Journal of Minerals, Metallurgy, and Materials**, 2013, 20, 759-769.
3. **Dharmendra Singh,** P. Nageswara Rao, R. Jayaganthan, "Effect of deformation temperature on mechanical properties of ultrafine grained Al-Mg alloys processed by rolling", **Materials and Design**, 2013, 50, 646-655.
4. **Dharmendra Singh,** P. Nageswara Rao, R. Jayaganthan, "Corrosion behaviour of ultrafine grained Al 5083 aluminium alloy developed by cryorolling", **Corrosion Science**, 2013, (Under review).
5. **Dharmendra Singh,** P. Nageswara Rao, R. Jayaganthan, "High cycle fatigue behaviour of Ultrafine grained 5083 Al aluminium alloy developed by cryorolling and cryorolling followed by warm rolling", **Journal of Material Science and Technology**, 2013, (Under review).

International Conference Proceedings (Presented/published)

6. **Dharmendra Singh,** P. Nageswara Rao, R. Jayaganthan "Effect of second phase particles on strengthening behaviour 0f Al 5083 and 6061 alloys processed by cryorolling" International conference on Recent Advances in Materials & Processing (RAMP -2011), **PSG Coimbatore,** 23-24 December, 2011.
7. **Dharmendra Singh,** P. Nageswara Rao, R. Jayaganthan "Study of microstructural evolution and Mechanical properties of 5083 Al alloy processed by cryorolling", International conference on Advanced Materials Processing: Challenges and Opportunities-2012, (AMPCO), **Indian Institute of Technology, Roorkee,** 2- 4 November, 2012.

8. **Dharmendra Singh,** P. Nageswara Rao, R. Jayaganthan, "Effect of grain size and microstructure on corrosion resistance of Al-Mg Alloy processed through cryorolling", TMS Annual Meeting & Exhibition 2013, Symposium: Aluminium Processing, **Warrendale, Texas, USA,** 3-7 March, 2013.

9. **Dharmendra Singh,** P. Nageswara Rao, R. Jayaganthan, "Fatigue behaviour of ultra-fine grained of 5083 Al alloy produced by cryorolling", TMS Annual Meeting & Exhibition 2013, Symposium: Aluminium Alloys: Fabrication, Characterization and Applications, **Warrendale, Texas, USA,** 3-7 March, 2013.

CHAPTER 1
Introduction

1.1 General introduction

Aluminium and its alloys are extensively used for various applications that are part of our daily lives, starting from utensils, aluminium foils used for food packaging, cans used for beverages, and to the structural applications in aircrafts, automobile and ships. This versatile use of aluminium alloys is due to a good combination of mechanical properties, combined with the ease with which it is being produced in a variety of shapes and forms for various industrial applications, which makes it the most widely used metal after steel. Aluminium is the third most abundant element found on earth's crust and the second most attractive metal used for making products after iron and steel. In 1809, Sir Humphrey Davy, the British electrochemist, established the existence of aluminium, and later on in 1825, Danish scientist Oersted transformed aluminium oxide into aluminium chloride and then produced pure aluminium from its chloride and subsequently the tiny pellet of aluminium metal. In 1920, modern aluminium alloys came into existence.

Global demand for lighter and stronger materials is ever increasing in engineering design because aluminium weighing 7 kg with equal width and length exhibit stiffness equal to steel beam weighing 10 kg (Polmear et al. 1995). The density of aluminium alloys is 2.7 g/cm^3 and their tensile properties are low as compared to steel, but they have excellent strength to weight ratio. Therefore, structural elements made from aluminium based alloys are vital for automotive, aerospace, marine industry, and other areas of transportation. According to International Energy Agency Research, around 20% of manmade greenhouse gas emissions are produced by the transportation sectors. The reduction in the weight of transportation vehicles is beneficial for mankind due to improved fuel efficiency, reduced energy consumption, and greenhouse gas emissions. About 140 million tons of saving in global CO_2 and about 55 billion liters of crude oil saving was reported in 2006 using light passenger cars and trucks (www.world-aluminium.org). Weight of structures is reduced by > 30% without losing performance in car bodies making use of aluminium (Hirsch et al. 2011). Thus, from an average of only 39 kg of aluminium in the passenger car in 1976, to 110 kg in 1996, its usage is expected to grow to around 250-340 kg by 2015. For better performance of ships, new Al alloys with improved mechanical properties, weldability, corrosion resistance, etc were developed. Weight savings from 50% in hulls to around

62% in commercial deckhouse structures were favorable, this saving in weight improves the ship stability with design of narrower ships, and fuel efficiency becomes significant in larger ships (Brown et al. 1999). Similarly, aluminium is the main material used from 50 to 70% in the aircraft structure. The A380 super sized aircraft shows that 61% of the aircraft structure is made up of aluminium alloys, 22% with composites, 10% in steel and titanium and 3% in fiber-metal laminates, and this allows a 12% increase in fuel efficiency (www.key to metals.com). The double-deck jetliner has a very low fuel burn of less than 3 liters per passenger per 100 kilometers making use of aluminium.

This extensive use of aluminium alloys raised its demand worldwide. The statistics shows that the global aluminium production which was 41.1 million tons in 2010 has increased to 45.54 million tons in 2011(as per CRU Monitor-Aluminium) as shown in Figure 1.1. The increase is about 8.23%, i.e. to 49.28 million tons in 2012. India produced approximately 4% of world production. The world aluminium consumption in 2010 and 2011 was 39.66 million tons and 44.88 million tons, respectively, as shown in Figure 1.2. Also, the excellent recycling of aluminium, together with its high value of scrap and the low energy requirements during recycling (nearly about 5% of the energy required by primary production), make recycling of aluminium to increase dramatically in the coming years.

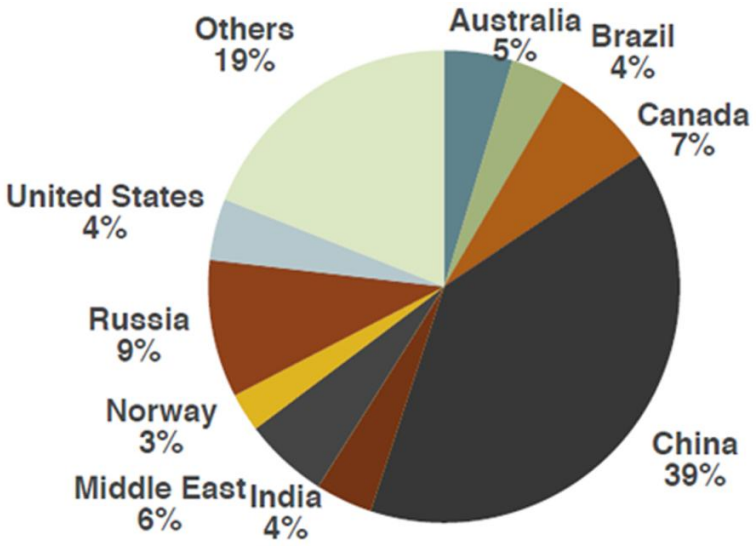

Figure 1.1: World production of aluminium (2010) (Source: WBMS and CRU).

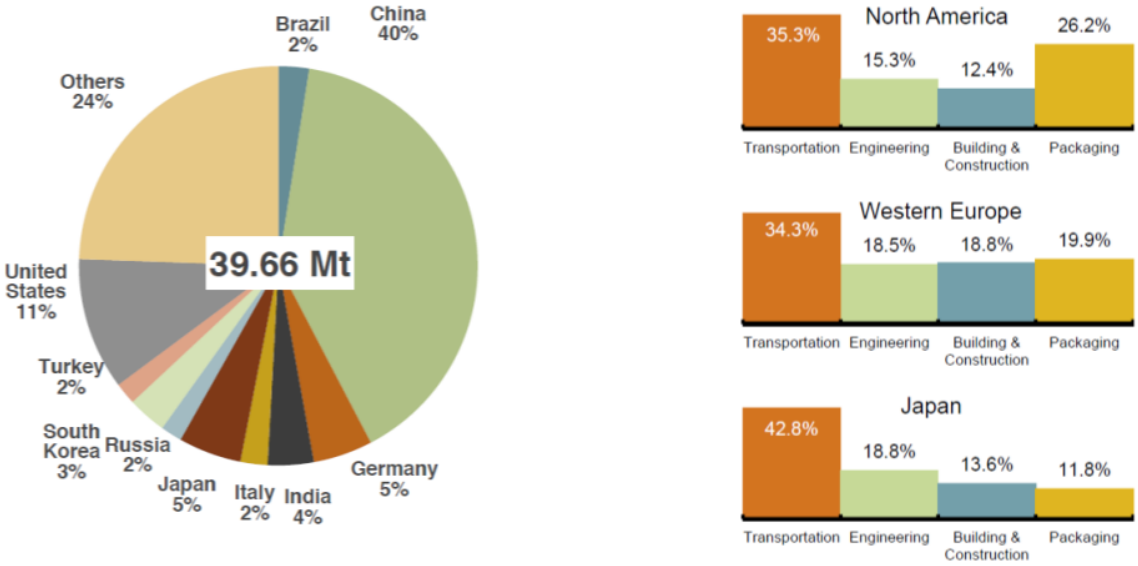

Figure 1.2: Primary aluminium consumption (2010) (Source: WBMS, July 2011).

As far as primary production is concerned globally, China (with around 40% market share) is leading because of its natural sources of comparative advantage (energy is abundant and relatively cheap), and also because of policies related to subsidies, trade and exchange rates. The leading role in global consumption is also played by China, whose market share is 40% today. Transportation has become the most significant end-use market (www.world-aluminium.org).

The demand for lighter and stronger materials with high strength, toughness, higher fatigue and corrosion resistance, ease of fabrication and cost effectiveness is ever growing due to its applications in aerospace, automobile, transportation, food and chemical processing industries. This provides an impetus for a significant growth in the development of new metals or materials with enhanced properties. To meet these requirements, the material scientists and engineers are modifying the existing alloys to alter its microstructural characteristics and improve their properties or use novel processing techniques for producing ultrafine-grained/nano materials with improved mechanical properties. Metals and alloys with ultra-fine (< 1 μm) and nanocrystalline (< 100 nm) grain size offers an increased strength and therefore serve as potential materials for structural applications. Iwahashi et al. (1998) have demonstrated that at low strains, dislocation cell structures formed consisting of low angle grain boundaries, which has transformed into ultrafine grained materials with predominantly high angle grain boundaries. Also, the presence of second-phase particles in matrix speeds up the rate of dislocation generation more uniformly (Cheng et al.

2007). Advancements in technology make it possible to develop such materials with excellent combination of mechanical properties and have been widely studied and attracted significant research interest worldwide. Generally two approaches were developed for the synthesis of these materials known as “top -down” and “bottom- up” approaches.

Review by Sabirov et al. (2013) have shown that aluminium alloys processed by SPD techniques contains four types of nano scale elements along with ultrafine grains such as i) non-equilibrium grain boundaries (Valiev et al. 1986, 2009), ii) stacking faults and nano twins (Chen et al. 2011, Liu et al. 2010); iii) segregation of clusters or clouds (Liddicoat et al. 2010, Sauvage et al. 2012), iv) nano sized particles and precipitates (Valiev et al. 2009). These materials are referred as bulk nanostructured materials. Recently, it was reported that nanostructured aluminium alloys not only increases their mechanical properties, but also improves chemical and physical properties, which makes them attractive for functional and structural applications (Valiev et al. 2006, Zhilyaev et al. 2008). Furthermore, the grain size reduction to the submicrometer level leads to the occurrence of very high strain rate superplasticity in comparison with conventional superplastic materials at elevated temperatures (Kawasaki et al. 2007).

The work hardenable wrought Al-Mg (5xxx) alloys are used for applications that require greater design efficiency, excellent resistance to corrosion, better welding characteristics, good super plasticity, and relatively higher strength-to-weight ratio coupled with low cost (Hecht et al. 1995). Specifically, 5083 Al alloy is attractive for ships and marine applications. US navy uses 5083 Al alloy in plates and extrusions on many of its ships including the HSV-1 Swift, Littoral Combat Ship and the Bollinger/Incat the charter for a High Speed Craft (HSC) due to its resistance to exposure on salt water in navy (Dean et al. 1995). Aluminium manufacturer, Pechiney of France have registered the 5383 Al alloy and promoted it to shipbuilding industry as a better material over the 5083 Al alloy. Weldability of 5083 Al alloy makes it an ideal material for those components, which demands for high welded strength (Hoeven et al. 2002). With the development of super plastic and quick plastic forming techniques, 5083 Al alloy is used for automobile and aerospace applications. Al-Mg-Mn alloys are mostly used for inner body panels because of their specific combination of strength and formability shown in figure 1.3. The SPF/QPF grades of the alloy are now commercially produced by a number of suppliers in Europe, USA and Japan. Grimes et al. (2007) have produced 5083 Al alloy with 1% Zr alloy on a laboratory scale and reported good super plastic ductility and significantly improved mechanical properties (YS - 210 MPa). Boeing’s

commercial fleet uses 5083 Al alloy for most of the parts of the aircraft, whose failure would not lead to the complete loss of the aircraft. By replacing these parts as older aluminium castings and fiberglass assemblies, makes Boeing's planes lighter with lower cost. 5083 Al alloy is non-heat treatable, therefore, cost associated with heat treatment, quenching, ageing is avoided and also provides distortion free structures (Hefti et al. 2007).

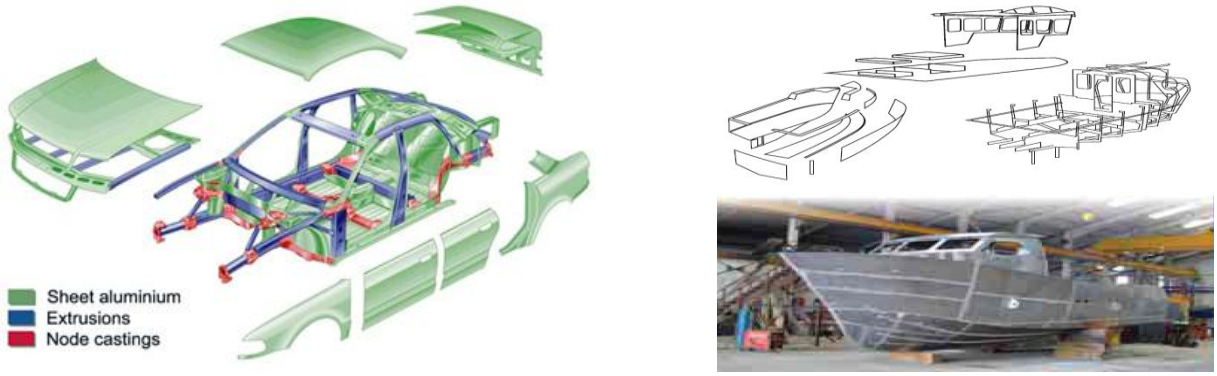

Figure 1.3: Application of 5083 Al alloy.

Aluminium alloys in all of the major industrial applications comprise the largest usage of flat rolled products. The extensive use of aluminium and its alloys in form of rolled products requires developing rolling technologies for production at large scale with high performance sheets, that not only have high strength but also high formability. Conventional rolling may be suitable for mass production of bulk ultrafine-grained alloys, but it is difficult to process high stacking fault energy aluminium and its alloys (Lee et al. 2004). To obviate these troubles, conventional rolling at liquid nitrogen temperature (cryorolling) has been identified as a potential route and has been used popularly to produce UFG structure in aluminium alloys (Panigrahi et al. 2008, Gang et al. 2009, Rao et al. 2012). Recently, cryorolling followed by warm rolling and asymmetric cryorolling have also been developed to produce ultrafine grained aluminium alloys (Kang et al. 2010, Rao et al. 2012).

Owing to the above mentioned views, the present work has been envisaged to develop high strength 5083 Al alloy by grain refinement processed through cryorolling and cryorolling followed by warm rolling. The microstructure of deformed Al alloys was characterized by Optical microscopy, TEM, and FE-SEM/EBSD to substantiate their influence on mechanical properties. Optimization of annealing conditions for the deformed Al alloy so as to achieve best combination of strength and ductility with impact strength has been carried out in the present work. High cycle

fatigue behaviour of the alloy was also investigated. The corrosion behaviour of coarse grained and ultrafine grained 5083 Al alloy has been carried out in the present study.

1.2 Outline of thesis

The outline and content of various chapters of the thesis are summarized as follows:

The brief description related to aluminium alloys, their strengthening mechanisms, properties of ultrafine grained/nanocrystalline materials, different techniques of their synthesis and introduction to cryorolling followed by exhaustive literature survey are summarized in **Chapter 2.** Based on literature review, the problem for present research work was identified and listed in S**ection 2.5**. Materials selection, different processing techniques adopted and their experimental procedures, methodology pertaining to their microstructural characterization, texture analysis and mechanical testing are discussed in detail in **Chapter 3.** Different experimental investigations performed on 5083 Al alloy processed through cryorolling and cryorolling followed by warm rolling and their results are discussed in **Chapter 4.** Microstructural studies of 5083 Al alloy deformed through cryorolling are discussed in **Section 4.1.** Microstructures and Impact toughness behaviour of 5083 Al alloy processed by cryorolling and afterwards annealing are discussed in **Section 4.2.** Effect of deformation temperature on microstructure and mechanical properties of ultrafine grained Al-Mg alloys processed by rolling is discussed in **Section 4.3.** An attempt has also been made to investigate the effect of rolling condition on high cycle fatigue behaviour and their comparison in S**ection 4.4.** Corrosion behaviour of ultrafine grained 5083 Al alloy developed by cryorolling and cryorolling followed by warm rolling was investigated and comparison with as received and solution treated and material are discussed in **Section 4.5.**

The observed mechanical behaviour of 5083 Al alloy is substantiated using microstructural observations and phase identification through Optical, FE-SEM, EBSD, TEM, DSC, and XRD. The conclusions drawn from experimental investigations of 5083 Al alloy are also reported at the end of each section of **Chapter 4.**

The final conclusions are summarized in **Chapter 5** with future scope followed by references in the present work.

CHAPTER 2
Literature Review

This chapter highlights a brief description of aluminium and their alloys, their strengthening mechanisms, development of ultrafine grained/nanocrystalline materials and different processing techniques used for producing these fine grained materials. Literature pertaining to cryorolling and other severe plastic deformation techniques used for producing ultrafine grain microstructure in aluminium and other materials are discussed in this chapter. The formulation of problem for the present dissertation work has been made based on the existing literature. The scope, objectives, and outline of the dissertation work are discussed in this chapter.

2.1. Aluminium alloys

Pure aluminium is soft and ductile, corrosion resistant and has a high electrical conductivity; therefore it is widely used for applications in foil and conductor cables. Alloying with other elements provides higher strength required for other applications. Aluminium and their alloys have the face centered cubic (FCC) structure that is stable up to melting point temperature at 657 $^{\circ}$C. The yield strength of pure aluminium is 7-11 MPa, while their alloys have yield strengths between 200 MPa to 600 MPa. Aluminium alloys are suitable for low temperature applications; they lose their strength and corrosion resistance when exposed to elevated temperatures during service. Aluminium alloys have ability to form a thin oxide film on the surface due to their high reactivity with oxygen. This air oxide film is stable in neutral and some acidic solutions. Further it works as an insulator and serves as a protective layer from the external environments.

The classification of aluminium alloys is made as wrought alloys which are mechanically formed by rolling, forging and extrusion into final products and cast aluminium alloys those are casted directly to the final finished shape. Further, classification of wrought aluminium alloys fall into two distinct categories as shown in Figure 2.1.

a. Non-heat treatable alloys

These are materials which derive their properties from work hardening and solid solution strengthening. The enhancement in properties of 1xxx, 3xxx, 4xxx and 5xxx series alloys is achieved through cold working, usually by cold rolling, and annealing or thermal treatment

required for their stabilization. They are not sufficient for load bearing structural applications because the strengthening properties obtained for the cold worked structures are lost at elevated temperatures.

b. Heat treatable alloys

These are materials whose improvement in strength is based on solution heat treatment and age hardening. 2xxx, 6xxx, 7xxx series contains solute elements in concentrations that exceed their equilibrium solubility at room temperature. After solution treatment (dissolution of soluble phase) and water quenching (development of super saturation phase) followed by low temperature ageing, the solute atoms precipitates, which significantly strengthen the materials. This type of strengthening mechanism is called precipitation hardening.

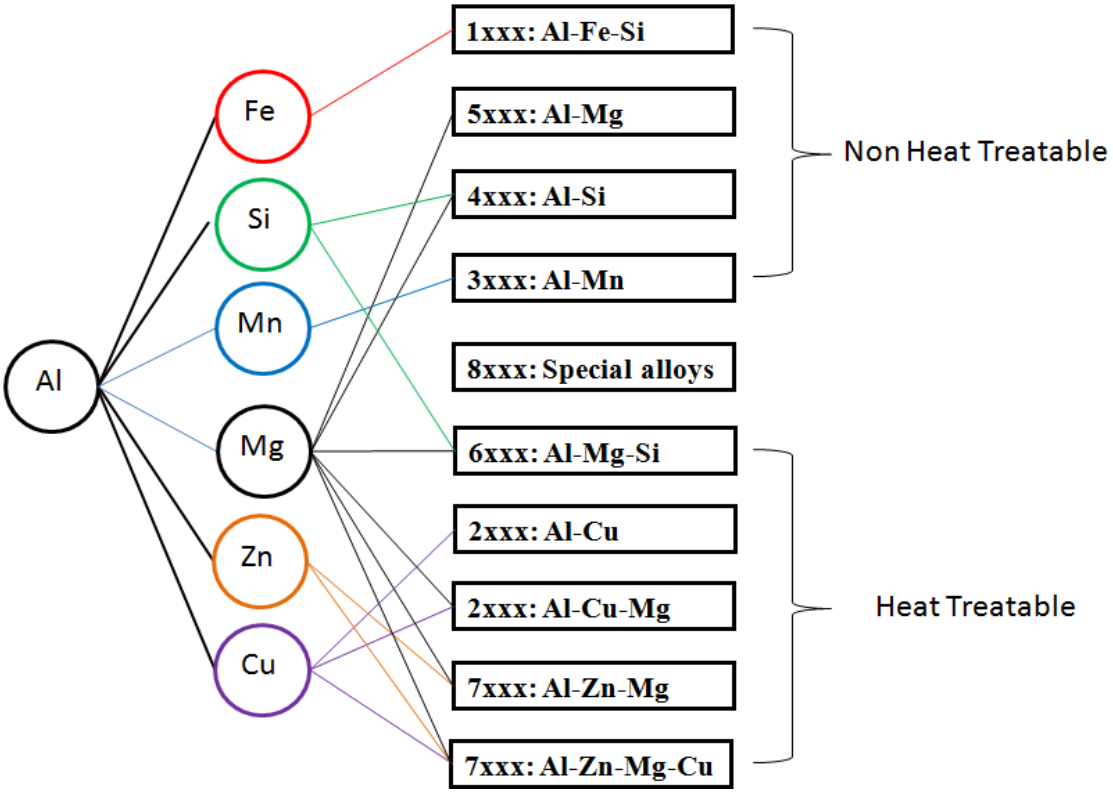

Figure 2.1: Principal alloying elements and the families of alloy derived from them (Hatch, 1984).

2.2. Alloy designations and temper

Wrought aluminium alloys are identified through 4 digit systems, where the first digit indicates major alloying element (the alloy group), the second digit indicates modifications in the original alloy or their impurity limits and the last two digits signify the aluminium alloy or indicate

the aluminium purity. A letter used as a prefix indicates an experimental alloy. A letter used as a suffix shows national variations. Figure 2.2 shows detailed temper designations for aluminium alloys. Cast alloys are designated through 3 digit system.

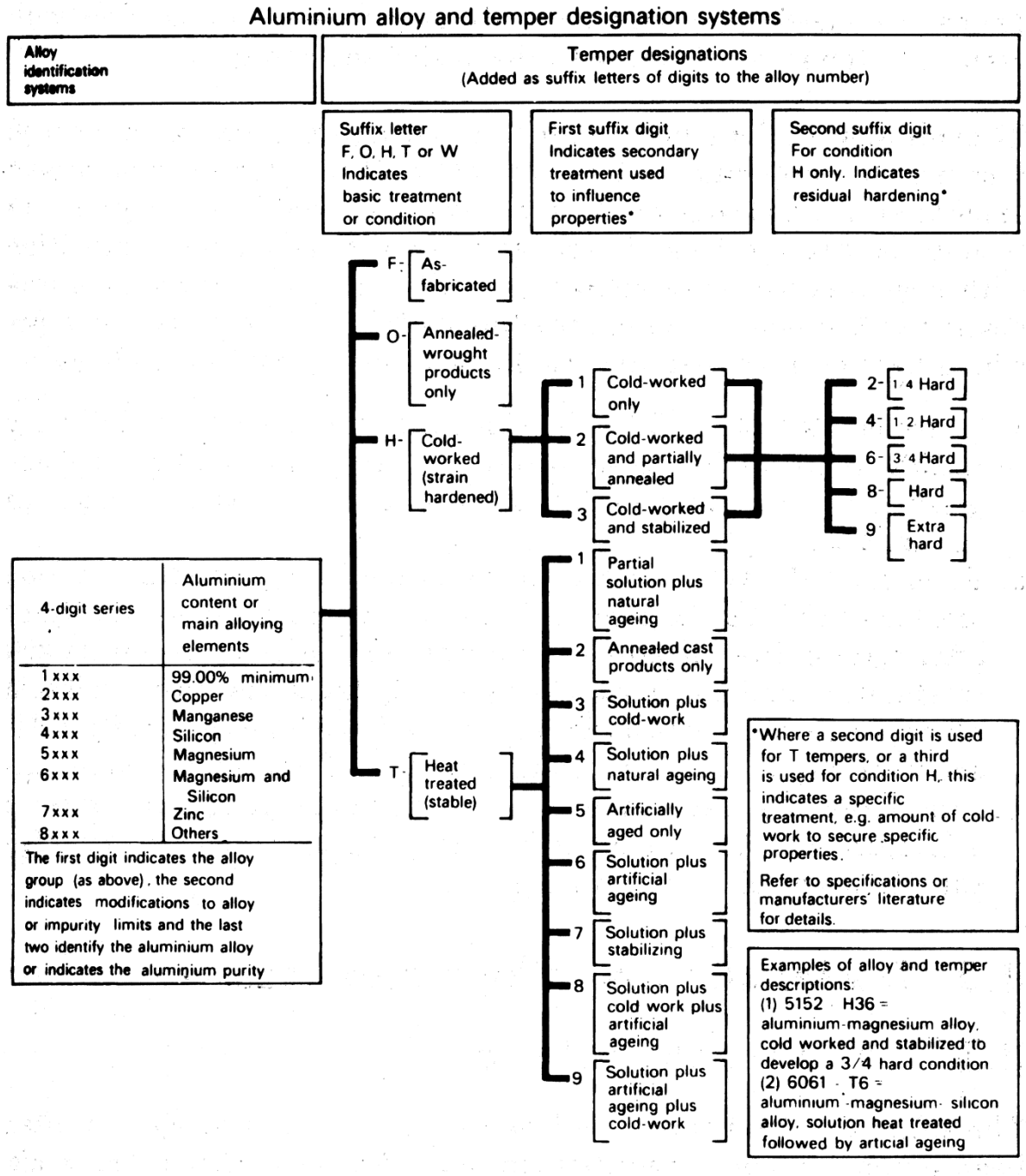

Figure 2.2: Designations for wrought aluminium alloys (Polmear, 1995).

2.3 Strengthening mechanisms for aluminium alloys

Ultrafine grained and nanostructured materials have shown a remarkable increment in strength as compared to their coarse-grained counterparts. High-strength aluminium alloys are of great interest because of their low densities, and recent works have reported that substantial strengthening of aluminium alloys can be accomplished through grain refinement (Zhao et al. 2001, Tellkamp et al. 2001, Youssef et al. 2006). Ability of a metal to deform plastically depends on ease of dislocation motion under external stresses. Therefore, hindering/restricting dislocation motion leads to enhancement in strength of material, that is, greater external forces will be required to initiate plastic deformation. In contrast, more unconstrained dislocation motion makes metal soft and weak due to ease in deformation. Dislocation motion can be blocked in many ways within the microstructure, such as the crystal lattice itself, precipitates, solute atoms, dislocations, and grain boundaries, thus increasing dislocation density in the matrix for enhancement in strength (Huskin et al. 2010).

The various strengthening mechanisms have been developed to produce aluminium alloys with higher strength and ductility improved through post processing treatments. Strengthening by grain-size reduction, solid-solution strengthening, and strain hardening applies for single-phase metals. Whereas, dispersion hardening, fiber strengthening and precipitation hardening are applicable for multi-phase metallic materials. Huskin et al. (2010), have reported some of the strengthening mechanism in 5083 Al alloys. A review of the strengthening mechanisms, which are relevant to the present dissertation work are discussed in detail.

2.3.1 Strengthening by Grain Size Reduction

In polycrystalline materials, orientation changes abruptly while moving from one grain to the next across the grain boundary. Therefore, it is difficult for the dislocations moving on a common slip plane in one crystal to pass over to a similar slip plane in another grain, especially if there is misalignment in orientation. Atomic disorder at the grain boundary causes discontinuity in slip planes, and dislocations are hindered by a grain boundary and piled up against it. Pile up of dislocations will be more frequent in smaller grain size. These pile-ups introduce stress concentrations ahead of their slip planes, which generate new dislocations in adjacent grains. Low angle grain boundaries are not effective in hindering dislocations due to small crystallographic misorientation across the boundary. Whereas, high angle grain boundaries block the slip and

increases the strength of the material. The schematic of a dislocation moving along a slip plane approaching grain boundary is shown in Figure 2.3 a. Schematic diagram showing low and high-angle grain boundaries with respect to atom positions adjacent to it is shown in Figure 2.3 b.

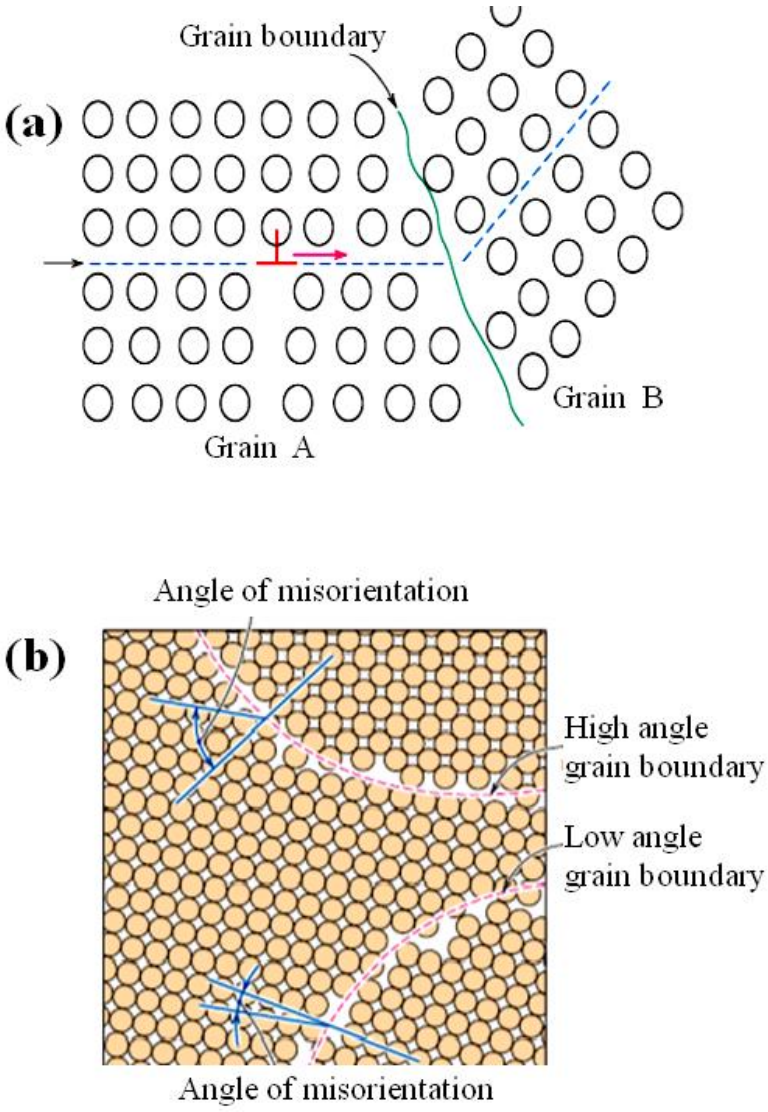

Figure 2.3: Schematic diagram showing; (a) Dislocation motion approaching a grain boundary, (b) Low and high-angle grain boundaries with respect to adjacent atom positions (Callister, 2007).

With reduction in grain size, the mean distance travelled by dislocation decreases, and starts pile up of dislocations at grain boundaries. This results in increase in yield strength of the material, which is explained from the well known relation known as Hall-Petch relation between yield strength (σ_y) and grain size (d) (Hall, 1951, Petch, 1953 and Hansen, 2004).

$$\sigma_y = \sigma_o + kd^{-1/2} \quad (2.1)$$

Where; 'σ_o' is the friction stress representing the resistance of the crystal lattice to dislocation movement, 'k' is the locking parameter that measures the hardening contribution made by grain boundaries and 'd' is the average grain diameter. The yield strength is inversely proportional to grain size; therefore, the fine grained materials are stronger than the coarse grained materials. The above equation is not valid for both very coarse grain and extremely fine grain in polycrystalline materials.

2.3.2 Solid solution strengthening

Solution hardening, or alloying, is a powerful method to improve the strength of a material. Adding atoms of another element, which is stronger than parent metal, occupies interstitial or substitutional sites in lattice, thus increasing the strength of parent material as shown in Figure 2.4. The stress fields thus generated around the solute atoms interact with the stress fields of a moving dislocation, impeding its motion thereby increasing the stress required for plastic deformation. Solid solution strengthening depends on: size of solute atoms, concentration of solute atoms, valency of solute atoms and shear modulus of solute atoms, The solute strengthening increment '$\Delta \sigma_{ss}$', due to concentration 'C' of a solute atom, is often defined as;

$$\Delta\sigma_{ss} = HC_\alpha \quad (2.2)$$

Where 'α' and 'H' are constants. A higher concentration of solute atoms will obstruct dislocations and slow their motion more than a smaller concentration, thus increasing strength (Suzuki et al. 1990).

The basic alloy strengthened by solid solution coupled with cold working is the aluminium-magnesium (5083 Al) alloy containing magnesium in range from 0.5 to 6 wt%. This alloy also contains small additives such as manganese or chromium, zirconium to control the grain or subgrain structure, silicon and iron impurities are present as intermetallic particles. Al -Mn acts as point defects within the lattice and impedes dislocation movement. Figure 2.5 illustrates the effect of magnesium in solid solution on the yield strength and tensile elongation for some of the common aluminium- magnesium alloys commercially available.

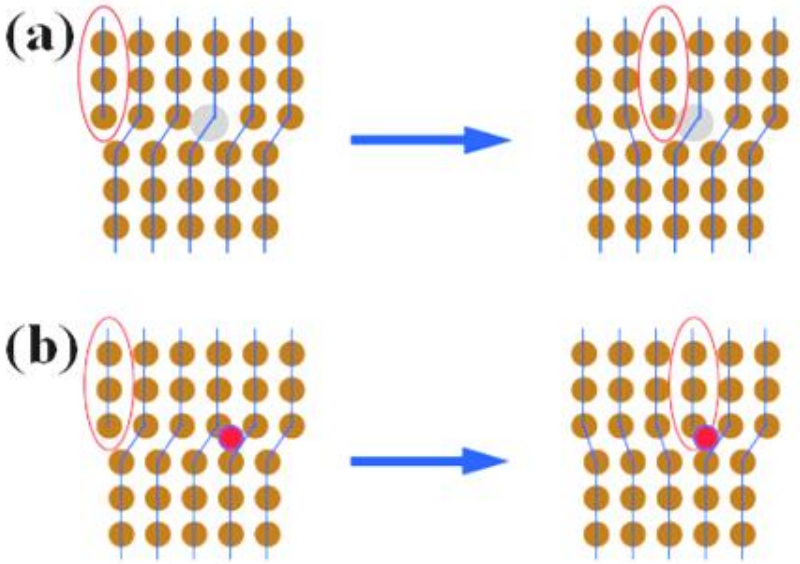

Figure 2.4: Representation of a dislocation stopped by; (a) Interstitial atom, (b) Substitutional atom (Brush wellman, 2010).

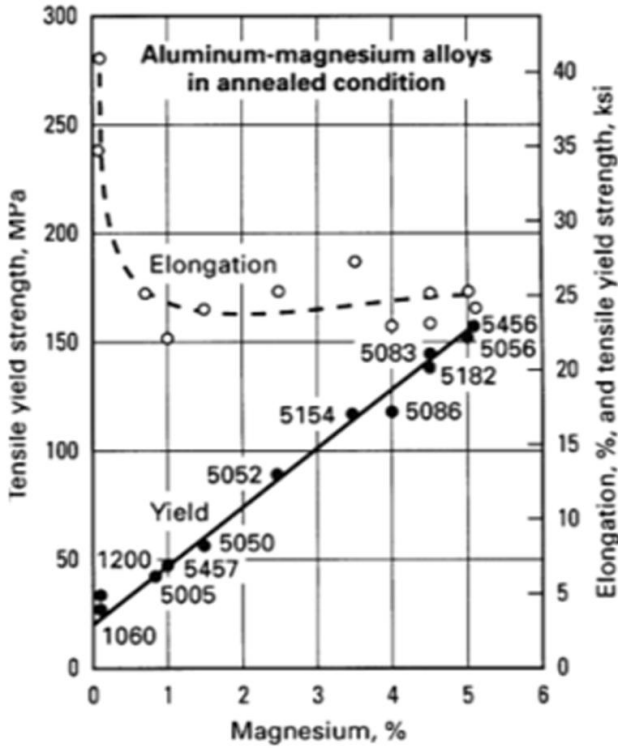

Figure 2.5: Effect of Magnesium (wt %) in solid solution on mechanical properties (ASM Handbook, Vol. 2).

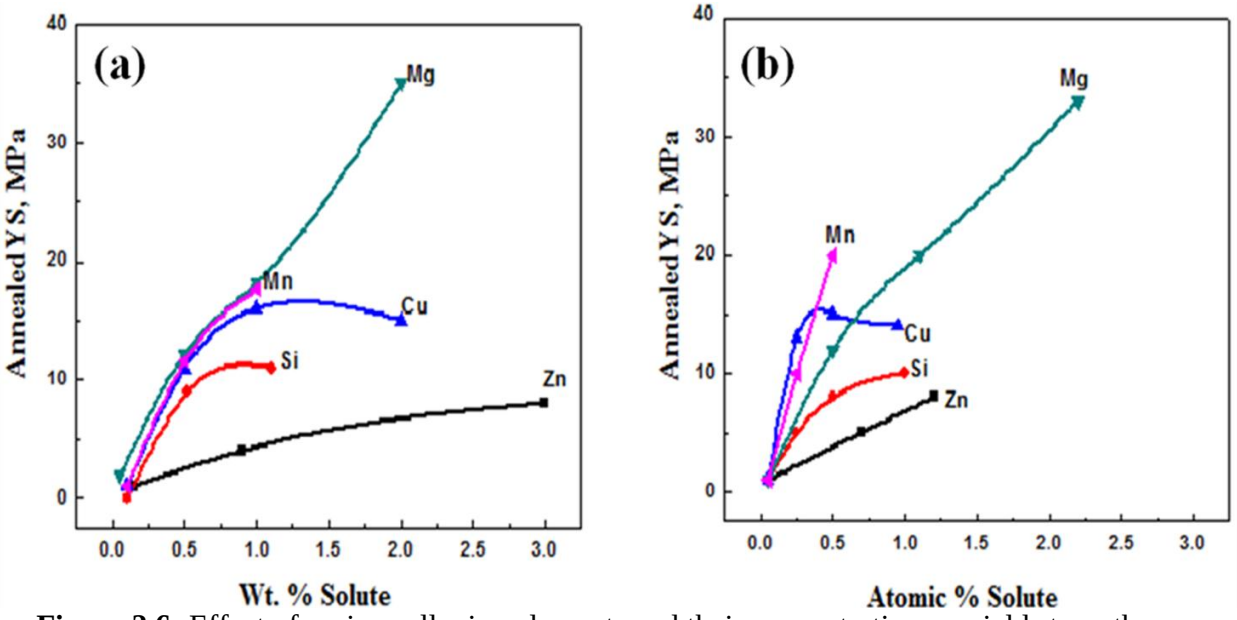

Figure 2.6: Effect of various alloying elements and their concentration on yield strength as a function of; (a) weight % solute, (b) atomic % solute. (Sanders et al. 1986, George E. Totten, 2003).

Figure 2.6 (a) and 2.6 (b) shows that upon alloying the elements with atomic % or weight %, the yield strength of annealed aluminium sheet increases. The effect of varying concentration is not linear; similarly, the various solute elements are not equally effective in strengthening the material. As seen in Figure 2.6 a, Cu and Mn are more effective in strengthening with less than 0.5%. Magnesium is not effective on atomic % basis, but more effective on weight % basis. When Mg level is < 1 atomic %, the yield strength increase is proportional to ($Mg^{2/3}$), whereas at higher concentration, the proportionality varies to ($Mg^{1/3}$). Therefore, Mg is more effective in solid solution strengthening of aluminium alloys. The presence of Cu and Si affects the amount of Mg retained in solution, as it forms Al-Cu-Mg, Al-Mg-Si phases in the matrix (Sanders, 2004, George E. Totten, 2003). Alloying of Cu to aluminium resulted in age hardening behaviour. Zinc is highly soluble in aluminium at low temperature, but has very less effect on strengthening due to its high density of 7.14 g/cm^3. Zn is added to non-heat treatable alloys at level of 1% to adjust the solution potential to enhance its resistance against stress corrosion cracking.

2.3.3 Strain hardening

Wrought alloys (e.g. 1xxx, 3xxx, 5xxx) are usually strengthened by strain hardening. This involves cold-working at ambient temperatures, where the dislocations multiply at a faster rate than destroyed by dynamic recovery**.** With increase in dislocation density, separation between dislocations decreases and they come closer. The average dislocation–dislocation strain interactions are repulsive and results in hindering the motion by the presence of other dislocations. This leads to an increase in the yield strength of the material at the expense of ductility. The strength contribution of dislocation structures to the macroscopic flow stress is often represented by an Orowan type equation (Mecking et al.1981and Gubicza et al. 2007).

$$\sigma_o = \alpha\, Gb\rho \tag{2.3}$$

Where, 'σ' is macroscopic flow stress, 'σ_o' is friction stress, 'α' is constant, 'G' is shear modulus, 'b' is Burger's vector and 'ρ' is total dislocation density. From equation (2.3), it is observed that yield strength is directly proportional to dislocation density. Therefore, with increasing dislocation density during plastic deformation, the yield strength increases significantly. Figure 2.7 shows the influence of cold working on the yield stress and ductility of the material.

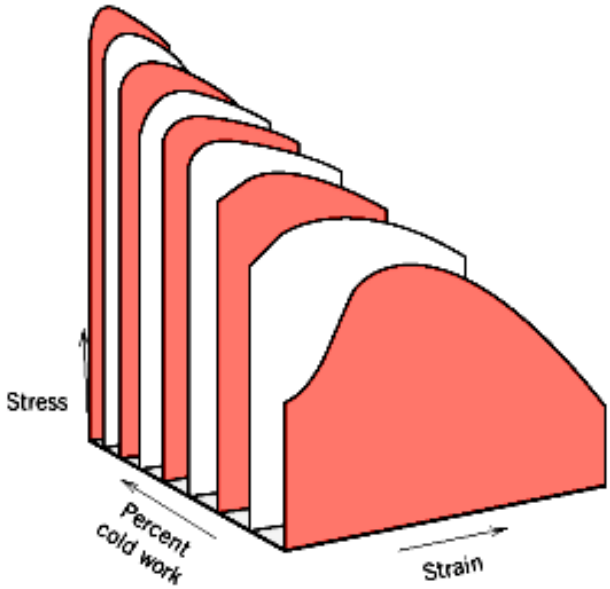

Figure 2.7: The influence of cold working on yield stress and ductility of a material (Callister, 2007).

2.2.4 Precipitation hardening

Precipitation hardening or age hardening is most widely used strengthening mechanisms of aluminium alloys in 2xxx, 6xxx and 7xxx series, where the hardness and strength of aluminium alloys is improved by the formation of extremely fine and uniformly dispersed second-phase particles of the solute atoms in supersaturated matrix. Precipitation hardening relies on changes in solid solubility with temperature.

These fine precipitates impede the movement of dislocations and strengthen the heat-treated alloys. The process mainly involves three steps; i) Homogenization or Solution heat treatment, where the alloy is heated above the solvus temperature and soaked there until solute dissolves and homogeneous solid solution is produced; ii) Quenching, where the solid solution is cooled rapidly to a lower temperature forming a supersaturated solid solution and the solute is not immediately able to diffuse out of a phase.; iii) Finally ageing is done where the supersaturated solid solution is heated below the solvus temperature to produce a finely dispersed precipitate. Figure 2.8, is schematic showing temperature-time plot for precipitation hardening mechanism. The fine precipitates in the alloy prevent dislocation movement. This mechanism of hardening has most extensively been studied for the Al-4% Cu (Duralium) alloys, where Al_2Cu is the phase that strengthens the alloy. The schematic diagram of various modes of interaction between precipitates and dislocations proposed by Ashby et al. (1992) is shown in Figure 2.9.

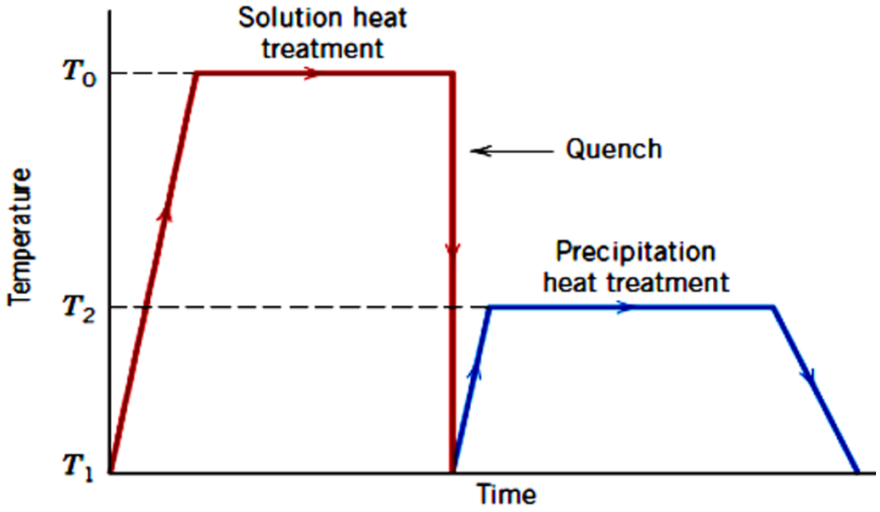

Figure 2.8: Schematic of temperature-time plot showing precipitation hardening mechanism.

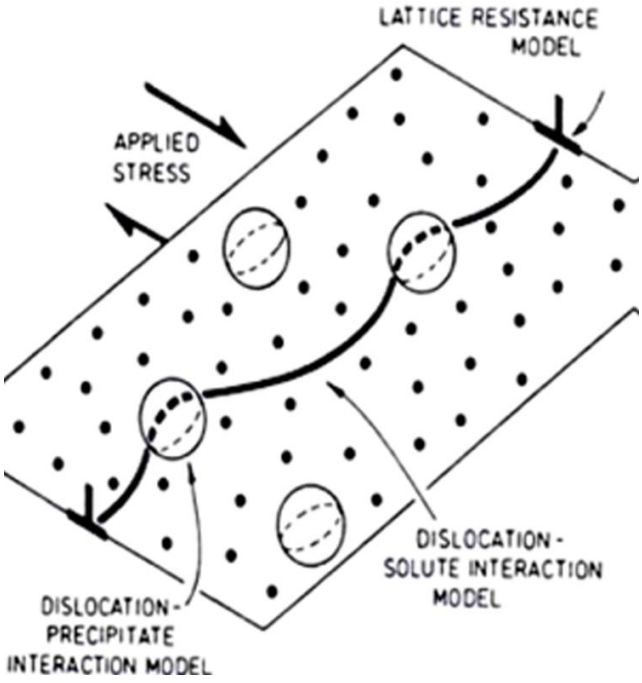

Figure 2.9: Schematic of interaction of dislocation line with precipitates (Ashby et al. 1992).

2.3.5 Dispersion hardening

The strength and hardness in metal and alloys may also be improved by the presence of extremely small and uniformly dispersed particles usually less than 0.1μm size within the soft matrix. These particles can hinder the dislocation motion and thus increase the strength of a material. These second phase particles can be added by mixing and consolidation or as precipitates in a solid state that has very little solubility in the matrix, even at higher temperatures. The size, shape, and amount of second phase particles control the strengthening of the alloy, for example hard fine particles of Al_2O_3 in soft ductile matrix of aluminium. Dislocations moving through the matrix can either cut through the precipitate particles or bend around and bypass them. When the precipitates are non-deformable or an abrupt change in orientation, it is very difficult for the dislocations to cut though the precipitate particles at even high applied stress. The moving dislocations bow to bypass instead of cutting through the precipitate particles. As the applied shear stress increases, the dislocation bows sufficiently and when a critical curvature is reached, the segments of the dislocation meet at the other side of the particle. The dislocation then moves forward leaving a dislocation loop around each particle. This is called Orowan mechanism (Orowan, 1948). Cutting of particles is easier for smaller particles which can be considered as segregated solute atoms. Figure 2.10 shows the Orwan mechanism of dispersion hardening.

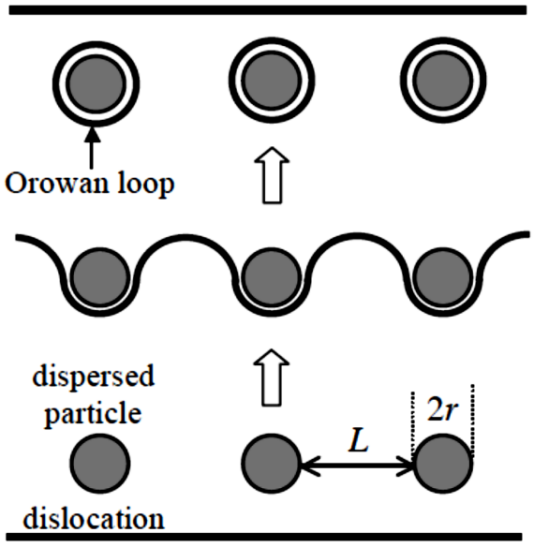

Figure 2.10: Schematic of Orwan mechanism for dispersion hardening (Orwan, 1948).

2.4 5xxx Series aluminium alloys

Magnesium is the principal alloying element in 5xxx series with moderate strength belongs to non heat treatable family of alloys. They posses good formability, better fatigue properties in higher temper conditions, resistance to marine atmosphere and salt water corrosion makes them an attractive material to be used in a various applications including home, marine, ground transportation, aircraft and cryogenic applications, but it is susceptible to corrosion above 60 °C. Some popular alloys of this series are listed in Table 2.1. Non-heat treatable aluminium alloys, especially the 5xxx series are strengthened primarily by solid solution strengthening with Mg, strain hardening through cold work, and also due to dispersion hardening by Al_6Mn precipitates.

As mentioned in the Table 2.1, impurities of iron and silicon are present (~0.5 wt % each) in low amounts. Iron is found in primary constituents as Al_3Fe, and in presence of Mn, mostly Fe is tied up in phases like $Al_6(MnFe)$. Minor additions of titanium (< 2 wt %) and chromium acts as a grain refiner. Manganese improves strength of the alloy, either in solid solution or as a finely precipitated inter-metallic phase. It also improves the corrosion properties by tying up the iron. Zinc content in high magnesium Al-Mg alloys reduces the electrochemical potential in the microstructure and thus enhances its resistance against stress corrosion cracking (SCC) by formation of a stable ternary Al-Mg-Zn phase. Addition of copper enhances the mechanical

properties, but reduces the hot ductility, corrosion resistance and the weldability. A small amount of Zr is also added for grain refinement, thus increases recrystallization temperature.

Table 2.1: Chemical compositions (wt %) of popular commercial 5xxx series alloys (balance Al)

Alloy Series	Mg	Mn	Cu	Si	Cr	Fe	Ti	Zn	Others
5005	0.5-1.1	0.20	0.20	0.30	0.10	0.70	-	0.25	0.15
5052	2.2-2.4	0.1	0.10	0.25	0.15-0.35	0.40	-	0.10	0.15
5083	4.0-4.9	0.4-1.0	0.10	0.40	0.05-0.25	0.40	0.15	0.25	0.15
5086	3.5-4.5	0.2-0.7	0.10	0.40	0.05-0.25	0.50	0.15	0.25	0.15
5154	3.1-3.9	0.10	0.10	0.25	0.15-0.35	0.40	0.20	0.20	0.15
5356	4.5-5.5	0.10	0.10	0.25	0.05-0.20	0.40	0.06- 0.20	0.10	0.15
5383	4.0- 5.2	0.7-1.0	0.20	0.25	0.20-0.25	0.25	0.12-0.15	0.40	0.15
5454	2.4-3.0	0.5-0.6	0.10	0.25	0.05-0.20	0.40	0.20	0.25	0.15
5456	4.7-5.5	0.5-1.0	0.10	0.25	0.05-0.20	0.40	0.20	0.25	0.15
5754	2.6-3.6	0.50	0.10	0.40	0.30	0.40	0.15	0.20	0.15

The stringent demand for lighter and stronger materials with high strength to weight ratio, toughness, fatigue and corrosion resistance, ease of fabrication and cost effectiveness, paves the way for the development of new metals or materials. The demand for improved strength along with excellent corrosion resistance of aluminium 5xxx series alloys is given due importance in naval applications. Aluminium manufacturer Pechiney marine group of France have registered the 5383 Al alloy and promoted it to shipbuilding industry as a better material over the 5083 Al alloy. 5383 Al alloy has ~ 15% higher welded strength, improved fatigue strength, as well as increased corrosion resistance than 5083 Al alloys.

2.4.1 The Al-Mg Phase diagram

Magnesium is the principal alloying element in the 5xxx series wrought aluminium alloys. Figure 2.11 shows that the maximum solubility of magnesium in aluminium is about 2 wt % at room temperature, and 17.4 wt % at 450 °C. Even though concentrations of up to 12-13 wt % Mg

can be found in cast Al-Mg alloys, wrought alloys containing beyond 3.5 wt % Mg are rarely used in the strain-hardened condition due to their high susceptibility for intergranular cracking and stress corrosion cracking, which overcomes its improvement in strength due to increasing magnesium content. This behaviour is attributed to Mg atoms which got precipitated as highly anodic β-phase (Mg_5Al_8 or Al_3Mg_2) particles, preferably distributed at grain boundaries and randomly distributed in structure, thus making them unsuitable for operating at temperatures above 65 °C. Therefore, an optimization between chemical composition and microstructure is prime requirement that has to be achieved during thermo mechanical treatments in order to have a better combination of mechanical properties and corrosion behaviour.

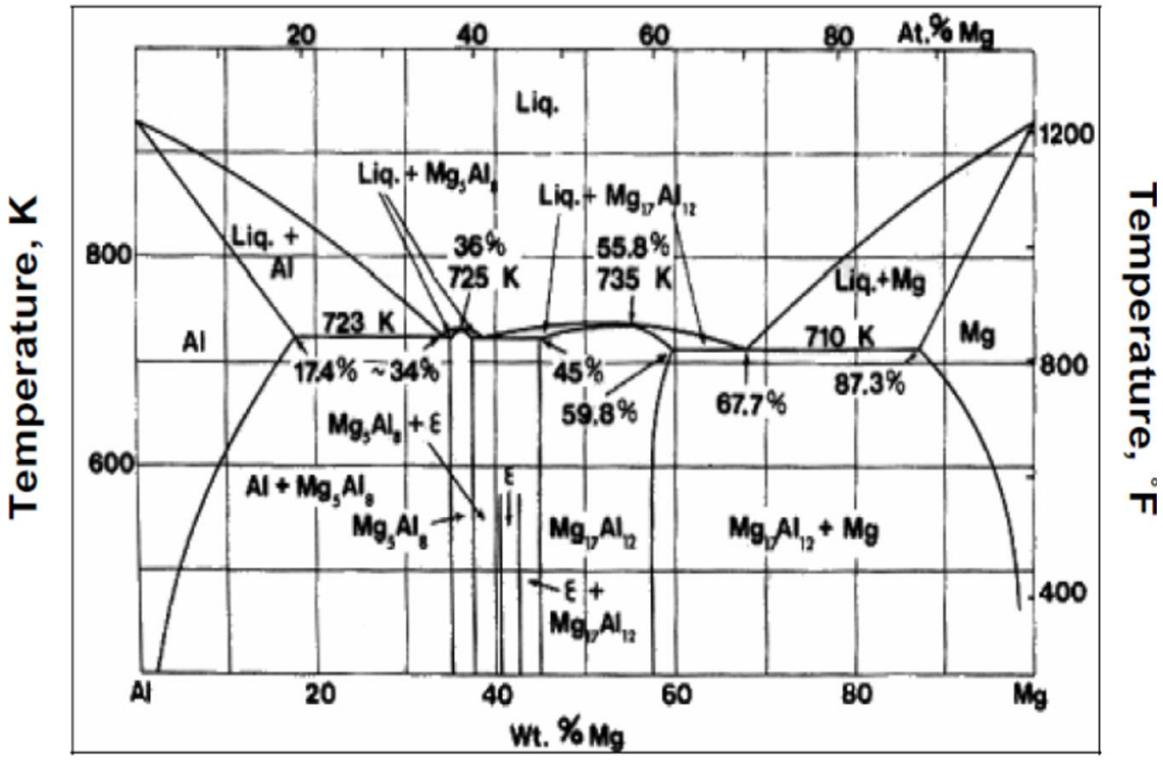

Figure 2.11: Schematic showing Al-Mg Phase diagram.

2.4.2. Intermetallic Particles in AA 5xxx (Polmear 1995, George E. Totten, 2003, Attalluah et al. 2007)

a. Constituents (Primary particle)

Constituent particles are formed when phase other than aluminium separates first during solidification, with size range 1-10 μm in wrought form (rolled sheets). Some of them are

Al(Fe,Mn)Si, Al_3Mg_2, Al_3Ti, Al_3Zr, Al_7Cr, Al_3Fe. These Iron–manganese rich particles cannot be redissolved during solution treatment or homogenization due to their low solubility and high melting point ~700 °C. It may be transformed from one phase to another, such as the transformation of $Al_6(Fe,Mn)$ to Al(Fe,Mn)Si, if sufficient silicon is present. Constituent particles that do not contain iron may be soluble depending on the solute content such as Al_2Cu, Al_2CuMg and Mg_2Si (having partial solubility) during homogenization. These particles are non coherent with the matrix, and do not interfere with the dislocation movement, but they impose deformed zones in surrounding, and may serve as sites for particle nucleated simulation during recrystallization.

b. Dispersoids (Secondary particles)

Smaller submicron particles (typically 0.05–0.5μm) that form during homogenization or solution treatment of the ingots by solid state precipitation of compounds containing elements, which have slow diffusivity and modest solubility with the matrix, such as chromium , manganese and zirconium. These dispersoids appear in various shapes like; plate, rod, rectangular or spherical and prevents or delays recrystallization through Zener drag, examples are $Al_{20}Mn_3Cu_2$, $Al_{12}Mg_2Cr$, Al_3Zr and $Al_6(Fe,Mn)$.

2.5 Ultrafine grained and Nanocrystalline materials

The unique structural and functional properties offered by ultrafine grained or nanocrystalline materials through severe plastic deformation have been active area of research among material scientists. The remarkable properties of high strength and ductility, toughness, creep, excellent fatigue life, electrical conductivity, enhanced diffusivity, high thermal expansion coefficient, and corrosion resistance makes them a potential material for various structural applications. Bridgman introduced SPD processing with combination of hydrostatic pressure and shear deformation (Bridgman, 1935). In 1981, Gleiter produced nanocrystalline powders using inert gas condensation and reported in situ consolidation of these nano powders. Later on, thousands of research papers and significant research articles have been published. Ultrafine grained (100-1000 nm) or nanocrystalline (< 100 nm) range materials contain very high density of grain boundaries, which may change their physical, mechanical, chemical, and functional properties of metals and alloys.

2.5.1 Synthesis of ultrafine grained / nanostructured materials

The market demand for exceptional material properties have led to a considerable interest in the development of ultrafine-grained/nanomaterials worldwide. There are two general approaches to produce bulk nanostructured/ultra-fine grain metallic materials. The first, "Top-down" is a subtractive approach from bulk starting material to make ufg/ns materials. "Bottom-Up" is an additive approach that involves precursor atoms or molecules to make nanomaterials. UFG materials obtained by both the approaches differ considerably in terms of dislocation density, grain boundaries, grain shape and size, the distribution elements, which in turn impart their mechanical properties. The schematic representation of building up of ultrafine grained and nano structured materials is shown in figure 2.12.

a. Top-down approach

In this approach, bulk starting material on application of strain / loading, through grain refinement, leads to formation of ultrafine/nanostructures. Typical examples are mechanical alloying through ball milling/cryomilling and consolidation of powder (Koch 1997, 2005, Dybiec 2007, Ullrich 2012), and severe plastic deformation techniques (SPD) (Valiev et al. 1991 and Horita et al. 1996). Aluminium alloys have received considerable attention and ultrafine grain microstructures in these alloys were developed through these techniques. SPD approach substantially requires large plastic strains for the development of homogeneous and equiaxed material with ultrafine and nano grain sizes.

b. Bottom up approach

In the "bottom-up" approach, the first step is synthesis of nano powders, which are then consolidated at some elevated temperature to form bulk nanostructured materials, such as electro deposition (Erb et al. 1995, Lu et al. 2005), spark plasma sintering (Tokita 1993), inert gas condensation (Gleiter, 1981 and 1989), crystallization from amorphous materials (Tong et al. 1992, Liu et al. 1993), chemical vapor deposition (Jaege et al. 2002, Choy 2003), etc. This gives rise to smaller grain sizes up to 100nm, used in electronic devices. This approach has some drawbacks of particle agglomeration, contamination and residual porosity.

TOP-DOWN approach

- Equal Channel angular pressing (ECAP)
- High pressure torsion (HPT)
- Accumulative roll bonding (ARB)
- Cyclic extrusion compression (CEC)
- Multipass coin forging (MCF)
- Repetitive Corrugation and Straightening (RCS)
- Conshearing Process
- Continuous confined strip shearing
- Multi-axial forging
- **Mechanical alloying/milling**
- **Cryorolling**

BOTTOM-UP approach

- Inert gas condensation (IGC)
- Electrodeposition
- Plasma synthesis
- Chemical vapor deposition
- Physical vapor deposition
- Rapid solidification
- Continuous confined strip shearing
- High temperature evaporation

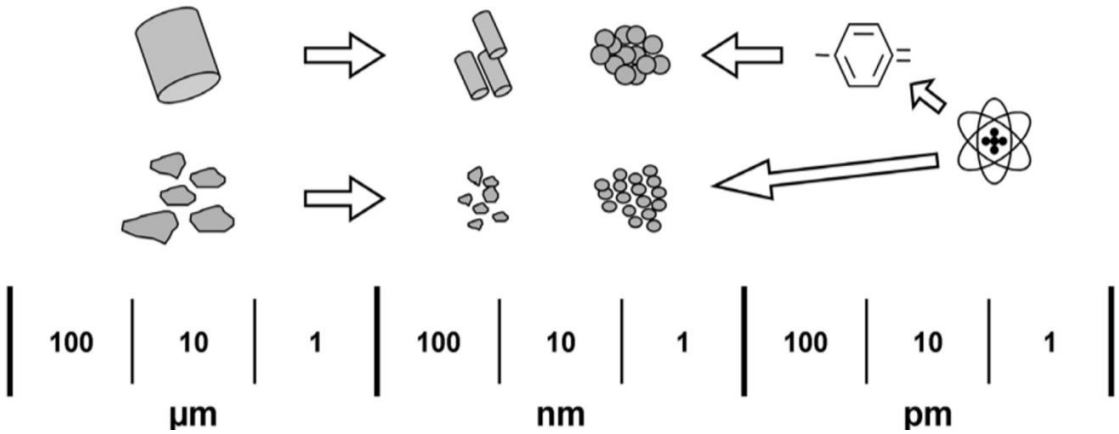

Figure 2.12: The schematic representation of building up of ultrafine grained and nanostructured materials.

2.5.2 Severe Plastic Deformation

Grain refinement through traditional thermo mechanical techniques (TMT) can produce material with 1-10 μm grain size. Cost for fabrication was very high due to specially designed processing routes associated with specific heat treatment processes. Therefore, the TMT methods were not effective for the production of bulk ultrafine grained materials. Severe plastic deformation (SPD) is a technique to obtain very fine grained structure in different metals and their alloys. Over a last decade, SPD techniques have been emerged and explored by many material scientists for the production of bulk ultrafine-grained (UFG) materials (Valiev et al. 1993, Valiev et al. 2000) with primary aim of grain refinement. The materials subjected to SPD induces very high plastic strains in the materials and produces micrometer and sub-micrometer (100- 1000 nm) size and nanometer (less than 100 nm) size grains in the initially coarse grain materials containing mainly high angle grain boundaries. Figure 2.13 shows grain refinement observed through different processing routes.

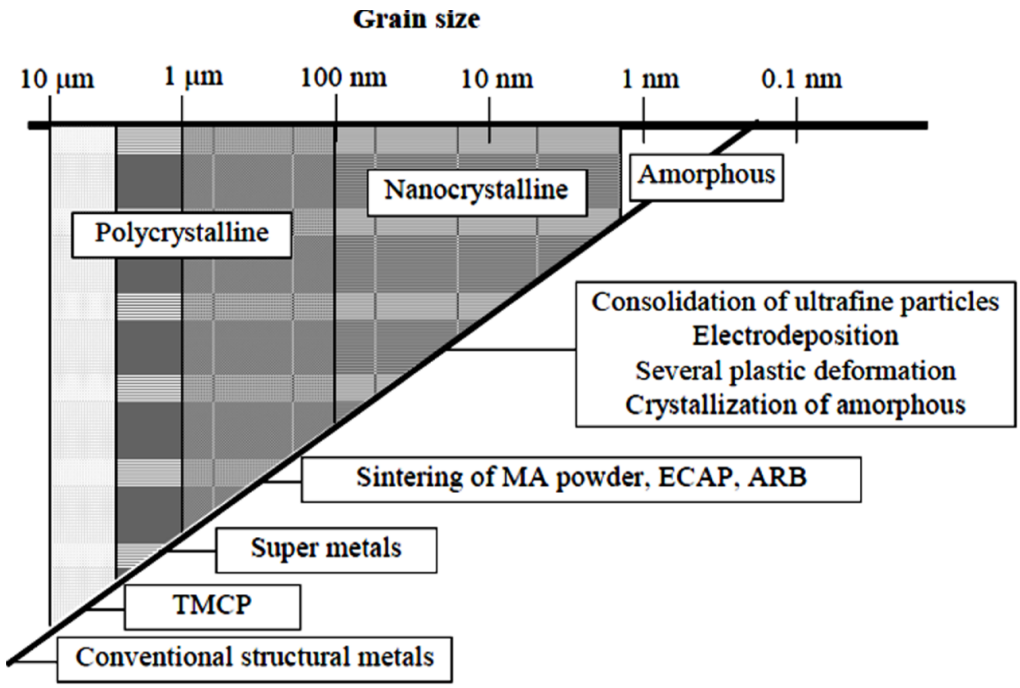

Figure 2.13: Schematic showing grain refinement observed through different processing routes.

These materials are 100% dense, free from contamination, and sufficiently large and found to have high strength, good ductility, superior super plasticity, low friction coefficient, higher wear resistance, and enhanced high cycle fatigue life (Zhu et al. 2004). Several SPD techniques are now

available for refinement of microstructure in order to achieve improved mechanical and functional properties. Several review articles on SPD are listed in Table 2.2.

Some of the SPD techniques are:

- Equal-channel angular pressing (ECAP, Segal et al. 1997, Azushima et al. 2000, Nishida et al. 2001, Suwas et al. 2005, Kim et al. 2005)
- High-pressure torsion (HPT, Bridgeman et al. 1935, Valiev et al. 1989, Zhilyaev et al. 2003)
- Accumulative roll-bonding (ARB, Saito et al. 1999, Chang et al. 2012)
- Repetitive corrugation and straightening (Huang et al. 2001 and Zhu et al. 2001, Krishnaiah et al. 2008)
- Multiaxial forging (MAF, Noda et al. 2005)
- Cyclic-extrusion/compression (CEC, Richert et. al 1986)
- Severe torsion straining (STS, Nakamura et al. 2004)
- Super short multi-pass rolling (SSMR, Kawano et at. 2005)

Other popular techniques of grain refinement in aluminium alloys are:

- Friction stir processing (FSP, Mishra et al. 2005)
- Cryorolling (Wang et al. 2002)

Table 2.2: Review of articles on severe plastic deformation (SPD) techniques.

Author Name, Year	**Journal Name**	**Title**
Valiev et al. 2000	Progress in Materials Science	Bulk nanostructured materials from severe plastic deformation.
Verlinden et al. 2002	Metalurgija - Journal of Metallurgy	Severe plastic deformation of metals.
Valiev et al. 2004	Nature Materials	Nanostructuring of metals by severe plastic deformation for advanced properties.
Valiev et al. 2006	Nanostructured Materials	Producing bulk ultrafine grained materials by severe plastic deformation.
Zernik et al. 2008	Metalurgija	Processing of metals by severe plastic deformation (SPD)- Structure and mechanical

		properties
Azushima et al. 2008	CIRP Annals - Manufacturing Technology	Severe plastic deformation (SPD) processes for metals.
Wang et al. 2010	Material Science Forum	Nanomaterials by Severe Plastic Deformation: NanoSPD5.
Wang et al. 2012	Science China Technological Sciences	Review on modified and novel techniques of severe plastic deformation.

The conventional equal channel angular pressing (ECAP) was invented by Segal et al. (1997). A shear strain is induced when the billet is passed through the two parts of the channel through a piston without corresponding change in dimensions of the sample. The pressings may be repeated to achieve exceptionally high strains. There are four different processing routes; the sample is pressed without rotation (route A). The sample is rotated by 90° in alternate directions during consecutive passes (route B_A). The sample is rotated by 90° either in clockwise or counterclockwise direction between each pass (route B_C). The sample is rotated by 180° between passes (route B_C). This has become most frequently used due to its low load requirement (with small press) and simple tool geometry resulting low tool pressure to develop microstructure and strength in material at applied strain (Park et al. 2005, Chatterjee et al. 2012). Figure 2.14 shows the schematic of various ECAP techniques.

Later on, ECAP was modified by various research groups; Lee et al. (2003) have developed modified equal channel angular rolling (ECAR), the process is represented schematically in Figure 2.14b. The strip is fed between rolls and extruded to reduce the strip thickness. The work piece is driven forward by frictional forces on the three contact interfaces with the groove and constrained to the groove by the stationary constraint die. This restricts the work piece and forces it to turn by shear deformation likewise the ECAP process.

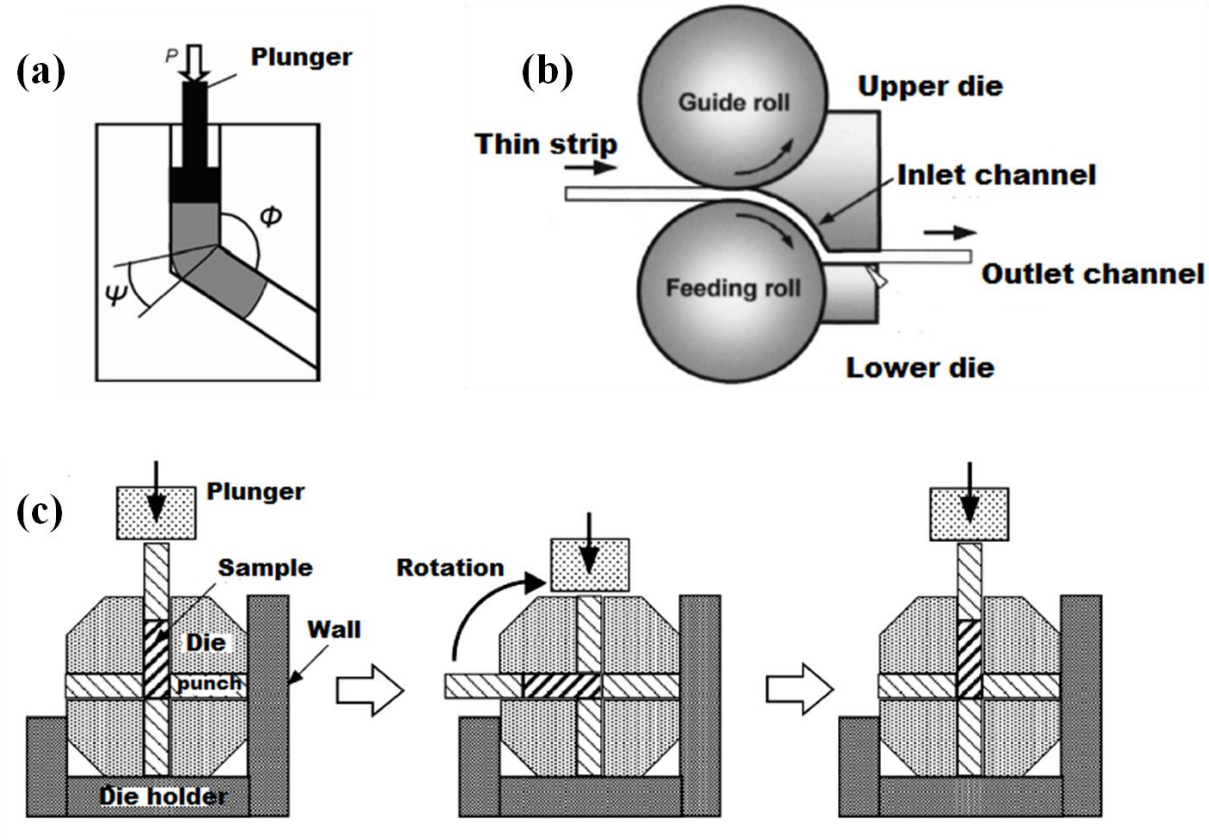

Figure 2.14: Schematic of equal channel angular processing (ECAP); (a) Conventional ECAP, (b) Conventional Equal channel angular rolling (ECAR), (c) Rotary die ECAP.

Nishida et al. (2000) developed a rotary-die ECAP shown in Figure 2.14c, which consists of two channels having the same cross-sections intersecting at the center with a right angle in order to remove the limitation of conventional ECAP. At first, the sample is inserted into the die consisting of plunger, and after pressing the sample, the die is rotated by 90°, and the sample is reinserted again.

Accumulative roll bonding (ARB) was developed by Saito et al. (1998), shown in figure 2.15a, where the two sheets to be roll bonded were cleaned by acetone and wire-brushed by steel wire, the sheets were then stacked together to form a thick sheet. The two stacked sheets are rolled to 50% of their initial thickness, and then cut into two halves, cleaned thoroughly with wire brushing, stacked together, and rolled again. This sequence is continued for several times till to achieve desired strain. The strength of the ARB processed material critically depends on the quality of the bond, which may be difficult to achieve. The process may be performed at room temperature or at some elevated temperature. Several researchers have shown that the process may

be repeated several times, if some precautions like removing the edge cracks are taken into account. UFG materials produced through ARB exhibit high strength and ductility (Toroghinejad et al. 2013). Nowadays, this technique is being used to develop composite materials with aim to have qualities of both the material (Lee et al. 2011, Liu et al. 2012).

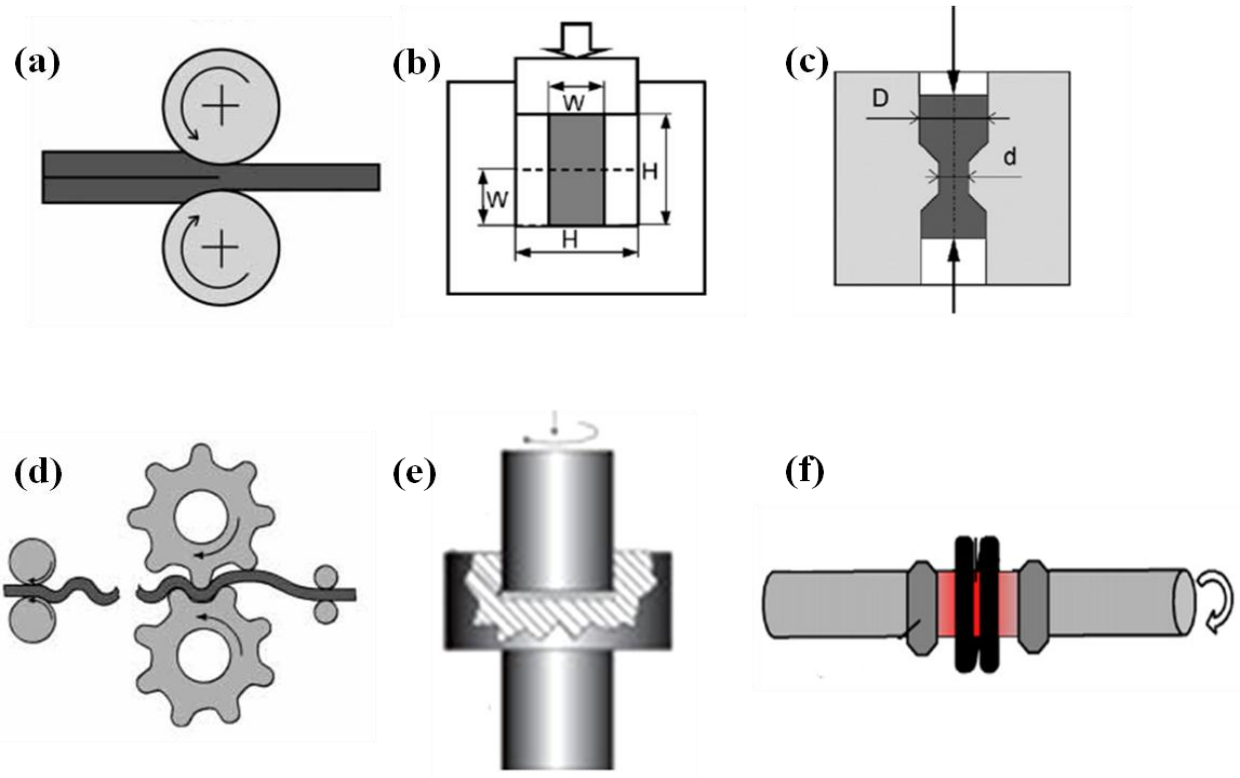

Figure 2.15: Schematic representation of few common SPD processes; (a) ARB, (b) MAF, (c) CEC, (d) RCS, (e) HPT, (f) STS.

Multiaxial forging (MAF) was initially developed by Noda et al. (2005), where the samples were cut to cubic shape generally prepared in ratio of 1.5:1.22:1.0, as shown in Figure 2.15b. Strains were applied to the test materials alternately in three directions by rotating the test materials by 90° after each pass up to a required true strain. Working temperature and deformation rates influences the microstructural evolution and mechanical properties of MAFed material. Severe strain induced in material resulted in increasing the active slip systems and the deformation bands, high-misorientation grain boundaries (94.8%), and ultrafine grains with a grain diameter of 0.8 μm were formed (Noda et al. 2005). Therefore, the MAF technique is an effective working method for producing ultrafine grains in the bulk materials.

Cyclic extrusion compression (CEC) is well known process to produce UFG materials developed by Richert et al. (1986), and represented schematically in Figure 2.15c. The enough counter-pressure is given to the samples to cause plastic deformation by alternating extrusion and compression by moving the workpiece cyclically between the two die chambers to accumulate desired plastic strain. The accumulated equivalent strain is approximately given by;

$$\varepsilon = 4\,n\ln(\frac{D}{d}) \tag{2.4}$$

Where; 'D' is the chamber diameter, 'd' is the channel diameter and 'n' the number of deformation cycles. A high hydrostatic pressure is imposed due to cyclic extrusion and compression, resulting in higher loads, which require special tooling. This process is most suited for processing of soft material such as aluminium alloys.

The principle of the repetitive corrugation and straightening (RCS) process was developed by Huang et al. (2001), and represented schematically in Figure 2.15d. The technique consists of repetitively bending and straightening of a billet with corrugated tools and then straightening the billet with flat tools without changing the cross-sectional area of the billet imposing high strain into the material. The equivalent strain per one sequence is given by;

$$\varepsilon = 4\ln\frac{[(r+t)/(r+0.5t)]}{\sqrt{3}} \tag{2.5}$$

Where,'t' is the thickness of sample and 'r' is the curvature of bent zone. By repeating this process in a cyclic manner, severe plastic strain can be introduced in to the work piece, which results in grain refinement.

The high pressure torsion (HPT) process was first investigated by Bridgman et al. (1935). Later on, Erb et al. (1993) reported the evolution of grain structure towards the structure of dislocation free subgrains with high angles of misorientation and submicrometer size. A small ring type sample with conical faces, whose virtual extensions met at the axis of the apparatus, is pressed between anvils and under hydrostatic pressure as shown in Figure 2.15e. The sample is pressed between anvil and burrs are formed at the edges. Then, one anvil is rotated with respect to another one and the speed of rotation is varied over a large range. The deformation of the sample takes place through simple shear. The high pressure suppresses the formation of cracks and therefore, it is possible to apply extremely high strain without failure of the deformed sample, and very fine grains of the order of nanometer range (100 nm) may be produced. The major drawback of this

process is that, it process the specimens in the form of relatively small discs, therefore, it is not applicable for bulk material.

The principle of the severe torsion straining (STS) process was developed by Nakamura et al. (2004), is represented schematically in Figure 2.15f. A locally heated zone is produced and tensile strain is created in the zone by rotating one end with respect to the other. The rod is moved along the longitudinal axis of apparatus creating the local strain. Therefore, a severe plastic strain can be induced continuously throughout the rod. To produce efficient STS, the locally heated zone should be narrow and rod should be rotated faster with respect to its moving speed. A modification can be made for the cooling system so that the heated zone is more localized to create torsion strain. The severe torsional straining (STS) process can be used for consolidation of powders to produce metal-ceramic and nano-composites having high density, and to produce ultrafine grain size and high strength materials.

All of the above explained procedures can introduce large plastic strain into the material leading to significant refinement in microstructural of bulk crystalline solids. Some of them are well established and being used by different research groups to fabricate bulk nanostructured or ultrafine grain samples of different materials, while others are under development stage and not fully commercialized for large-scale industrial applications due to their limited production rates.

2.6 Cryorolling

The major drawback of SPD processes is that, a large amount of plastic strain has to be imposed on material for formation of ufg/ nanocrystalline metals. The drawback of SPD is that, it requires severe plastic strain, production of relatively small quantities of material, expensive tooling, design difficulties, and cost associated makes it difficult to be used at industrial scale for bulk production. Therefore, in order to obviate the mentioned drawbacks, Wang et al. (2002) had proposed an alternative method of rolling at liquid nitrogen temperature (-196 °C) and called this procedure as cryorolling (CR). He developed grains in nanocrystalline to ultrafine range (<300 nm) with high yield strength and low tensile ductility by deforming copper to about 93% reduction through cryorolling. He has also reported that after annealing, a remarkable increment in uniform elongation was found with strain hardening, without giving up the strength, in material with the bimodal grain size microstructure. Since then, the CR has got significant research importance and an extensive work has been reported on mechanical behaviour and development

of ultrafine grained material with less than 1μm grain size in pure metals and their alloys like copper (Kauffmann et al. 2011, Raju et al. 2013), aluminium (Panigrahi et al. 2008, 2009, Kumar et al. 2009, Rao et al. 2010, 2012, Gopal Krishna et al. 2012, 2012, Sarma et al. 2008, Taylor et al. 2012), nickel (Lee et al. 2005, Zhao et al. 2008), titanium (Fomenko et al 2010, Yang et al. 2010), zirconium (Defeng et al. 2012), and vanadium (Chun et al. 2009) and brass (Das et al. 2011).

Cryorolling is a conventional rolling of the materials at low temperature that needs comparatively much lower loads to induce severe strains as compared to SPD techniques, and refines their grains to submicrometer level or ultrafine grained level. Samples subjected to rolling are dipped into liquid nitrogen (-196 °C) for initial pass till it attains uniform temperature and then rolled and dipped immediately for successive passes. The process is repeated continuously till required strain is achieved. Due to rolling at liquid nitrogen temperature, the dynamic recovery is suppressed in the material and the strain is retained in the up to the extent to which rolling is carried out. This is associated with cross slip and climb of dislocation, thereby increasing dislocation density generated into material. Therefore, cryorolling process increases the hardness and yield strength of materials with decrease in ductility of materials. Post process annealing treatment of CR material provides a good combination of strength and ductility. Therefore, CR has been identified as a potential route to develop UFG material as reported in literature. Recently, asymmetric rolling (Hailiang et al, 2012) and cryorolling followed by warm rolling (Kang et al. 2010, Rao et al. 2012) has also been reported to fabricate bulk nanostructure or ultrafine grained structure in aluminium alloys. An extensive literature related to the strength, ductility and microstructural studies of the cryorolled materials upto year 2006 has been reported in Ph.D. dissertation (Panigrahi et. al. 2009). So, literature related to cryorolling of Al alloys is discussed in detail from year 2006 onwards.

Lee et al. (2004) have reported that cryorolling followed by subsequent annealing develops duplex microstructure consisting of equiaxed grains with an average grain size of 200 nm in 5083 Al alloy with improved strength and enhanced ductility, at least 10% more than room temperature rolled material. Annealing above 300 ^{o}C leads to coarsen recrystallized grains, which has little influence on hardness.

Panigrahi et al. (2008, 2010, 2010) have investigated 6063 Al alloy subjected to cryorolling at different strains and observed the formation of recrystallized ultrafine grains structure with the high angle grain boundaries at the strain value of 3.8. He also reported evolution of precipitates,

during annealing of cryorolled 6063 Al alloy that follows a sequence; the formation of GP zones (spherical), β'' phase (needle), β' phase (rod), and stable β phase (plate) shaped morphology after annealing in temperature range of 150 - 250 °C for 1 hr respectively. The DSC analysis of cryorolled 6063 Al alloy obtained at different heating rate was used to evaluate activation energies using Kissinger analysis for the evolution of precipitates. The reduced activation energy was observed for the formation and dissolution of precipitates in cryorolled Al 6063 alloy as compared to solution treated and water quenched condition. This may be attributed to an excess free energy associated with higher volume fraction of low angle grain boundaries in Al 6063 alloy, that promotes precipitation kinetics by providing high diffusion path due to precipitation growth and reducing activation energy of precipitates by providing enhancement in nucleation sites.

Panigrahi et al. (2010, 2011) have shown combined treatment of solution treatment on the 6063 Al alloy to dissolve the second-phase particles, cryorolling (CR) produces a high density of dislocations, short annealing (SA) treatment recrystallizes partially the microstructure without affecting the age-hardening effect. Finally aging treatment was given to generate highly dispersed nano precipitates. CR samples with optimum SA and PA treatment (155 °C for 5 min and 125 °C for 12 hr) shows the enhancement in yield strength (240 MPa to 265 MPa), UTS (248 MPa to 286 MPa), and ductility (5 to 14) than the CR materials.

Gang et al. (2009) have observed that combined treatment of cryogenic-rolling with warm rolling (175 °C) was found more effective than a single cryogenic-rolling alone in 5052 Al alloy and remarkable increment in ultimate tensile strength (452 MPa) observed was attributed to the formation of fine precipitates during warm-rolling. Enhanced ductility observed after annealing at 175 °C for 48 hr was attributed to the formation of fine equiaxed grains (100-200 nm) as well as the reduction in dislocation density.

Rao et al. (2009, 2012) have studied the effect of annealing and ageing on strength and ductility of UFG Al 6061 alloy, and reported that short annealing before ageing has significant effect on improvement in ductility without decreasing strength. Later, they reported microstructural evolution in 6061 with combined effect of cryorolling followed by warm rolling performed at 145 °C. Significant improvement in strength (376 MPa) and partial improvement in ductility (5%) was observed in cryorolled followed by warm rolled sample as compared to CR samples alone. Further enhancement in UTS (406 MPa) and ductility (7.9%) of cryorolling

followed by warm rolling followed by peak ageing sample was reported on ageing at 125 °C for 45 hr.

Sarma V.S. et al. (2010) have compared the effectiveness of the cryogenic rolling (CR) with room temperature rolling (RT) of materials with different stacking fault energies (SFE) and reported that there is an optimum SFE at which CR rolling is more effective. They reported that high SFE metals and low SFE metals were deformed by dislocation slip and twinning, respectively, during CR and RT rolling. Metals with intermediate SFEs deformed by twinning, during CR rolling but by dislocation slip during RT rolling. CR rolling is the most effective route over RT rolling in improving the strength.

Jayaganthan et al. (2010) have reported the microstructural and texure evolution in cryorolled 7075 Al alloy, and observed that ideal fibers observed in the starting solution treated alloy has been destructed during cryorolling. The increase in thickness reduction weakens all the texture components, and there is shift in Goss/Brass orientation of the cryorolled Al alloy towards the Brass components. This weakening in texture components with thickness reduction (induced strain) alleviates the fragmentation and reorientation of grains to form subgrains and ultrafine grained microstructures in the cryorolled samples confirmed with the EBSD and HRTEM micrographs.

Malekjani et al. (2011) have investigated cyclic fatigue and electron microscopy of cryo-rolled 2024 aluminium alloy. Cryorolled 2024 Al alloy was cyclically deformed under fully reversed total strain control (R= -1) in the plastic strain amplitude, strain range $8x10^{-4}$ to 1×10^{-2}. It revealed the beneficial effect of the presence of precipitates on the microstructure and the cyclic stability. Artificial ageing of cryorolled 2024 Al alloy was found to be ineffective in terms of improving fatigue life.

Taylor et al. (2012) have processed pure aluminium through cryorolling followed by annealing. FLD (forming limit diagram) measurement has shown that although the strain to failure in uniaxial tension is poor, strain in biaxial stretching was relatively good, having forming limit strain >20%. They have demonstrated that fine grained material exhibits poor formability in tension less than 5%, but in biaxial deformation, it has shown sufficient formability.

The literature reported above is mainly concentrated on the cryorolling of pure aluminium or precipitation hardenable alloys. Lee et al. (2004) and Kang et al. (2009) have reported formation

of ultrafine grained material on cryorolling of non-heat treatable aluminium alloys. The present research work is focused to develop ultrafine grained (UFG) microstructure in bulk 5083 Al alloy sheets for high strength structural applications through grain refinement. The microstructural characteristics, mechanical properties, high cycle fatigue behaviour and corrosion behaviour of Al alloys processed through cryorolling were investigated.

2.6.1 Mechanical properties of cryorolled materials

Deformation at cryogenic temperature has gained significant importance to develop UFG material with high density of dislocation at lower strain values for realizing the improved mechanical properties. Recently cryo-ECAP (Chatterjee et al. 2012), cryo- forging (Wu et al. 2013), cryo-HPT (Konkova et al. 2012), cryogenic channel die compression (Kim et al. 2011) were adopted to develop ultrafine aluminium alloys. Deformation at cryogenic temperature (cryorolling) suppresses dynamic recovery, which leads to accumulation of high dislocation density. This preservation of high density of defects acts as a potential recrystallization sites during annealing. Cryorolling followed with ageing treatments has been observed to improve strength and ductility in the heat treatable aluminium alloys as discussed above. Table 2.3, shows review on mechanical properties of different alloys processed through cryorolling.

Table 2.3: Review of the mechanical properties of cryorolled materials; the upward arrow marks (↑) indicates increase and the downward arrow mark (↓) indicates the decrease in the properties.

Author, Year	**Alloy**	**Microstructure**	**Key results**
Panigrahi et al. 2008, 2010	Al 6063 alloy,	Ultrafine grained material with nano sized precipitates	Strength ↑, Ductility ↑ after ageing
Sarma et al. 2008	Cu-Zn and Cu-Al alloys	Ultrafine grained microstructures with very fine annealing twins	Young's modulus ↑
Panigrahi et al. 2009	Al 7075 alloy	Ultrafine grained material with fine precipitates	Strength ↑, Ductility ↑ after ageing
Kumar et al. 2009	Al- 4Cu-5TiB2 in situ composite	Fine grained structure	Hardness ↑, Wear resistance ↑
Gang et al. 2009, 2010	Al 5052 alloy	Ultrafine grained material with fine precipitates	Ductility ↑, Strength↑ after CR +WR

Yang et al. 2010	Pure Zirconium	Multi modal grain structure (nano scale and ultrafine graines)	Ductility ↑, Strength↑
Niranjani et al. 2011	Al 6061 alloy	Ultrafine grained material	Strength ↓, ductility ↓ less than RTR
Das et al. 2011	α-Brass	Microscopic shear bands, forms primary and secondary twins	Hardness ↑
Rao et al. 2012, 2012	Al 6061 alloy	Ultrafine grained material with very fine precipitates	Ductility ↑, Strength↑ after ageing, CR+WR
Malekjani et al. 2011	Al 2024 alloy	Ultrafine grained material	Low cycle fatigue life ↓
Das et al. 2011, 2011	7075 Al alloy	Ultrafine grained material	Impact strength ↑ High cycle fatigue life↑ Fracture toughness ↑
Fomenko et al. 2010	Titanium	Nanocrystalline and coarse-grain	Microhardness ↑
Hailiang et al. 2012	Pure aluminium	Nanostructures.	Ductility ↑, Strength↑

Grain size refinement to submicrometer or nanometer level is regarded as key factor in order to obtain extreme mechanical properties of polycrystalline metals. A significant research work has been reported on the microstructural evolution and mechanical behaviour of ultrafine grained precipitation hardenable aluminium alloys processed through different SPD techniques, especially cryorolling due to response of the precipitation to different thermal treatments. The literature is very scarce on the mechanical properties of the ultrafine grained non-precipitation hardenable Al alloys, where strengthening is achieved mainly due to solid solution strengthening and work hardening. Presence of magnesium in alloy promotes work hardening by lowering the stacking fault energy, thus reduces the propensity for dynamic recovery.

During the last decade, the growth of non-heat treatable (5083 Al) alloys has been most dramatic in the transportation sector (automobile, ship, aerospace) with the volume of sheet and foil produced nearly double to more than 600,000 tons (Sanders et al. 2004). Therefore, it is required to

investigate the influence of microstructural features on mechanical properties, and on corrosion behaviour of the ultrafine grained Al alloys processed through cryorolling.

2.7 Mechanical properties of aluminium alloys processed through different techniques

Strength of polycrystalline material is improved by grain size reduction with solid solution hardening or precipitation hardening. The dependence of yield strength on grain size can be well understood with Hall-Petch relation (Hall 1951, Petch 1953), which leads to lower ductility. Substantial increase in strength and ductility after optimizing annealing treatments is reported repeatedly, is however tricky and challenging task. The fraction of grain boundary increases with reduction in grain size, therefore, the mode of deformation transfers to grain boundary dominated mode in fine grains as compared to grain size mode in coarse grains. Fatigue resistance and toughness are properties governed by strength and ductility. Various strategies have been developed to enhance the ductility in Al alloys are; i) Increasing work hardening rate or strain rate sensitivity (Miyamoto et al. 2006, Valiev et al. 2010), ii) developing bi-modal microstructure in 5083 Al alloys (Han et al. 2006, Witkin at el. 2006), iii) fine distribution of nano second phase precipitates to trap and accumulate dislocations, resulted in increased strain hardening rate and enhanced ductility in Al 7075 alloy (Zhao et at. 2001), iv) addition of Zn content in solid solution (solute enhanced ductility) increase work hardening that increases ductility in FSP processed Al alloys (Hu et al. 2009).

Creep resistance in 99.9% pure Al alloy processed by ECAP is improved by grain refinement (Sclenicka et al. 2013), this may be attributed to homogenization of microstructure, microtexture and nanoporosity during ECAP passes, which shows that intergranular process including dislocation glide and climb of dislocation, controls the deformation rate. Estrin et al. (2004), reported diffusion controlled creep in nanocrystalline materials on concurrent grain growth.

Superplasticity in ultrafine grained aluminium alloys is demonstrated at higher strain rates (10^{-2} to 10^{0} s^{-1}) and lower temperature (200-350 °C) (Kaibyshev et al. 2001, Ma et al. 2005). It is very attractive due to its lower power consumption, increased life of dies and better forming properties up to 1000% elongation due to grain boundary sliding when ultrafine grains move over another during application of load. Superplastic forming of UFG alloys alloys is the potential route for developing structural components in aeroplanes, automobiles and ships. Increase in high angle

grain structure is critical parameter to achieve notable superplasticity due to activation or grain boundary sliding (Nieh et al. 1997). Lee et al. (2007) have observed that addition of Zr to 5083 Al alloy enhanced the high strain rate superplasticity, caused by the fineness and the coherency of Zr-rich dispersoids in the matrix.

Cyclic properties of ultrafine grained material are widely reported in last few years, UFG materials possess high strength compared to its coarse-grained counterpart with limited ductility, therefore, the high cycle fatigue life of UFG metal is more, and the low-cycle fatigue life is less (Maghurabi et al. 2004, Chung et al. 2002). UFG Al-7.5 Mg alloys (Hanlon et al. 2003) developed through cryomilling have shown high resistance to stress controlled fatigue compared to conventional microcrystalline material.

UFG materials also possess superior properties other than explained above like improved corrosion resistance, enhanced electrical conductivity, wear characteristics, higher specific heat, enhanced thermal coefficient, superior magnetic properties (Meyers et at. 2006). Varying chemical composition and modifying SPD process parameter may provide microstructural property correlation, which gives flexibility in properties to design engineers for various functional applications.

2.8 Corrosion of aluminium and alloys

Aluminium is an active metal with a corrosion potential of -1.66 mV vs. SCE (Vargel et al. 2004). It is anodic to other structural materials, therefore, used as a sacrificial anode to protect less active materials against corrosion (Xu et al. 2010). Aluminium and its alloys forms a protective oxide film on the surface (Al_2O_3) which shows good resistance to corrosion in neutral solutions, the atmospheric environment and some acidic solutions.

$$4\ Al + 3\ O_2 \rightarrow 2\ Al_2O_3 \tag{2.6}$$

$$2Al(s) + 3H_2O\ (l) \rightarrow Al_2O_{3(s)} + 6H^+_{(aq)} + 6e^- \tag{2.7}$$

The thickness of the oxide film formed in air and aqueous solutions at room temperature is 2-3 nm and increases with oxidation at temperatures below 425˚C to 20 nm (Shimizu et al. 1991). This is self-repaired when scratched or damaged. On anodizing, the thickness can reach upto 10-20 μm (Polmear et al. 2006).In aqueous solutions with pH value of 4.0 to 9, the oxide film shows low dissolution rate. It dissolves in solution with low pH value of less than 4 and, high alkalinity solutions of pH higher than 9. In solution of acidic and high alkalinity, the aluminium oxide film is

attacked more uniformly, and the corrosion type is general corrosion. However, in neutral solutions, the oxide film is attacked locally due to increased alkalinity in surrounding to the intermetallic particles and the impurities in the alloy. This exposes the aluminium substrate and speeds up its attack, resulting in loss of bond between the aluminium matrix and the intermetallic particles, which leads to formation of localized corrosion, and corrosion type is pitting corrosion. The susceptibility of the aluminium and its alloys to pitting corrosion increases with raise in concentration of chloride and oxygen, pH value, flow rate of the environment, impurities and grain boundary segregation, presence of second phase precipitates, and the effect of stresses (Carrol et al. 1991, Ghali et al. 2010).

2.9 Problem formulation

Based on the literature review, it can be concluded that aluminium alloys due to its unique mechanical properties and corrosion resistance makes it an ideal material for various structural applications. The brief summary of the literature is given below to identify the gap and for the formulation of a research problem in the present work.

- The worldwide demand for Al based alloys is ever increasing due to its extensive use in various engineering applications after steel such as, automotive, aerospace, marine industry and products that are part of our daily lives. Therefore, emphasis on materials with high strength to weight ratio for better design of complex shaped products, fuel economy, and cost effectiveness is ever growing to develop ultrafine grained aluminium alloys with improved mechanical properties.

- The largest usage of aluminium alloys is in the form of flat rolled products. Development of rolling technologies for production of high performance sheets at industrial scale, with combination of high strength and high formability, which is still a challenging task.

- Improvement in properties can be achieved either by controlling chemical composition and modifying processing techniques. In the race for better materials based on grain size alteration, several SPD techniques gained popularity in last two decades.

- Non-heat treatable aluminium alloys are strengthened by cold working and solid solution strengthening containing Mg, Mn, and Cr as alloying elements. Theoretical understanding

of different mechanisms has been established. 5083 Al alloy is popular for ship building, automobile and aerospace industries.

- The presence of intermetallic particles in matrix has a significant influence on microstructural refinement during deformation, which consequently improves the mechanical properties. Post process annealing results in good combination of strength and ductility.
- Cryorolling (CR) has been used popularly to produce UFG structure in aluminium alloys. Ultrafine grained materials produced through CR have shown good combination of yield strength and ductility, after thermal treatments.
- New advancements in cryorolling through combined effect of cryorolling followed by warm rolling and asymmetric cryorolling have also been made to produce ultrafine grained aluminium alloys.

The following key objectives are identified for current dissertation work based on the extensive literature review.

- Production of ultrafine grained microstructure in 5083 Al alloy through cryorolling and give an insight into microstructural evolution and their effect on mechanical behaviour such as tensile properties, hardness. Effect of short annealing on development of ultrafine grained materials is also investigated.
- To observe the energy absorption capability of fine grained materials after cryorolling to different strains and post annealing treatments on energy absorption capability of deformed materials and their comparison through Charpy impact test.
- Investigation of the effect of deformation temperature on microstructural and mechanical properties, and effect of second phase particles on pinning the dislocation movement, along with the effect of precipitation, if any during cryorolling followed by warm rolling.
- Characterization of the microstructural features of ultrafine grained aluminium alloys produced by cryorolling, and cryorolling followed by warm rolling, and to substantiate their influence on mechanical properties through techniques such as optical microscopy, FE-SEM, TEM, EBSD, DSC, and identification of the formation of different phases in the system by X-ray diffraction.

- To investigate high cycle fatigue properties of ultrafine grained 5083 Al alloy by processed by cryorolling and cryorolling followed by warm rolling.
- To investigate the resistance to corrosion behaviour of ultra fine grained 5083 Al alloy exposed to aggressive salt environment using electrochemical technique, salt immersion test and nitric acid mass loss test.

In order to achieve the objectives of the present work, the plan of the proposed work is schematically presented in Figure 2.16.

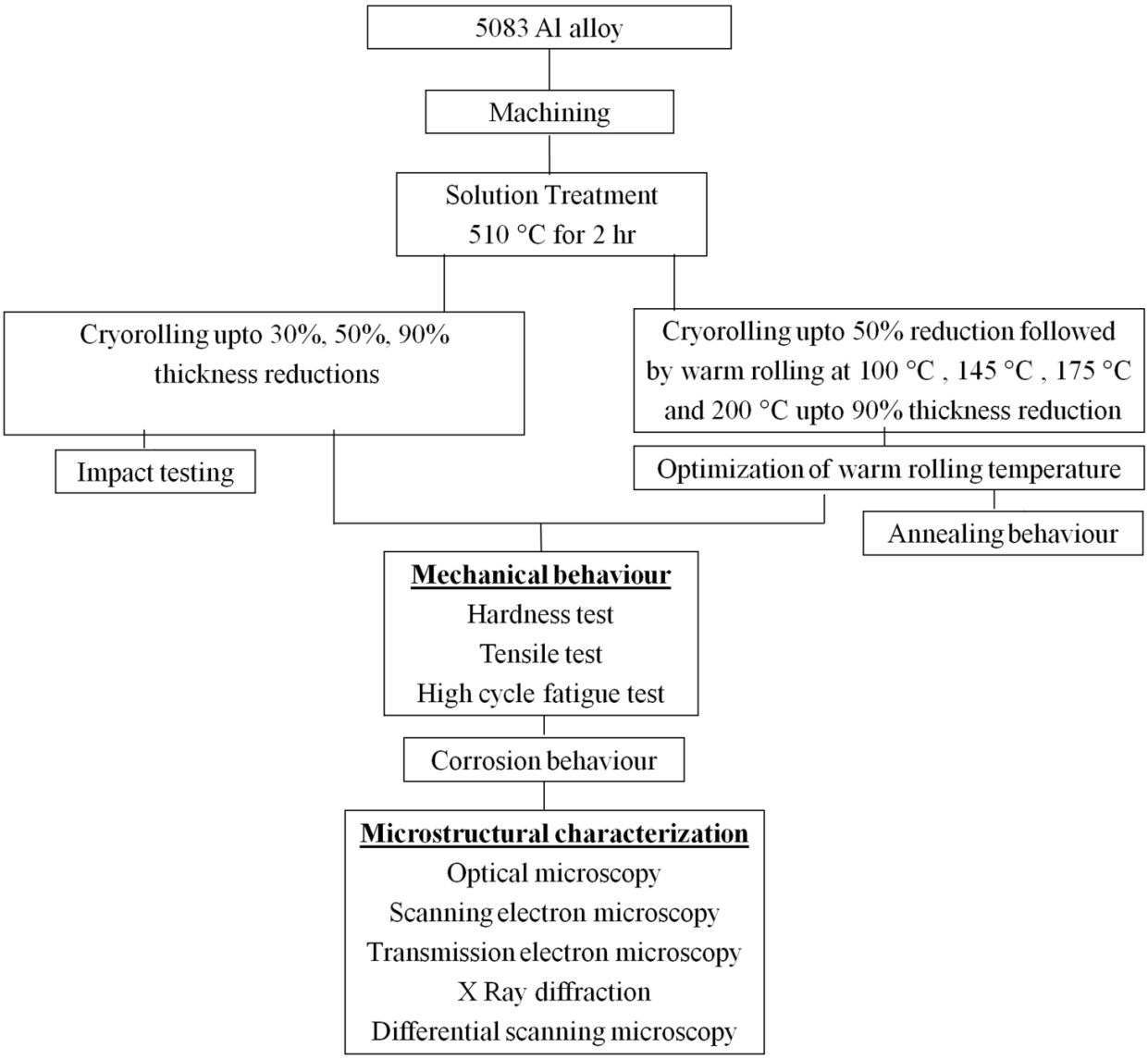

Figure 2.16: Proposed research plan.

.

CHAPTER 3
Experimental Details: Material and Methods

In this chapter, the selection of materials, various experimental techniques employed to process the material for grain refinement, their characterization techniques, and mechanical testing used in dissertation work are discussed.

3.1 Material Selection

Commercially available Al-Mg (5083 Al alloy) plate of 16 mm thickness with chemical composition as shown in Table 3.1 has been taken as a initial material for the present work. The samples were cut from the as received (AR) plate, solution treated (ST) at 510 °C for 2 hr and then quenched in water at room temperature. The samples after ST are free from defects and resulted in homogenized structure with approximately 85 μm grain size. The sample dimensions depend upon process as described below.

- For cryorolling (CR), samples with dimension of 40 × 30 × 10 mm^3 were used; the length may vary depending upon percentage of thickness reduction given to sample. These plates were deformed at liquid nitrogen temperature (CR) upto 30%, 50%, and 90% thickness reductions with equivalent true strain of 0.35, 0.69 and 2.3, respectively.
- For cryorolling followed by warm rolling (WR), samples are initially cryorolled upto (50% reduction) followed by warm rolling at 175 ^oC up to 90% thickness reduction was performed with same sample dimensions as used for CR.
- For impact testing of CR conditions, samples with 90 × 60 × 16 mm^3 were used and given 30% and 50% reductions only due to limitation of sample size for testing as per ASTM standards.
- For corrosion testing, samples of 10 × 10 mm^2 with different thickness, depending upon different percentage reductions of samples were used.

Table 3.1: Chemical composition of commercial 5083 Al alloy (Weight %).

Component	Mg	Mn	Cr	Si	Fe	Cu	Al
Wt %	4.6	0.7	0.08	0.07	0.17	0.02	Balance

3.2 Experimental techniques

3.2.1 Experimental set up for rolling

Cryorolling (CR) is found to be one of the potential techniques to produce ultrafine grained materials. Cryorolling was performed with different thickness reductions up to 90%, and cryorolling (upto 50% thickness reduction) followed by warm rolling (WR at 175 °C) up to 90% reduction was performed in the present study. Initial thickness was same for all conditions. The schematic of experimental set up used in present study to carry out cryorolling and warm rolling is shown in Figure 3.1. The equipment and accessories used during rolling are given below:

- Samples were rolled on two high laboratory rolling mill having rolling speed and roll diameter of 8 rpm and 110 mm, respectively.
- In order to reduce the frictional force and heat generated between the sample and the rollers, molybdenum disulphide is used as lubricant.
- A cryocan is used to procure and store liquid nitrogen.
- The containers were prepared to dip the sample in liquid nitrogen during rolling. It consists of long stainless steel tubular type container covered with glass wool, refractory cloth and asbestos sheets kept in thermocole box to minimize the evaporation of liquid nitrogen to surroundings.
- Oil bath furnace is used to perform warm rolling.
- A digital vernier caliper is used to measure the thickness reduction achieved after each pass.
- A set of gloves for handling the samples during rolling.

3.2.2 Cryorolling Procedure

The samples after machining to required dimension and solution treatment are subjected to rolling at different temperature. The schematic illustration of cryorolling (CR) and warm rolling (WR) process is shown in Figure 3.2. The schematic of ST sample before processing is shown in Figure 3.3. The photographs of the ST samples before rolling and after cryorolling and cryorolling followed by warm rolling upto 90% reduction (true strain of 2.3) are shown in Figure 3.4 and Figure 3.5, respectively.

Figure 3.1: Experimental set up of cryorolling.

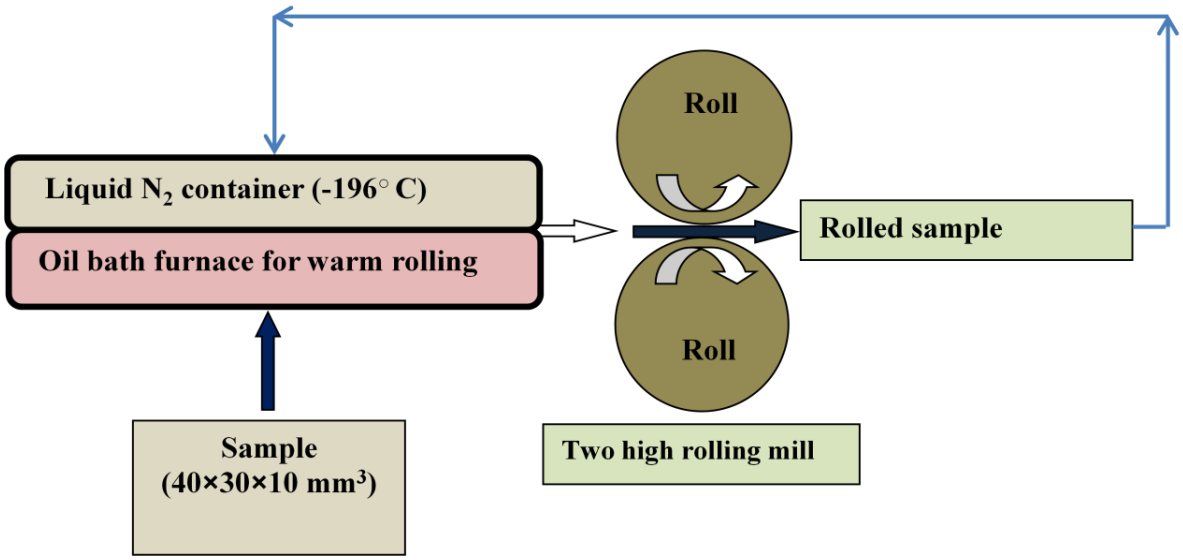

Figure 3.2: Schematic diagrams of cryorolling and cryorolling followed by warm rolling.

The detailed procedures adopted for cryorolling and warm rolling is given below.

- The rolling mill used in present work was cleaned thoroughly by using emery papers, tissue papers and acetone to remove rust, burrs, oxides and oil or grease, if any. The samples were also cleaned properly.
- Samples subjected to cryorolling are dipped into liquid nitrogen (-196 °C) kept in container for 15 min for initial pass and then 10 min for the successive passes. The process is repeated continuously till required strain is achieved and these samples are denoted as CR samples.
- The time span for removing sample from container, rolling of sample and keeping it again into container was observed to be 10 seconds to minimize the raise in temperature. The temperature measured before and after the rolling pass was found to be -150 $^{\circ}$C and -75 $^{\circ}$C, respectively.
- Samples subjected to warm rolling are initially cryorolled up to 50% reduction (0.7 true strains), further deformed at 100 °C, 145 °C, 175 °C and 200 °C by using oil bath furnace. Soaking time given for each pass was 4 min and these samples are denoted as cryorolled + warm rolled (WR) samples. The total reduction achieved was 90% (equivalent true strain of 2.3) and the reduction per pass was 4%.
- After rolling, the sample thickness was measured by digital vernier caliper.
- The strain per each pass (e) during rolling is calculated by using the following formula:

$$e = \ln \frac{\text{Thickness after cryorolling}}{\text{Initial thickness before cryorolling}} \quad (3.1)$$

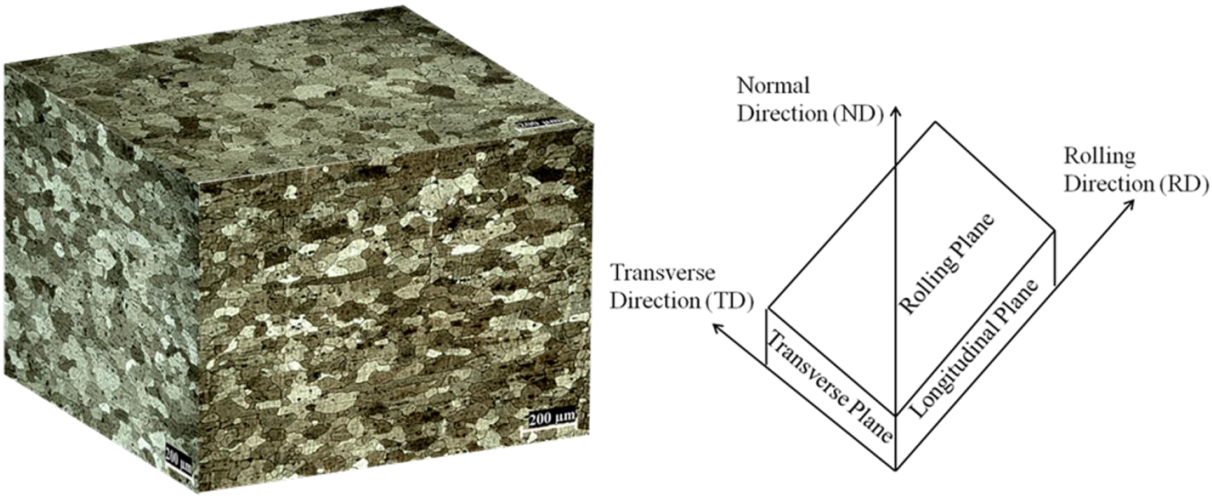

Figure 3.3: Tri-planar optical micrograph illustrating the grain morphology of 5083 Al alloy.

Figure 3.4: The photographs of the ST samples before subjecting to cryorolling.

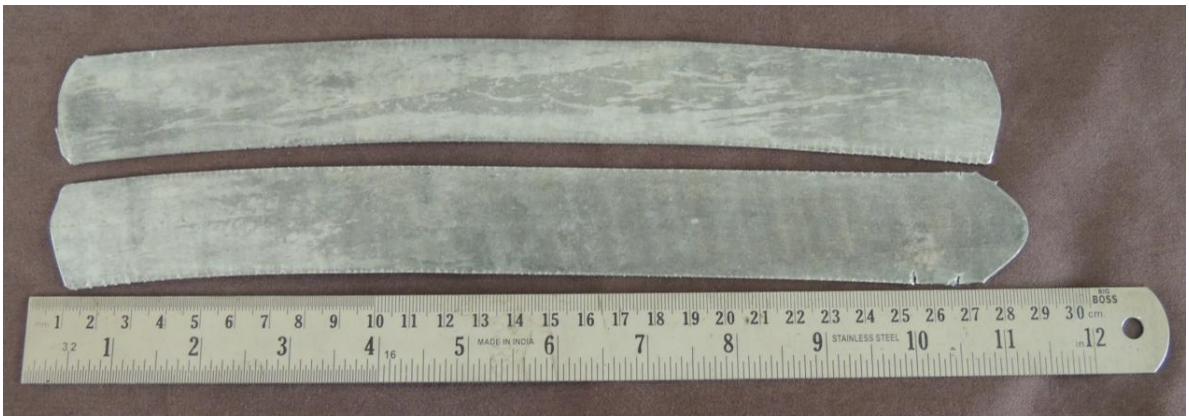

Figure 3.5: The photograph of the 5083 Al alloy subjected to CR 90% reduction.

3.3 Characterization techniques

3.3.1 Optical microscopy

Optical Microscopy provides images at higher resolution of variety of specimens. The samples after ST, CR and WR were characterized to examine the effect of homogenization after ST and evolution of microstructure along the rolling direction using a LEICA DMI5000 M optical microscope. Figure 3.6 shows the photograph of the LEICA DMI5000 M optical microscope used in the present study.

Figure 3.6: The Photograph of LEICA DMI5000 M optical microscope.

Initially, the selected part of the material is cut on diamond cutter at a certain distance from the plane to be observed using lubricant to avoid rise in temperature. These samples were then mounted on the sample holders and mechanically ground using SiC water proof abrasive papers of different grit sizes, usually 320, 600, 800, 1000, 1200, 1500 and 2000 grit. To avoid embedding of abrasive particles into soft aluminium alloys, water is used to flush away these particles. These mechanically polished samples were finally polished on polishing machine using fine velvet cloth and paste of magnesium oxide with water. The quality of the polishing influences the development of the true microstructure. Finally, the polished samples were etched with 50 ml of Poulton's reagent mixed with 25 ml HNO_3, 40 ml solution of 3 g chromic acid per 10 ml of water. After etching for 1 min, the samples were examined under Leica optical microscope with different magnifications under polarized light.

3.3.2 Electron back scattered diffraction (EBSD) analysis

Electron backscatter diffraction (EBSD), used with a high resolution field emission gun scanning electron microscope (FEGSEM) has emerged as a potential technique of microstructural analysis during the last decade. EBSD technique examines the surface of a bulk sample and an area scanned is larger as compared with TEM. It also furnishes information about the orientations of the subgrains and grains that cannot be easily obtained from the TEM. The structure of the deformed alloys and the mechanism for the formation of submicron grains or ultrafine grain structure, through quantitative measurement of boundaries present and their distribution in deformed state can be examined using EBSD technique. Therefore, in the present study, samples after ST, CR and WR and after different annealing conditions were characterized through EBSD. Figure 3.7 shows the photograph of the FEG-SEM equipped with EBSD.

The samples after electro polishing are placed in the equipment and inclined approximately 70^{o} with horizontal. The detector (camera) is equipped with a phosphor screen. The phosphor changes the diffracted electrons into light, suitable for the recording by charge coupled device (CCD) camera. Figure 3.8 shows the schematic of EBSD setup. The Kikuchi lines are collected by CCD camera. Specialized computer software analyzes the EBSD pattern by detecting a number of Kikuchi bands (a set of parallel Kikuchi lines) using an optimized Hough transform. The data obtained are used for identification of the phase, indexing of the pattern, and to determine the orientation of the crystal from which the pattern was generated. It also reveals systematic textural relations between individual grains and phases.

In order to get better diffraction patterns/Kikuchi bands, the specimen or sample surface should be well prepared. The selected part of the material is cut on diamond cutter at a certain distance from the plane to be observed using lubricant to avoid rise in temperature. These samples were then mounted on the sample holders and mechanically ground using SiC water proof abrasive papers of different grit sizes, usually 320, 600, 800, 1000, 1200, 1500 and 2000 grit. To avoid embedding of abrasive particles into soft aluminium alloys, water is used to flush away these particles. These mechanically polished samples were polished on polishing machine using fine velvet cloth and paste of magnesium oxide with water. Finally, electro polishing was performed at -15 °C using solution of methanol: perchloric acid (80:20) at potential of 11 volts.

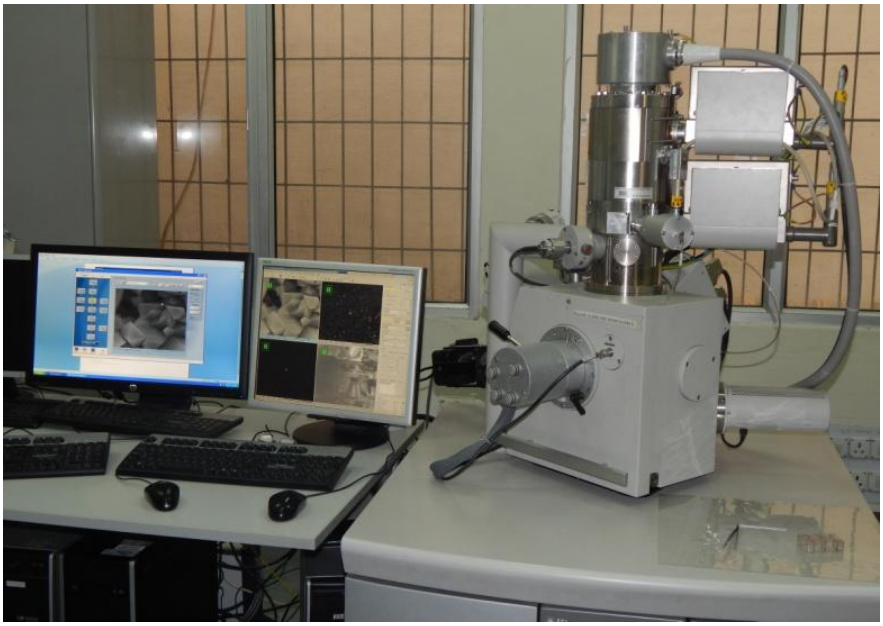

Figure 3.7: The Photograph of FEI Quanta 200 FEG-SEM.

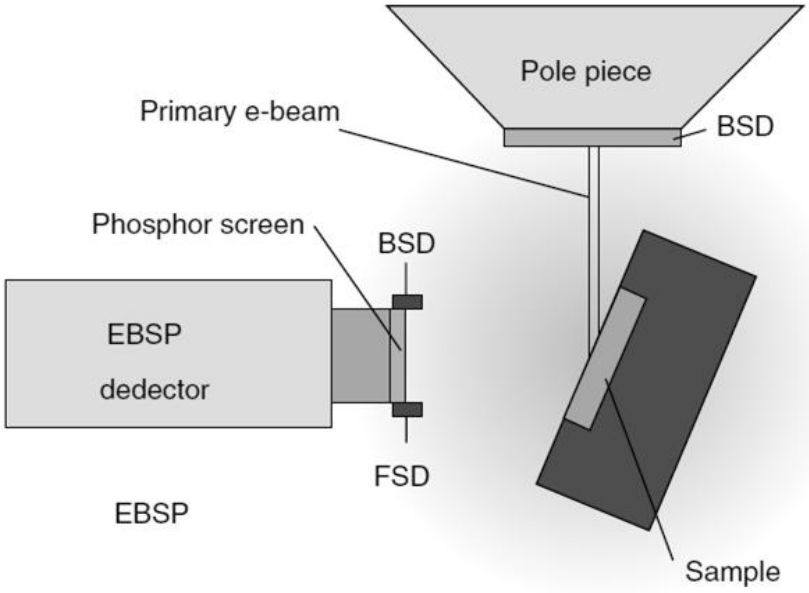

Figure 3.8: Schematic diagram of a typical EBSD sample installation (A. P. Day et al. Channel 5 User Manual, HKL Technology A/S, Hobro, Denmark (2001).

The EBSD measurements were performed on the samples cut from the mid centre of the rolled sheet. A scan rate for the solution treated (ST) samples was higher and lower scan rate for the CR, and WR samples with and without different annealing treatments. The larger step size of 1 μm was used for ST and annealed samples, whereas 0.1 μm for deformed samples like CR and WR samples. EBSD was performed on FEI, Quanta 200 F using TSL OIM analysis 4.6 software developed by TEXSEM laboratories Inc. Measurement points with confidence index (an approximate measure of accuracy of indexing) more than 0.03 are partitioned for analysis and less than 0.03 are shown as black in the EBSD maps. Misorientation angle which are less than 1.5º were neglected to avoid noise in the maps. Black area in EBSD maps represents partitioned area.

3.3.3 Field emission gun scanning electron microscopy (FEG-SEM)/ SEM

The fracture morphology of the 5083 Al alloys, cryorolled at different strains was studied by using field emission gun scanning electron microscope (FEG-SEM). The tensile fractured samples were examined in a FEI Quanta 200 FEG-SEM in the present work. Since the tensile fractured samples were conductive, the special sample preparation was not required for FEG-SEM study. Figure 3.7 shows the photograph of FEG- SEM used in present work for investigation of fractured surface morphology. The fractured morphology of fatigue samples and corrosion samples after immersion test are characterized by using SEM (Carl Zeiss).

3.3.4 Transmission electron microscopy (TEM)

Transmission Electron Microscopy (TEM) is a tool to characterize specimens in the region of 10^{-6} m to 10^{-9} m by diffraction and imaging techniques. It reveals the information that is inaccessible by optical microscopy because it uses a focused beam of high energy electrons that is related to the wavelength of the energy source used to form the images. TEM is mainly used to characterize the grain size, crystal structures, and specimen orientations, chemical compositions of phases, dislocation density, and precipitation morphology through diffraction pattern, X-ray and electron-energy analysis. In present work, investigation of ultrafine grained microstructure of CR, and WR samples (with and without different annealing treatments) were carried out by using a FEI Technai 20 TEM operated at 200 KV. The photograph of the FEI Technai 20 TEM is shown in Figure 3.9a, whereas, schematic diagram of the different hardware components inside the closed chamber of the TEM is shown in Figure 3.9b. TEM is a characterization technique wherein a beam of electrons interact the specimen within a high vacuum chamber. An image is formed from the

interaction of the electrons transmitted through sample. It is magnified and focused to have an enlarged version on fluorescent screen or to be detected by a sensor such as a CCD camera.

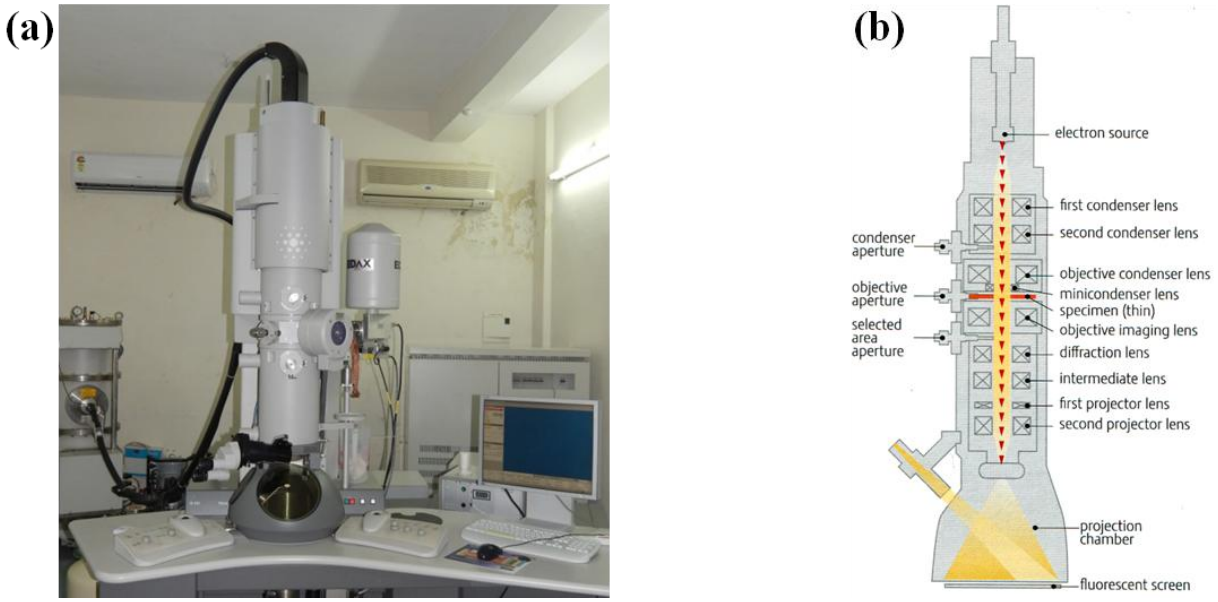

Figure 3.9: (a) Photograph of the TEM unit (FEI Tecnai-20), (b) Schematic diagram of TEM (*micron.ucr.edu/public/manuals/Tem-intro*).

For simplicity, TEM is divided into three sections: the illumination system, the objective lens/stage, and the imaging system. The illumination system consists of an electron gun having tungsten filament, or a lanthanum hexaboride (LaB_6) source. When this gun is connected to a high voltage source (typically ~100–300 kV), it begins to emit electron beam, operating in vacuum, which passes from set of condenser lenses in order to produce a beam of desired size and interacts with the sample. The specimen holder and objective lens are the main parts of the TEM. A beam-specimen interaction takes place and creates various images and diffraction patterns (DP). The imaging system makes use of lenses that subsequently magnify the image generated by the objective lens and focus these on the viewing screen via CCD camera.

For TEM investigation, the samples were initially cut into square pieces of 10 mm × 10 mm dimension and then fixed to the holders. These pieces were thinned up to 100 µm thicknesses through mechanically polishing from both sides by using silicon carbide emery papers (water proof) of 220, 400, 600,800, 1000, 1200 and 1500 and 2000 grit sizes. Thin foils were punched to 3mm diameter disks and then cleaned with acetone. The samples were thereafter further thinned by a twin-jet electro polishing unit with a solution of 20% perchloric acid and 80% methanol at a

temperature of -40 °C and at potential of 40 volts. After electro polishing, the samples were washed 3- 4 times in ethanol held in different containers to remove any layer of etchant and clean surface. Thereafter, the thinned dimpled samples were characterized by using TEM.

3.3.5 X-ray diffraction

XRD technique is used for qualitative identification and to get quantitative estimation of various crystalline phases and can provide information related to unit cell dimensions. The X-ray diffraction technique was utilized in the present study to characterize the different phases in the ST, CR and WR samples at different strains, and also for different annealing states. Bruker AXS D8 Advance instrument, using Cu Kα radiation was used to perform X-ray diffraction measurements for all the above mentioned samples. The photograph of the Bruker AXS D8 XRD equipment is shown in Figure 3.10a.

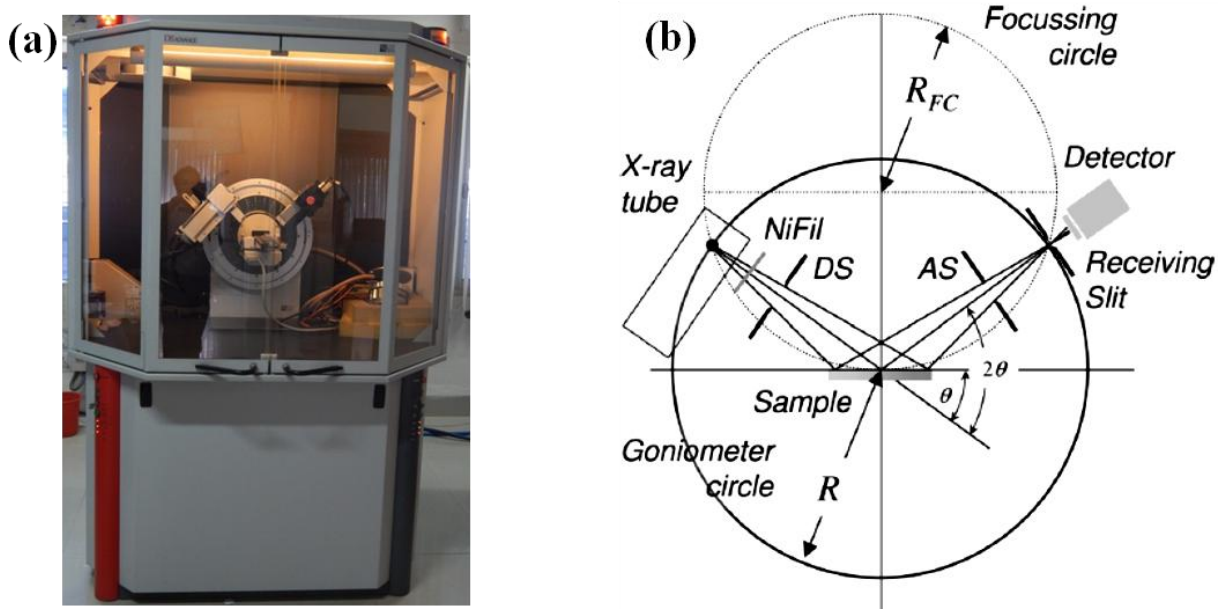

Figure 3.10: (a) Photograph of the XRD unit θ/2θ (Bruker AXS D8 Advance diffractometer, (b) Schematic representation of diffraction in Bragg–Brentano geometry (WILEY-VCH Verlag GmbH & Co. KGaA, weinhei).

The X-rays produced by a cathode ray tube are filtered and produces monochromatic radiation that are collimated and directed toward the sample. X-ray diffractometer has geometry such that the sample rotates in the path of the collimated X-ray beam by an angle ‘θ’, whereas, the X-ray detector is mounted to collect the diffracted X-rays and rotates by an angle of ‘2θ’. The

working principal is shown in the Fig. 3.10b. Whenever, the Bragg condition, $2d \sin \theta = n\lambda$ is satisfied, the incident X-ray beam is diffracted at the specimen and constructive interference takes place and peak in intensity occurs. The detector records the X-ray signals; Bruker D8 Advance diffractometer uses NaI scintillation counter as a detector. It can detect the diffracted radiations in the wavelength ranging from 0.5 to 3 Å. The diffraction pattern provides information such as; inter planar spacing, unit cell size or lattice parameters, crystallite size and strain in the sample.

3.3.6 Differential scanning calorimetry (DSC)

Differential scanning calorimetry (DSC) is a thermo analytical technique for measuring the temperatures and heat flows (into and out of the material) associated with phase transformation and chemical reactions in materials as a function of temperature and time in a controlled atmosphere. Although 5083 Al alloy is non-heat treatable alloy, some of the second phase constituents may affect the reactions. The effect of precipitation during CR, WR and annealing treatments are investigated through DSC. The energy associated with the formation or dissolution of different precipitate reactions is found to be within few joules per gram. Also, recovery, recrystallization, and grain growth phenomenon can also be detected during annealing using DSC. The thermal behaviours of the above mentioned samples were estimated in the present work using Perkin Elmer paris Diamond DSC with pure nitrogen atmosphere at the rate of 100 ml per min. The photograph of Perkin Elmer paris Diamond DSC unit is shown in Figure 3.11.

DSC consists of a sample holder and a reference holder and under each holder, a resistance heater and a temperature sensor is placed. Currents are applied to the heaters to increase the temperature with the selected rate. Both the holders ought to be kept at same temperature; however, power required to maintain the temperature is different, is used to calculate heat flow difference between sample and reference $\Delta dH/dt$. The recorded difference provides the exothermic or endothermic reactions associated with the formation or dissolution of different reactions in the samples. Peak observed in pattern corresponds to heat effect associated with process, such as crystallization as an exothermic process or melting as endothermic process. The area under endothermic or exothermic peaks superimposed on the baseline is proportional to ΔdH i.e., the heat absorbed or released by the material, and also the temperature scan rate.

The samples for DSC study were cut for different conditions and thinned 0.8 mm by using the silicon carbide emery paper (water proof) upto 1000 grit sizes and water was continuously

poured to avoid heating of sample. The thin samples were then punched to 5mm diameter disks by using a specially prepared set of punch and die and were cleaned using acetone.

Figure 3.11: The Photograph of Perkin Elmer Paris Diamond DSC instrument.

3.4 Mechanical testing procedures

3.4.1 Vickers hardness test

Hardness is the property of a material by virtue of which it resists plastic deformation, usually by penetration or scratch. In Vickers hardness test method, both soft and hard materials can be tested and their accurate results are widely acclaimed. It consists of diamond indenter, of right pyramid shape having square base and an angle of 136° between opposite faces, subjected to a load in range of 1 to 30 kgf. The hardness tests were performed to evaluate hardness values (HV) of ST samples, CR, WR samples after rolling to different strains, and at different annealing conditions. This is an economical method and a conventional way for evaluating the material properties due to its simplicity. Figure 3.12 shows a photograph of Vickers hardness testing machine, used in the present study.

Figure 3.12: The Photograph of Vickers hardness testing machine.

The sample of different conditions were cut into small pieces (15 × 15 mm^2) using diamond cutter. These samples were then mechanically polished by using silicon carbide emery papers (water proof) of 220, 600, 800 and 1200, grit sizes. These samples were further polished on a rotating cloth polisher using a paste of magnesium oxide. Vickers hardness testing was performed on plane parallel to rolling direction with load of 5 kg having dwell time of 15 s. An average of at least ten readings was taken to obtain a hardness (HV) value of sample.

3.4.2 Tensile test

Mechanical behaviour was investigated by performing tensile tests at room temperature to estimate the strength and ductility of the starting material after solution treatment (ST), CR, WR, samples at different thickness reductions (different true strains). Samples after different annealing treatments were also tested. The tensile tests were performed on S-Series, H25K-S materials testing machine operated at a constant crosshead speed with an initial strain rate of 5×10^{-4} S^{-1}. Samples for tensile testing were machined along the plane parallel to rolling direction according to the ASTM E-8 sub size specimen of 25 mm gauge length as shown in Figure 3.13. The tensile samples were properly polished before performing tensile test, to remove burrs, sharp corners, and scratches of machining to avoid surface roughness that may act as stress concentrators. Four samples were tested and were averaged to make final values. The photograph of tensile S-Series, H25K-S materials testing machine for present work is shown in figure 3.14.

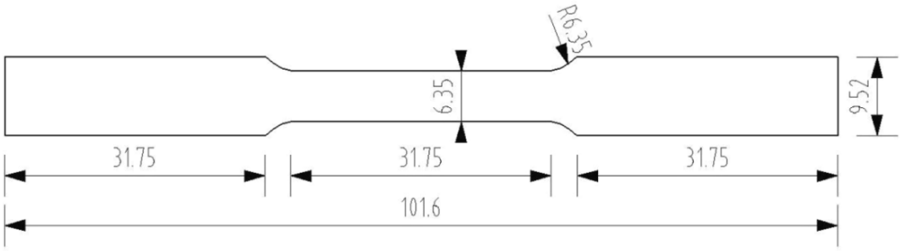

All dimensions are in mm.

Figure 3.13: Schematic diagram of a tensile specimen.

Figure 3.14: The photograph of the S-Series, H25K-S tensile testing machine.

3.4.3 Impact test

Impact test determines whether material is tough or brittle when it is subjected to suddenly applied load. A notched test specimen is employed and two methods generally used are the Izod or Charpy test. Charpy V-notch test is a high strain-rate test that estimates the amount of energy absorbed by a material up to fracture. This study is used to identify temperature-dependent ductile-brittle transition phenomena. The temperature at which the energy absorbed by material, suddenly drops to a lower value, and the shifting from ductile to brittle fracture, is called the transition temperature. Therefore, in present work, to quantify the energy absorption capability of ST, CR,

and annealed after CR sample, they are subjected to impact loading by Charpy impact test. The samples were cut in rolling (longitudinal) direction with a dimension of 10 mm × 7.5 mm × 55 mm with a 2 mm deep, 45^{o} V-notch having a 0.25 mm tip radius at the center of the specimen in the transverse direction as per ASTM standard E-23-07. The photograph of Charpy impact specimen and impact testing machine used in testing are shown in Figure 3.15 and Figure 3.16 respectively.

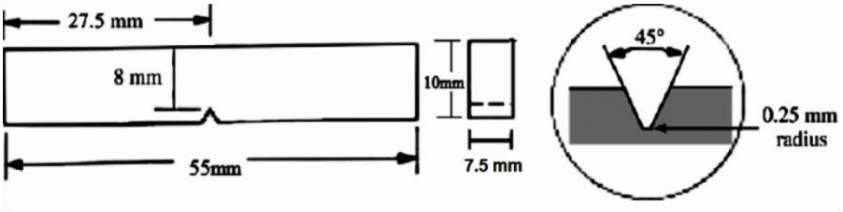

Figure 3.15: Schematic diagram of a Charpy impact specimen.

Figure 3.16: The photograph of Impact testing machine.

3.4.4 Fatigue test

The stress-life (S-N) fatigue test of ST, CR, WR conditions were performed under high-cycle fatigue experiments carried out on 25 kN servo hydraulic universal testing machine in a laboratory air environment. The specimens were axially loaded under stress control mode keeping stress ratio 0.1 and frequency of 20 Hz using a sinusoidal waveform in all cases. The samples for

fatigue testing were machined along the plane parallel to rolling direction according to ASTM E 466-07, as shown in figure 3.17. The samples of all the conditions were polished using abrasive grit emery papers up to 1200 to eliminate irregularities after machining and notches that may act as stress concentration during tests. Figure 3.18 shows the photograph of fatigue machine used in present study.

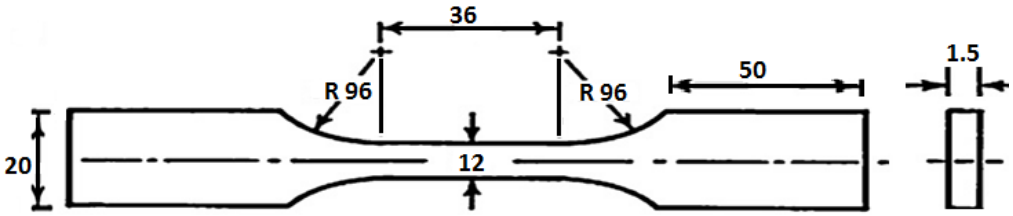

Figure 3.17: Schematic diagram of fatigue sample (All dimensions in mm).

Figure 3.18: Schematic showing type of loading on servo hydraulic machine.

3.5 Corrosion testing

The knowledge of corrosion behaviour of ultrafine grained material is essential for various engineering applications. Corrosion behaviour of ultra-fine grained (UFG) 5083 Al alloy fabricated by CR upto 90% reduction, WR up to 90% reduction was investigated by electrochemical

polarization test, immersion test, and nitric acid mass loss test, and their surface analyses was carried out through optical and scanning electron microscopy (OM and SEM). The potentiostatic polarization tests were performed to analyze the passive film breakdown (pit initiation and propagation) under the pitting potential. The corrosion behaviour of CR and WR samples were compared with as received and solution treated material.

Figure 3.19: The photograph of Voltalab PGZ301.

Electrochemical polarization test was carried out on 10 x 10 mm^2 dimension samples in 3.5% NaCl solution. This solution is best suitable for observing the pitting resistance and passivation behaviour of 5083 Al alloy, as it is extensively used in ships, submarines. Experiments were performed at scanning rate of 1 mV/s using "Voltamaster -4'' software of electrochemical laboratory voltalab PGZ301. Figure 3.19 shows the photograph of voltalab PGZ301 used in present study. Samples were prepared by putting a copper wire on one face of the sample and then cold mounted in resin. The samples were mechanically polished up to 1200 grade emery paper, degreased with acetone. Tests were conducted with conventional three-electrode cell using saturated calomel electrode (SCE) as the reference electrode, and a platinum rod as a counter electrode.

Immersion test was carried out in accordance to the ASTM G-31 standard. The samples were immersed in the 3.5% NaCl solution at room temperature for 15 days, and corrosion rate is calculated by measuring the weight loss of the test material. Samples were descaled with CrO_3

solution at 90 °C for 5 min followed by ultrasonic cleaning and rinsed with distilled water. The samples were weighed to determine mass loss per unit area.

Nitric acid mass loss test (NAML) is a standard test procedure to evaluate the susceptibility of the 5083 Al alloy to intergranular corrosion (IGC) in accordance with ASTM G-67. According to the standard, the material is considered as resistant to IGC, if the mass loss per unit area is less than or equal to 15 mg/cm ^{2}, while if, it is more than or equal to 25 mg/cm^2, then the material is considered to be susceptible for ICG. Sample with 50 mm length parallel to longitudinal direction and 6 mm width by sample thickness are grounded with 300 SiC grit paper to remove sharp edges, and cleaned with ethanol, and air dried. Dimensions were measured using Vernier caliper. The samples were then immersed in 5% NaOH solution at 80°C for 1 min followed by water rinse. Again 30 sec, immersion in HNO_3 (desmut), washed thoroughly, dried in air, and weighed before keeping sample in etchant for IGC. The samples were immersed in nitric acid and kept standing over glass beaker, and maintain the test solution temperature at 30°C for 24 hr. After completion, the sample was removed, rinsed thoroughly with deionised water while brushing with tooth brush and allowed to dry in air. The samples were weighed to determine mass loss per unit area.

CHAPTER 4
Results and Discussion

In this chapter, the results obtained on mechanical and corrosion behaviour of ultrafine grained 5083 Al alloy processed by cryorolling and warm rolling are discussed. The present research work was focused on various experimental investigations of the alloy such as: (i) Mechanical and microstructural studies of 5083 Al alloy deformed through cryorolling; (ii) Microstructures and impact toughness behavior of 5083 Al alloy processed by cryorolling and annealing; (iii) Effect of deformation temperature on mechanical properties of ultra fine grained Al-Mg alloys processed by rolling; (iv) High cyclic fatigue behaviour of ultrafine grained 5083 Al alloy; (v) Corrosion behavior of ultrafine grained 5083 Al alloy developed by cryorolling. The results of each study are substantiated using detailed microstructural characterizations of the samples processed under different conditions.

4.1 Mechanical and microstructural studies of 5083 Al alloy deformed through cryorolling

4.1.1 Introduction

Severe plastic deformation (SPD) techniques have emerged as novel processing routes to produce bulk ultrafine grained/nanostructured material from its counterpart by deforming relatively at higher plastic strains as reported in literature (Prangnell et al. 2004). These techniques also have limitations, and the efforts are being made on modification of SPD techniques to produce the materials in an effective way. Cryorolling is one of the simple technique to produce ultrafine grained structure in the material. It is performed by rolling the samples at room temperature and immediate quenching at cryogenic temperature by using liquid nitrogen. UFG structures can be produced in the material by deforming at relatively low plastic strain (~2.3) followed by annealing. Cryorolling has been used in recent years to produce UFG structure in pure metals and alloys like Cu, Al, Ti, Zr, Br and V as already discussed in literature review in Chapter 2.The effect of cryorolling on microstructural evolution and mechanical behaviour of pure metals and heat treatable aluminium alloys is reported in literature; however there is scarcity of literature in non-heat treatable alloys, especially in 5083 Al alloys. The presence of coarse second-phase particles can increase the rate of dislocation generation and develop surrounding deformation zones in the matrix. Low angle boundaries can form within such deformation zones at relatively low strain, whereas very fine particles are sheared and dissolved in the matrix (Apps et al. 2003, Humphreys et al. 2004, Urrutia et al., 2005). It has also been reported that in deformed materials, strengthening is attributed to their arrangement of dislocations and their density (Morris et al. 2003). Nikulin et al. (2012) investigated the formation of coarse recrystallized grains in 1561Al alloy due to discontinuous growth of recrystallized grains during interpass annealing between ECA passes. In the present work, the effect of second phase particles in the alloy are investigated subjected to different strains up to 2.3 at cryogenic temperature, especially the evolution of microstructre and grain refinement in terms of pinning and driving forces for recrystallization.

In the present study, 5083 Al alloy is deformed at different true strains levels with the aim: i) To study the effect of very low temperature deformation on microstructural evolution and mechanical properties and, ii) To investigate the influence of short time annealing on final microstructure and dislocation density.

4.1.2 Experimental procedure

The as rolled commercial grade 5083 Al alloy of 16 mm thickness plate with chemical composition given in Table 3.1 was selected for grain refinement in the present work. Samples with dimensions 10×30×40 mm^3 were machined from the as received material and solution treated (ST) at 510 ºC for 2 hr, then cryorolled (CR) to different thickness reductions of 30%, 50% and 90% (true strains of 0.35, 0.7, and 2.3 respectively). CR samples (true strain 2.3) were short annealed (SA) at 300 ^{o}C for 6 min in muffle furnace. The microstructure of material after ST and CR at different true strains was characterized using optical microscopy under polarized light, EBSD and TEM techniques. The details of material selected, sample preparation for optical microscopy, EBSD and TEM and mechanical testing and their procedures were discussed in Chapter 3. In EBSD scans, a step size of 1 μm was used for ST sample and 0.1 μm for the deformed samples.

4.1.3 Results and discussion

4.1.3.1 Microstructural evolution during cryorolling

Figure 4.1 shows the optical micrographs of ST. After ST, the material possesses equiaxed grains and the average grain size estimated from line intercept method was 85 μm. The positions of the particles are clearly visible irrespective of the grain boundaries after etching as shown.

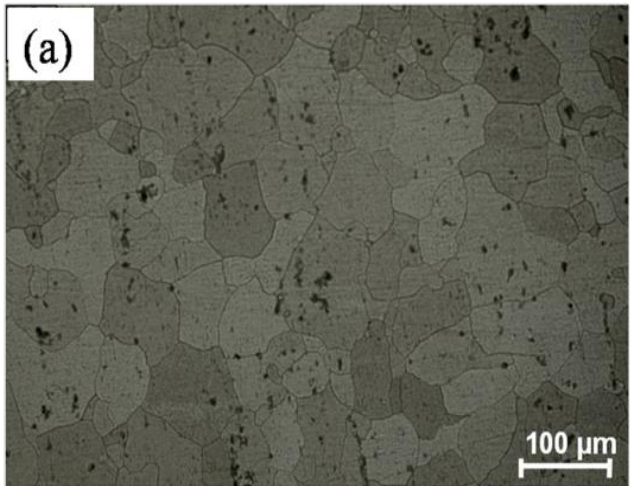

Figure 4.1: Optical micrographs of solution treated 5083 Al alloy after etching.

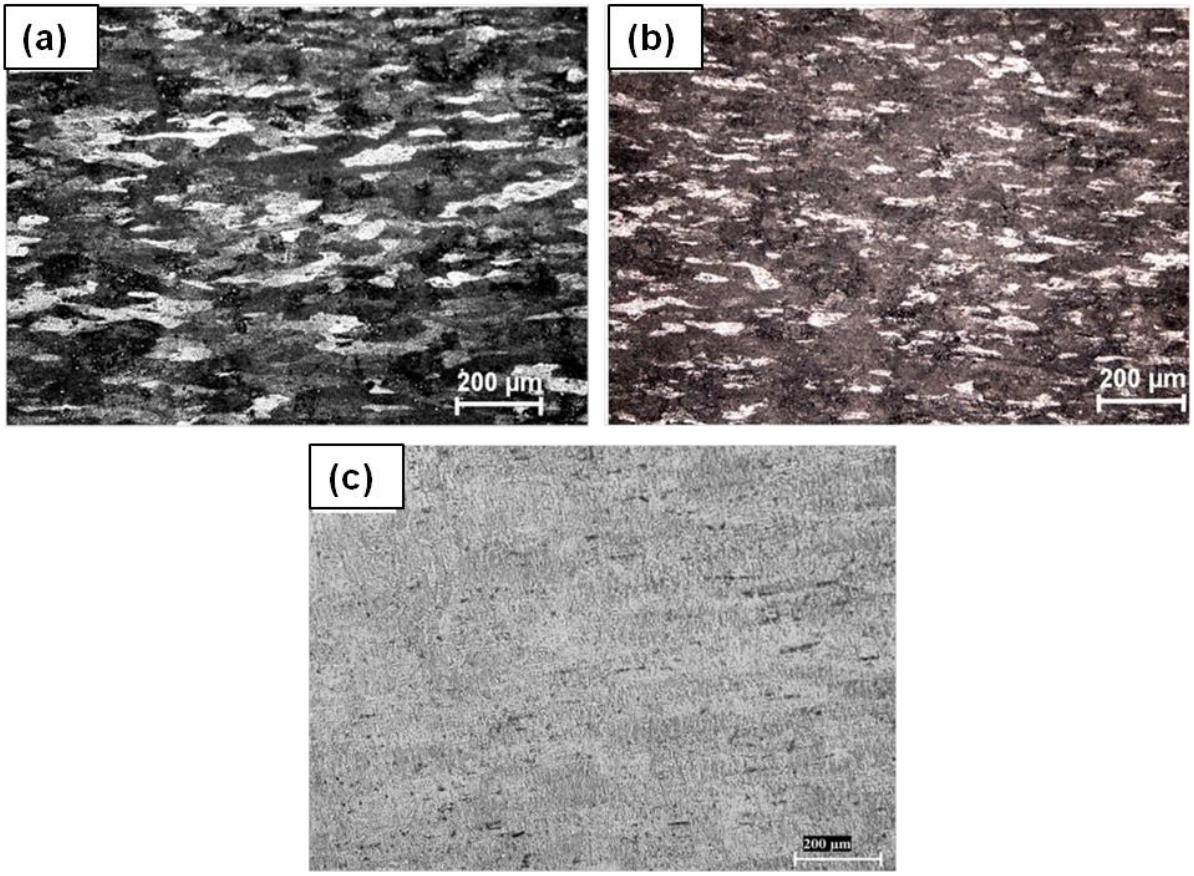

Figure 4.2: Optical micrographs of 5083 Al alloy after etching; (a) CR 30% reduction, (b) CR 50% reduction, (c) CR 90% reduction.

Figure 4.2 shows optical micrograph of CR at different percentage of thickness reductions after etching. After cryorolling to 30% reduction, the grains got elongated in rolling direction and aspect ratio increase to 1.32:1 as shown in Figure 4.2a. With further increase in rolling strain, the grains are more elongated in the rolling direction and it became denser as seen in Figure 4.2b. In Figure 4.2c, it can be seen that second phase particles got broken and redistributed throughout the matrix, which results in reduction of segregation effect. It is also not possible to observe the micrographs clearly due to limited resolution of optical microscopy at higher strain level. Therefore, the deformed microstructures were investigated through EBSD and TEM techniques.

EBSD micrograph of ST, CR samples at different percentage of reductions and CR 90% after short annealing (SA) at 300 ºC for 6 min with its image quality map are shown in Figure 4.3. Measurement points with confidence index (an approximate measure of accuracy of indexing) more than 0.03 are partitioned for analysis and less than 0.03 are shown as black in the EBSD

maps. Low angle grain boundaries (1.5° ≤ 15°) are shown in grey colour, whereas high angle grain boundaries (<15º) are in black colour. Misorientation angle which is less than 1.5º were neglected to avoid noise in the maps. Black portion in EBSD maps represents partitioned area. The frequency histogram of boundary misorientation distribution of initial solution treated condition shows with full of high angle (15°) grain boundaries as shown in Figure 4.3a. Figure 4.3b shows EBSD map of CR samples after 30% thickness reduction, where the grains are deformed in the rolling direction. Grain fragmentation can be observed from the EBSD map and TEM image (Figure 4.5a).

With increasing percentage of deformation, the aspect ratio of the grains increased and the fraction of low angle grain boundaries increased due to the formation of fine subgrain structure inside the original grain as seen from the Figure 4.4b to Figure 4.4d. These results are supported by TEM microscopy, where the initial microstructure of 5083 Al sample after annealing at 510 °C for 2 hr exhibits high density of fine second phase particles with very low density of dislocations as shown in Figure 4.5a. During cryorolling, dislocation density is increased with increasing percentage of reduction as shown in Figure 4.5a,b,c &d. Fine second phase particles are promoting dislocation accumulation by acting as an obstacles for dislocation movement. Cryorolled sample after 90% reduction has shown substructure formation with unclear dislocation cell network. Dislocation cells with dense dislocation walls and dislocation tangling zones were observed. The reason for high fraction of low angle grain boundaries and high dislocation density during cryorolling is due to effective suppression of dynamic recovery. Pinning of dislocation movement by fragmented second phase particles also leads to accumulation of high dislocation density and develop local deformation zones with large misorientaion gradients (Apps et al. 2003). These microstructure features have significant role on improvement of mechanical properties. Figure 4.3e shows EBSD micrograph of CR 90% and short annealing at 300 ºC for 6 min. After short annealing at relatively high temperature, recovery has occurred and there is significant change in dislocation density network and ultrafine grains with well defined grain boundaries of grain size ~300 nm were formed.

Formation of homogeneous fine grained structure is clearly evident from image quality micrograph of CR 90% after short annealing is shown in Figure 4.3f and Figure 4.5e. Some recrystallized grains free from dislocation are also observed in CR 90% and short annealed samples. The volume fraction of high angle grain boundaries were increased after short annealing treatment due to formation of recrystallized grains (Figure 4.4e). The sizes of the recrystallized

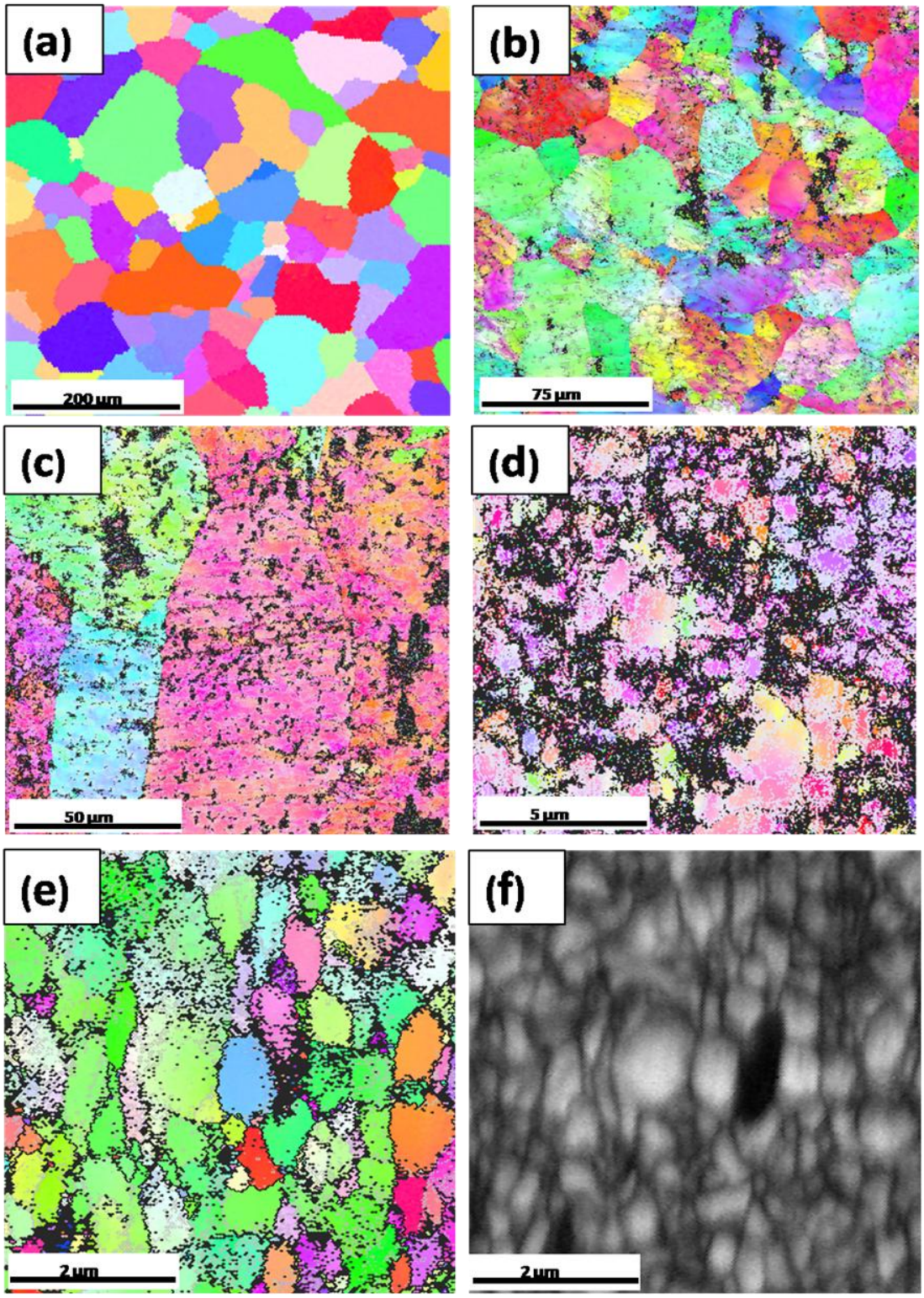

Figure 4.3: EBSD micrographs of 5083 Al alloy; (a) ST, (b) CR 30% reduction, (c) 50% reduction, (d) CR 90% reduction, (e) CR 90% and SA, (f) Image quality map of CR 90% and SA.

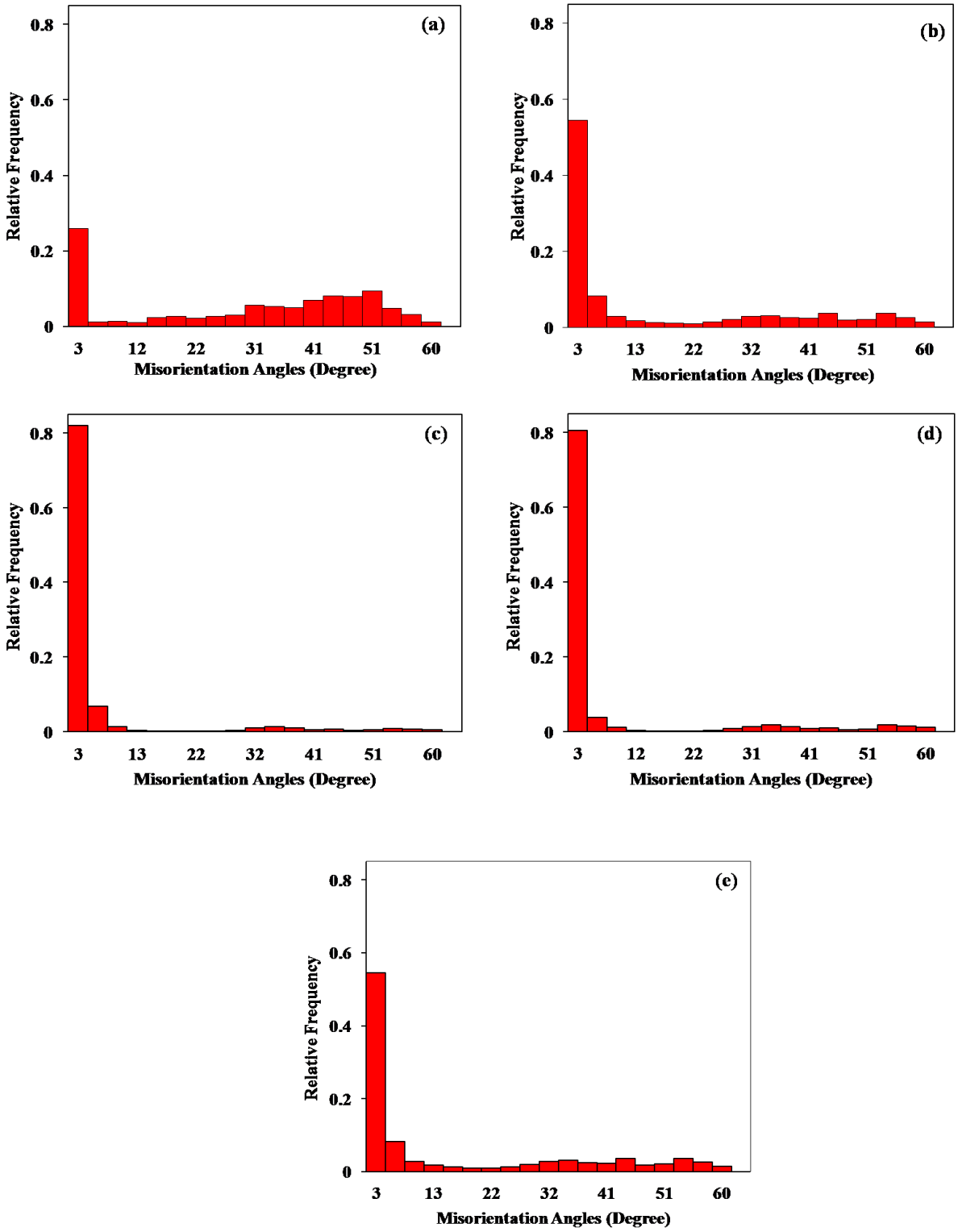

Figure 4.4: Frequency histograms of grain boundary misorienation of; (a) ST, (b) CR 30% reduction, (c) 50% reduction, (d) CR 90% reduction,(e) CR 90% and SA, (f) Image quality map of CR 90% and SA.

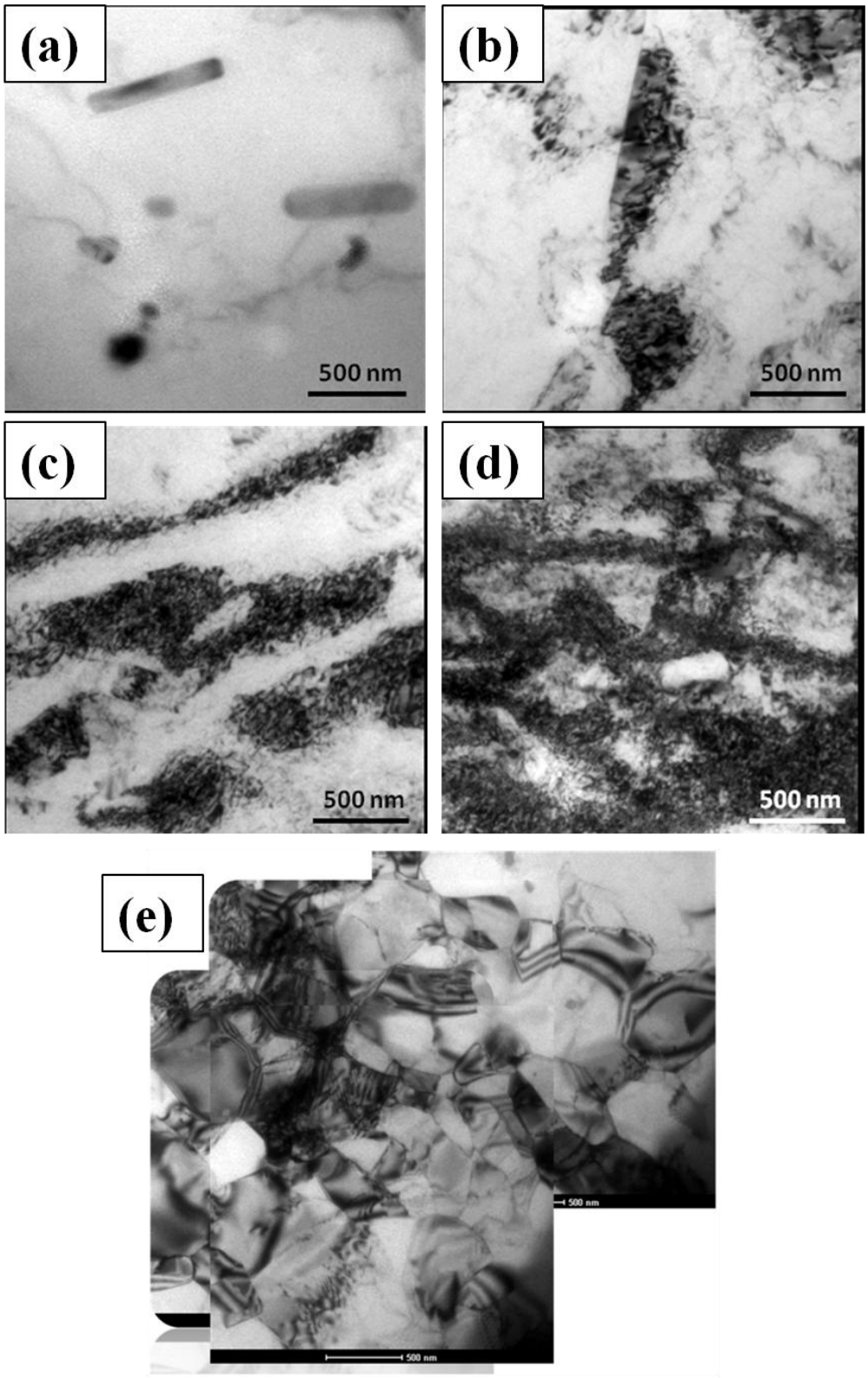

Figure 4.5: TEM micrographs of 5083 Al alloy (a) ST, (b) CR 30% reduction, (c) CR 50% reduction, (d) CR 90% reduction, (e) CR 90% and SA.

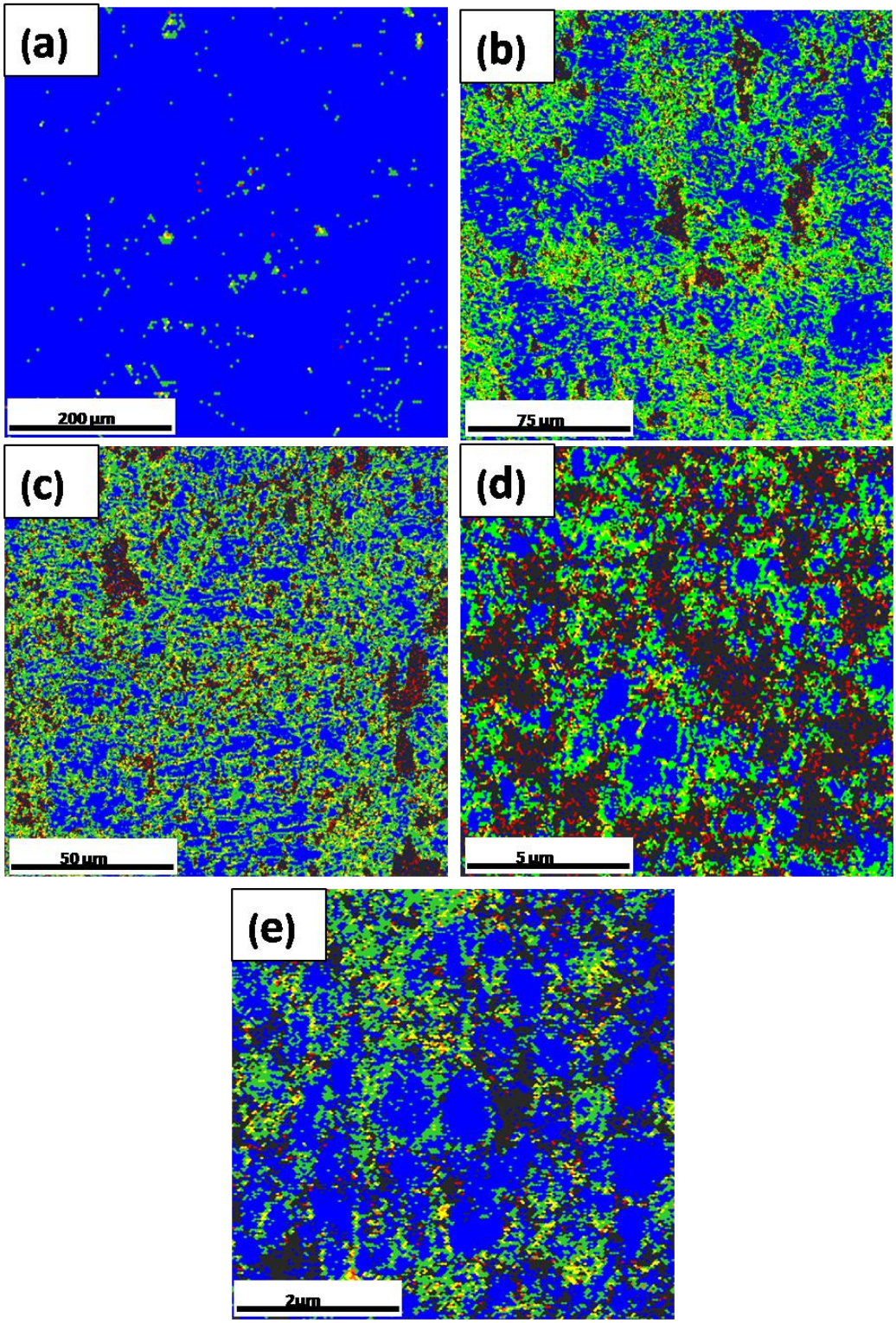

Figure 4.6: Kernels average misorientation (KAM) analysis; (a)-(e) are Kernels average misorientation (KAM) micrographs of (a) ST, (b) CR 30% reduction, (c) CR 50% reduction, (d) CR 90% reduction, (e) CR 90% and SA.

grains are slightly bigger in size than recovered fine grains. These predictions were supported by Jiang et al. (2008), who have examined the grain misorientation in similar Al-Mg-Mn alloy subjected to 6 passes by ECAP and annealing for 1 hr at 673K and 723K, respectively. The observation shows that the average misorientation and the fraction of high-angle boundaries exhibit increasing trend as the annealing temperature increases. This depicts that the fraction of LAGB decreases with increasing annealing temperature.

In order to find the stored energy in the material, the most appropriate quantity is Kernels average misorientation (KAM) (Takayama et al. 2005). In the Kernel maps, the degree of misorientations are correlated to the neighbouring data points and indicated by a colour scheme. A Kernel map and the associated colours are shown in Figure 4.6a to 4.6e, and Figure 4.7 gives the misorientation in degrees. Red colours indicate a high degree of misorientation compared to the surrounding data points; blue colours indicate a low misorientation and thus low strains. From Figure 4.6e, it can be observed that short annealing at 300 ºC for 6 min have not recrystallized the material completely. The dislocation content is still remained in the material. The fine grains which are formed after short annealing of CR 90% reduction were due to combined effect of static recovery and recrystallization.

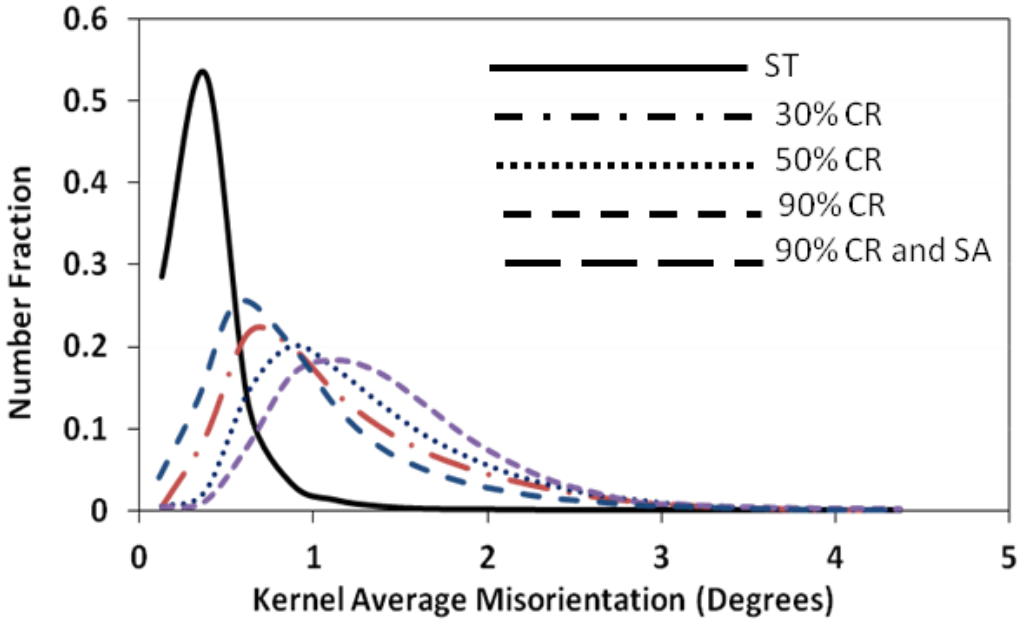

Figure 4.7: Kernels average misorientation (KAM) plots of; (a) ST (b) CR 30% reduction, (c) CR 50% reduction, (d) CR 90% reduction, (e) CR 90% and SA.

4.1.3.2 Mechanical properties

Figure 4.8 shows the effect of CR on the hardness of 5083 Al alloy at various strains. In 5083 Al alloy, hardness value has increased from 58 HV to 98 HV (nearly ~69%) after imparting true stain of 0.35 (30% reduction) at cryorolling temperature. The enhancement in hardness value is attributed to high dislocation density generated in the samples during rolling at liquid nitrogen temperature and effective suppression of cross slip or climb of dislocations associated with dynamic recovery (Wang et al. 2002, Cheng et al. 2007, Rao et al. 2012). Further reduction of samples from 30% to 50% at the same temperature leads to the 6 HV increase in hardness and from 50% to 90%, the rise in hardness is 23 HV. There is remarkable improvement (119%) in hardness of 90% CR sample with respect to initial solution treated condition.

Tensile tests were carried out on S-series, H25K-S testing machine operated at constant cross head speed with strain rate of $5x10^{-4}$ s^{-1} on the samples machined as per ASTM E-8/E8M-0 9 sub-size specifications parallel to the rolling direction with gauge lengths and width of 25 mm and 6 mm respectively. Microstructure of rolled sheet at CR 30% reduction (0.75 true starin) has significant effect on yield strength and ultimate tensile strength as shown in Figure 4.9.

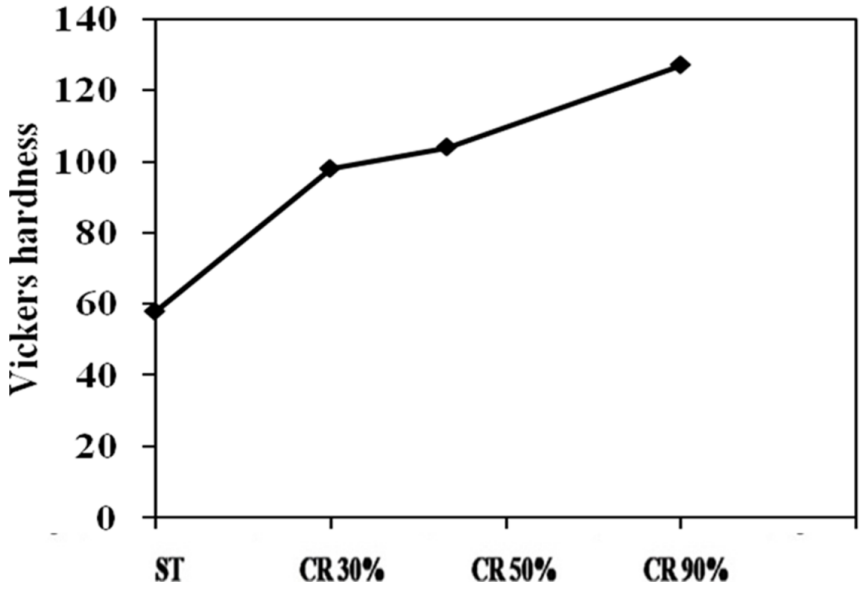

Figure 4.8 Variation in Vickers hardness at different conditions of samples.

Ultimate Tensile strength (UTS) has increased from 277 MPa to 340 MPa (22.7% increment), and yield strength (YS) has increased from 180 MPa to 290 MPa (61.1% increment), whereas the percentage of elongation drops from 22 % to 12.3% for CR samples with 30% thickness reduction. Similarly, as the degree of CR increases to 50% thickness reduction, UTS increased from 277 MPa to 390 MPa (40.8% increment) and YS has increased from 180 MPa to 366 MPa (103% increment), whereas elongation drops to 8%.

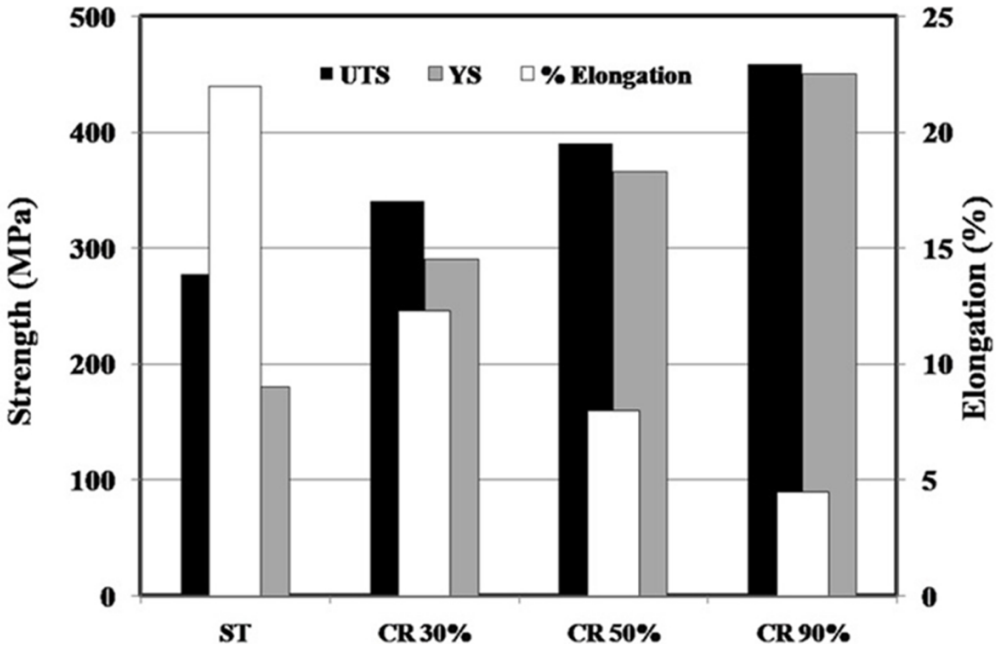

Figure 4.9: Variation in UTS, YS and elongation values at different conditions of samples.

4.1.4 Summary

- A homogeneous ultrafine grained structure with an average grains size of 300 nm was achieved after short annealing treatment at 300 ºC for 6 min of CR 90% thickness reduction sample.
- With the increase in % reduction, fraction of low angle grain boundaries increases due to formation of subgrain structure and retention of high dislocation density, which acts as a driving force for the formation of ultrafine grains.
- The volume fraction of high angle grain boundaries has increased after short annealing treatment due to formation of recrystallized grains.
- The formation of ultrafine grained structure after short annealing treatment is

due to the combined effect of static recovery and recrystallization.

- From the KAM analysis, the average misorienation of CR 90% and SA is found to be 0.8 degrees, which lies in between ST and CR 30% thickness reduction.
- The significant improvement in yield strength (103%) and ultimate tensile strength (40.8%) of 90% cryorolled sample is due to the effective suppression of dynamic recovery and accumulation of high density of dislocations during low temperature deformation.

4.2 Microstructures and impact toughness behaviour of 5083 Al alloy processed by cryorolling and annealing

4.2.1 Introduction

Structural components and machines having various industrial applications, made of metals and their alloys are subjected to impact loadings frequently during their service. Therefore, material should have high impact strength to prevent catastrophic failure while subjected to impact loading. High impact strength is particularly important at low service temperatures because metals show low impact toughness at lower temperatures. The metals including steel and aluminium with lower impact, on decrease in working temperature, limit their applications. The great historical tragedy of Titanic ship was result of freezing sea temperature at which the plates of ship become brittle, this may be attribute to ductile to brittle transition temperature of metals. Therefore, fracture and impact-toughness studies of metals and their alloys are of great technological importance for ensuring safe material design in structural application when subjected to sudden loadings. Efforts are being made since 1950 to investigate the behaviour of material. The energy absorption capabilities of materials can be investigated with classical experimental mechanics approach subjected to impact loading through Charpy impact test. With advancements in microscopy techniques through SEM and TEM, fracography studies of engineering materials become easier, which provides a new insight to fracture studies. The lower fracture toughness may be due to microstructural changes in material, which can be improved by alloying, processing techniques and heat treatment. Microstructural changes can be observed through severe plastic deformation (SPD) techniques, cryorolling is also a potential route that obviates the drawbacks of SPD. All these techniques have reported high strength and improved ductility through different heat treatments, but very few have reported impact toughness of these fine grained materials.

It has been reported that impact toughness decreases with cold working in 7075 AA, which can be improved by recrystallization at appropriate temperature (Tajally et al. 2010). ECAP is proved to be effective in improving the strength and toughness of Al-Cu alloy as the fracture behaviour changes from brittle to ductile mode by multiple passes ECAP (Fang et al. 2011). Ozden et al. (2007) have studied that, impact toughness of Al 5083+SiC MMCs for different temperatures are fairly constant and lower than those of Al 5083 unreinforced alloys. Impact toughness as a function of temperature in case of initial coarse grain Ti and nanostructured Ti has been studied by

Stolyarov et al. (2006) and observed that impact toughness of coarse grain Ti decreases with decreasing temperature while for nanostructured Ti, it increases with decreasing temperature.

Although substantial work has been reported on microstructural evolution and mechanical behaviour of deformed and annealed 5083 Al alloy, studies on fracture and impact toughness behaviour of rolled sheet and plate are scarce in the literature. Therefore, the present research work has been envisaged to quantify the energy absorption capability of cryorolled 5083 Al alloy subjected to impact loading by Charpy impact test, tensile properties, and effect of cryorolling followed by annealing treatment on impact and tensile properties of 5083 Al alloy. The microstructure of the CR 5083 Al alloy and CR and annealed 5083 Al alloy was characterized by using optical microscopy, Electron back scattered diffraction technique (EBSD), and Transmission electron microscopy technique (TEM). The fracture surface of tensile and impact test samples were characterized by FE-SEM to reveal the mode of failure in the CR 5083 Al alloy.

4.2.2 Experimental procedure

The 5083 Al alloy, after solution treatment were cryorolled to 30%, 50% and 90% reductions. 30%, 50% cryorolled samples were annealed for 1 hr at different temperatures ranging from 150 °C to 400 °C with an interval of 50 °C. Microstructural evolution of solution treated (ST), cryorolled (CR) and cryorolled and annealed sample were examined through optical microscopy, EBSD and TEM along the plane parallel to the transverse direction. To study the effect of cryorolling strain and cryorolling followed by annealing, Vickers hardness and uniaxial tensile tests were performed at room temperature. To determine impact toughness, Charpy impact tests were conducted on homogenized starting material, CR and annealed samples. To study the effect of temperature on impact energy of CR 30%, 50% samples, Charpy impact test were performed at different temperatures -190, -50, 0, 25, 100, 225 °C and compared with ST samples at the same temperature. Minimum four samples were tested in each condition to obtain impact toughness value. Samples tested at -50 °C were pre-cooled in acetone which was in turn cooled by liquid nitrogen, samples tested at -190 °C were directly cooled at liquid nitrogen and samples tested at 100 and 225 °C were preheated in a muffle furnace for 10 minutes. The fractography examinations were carried out for all conditions of sample on the fractured surfaces by using scanning electron microscope (SEM). The details of material selected for present work, the testing procedures for hardness, tensile strength and Charpy impact toughness test and their sample

preparation and procedures for microstructural observations and fractography analysis are discussed in Chapter 3.

4.2.3 Results and discussion

4.2.3.1 Effect of cryorolling on microstructure and mechanical properties

In Section 4.1, the effect of CR on the microstructural evolution and their effect on hardness and tensile properties of 5083 Al alloy at various strains is described in detail. The results shows significant improvement in properties due to high dislocation density generated due to low temperature rolling and pinning of dislocations by fragmented second phase particles.

4.2.3.2 Effect of cryorolling on impact toughness

The instrumented impact results of the Al 5083 with ST, CR 30% and CR 50% reduction at different temperatures are presented in Figure 4.10. The impact behaviour of all three conditions at different temperatures exhibited a similar trend. However, the observed values of impact toughness of CR 30% and 50% reductions got reduced in all temperatures compared to ST condition. The lower impact strength of CR 30% and 50% reduction samples can be attributed to increase in dislocation density due to suppression of dynamic recovery taking place during deformation at liquid nitrogen temperature. The loss in impact energy after cryorolling is due to lack of plastic deformation in the sample due to increase in yield strength. Yield stress and propagation energy are inverse to each other (Tajally et al. 2010). Hence, it may be mentioned that cold working of 5083 Al alloy results in loss in impact toughness and increases its brittle fracture behaviour. It is evident from the literature that dislocations and micro cracks are most important defects affecting fracture toughness in the metallic materials (Tajally et al. 2010, Jayatilaka 1979). The drop in impact toughness of ST, CR 30% and 50% at -190 °C with respect to room temperatures is 20%, 30% and 46%, respectively. The drop in toughness at -190 °C is more significant in CR 50% reduction sample than the other samples (ST, CR 30% reduction). The behaviour of starting solution treated material is in agreement with reported literature (Ozden et al. 2007), where the impact strength increased with increasing temperature up to room temperature and then started decreasing to minimum at 225 °C. Whereas, in the cryorolled samples, impact strength increased with increasing temperature upto 100 °C and then decreased. The increase of impact toughness with increasing temperature is an anticipated result as the ductility increases with increase in

temperature up to critical values. The material will start yielding and its load carrying capacity will decrease with increasing temperature beyond critical value.

Figure 4.11 shows the SEM images of fractured surfaces of ST, 30% CR and 50% CR after Charpy impact test at room temperature. Figure 4.11a reveals the well developed large dimples, with lateral expansion in macroscopic view in bulk sample, which indicates ductile mode fracture leading to a high tensile elongation. The characteristics of ductile fractures are supposed to be tearing of metal accompanied by considerable plastic deformation and expenditure of substantial energy.

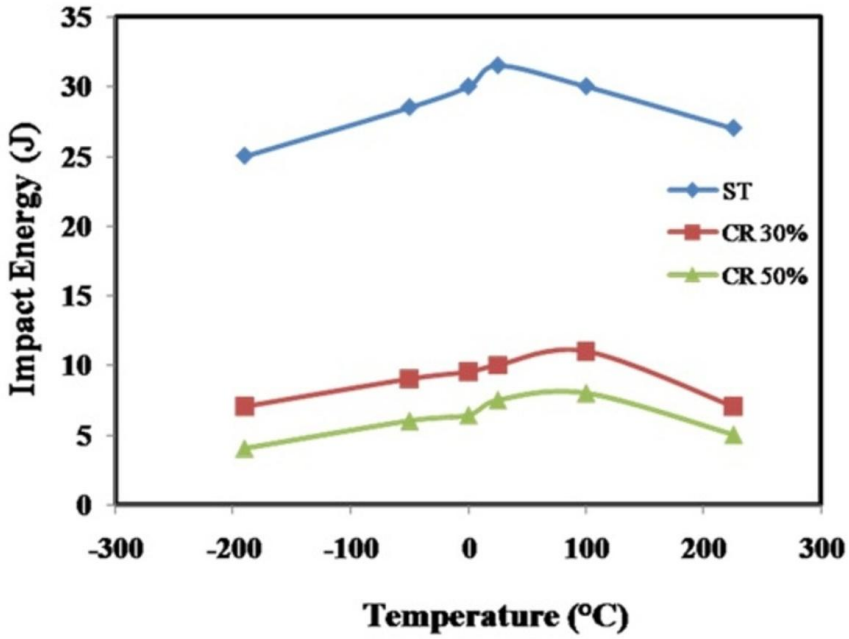

Figure 4.10: Variation in impact energy with respect to temperature of ST, CR 30% and CR 50% reduction samples.

However, brittle fractures are defined by rapid crack propagation with less expenditure of energy than ductile fractures and without considerable gross plastic deformation. In ductile materials, a crack is formed by coalescence of micro voids that form as a result of particle-matrix decohesion or cracking of second phase particle. The ST material in Figure 4.11d shows association of micro voids with Mg and Si particles. It is evident from Figure 4.11a-c that dimples formed in CR 30% reduction sample are finer and it is much finer and more in density in 50% CR samples than those formed in ST sample. Formation of fine and denser dimples may be attributed to nucleation of large number of micro voids due to severe strain induced during deformation by

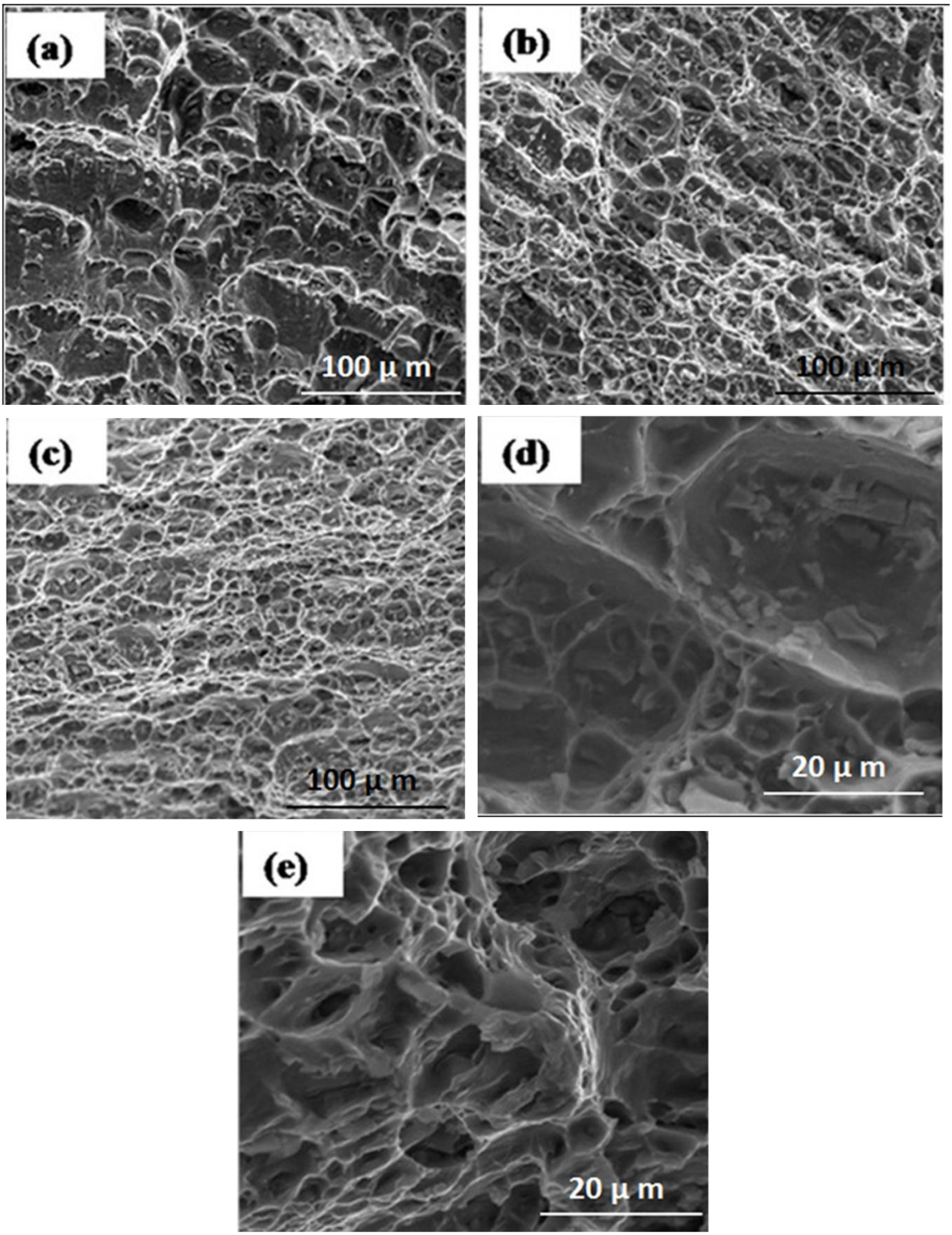

Figure 4.11: SEM fractographs of 5083 Al alloy after Charpy impact testing at room temperature, (a) ST, (b) CR 30% reduction, (c) CR 50% reduction, (d) Higher magnification of ST, (e) Higher magnification of CR 50% reduction.

cryorolling. It is mentioned that material with high strength and high ductility contribute for high fracture propagation energy, hence impact toughness is more (Stolyarov et al. 2006).

The ultimate tensile strength of CR 50% sample has increased up to 40% but the reduction in percentage of elongation is 55% compared to ST condition. Figure 4.12 shows fractographs of ST 5083 Al alloy after Charpy impact test at different temperatures. Figure 4.12a & c shows fractured morphology with significant difference in features on fractured surface at test temperatures -190 °C and 25 °C, respectively, where the sample has shown low and high impact toughness values. Sample tested at -190 °C shows rough fractured surface and displays a brittle fracture mode as shown in Figure 4.12a.

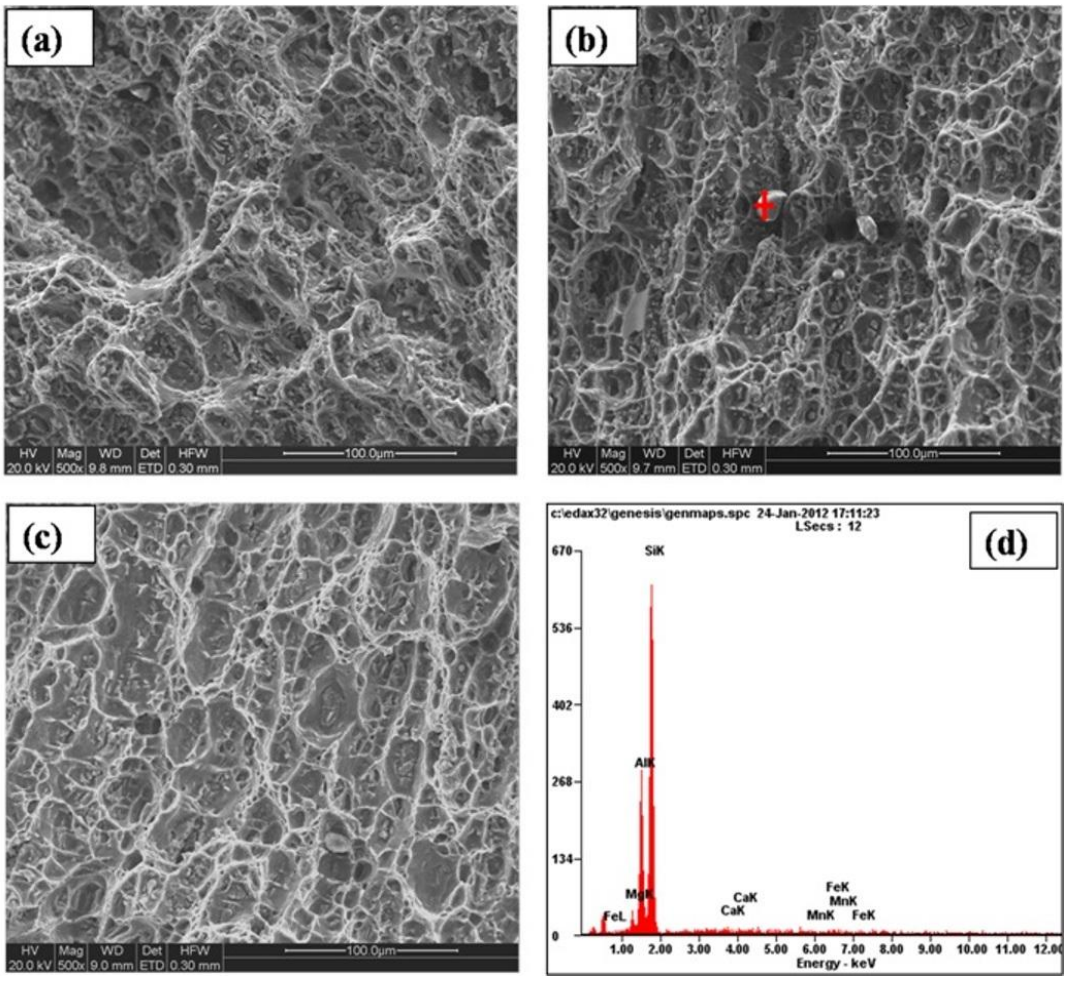

Figure 4.12: SEM fractographs of ST 5083 Al alloy after Charpy impact testing at different temperatures; (a) -190 °C, (b) -50 °C, (c) 25 °C, (d) EDAX mapping on spot taken on Figure 4.12(b).

Whereas, the sample tested at 25 °C shows equiaxed large size dimples, which resembles ductile character. Equiaxed dimple formation and growth has been observed with increasing temperature from -190 to 25 °C. The features observed in fractured surface of CR 50% are finer than ST sample in all tested temperatures as shown in Figure 4.13. This is attributed to brittle nature of CR 50% reduction.

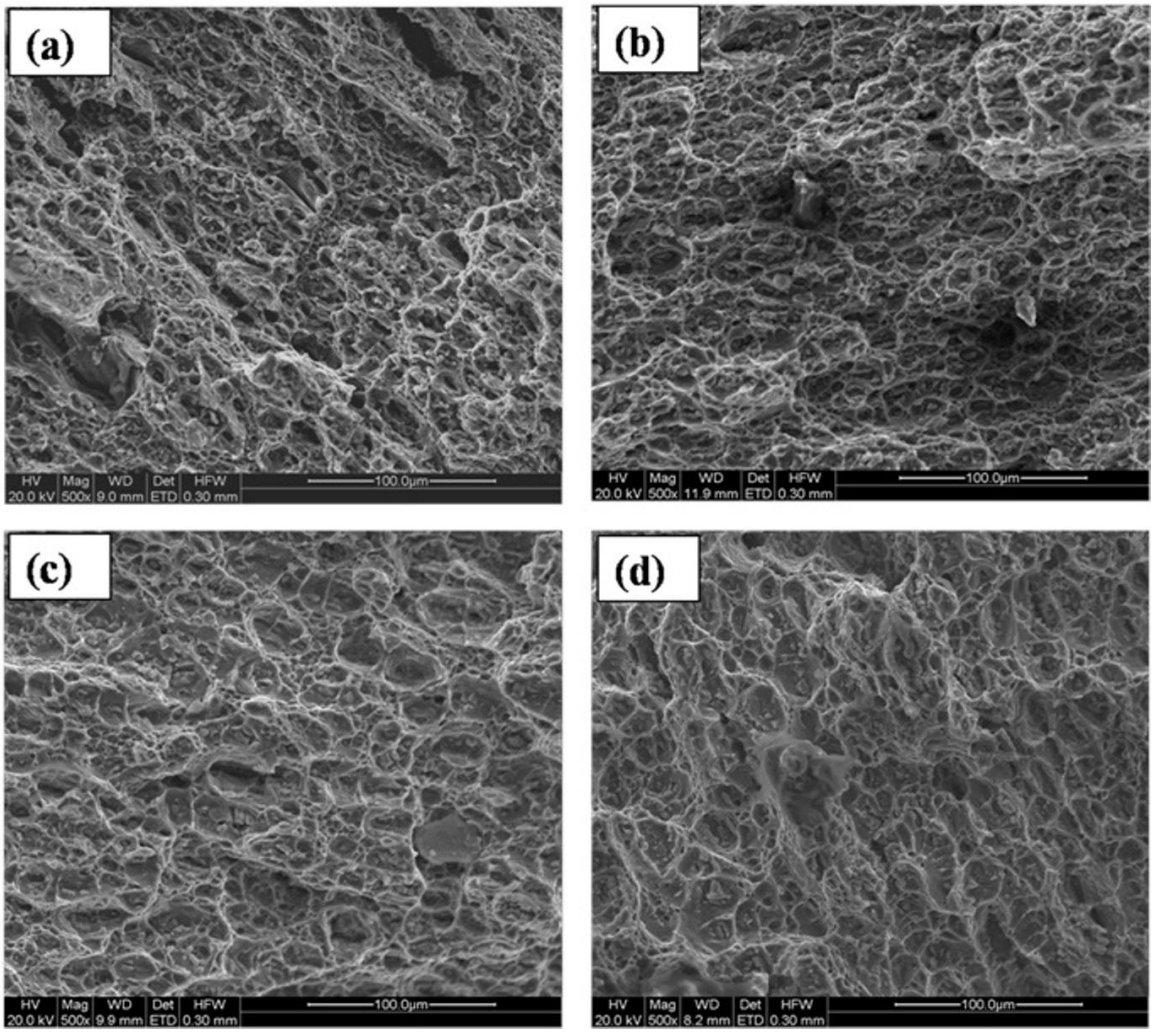

Figure 4.13: SEM micrographs of 30%, 50% cryorolled 5083 Al alloy after annealing at different temperatures for 1 hr; (a) CR 30% annealed at 200 °C, (b) CR 50% annealed at 200 °C, (c) CR 30% annealed at 250 °C , (d) CR 50% annealed at 250 °C.

4.2.3.3 Effect of annealing on microstructure

The EBSD micrographs of cryorolled 30% and 50% reduction samples after annealing at different temperatures from 200 °C to 350 °C with 50 °C intervals are shown in Figure 4.14, 4.15. In the micrographs, grey lines represents for low angle grain boundaries ($1.5° \leq 15°$) and black lines represent for high angle grain boundaries ($15° \leq$). These low angle grain boundaries are generated during deformation process. Annealing after 250 °C for 1 hr, fine crystallites along with high fraction of low angle grain boundaries were observed in both condition of the samples (Figure 4.14c, d). The fractions of low angle grain boundaries after annealing at 250 ° for 1 hr are 0.85 and 0.78 in CR 30% and 50% samples, respectively. After annealing at 300 °C for 1 hr, the observed fraction of high angle grain boundaries are 0.25, 0.55 in CR 30% and 50% reductions, respectively. Complete recrystallization is observed after annealing at 350 °C for 1 hr. The grain size distribution in CR 30% and 50% reduction after annealing at 350 °C 1 hr is shown in Figure 4.15e. CR 50% reduction sample shows an average grain size of 14 μm, whereas in CR 30%, the average grain size is 25 μm. This difference in the size of recrystallized grains after annealing may be due to the strain induced during CR 50% reduction leads to generation of more nuclei, therefore the resulting grain size is small, which can be seen from the EBSD micrograph in Figure 4.15b.

4.2.3.4 Effect of annealing on mechanical properties

In order to investigate the effect of microstructure evolved after annealing at different temperatures ranging from 150 °C to 350 °C with 50 °C interval on mechanical properties, Vickers hardness test and Charpy impact test were performed at room temperature. Figure 4.16 shows the variation in hardness with increasing annealing temperature. The initial hardness of the CR 30% and 50% reductions is 98 and 104 HV, respectively. With increasing annealing temperature, hardness has decreased slightly up to 250 °C, and suddenly dropped to nearly same value for CR 30% and 50% reductions irrespective of cryorolling strain from 250-350 °C. The sudden drop in hardness within the range 250-350 °C is due to nucleation and growth of dislocation free recrystallized grains during annealing treatment.

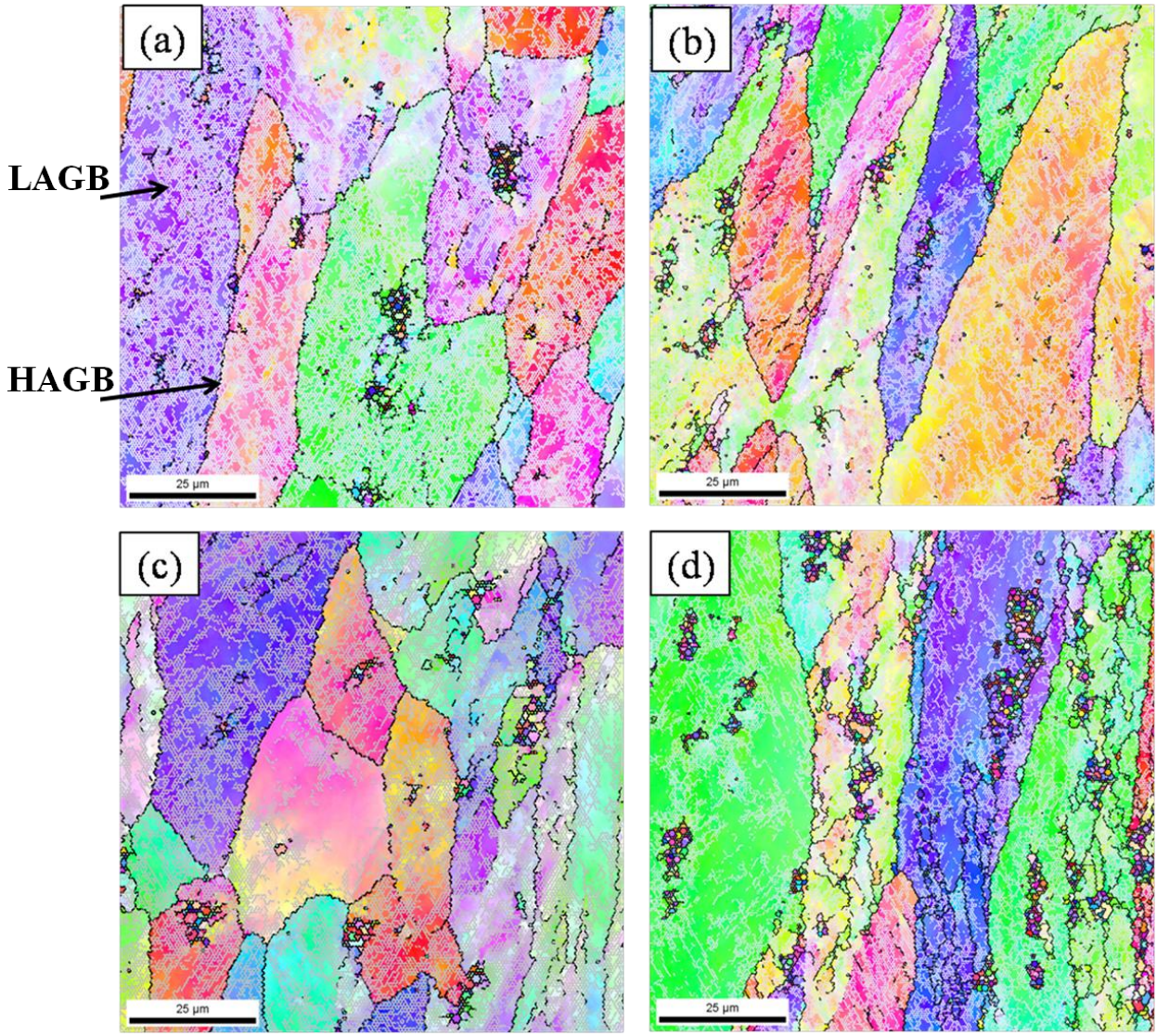

Figure 4.14: EBSD micrographs of cryorolled 30%, and 50% reductions 5083 Al alloy after annealing at different temperatures for 1 hr; (a) CR 30% annealed at 200 °C, (b) CR 50% annealed at 200 °C, (c) CR 30% annealed at 250 °C, (d) CR 50% annealed at 250 °C.

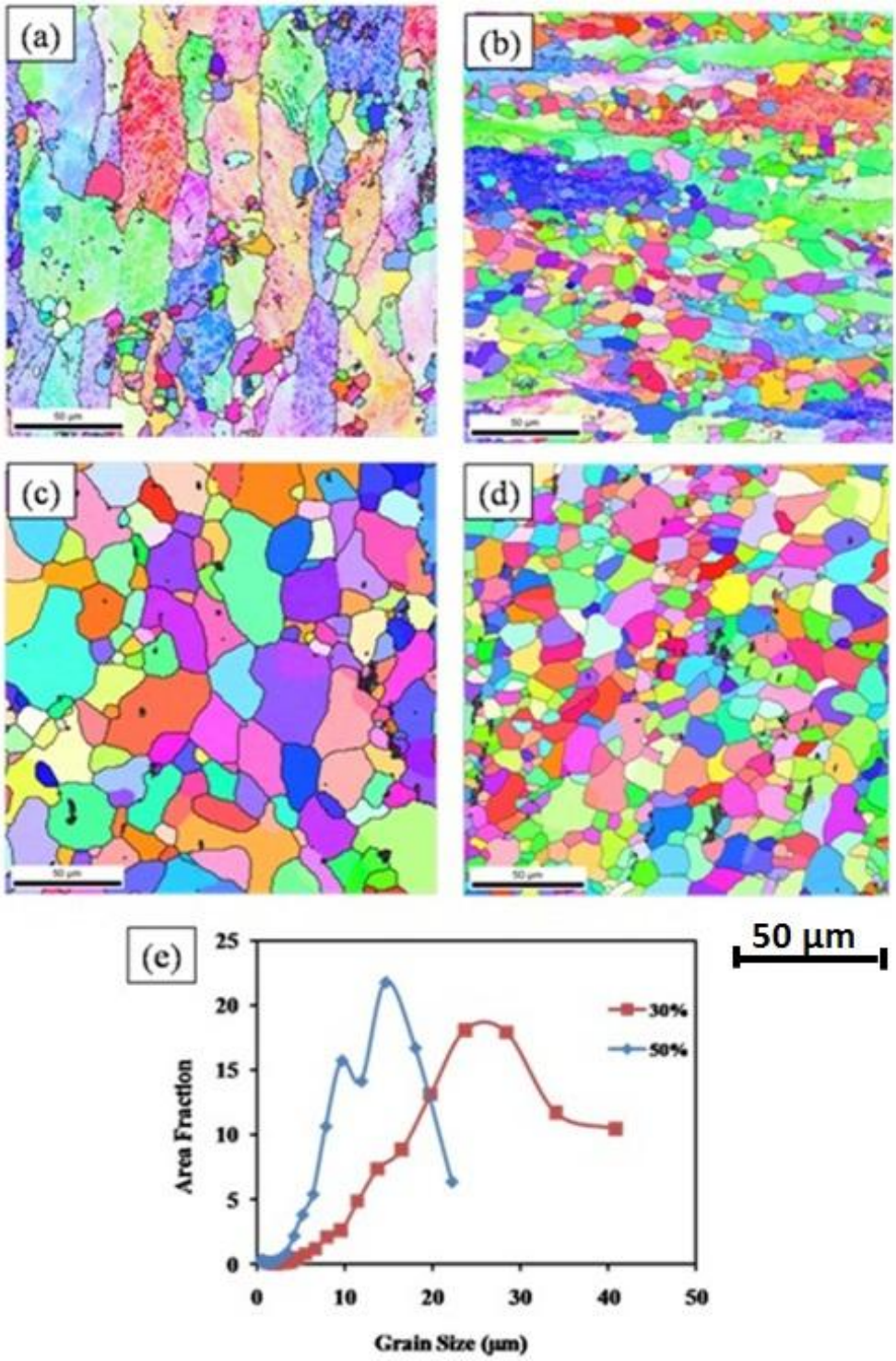

Figure 4.15: EBSD micrographs of cryorolled 30%, 50%, 5083 Al alloy after annealing at different temperatures for 1 hr; (a) CR 30% annealed at 300 °C, (b) CR 50% annealed at 300 °C, (c) CR 30% annealed at 350 °C, (d) CR 50% annealed at 350 °C, (e) Grain size distribution after annealing at 350 °C for 1 hr in CR 30% and 50% reductions 5083 Al alloy.

The variation in impact energy of CR 30% and CR 50% reduction after annealing at various temperatures is shown in Figure 4.17. With increasing annealing temperature, the energy absorption capacity of the material is gradually increased up to 250 °C due to availability of enough room created by annihilation of dislocations during recovery process in both CR 30% and 50% reduction samples to accept dislocations further. After annealing at 300 °C for 1 hr, absorbed impact energy is suddenly increased about 78.5% in CR 50% reduction sample, whereas it is 36.8% in CR 30% reduction sample. The sudden rise in impact energy of CR 50% reduction sample, upon annealing, is due to nucleation and growth of dislocation free recrystallized grains, which can absorb more amounts of dislocations before fracture. The observed impact energies of CR 30% and 50% alloy after annealing at 350 °C are slightly lower than the initial ST condition. In the literature, it was reported that ECAPed Al-Si alloy has shown improved impact toughness compared to unprocessed material (Ma et al. 2005) due to presence of large dendritic and interdendritic networks of eutectic Si plates, which could lower the toughness of the starting material. However, in the present study, the starting material is in the wrought form, where the dendritic networks are already broken. The difference in amount of increment in impact energy with respect to temperature in CR 30% and 50% reduction samples may be dependent on the number of nucleation points generated at the starting of recrystallization process. It is evident from the fractography images of CR 50% reduction and annealed samples at different temperatures shown in Figure 4.18, that there is a remarkable change in the appearance of dimple shape and size. After annealing at 300 °C, the dimple size of sample becomes larger and deeper than that of it at 250 °C.

On the other hand, the same observation is not true in CR 30% reduction sample after annealing at different temperatures as shown in Figure 4.19. The changes in the features of fractography images are gradual from CR sample to CR and annealed at 350 °C sample. This may be due to the strain imparted to material by CR 50% reduction speeds up the recrystallization phenomena, which results in nucleation of more number of fresh grains, contributing to increase in ductility and decrease in strength.

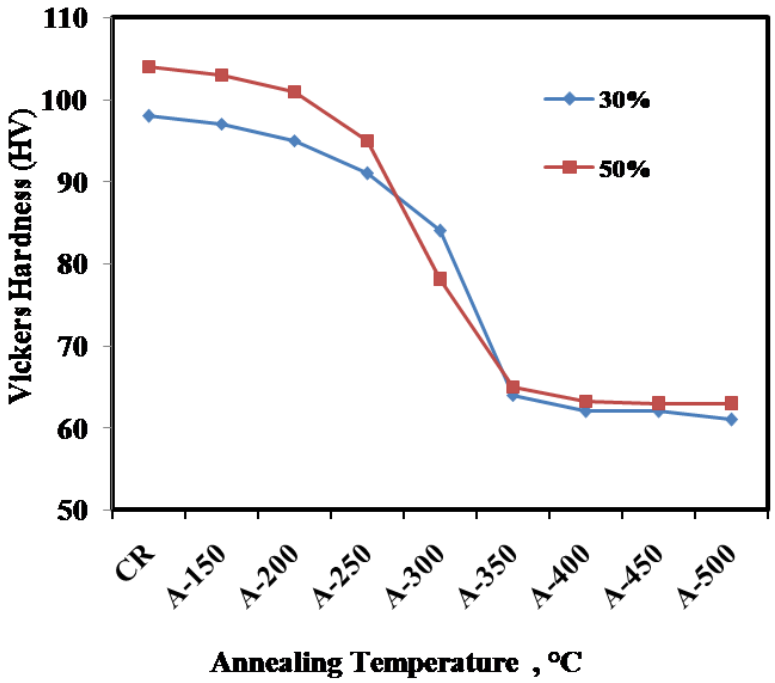

Figure 4.16: Variation in Vickers hardness of 5083 Al alloy of CR, CR and annealed at various temperatures; (a) 150 °C, (b) 200 °C, (c) 250 °C, (d) 300 °C, (e) 350 °C.

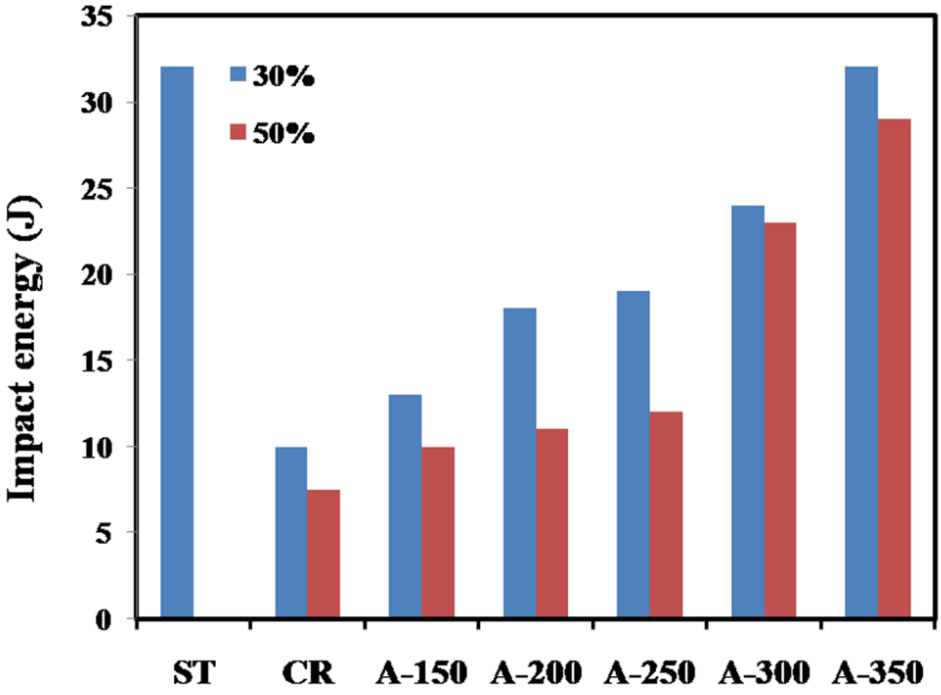

Figure 4.17: Variation in Impact energy of 5083 Al alloy of ST, CR, CR and annealed at various temperatures; (a) 150 °C, (b) 200 °C, (c) 250 °C, (d) 300 °C, (e) 350 °C.

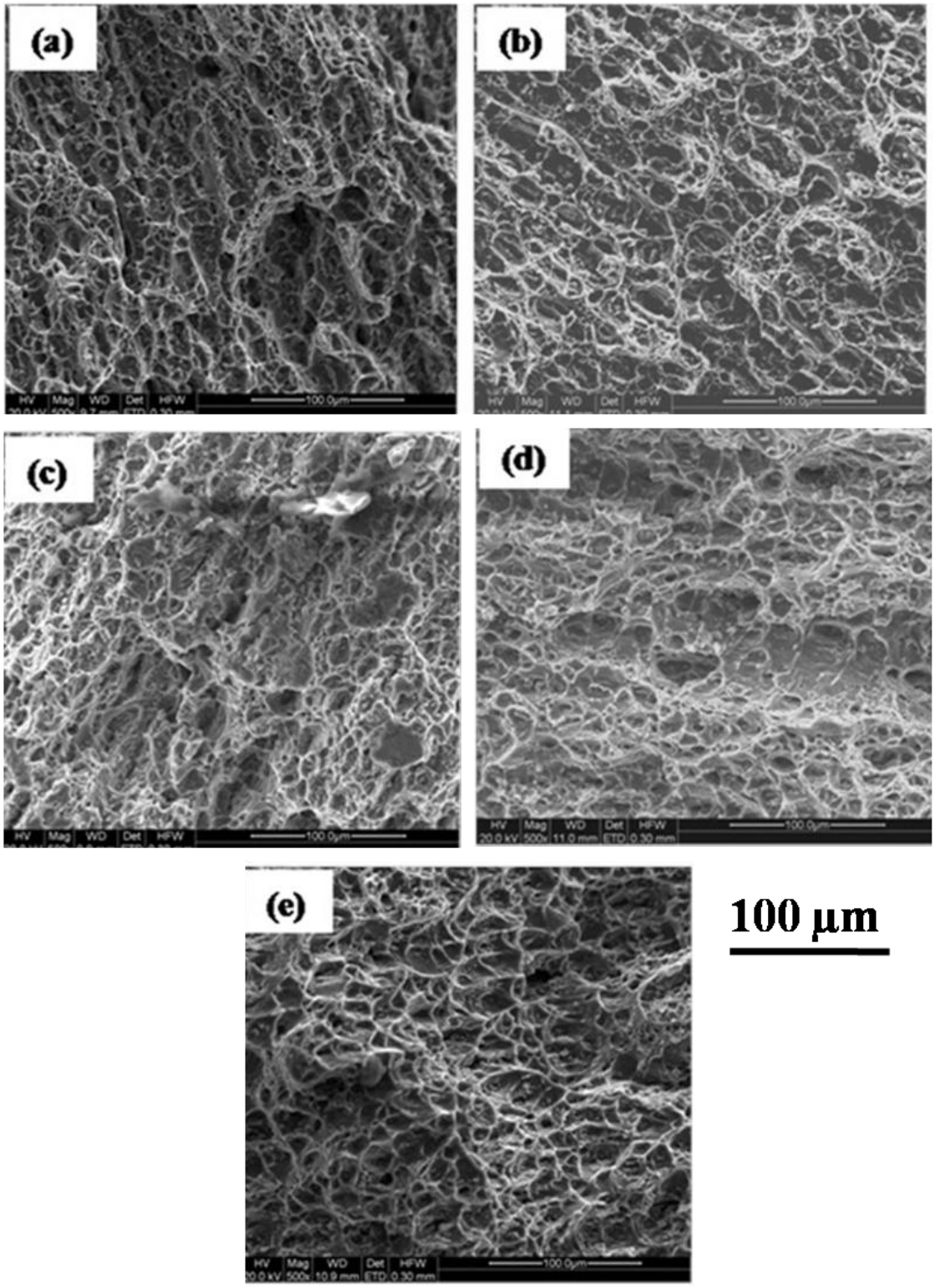

Figure 4.18: SEM fractography images of Charpy Impact tested samples of 5083 Al alloy; CR 50% reduction and annealed at various temperatures; (a) 150 °C, (b) 200 °C, (c) 250 °C, (d) 300 °C, (e) 350 °C.

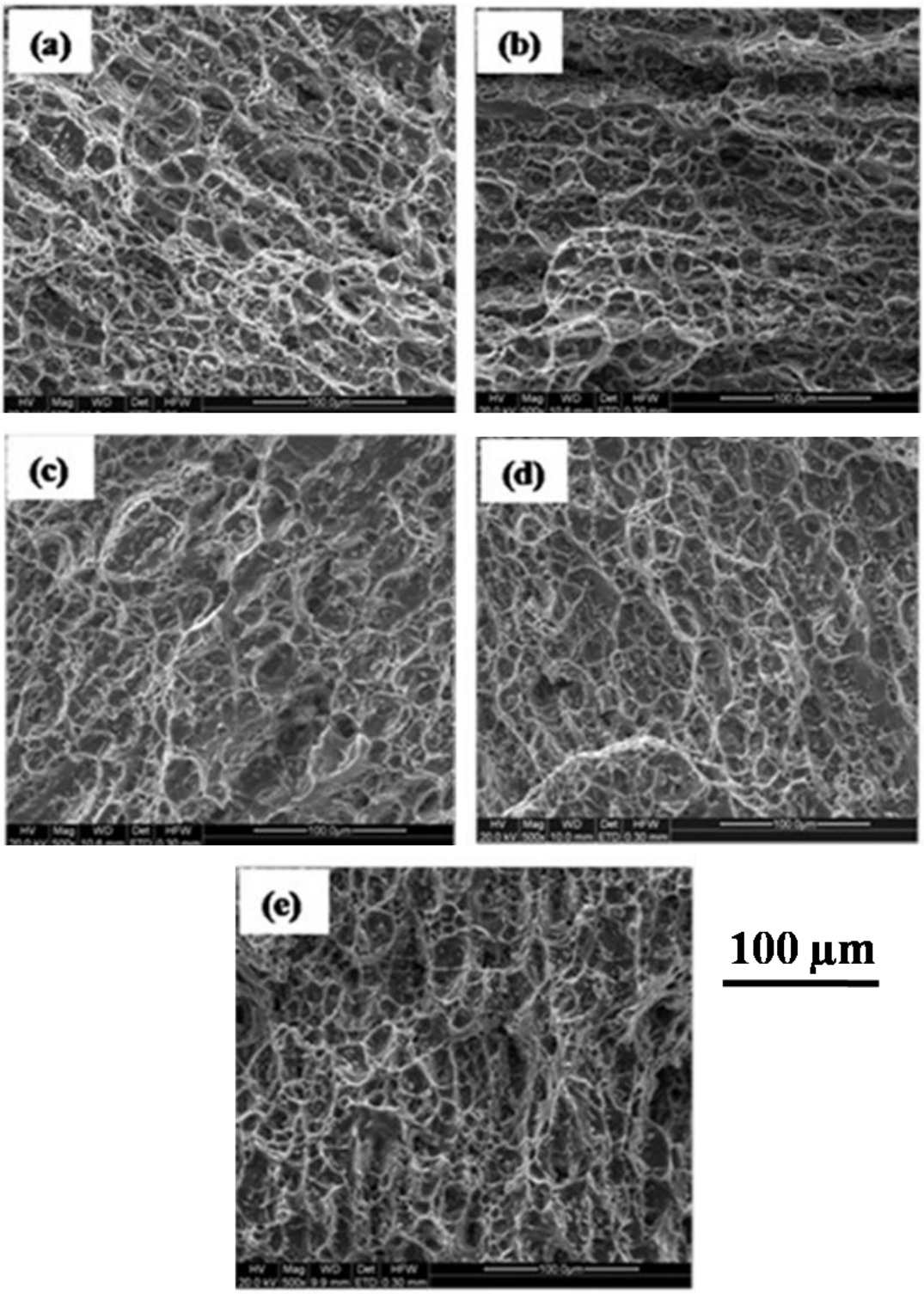

Figure 4.19: SEM fractography images of Charpy Impact tested samples of 5083 Al alloy; CR 30% reduction and annealed at various temperatures; (a) 150 °C, (b) 200 °C, (c) 250 °C, (d) 300 °C, (e) 350 °C.

As evident from the EBSD micrographs of CR 30% and 50% reduction samples (Figure 4.14 and figure 4.15) annealed at different temperatures, the trend in evolution of microstructure is similar in both conditions with increasing temperature. Significant changes were observed in microstructures of the samples annealed at 250, 300 and 350 °C. To study the effect of microstructure on impact toughness, CR 50% reduction sample annealed at 250, 300 and 350 °C were chosen.

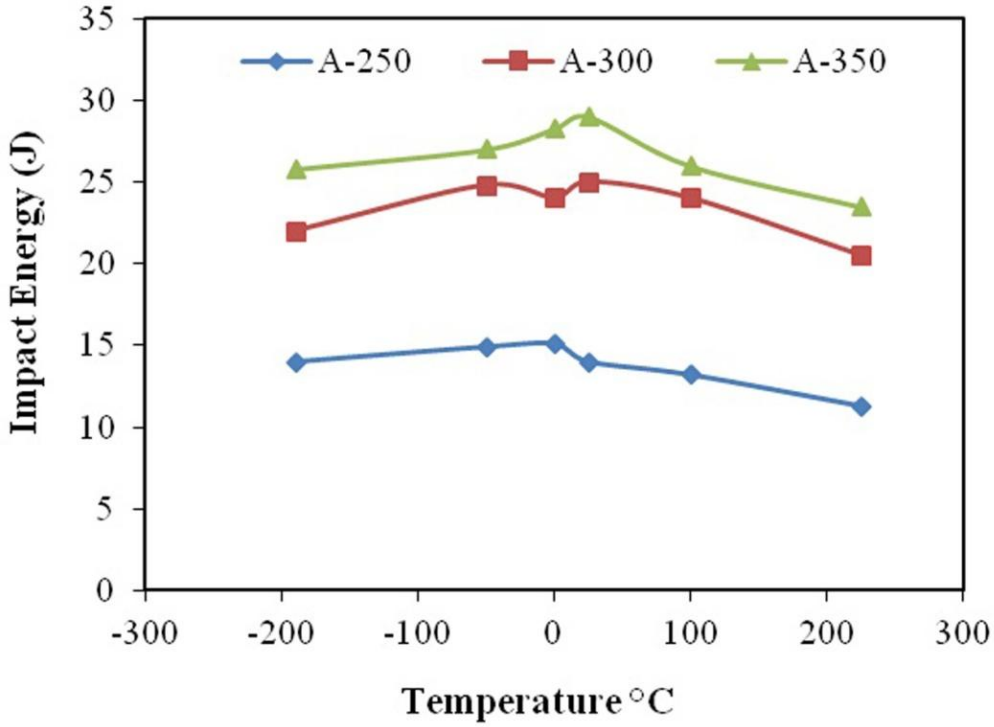

Figure 4.20: Variation in Impact energy with respect to temperature of CR 50% sample annealed at 250 °C, 300 °C and 350 °C.

Figure 4.20 shows the impact toughness as a function of temperature for samples of CR 50% and annealed at 250 °C, 300 °C & 350 °C. As shown, the behaviour of CR 50% and annealed at 250 °C, 300 °C & 350 °C is similar; there is no significant change in the trend. The drop in impact toughness of all three conditions at -190 °C is ~ 7% only. The shift in temperature of maximum impact toughness in CR 50% reductions and annealed at 300 °C needs further investigation. Sample with fully recrystallized microstructure (CR 50% reduction and annealed at 350 °C) has shown maximum impact toughness compared to the rest, at all temperatures. Impact toughness of the sample with 55% recrystallized microstructure (CR 50% reduction and annealed

at 300 °C) is slightly lower than that of the sample with fully recrystallized microstructure. Sample with CR 50% reduction and annealed 250 °C in which the fraction of low angle grain boundaries are very high (78%) has shown very low impact toughness value as compared to other two conditions at all temperatures. Reduction of grain size from 85 µm (ST sample) to 14 µm (CR 50% reduction and annealed 350 °C for 1 hr) has little effect on improving impact toughness value at room temperature. Stolyarov et al. (2006) have achieved high impact toughness in nanostructured Ti than its coarse grained counterpart at temperatures much lower than room temperatures. It has been reported that for a material to possess high impact toughness at lower temperatures, the saturation density of dislocations should be high at much lower temperatures (Wang et al. 2003, Zhu et al. 2005). This leads to higher work hardening rate, which further results in high ductility. The drop in impact toughness of the 5083 Al alloy at liquid nitrogen temperatures discussed in the present paper may be attributed to low work hardening rate and hence poor ductility at liquid nitrogen temperatures than room temperature.

4.2.4 Summary

The following conclusions are drawn from the systematic study made on effect of cryorolling and annealing temperatures on impact toughness behaviour of 5083 Al alloy.

- It is observed that there is a significant improvement in yield strength (103%) and ultimate tensile strength (40.8%) with 50% of cryorolling due to high density of dislocations.
- The percentage of elongation in 30% and 50% cryorolled samples after annealing at 350 °C 1 hr has reached up to 20.5%, 19% respectively, whereas the hardness value drops suddenly to ~ 64HV.
- The Charpy impact test results show that cryorolling has a significant effect on decreasing impact toughness of the alloy (ST - 32 J to CR 30% - 10 J) and it further decreases with increasing % of cryorolling (CR 30% - 10 J to CR 50% - 7.5 J).
- The loss in impact energy after cryorolling is due to lack of plastic deformation in the sample due to increase in yield strength, and brittle fracture as observed from SEM micrographs.
- ST samples have well developed large dimples over entire surface, whereas the dimples formed in CR 30% reduction sample are finer and it is much finer and more in density in 50% CR samples.

- After annealing at 350 °C for 1 hr, CR 50% sample shows an average grain size of 14 µm, whereas in CR 30%, the average grain size is 25 µm. The difference in the size is due to more nuclei generated during CR 50% leading to the formation of smaller grain size.
- A comparative study of impact toughness behaviour of starting solution treated material with CR 50% sample annealed at 350 °C shows that the loss in impact toughness due to cryorolling has been compensated by occurrence of recrystallization after annealing treatment (7.5 J to 28 J)**.**

4.3 Effect of deformation temperature on mechanical properties of ultrafine grained Al-Mg alloy processed by cryorolling

4.3.1 Introduction

Metals and their alloys with ultrafine grained (UFG)/nanocrystalline microstructure exhibit excellent combination of strength and ductility, and toughness as compared to bulk material. In last decade, the stringent demand to develop such materials has attracted significant research interest worldwide. To meet these demands, the material scientists and engineers are modifying the existing alloys to alter its microstructural characteristics and improve their properties or use novel processing techniques for producing ultrafine-grained/nano materials with improved mechanical properties. Cryorolling (CR) has been used popularly to produce UFG structure in aluminium alloys (Lee et al. 2004) with high density of dislocation for realizing the improved mechanical properties.

Non - heat treatable Al-Mg (5083 Al) alloy has excellent corrosion resistance, high strength to weight ratio and better formability and therefore makes it suitable for structural applications. Lee et al. (2004) have reported that cryorolling followed by subsequent annealing is effective to develop ultrafine grained 5083 Al alloy with improved strength and good ductility. A modification in process was reported by Gang et al. (2009) and Kang et al. (2010) where combined effect of Cryorolling followed by warm rolling in 5052 Al alloy on mechanical behaviour and evolution of microstructure was observed. A significant improvement in their properties was reported due to work hardening and formation of fine precipitates, and high ductility on subsequent annealing attributed to formation of equiaxed fine grains and reduction in dislocation density due to recovery. Later on Kang et al. (2012) and Rao et al. (2012) have reported the combined effect of CR followed by WR in Al 6061 alloy on mechanical behaviour and evolution of microstructure, and observed significant improvement in their properties as well as for CR followed by WR with peak aging (CR +WR + PA) samples due to precipitation of second phase particles. There is no reported literature on mechanical behaviour and microstructural evolution during combined effect of cryorolling followed with warm rolling (WR) on Al-Mg (5083 Al) alloy. Therefore, an attempt has been made in present study to investigate the combined effect of work hardening, grain refinement, and dynamic recovery on the mechanical behaviour, microstructural evolution and strengthening mechanisms of Al-Mg alloy processed by cryorolling followed by warm rolling at different temperatures (100 -200 °C).

4.3.2 Experimental procedure

Commercially available Al-Mg alloy plate with chemical composition as mentioned in Table 3.1 has been taken as starting material in the present work. The schematic illustration of cryorolling (CR) and warm rolling (WR) process is shown in Figure 3.2 in Chapter 3. Samples after machining to required dimension and solution treatment were deformed at liquid nitrogen temperature up to 50% and 90% reduction. Cryorolled samples with 2.3 true strain deformations are denoted as CR. Room temperature rolled samples up to 90% reduction are denoted as RTR. Cryorolled samples upto 50% reduction were further deformed at 100 °C, 145 °C, 175 °C and 200 °C by using oil bath furnace upto total reduction of 90%. Soaking time given for each pass was 4 min and these samples are denoted as cryorolled followed by warm rolled (WR) samples. The total reduction achieved was 90% (equivalent true strain of 2.3) and the reduction per pass was 4%. Samples were rolled on two high mill having rolling speed and roll diameter of 8 rpm and 110 mm, respectively. Mechanical behaviour was investigated by performing tensile test and Vickers hardness test at room temperature. From the hardness data, WR at 175 °C was selected which has shown maximum hardness for further analysis. In order to investigate the microstructure and thermal stability of selected condition (WR at 175 °C), samples were annealed between temperature range 150-300 ˚C for 1 hr in a muffle furnace.

Microstructure of starting material, CR and WR was characterized through Electron Back Scattered diffraction analysis (EBSD) and Transmission Electron microscopy (TEM). All microstructure observations were made at the mid-thickness of the rolled specimens. In EBSD scans, step size 0.1 µm is used for all the samples. In order to investigate the thermal behaviour of CR and WR samples, differential scanning calorimetry (DSC) was performed under nitrogen atmosphere using Perkin Elmer Paris Diamond DSC. The scan rate used in the current study was 25 °C/min. Sample dimensions and its preparation, rolling procedure, sample preparation for mechanical testing and for EBSD, TEM, DSC, XRD characterization techniques are discussed in Chapter 3.

4.3.3 Results and discussion

4.3.3.1 Effect of warm rolling on mechanical properties and microstructure evolution

The Vickers hardness of starting material after solutionizing and water quenching is 58 HV. After deformation at liquid nitrogen temperature (CR) up to true strain of 2.3 (90% reduction), the hardness has increased from 58 HV to 127 HV. The hardness of RTR sample has increased from

58 HV to 122 HV, but this value is 5 HV less than CR sample for same deformation strain. The increase in hardness of CR sample is due to the microstructure refinement occurred during cryorolling. To investigate the effect of warm rolling on cryorolled samples, warm rolling was performed at different temperatures of 100, 145, 175, 200 °C on 50% cryorolled samples up to 90% reduction. The effect of cryorolling followed by warm rolling (WR) performed at various temperatures on hardness of 5083 Al alloy is shown in Figure 4.21. WR performed at 100 °C has shown hardness value of 134 HV, which is 7 HV more than CR condition. With further increase in WR temperature up to 175 °C, the hardness value has increased to 146 HV and on WR at 200 °C, the hardness has decreased to 138 HV. Microstructural evolution and mechanical behaviour of CR alloy are discussed in previous sections, and described here for comparison purpose.

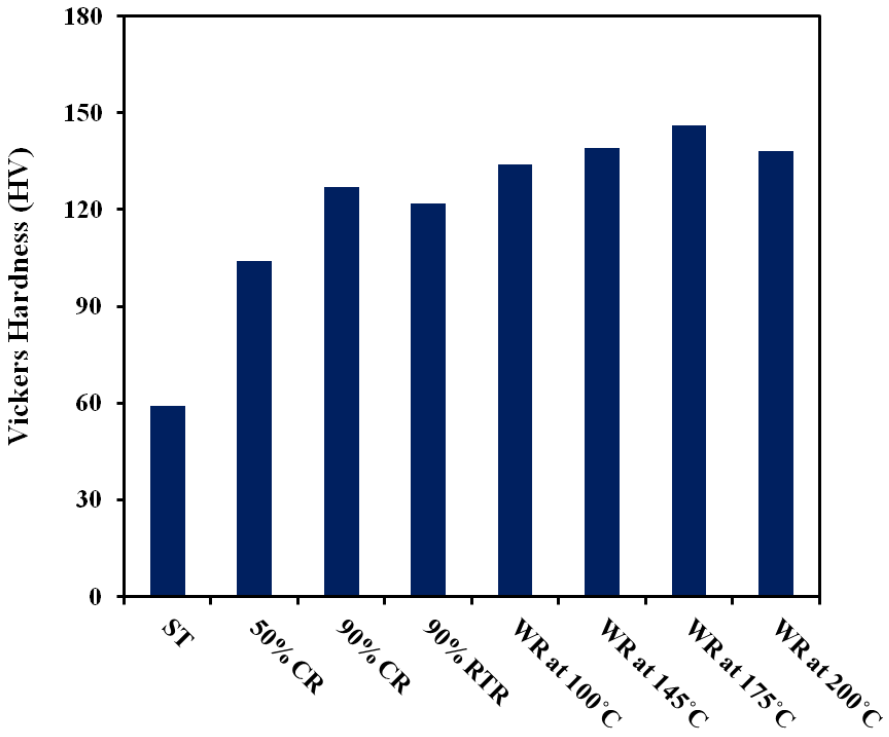

Figure 4.21: Variation in hardness with respect to rolling condition.

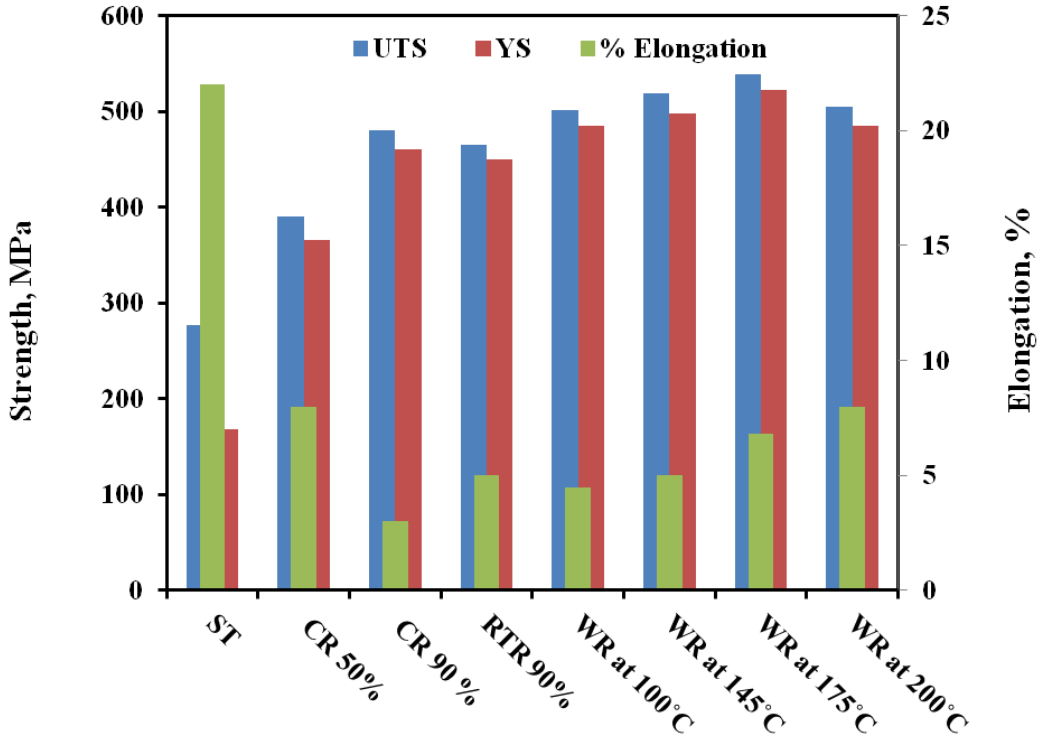

Figure 4.22: Variation in UTS, YS, and elongation with respect to rolling condition.

The ultimate tensile strength (UTS) and yield strength(YS) of starting solution treated material has significantly improved after cryorolling up to 90% reduction (UTS- 277 to 478 MPa, YS-168 to 460 MPa), but its elongation to failure has decreased from 22% to 3% (Figure 4.22), which is distinctive behaviour of cold worked samples. Whereas, after RTR up to 90% reduction, the UTS and YS has improved to 465 MPa and 450 MPa, respectively, which is less than CR , but the elongation observed was 4.0% (1% more than CR). This may be due to softening occurred during RTR and the temperature was not sufficient for precipitation to occur. Warm rolling of 50% cryorolled sample at 100 °C has increased not only tensile strength but also ductility (Figure 4.22b). With increasing warm rolling temperature from 100 °C to 175 °C, simultaneous improvement in strength and ductility is observed. The further increase in warm rolling temperature to 200 °C led to increase in elongation to failure, but decrease in its tensile strength. The ultimate tensile strength achieved in WR sample at 175 °C is (539 MPa) is nearly two times more than that of ST sample (277 MPa) and 13% more than CR sample. Furthermore, the elongation to failure in WR sample at 175 °C is 6.8%, which is more than CR sample (3%). The improvement in mechanical properties achieved in 5083 Al alloy through cryorolling followed by warm rolling are similar to earlier reported results on Al 6061 alloy (Rao et al. 2012). Kang et al.

(2010) have reported formation of fine precipitates, during warm rolling, leading to significant improvement in mechanical properties observed in Al 5052 alloy.

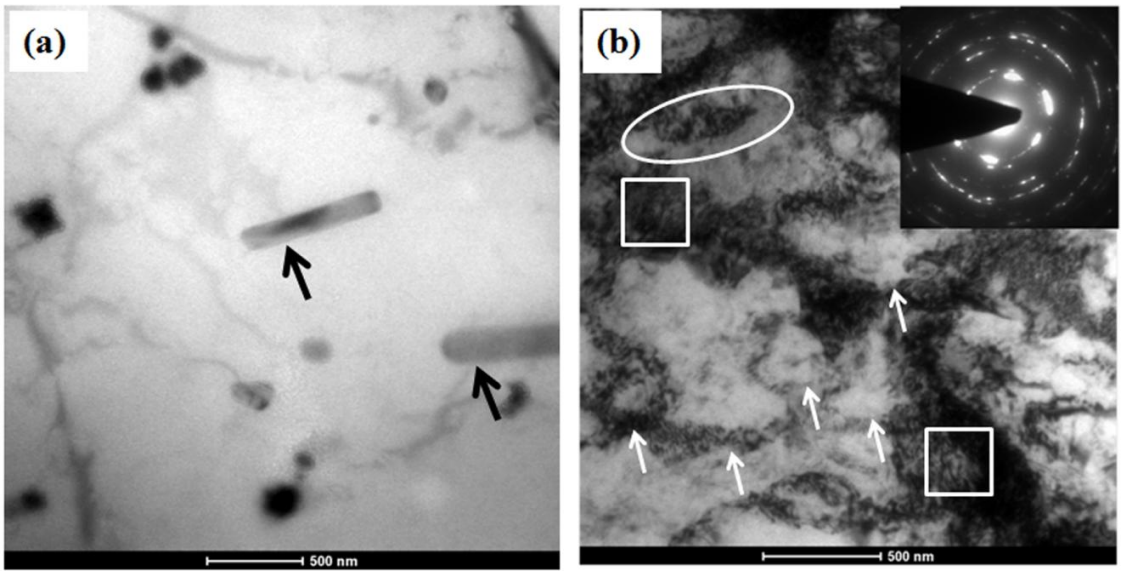

Figure 4.23: TEM micrographs of 5083 Al alloy; (a) Solution treated (ST), (b) Cryorolled 90% reduction (CR).

From the hardness and tensile testing data, it is reasonable to state that to achieve better strength and ductility in 5083 Al alloy, cryorolling followed by warm rolling at 175 °C is an optimum condition. Therefore, CR and WR samples at 175 °C were considered for further study. The mechanical behaviour of CR and WR samples can be well realized by examining the microstructural changes. WR at 175 °C sample has been chosen for detailed microstructural study. The optical microstructure of as received material consisting of equiaxed grains after solutionizing treatment is shown in Figure 4.1, the average grain size was found to be 85 µm. In Figure 4.23a, TEM micrograph of ST material reveals existing of rod shaped intermetallic particles of Al_6Mn, which is evident from XRD analysis of ST sample as shown in Fig. 4.24. These are in accordance with the findings on 5083 Al alloy annealed at 450 °C and water quenched (Lee et al. 2012). The existence Al_6Mn intermetallic phase even after solutionizing treatment may be due to the low diffusion rate of Mn, which requires high temperature and long annealing time to dissolve completely in to the matrix (Warmuzreka et al. 2004). Figure 4.23b shows the TEM bright field micrograph of CR sample and corresponding SAED pattern (in inset) after undergoing deformation up to true strains of 2.3. From the bright field micrograph and SAED pattern of the CR sample, it is clear that the refinement of initial microstructure has occurred. The diffraction pattern shows

diffused rings indicating formation of low angle grain boundaries. It is evident from bright field micrograph of CR sample that number of fine dislocation cells (indicated with arrow marks in Figure 4.23b), and sub-grains (indicated with oval in Figure 4.23b) along with dislocation tangle zones (indicated with squares in Figure 4.23b) are observed. Figure 4.25a gives the clear evidence of accumulation of dislocations around the second phase Al_6Mn particle. High dislocation density areas can be seen around the particle. SAED pattern (Figure 4.25b) of Figure 4.25a is taken with an aperture size of 500 nm. The increase in hardness and strength of CR sample can be attributed to grain refinement and increase in dislocation density. The dislocation density of the CR material has increased with increasing rolling strain. There are two factors contributing to enhancement of the dislocation density; i) Effective suppression of dynamic recovery during rolling at liquid nitrogen temperature, ii) Presence of undissolved second phase before cryorolling effectively increased the dislocation density by pinning dislocations around them (Cheng et al. 2007).

Figure 4.26a-e corresponds to the TEM micrographs of the samples subjected to 50% cryorolling and cryorolling followed by warm rolling (WR) at 175 °C. Figure 4.26a shows nearly equiaxed dislocation cell structure after cryorolling up to 50% reduction. These dislocations cells are formed from dislocation tangled structure with increasing strain. These cells further subdivide in to cell blocks by formation of dense dislocation walls with increasing strain (Bay et al. 1992). Figure 4.26b shows the bright field TEM micrograph of WR at 175 °C sample with an average grain size of 100-200 nm and the corresponding SAED pattern is shown in Figure 4.26c. The ring pattern formed in SAED image indicated existence of sub grains with high angle grain boundaries. It is mixture of low angle and high angle grain boundaries. The subgrain structure has developed in WR sample from dislocation cell structure, observed in CR 50% reduction sample is due to annihilation of dislocations through static recovery(during soaking time in the furnace), dynamic recovery (during rolling at warm temperature), and dislocation generation due to deformation occurring simultaneously at warm temperature.

Figure 4.26d shows the big second phase particles (marked as S) surrounded with sub grains (marked with number from 1-7). Figure 4.26e shows the fragmentation of second phase, which is shown with white line and black arrow. More subgrains are observed in WR samples, unlike CR sample, where dislocation cells and dislocation tangled zones are dominant features.

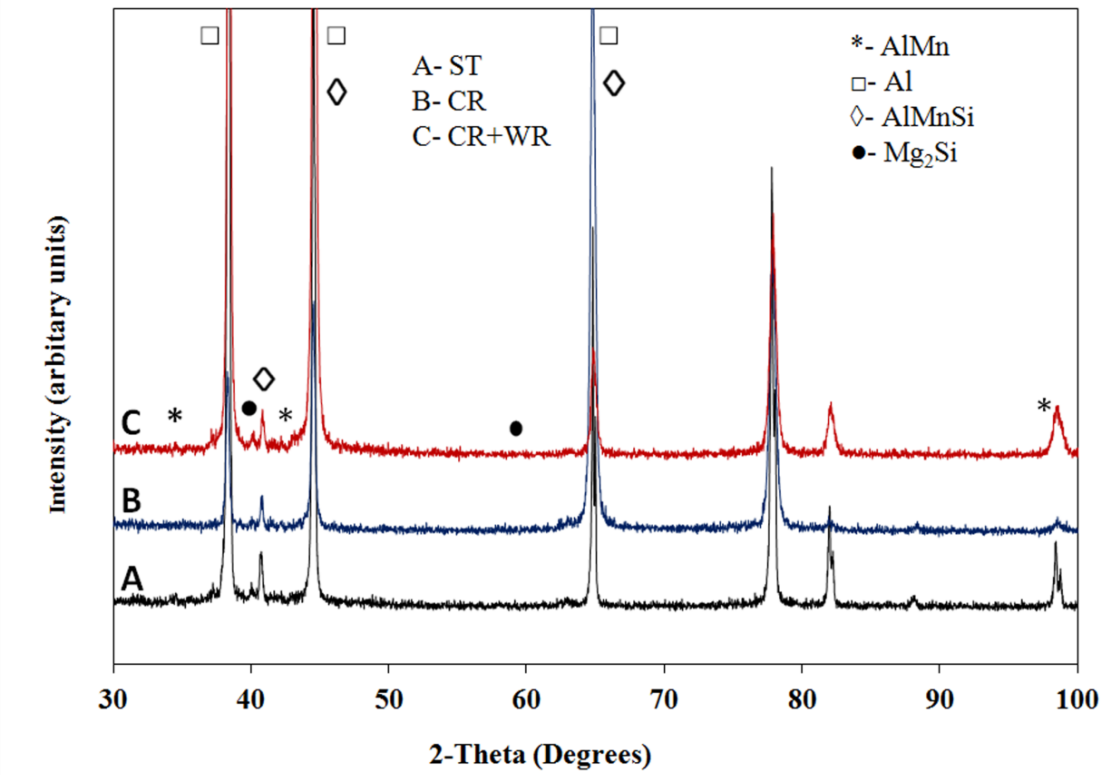

Figure: 4.24: XRD plots of 5083 Al alloy; (a) ST, (b) CR 90% reduction, (c) WR 90% reduction.

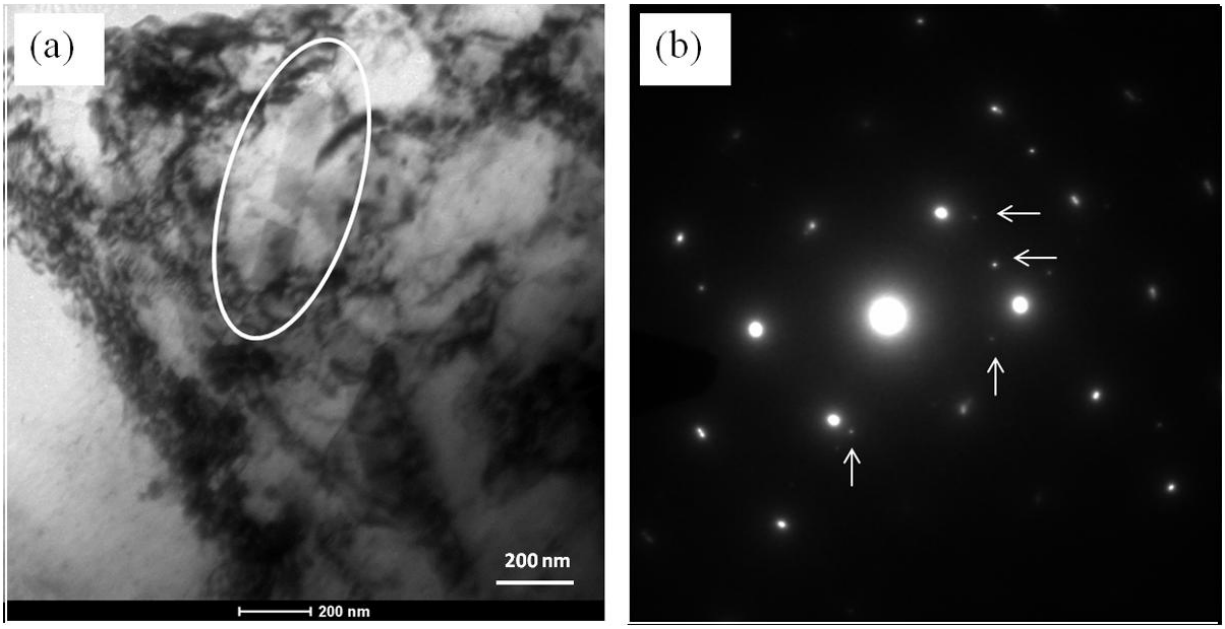

Figure 4.25: TEM micrographs of 5083 Al alloy; (a) CR 90% reduction, (b) SEAD image of CR.

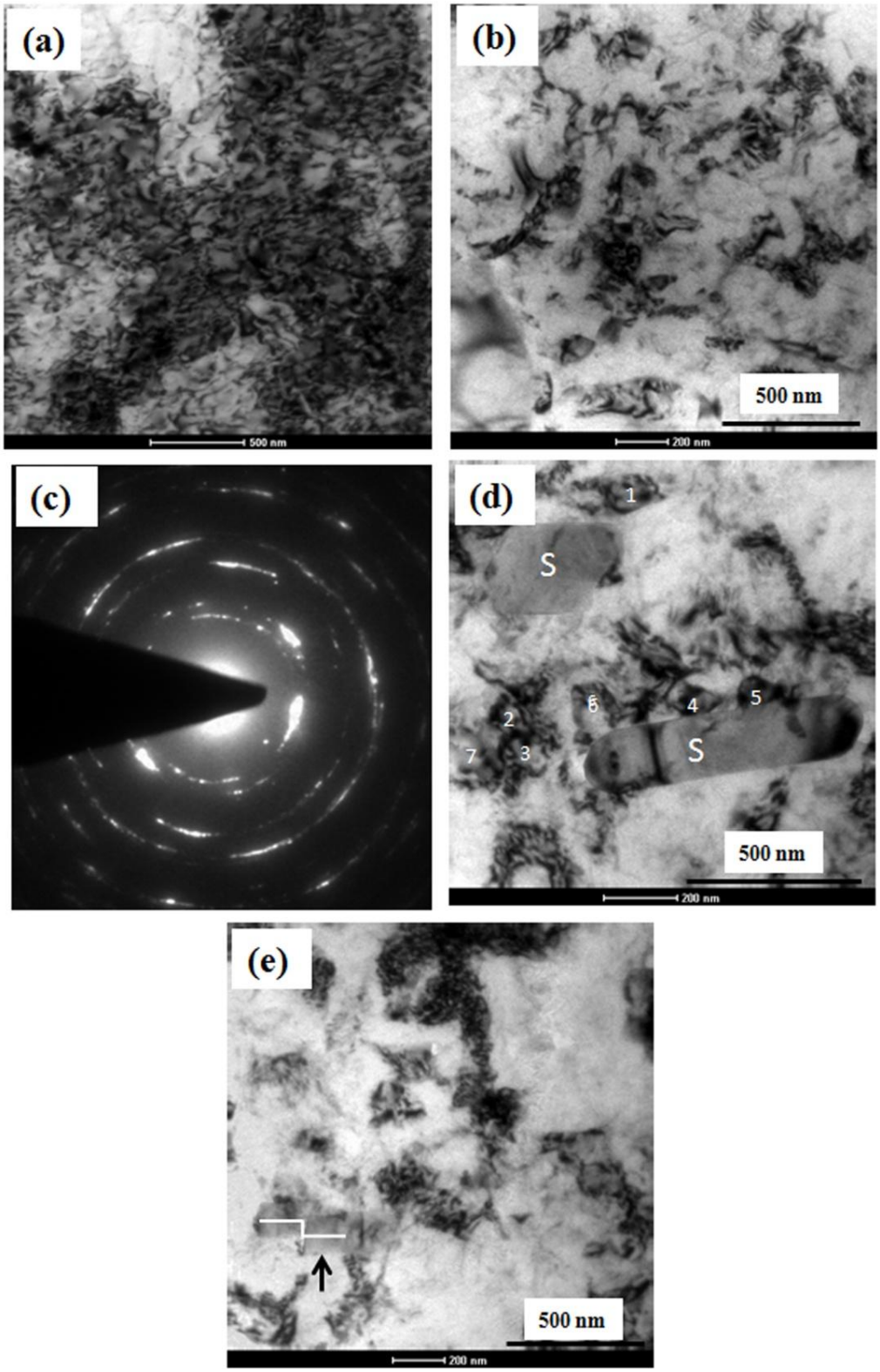

Figure 4.26: TEM micrographs of 5083 Al alloy; (a) CR 50% reduction, (b) WR at 175 °C, (c) SEAD pattern of image(b), (d) WR at 175 °C showing subgrain structure, (e) Fragmented second phase particle observed in WR at 175 °C.

The dislocation density of WR samples has decreased due to dynamic recovery during the WR process. Still there are dislocations observed within the grains, which are not annihilated during warm rolling, which are seen in Figure 4.26d. The grain refinement achieved in WR sample can be attributed to the following phenomenon occurring simultaneously during warm rolling: i) Annihilation of dislocations through dynamic recovery, ii) Continuous generation of dislocations through deformation, iii) Evolution of fine precipitates through dynamic ageing effect, iv) Accumulation of dislocations by precipitate - dislocation interaction.

The increase in percentage elongation to failure of WR sample is attributed to decrease in dislocation density and subgrain formation due to dynamic and static recovery during warm rolling process. Even though the decrease in dislocation density of warm rolled sample, which is clearly evident from increment in percentage elongation to failure, significant improvement in yield and ultimate tensile strength is shown. The reason for this unusual behaviour of the warm rolled material is due to the formation of fine precipitates during warm rolling as reported in the literature (Gang et al. 2009). 5083 Al alloy is typical non-heat treatable alloy where magnesium is the primary alloying element in 5xxx series, which imparts strength to the material by forming solid solution. The maximum solubility of the Mg in Al at room temperature is 2% and 14-15% at 447 °C. The starting material in the present investigation was solution treated and water quenched.

Magnesium is completely dissolved into the matrix by diffusion and supersaturated solid solution is developed after quenching immediately to room temperature. To understand the thermal behaviour of WR 5083 Al alloy, DSC measurements were performed. Figure 4.27 shows DSC plots of CR and WR samples at 175 °C performed with heating rate of 25 °C/ min. Two exothermic peaks were observed at 219 °C and 319 °C, where the peak positions are almost identical in both the conditions. Osamura et al. (1984) have carried out resistivity measurements in Al-4.64 Mg wt %, and reported the precipitation sequence as SSSS-G.P zones→ β” → β' → β, where β is an equilibrium phase (Al_3Mg_2) having f.c.c structure. Thermal analysis of Al-Mg alloy reported by Starnik et al. (1998) shows that the formation of β' with exothermic peak occurs between 180-290 °C and transformation of β' to β with an exothermic peak occurs between 280-330 °C. Whereas, Lee et al. (2012) have reported formation of two endothermic peaks (at 294 °C and 360 °C) and one exothermic peak (at 340 °C), where the two endothermic peaks corresponds to β' formation and β dissolution, one exothermic peak corresponds to transformation of β' to β for the 5083 Al alloy processed by ECAP. DSC plot of CR sample shown in Figure 4.28 reveals first exothermic DSC peak at 219 °C, due to the formation of β' and second exothermic peak at 319 °C

corresponds to transformation of β' to β. Exothermic peak positions observed in our results are similar to reported literature (Starnik et al. 1998). The position of the DSC peak also depends on the temperature scanning rate (Zhou et al. 2003). From the DSC plot of WR sample as shown in Figure 4.27, the intensity of both exothermic peaks are comparatively smaller than CR sample.

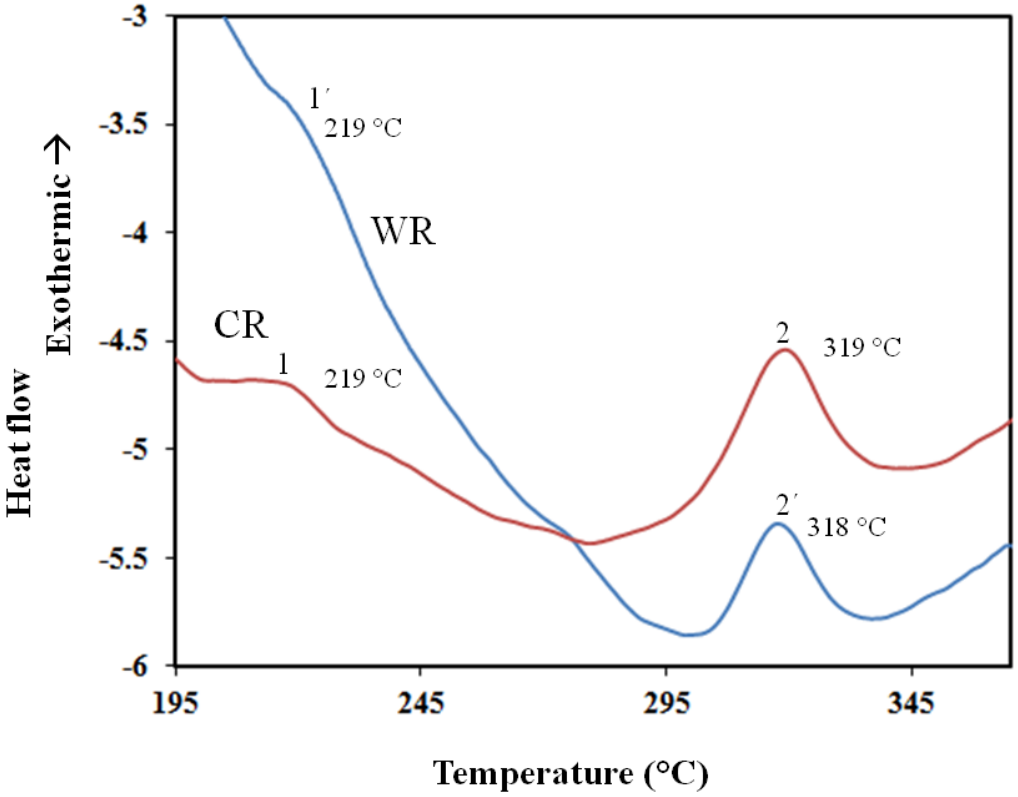

Figure 4.27: DSC curves of 5083 Al alloy at the heating rates of 25 °C/min; (a) CR, (b) WR at 175 °C.

Due to the already formed precipitates during warm rolling at 175 °C, it led to suppression of the first exothermic peak at 219 °C in WR sample, which in turn showed improvement in mechanical properties of WR sample. Another possibility of formation of exothermic peaks in severely deformed sample is due to recovery and recrystallization. Kang et al. (2010) have measured the activation energy of the peaks, which are reasonably matching with the recovery and recrystallization activation energies in Al-Mg alloys (Kang et al. 2010, 2012). The enthalpy value associated with recrystallization phenomenon of CR (0.99 mj/mg) is higher than that of WR at 175 °C (0.55 mj/mg) sample. This implies that stored strain energy of CR sample is higher than that of the WR (175 °C). Plastic deformation at cryogenic temperature generates high dislocation density, which has significant effect on stored strain energy (Zhou et al. 2003, Hirth et al. 1982). The

improvement in strength and hardness of cryorolled sample is purely due to increase in dislocation density, during cryorolling process, due to effective suppression of cross slip or climb of dislocation associated with dynamic recovery. The lower enthalpy value associated with recrystallization peak in WR at 175 °C indicates decrease in dislocation density during warm rolling, which reflects the improvement in ductility (6.8%). The improvement in strength and hardness of WR at 175 °C is due to the combined effect of precipitation and dislocation strengthening mechanisms (Kang et al. 2010, 2012, Rao et al. 2012, Gang et al. 2009).

4.3.3.2 Effect of annealing on microstructure and mechanical properties

In order to investigate the thermal stability of microstructure and mechanical properties 5083 Al alloy processed through WR at 175°C, the samples were subjected to annealing at different temperatures such as 150 °C, 200 °C, 250 °C, 275 °C, and 300 °C for 1 hr. The EBSD micrographs of WR at 175 °C of 5083 Al alloy subjected to annealing at different temperatures are shown in Figure 4.28. During recovery or recrystallization, formation of very fine subgrains are observed through TEM analysis (Figure 4.29) of respective EBSD micrographs of the samples shown in Figure 4.28. These fine subgrains were not observed in EBSD micrographs due to the limitation of grain size and dislocation density observable in EBSD technique. To generate meaningful results through EBSD technique, it requires sufficient grain coarsening leading to measurable diffraction patterns (Mani Krishna at al. 2008). In Figure 4.28, low angle grain boundaries are shown in black line and high angle grain boundaries are shown in white lines. With increasing annealing temperature, the length of low angle grain boundaries is decreasing and the length of high angle grain boundaries is increasing, listed in Table 4.1. To find the fraction of recrystallization, during annealing, grain orientation spread (GOS) between 0-1 is used as criteria (Mani Krishna et al. 2008). Figure 4.29a-b shows the TEM micrograph of WR at 175 °C sample after annealing at 150 °C for 1 hr. In Figure 4.29a, formation of elongated sub grains (indicated with number 1-3) with an average width of 170 nm was observed. Within the sub grains, arrow marks indicates dislocation arrays and circled area indicates formation of fringes. Figure 4.29b shows the enlarged view of area marked with square in Figure 4.29a. White dotted line in Figure 4.29b indicates the subgrain boundary. The dislocation density inside the sub grains are reduced and the tangled thick cell walls became more regular dislocation arrays after annealing at 150 °C as shown in Figure 4.28a (Humphreys et al. 2004). Through EBSD, the fraction of recrystallized grains is observed as 3% (Figure 4.32), which is very low and micro structural changes occurred

predominantly due to recovery at 150 °C, annealing temperature. The reduction in dislocation density, which has been reflected in hardness and tensile properties, is shown in Figure 4.30.

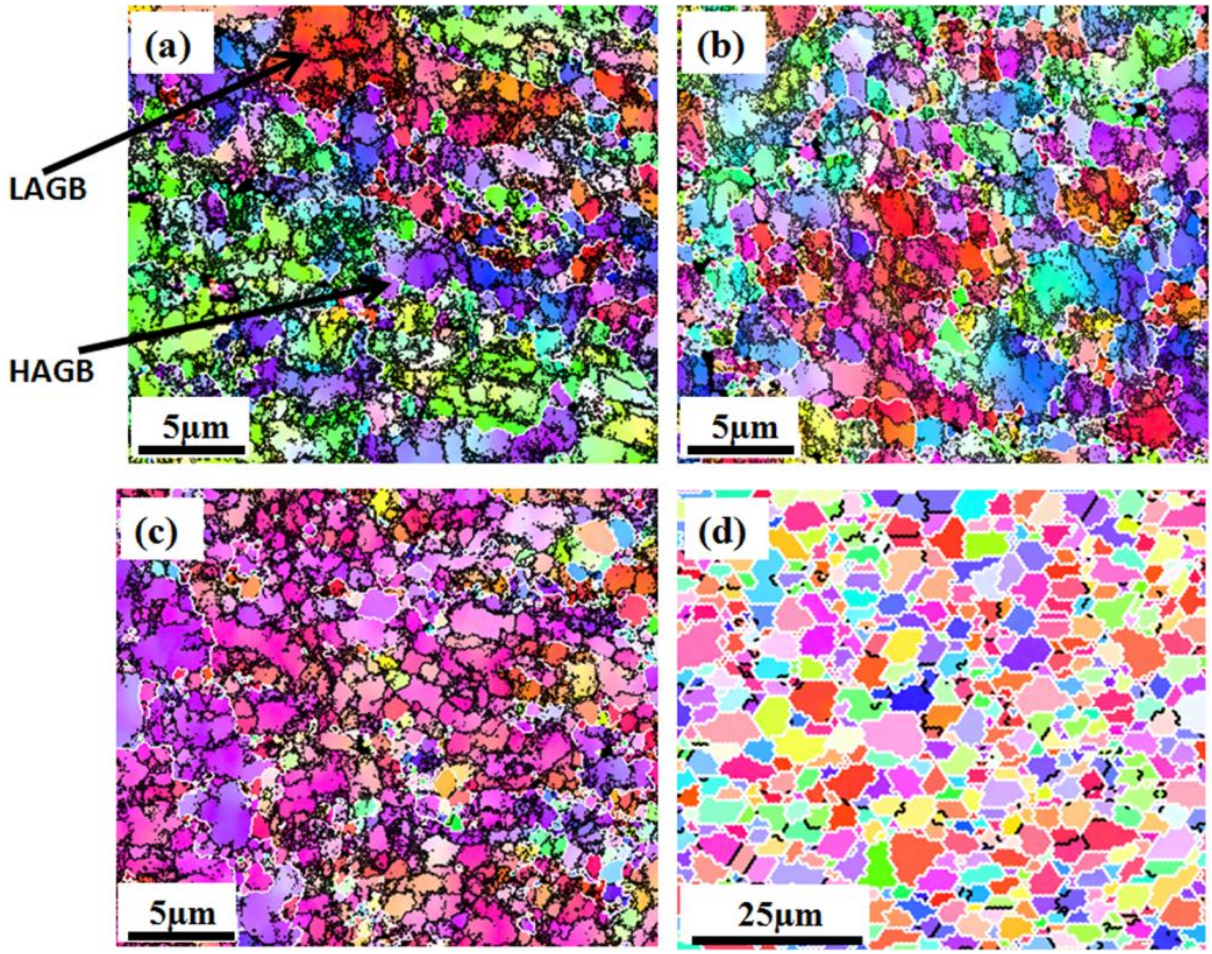

Figure 4.28: EBSD micrographs of 5083 Al alloy WR at 175 ˚C, annealed at temperatures; (a) 150 °C, (b) 200 °C, (c) 250 °C, (d) 275 °C.

Table 4.1: Total length fraction of LAGB and HAGB

Condition	High angle grain boundary length	Low angle grain boundary length
Annealed at 150 °C	458.88 microns	3.04 mm
Annealed at 200 °C	685.72 microns	2.68 mm
Annealed at 250 °C	638.78 microns	2.60 mm
Annealed at 275 °C	5.22 mm	547.91 microns
Annealed at 300 °C	4.24 mm	923.47 microns

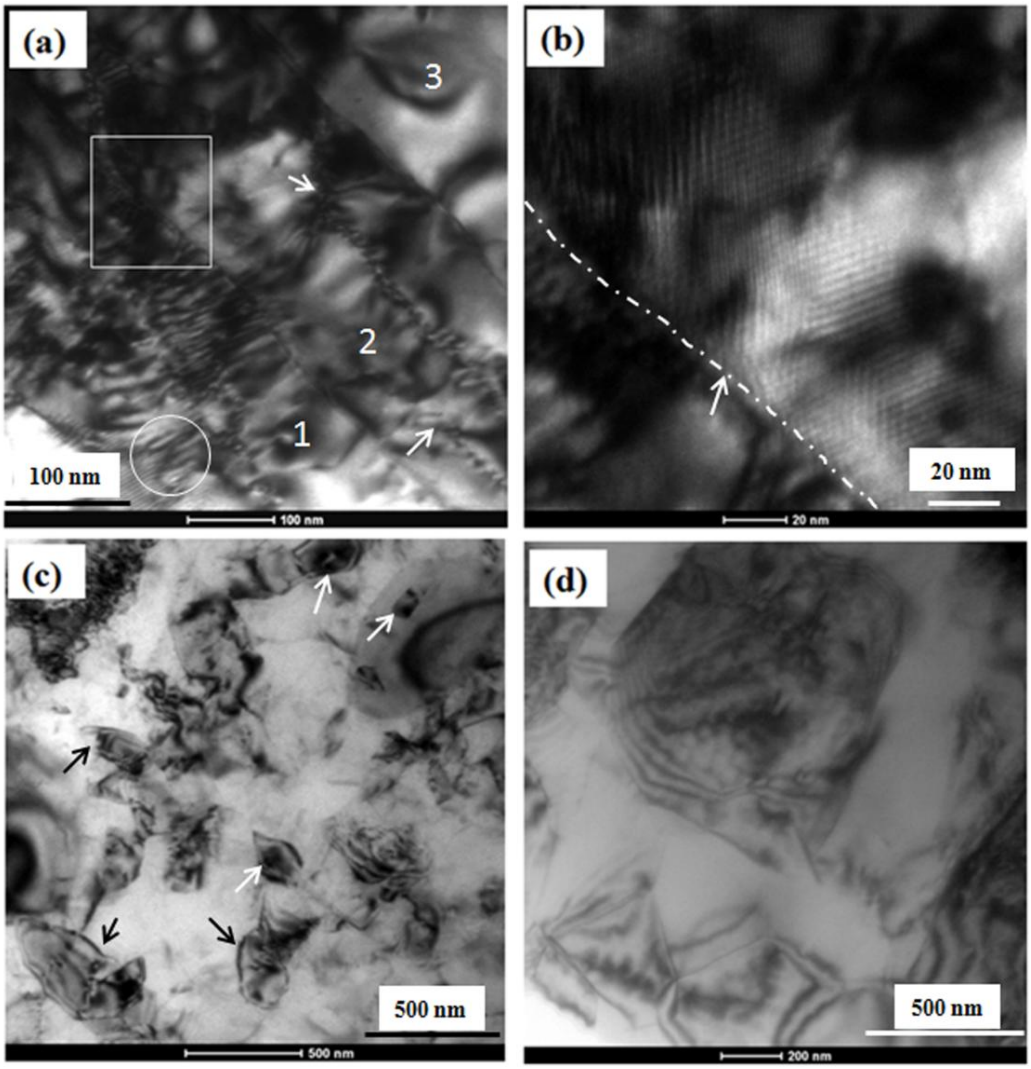

Figure 4.29: TEM micrographs of 5083 Al alloy WR at 175°C, annealed at temperatures; (a) 150°C, (b) Magnified view of marked area with square in Figure a, (c) 200 °C, (d) 250 °C.

The Vickers hardness has dropped from 145 HV to 136 HV after annealing at 150 °C .The ductility has improved from 6.8% to 9%. The UTS has dropped from 539 MPa to 490 MPa, and YS from 522 MPa to 470 MPa. LAGB length has decreased (3.41 mm to 3.04 mm) and slight increment in HAGB (250 µm to 458 µm) are observed. Further increasing annealing temperature to 200 °C, the fraction of recrystallization (Figure 4.31b & Figure 4.32) has increased from 3% to 8%. In the present study, after annealing at 150 °C and 200 °C, recrystallized grains are observed preferably nearby second phase particles. Due to increased localized strain around the second phase particles, it resulted in particle stimulated nucleation even at low temperatures. After annealing at 200 °C, hardness value has dropped from 145 HV to 124 HV and the YS and UTS have dropped (522 MPa to 340 MPa and 539 MPa to 395 MPa) and elongation to failure has

increased from 6.8% to 10.5%. Very fine grains with an average size of 300 nm are observed from TEM analysis as shown in Figure 4.29c. With increasing annealing temperature, the softening rate is increased. The volume fraction of recrystallized grains during annealing might show effect on softening rate of the material, which is related to the accumulated dislocation density (Lee at al. 2004). Due to reduction in dislocation density and formation of fine grains (as indicated in Figure. 4.29c), work hardening rate is increased. The fraction of recrystallization observed in samples annealed at 250 °C was 11% (Figure 4.31c, 4.32). The recrystallization is mainly around the second phase particles as observed in lower temperatures (150 °C, 200 °C). Nearly 35 HV drop was observed with 73% reduction and ductility improvement (from 6.8% to 13%). The YS and UTS have dropped (522 MPa to 270 MPa and 539 MPa to 330 MPa) and elongation to failure has increased from 6.8% to 13%. From TEM micrograph (Figure 4.29d) of the samples subjected to annealing treatment at 250 °C, coarsened (~ 500 nm) grains were observed. Complete dislocations were not removed at this temperature. EBSD micrograph (Figure 4.28c) shows the recovered substructure with thin sharp grain boundaries. In cryorolled 5083 Al alloy, maximum drop in strength values are observed due to high fraction of recrystallized grains. In WR at 175 °C in 5083 Al alloy, recrystallization is delayed due to recovery at 175 °C or it could be due to formation of fine precipitates, during warm rolling, caused pinning of the grain boundaries (Kaibyshev et al. 2006). Annealing at 300 °C leads to nearly 50% drop in hardness (146 HV-72 HV), fully recrystallized equiaxed structure with an average grain size of 6 µm was observed as shown in Figure 4.33a-b.

Strength values have dropped, UTS (539MPa- 272 MPa) and YS (522 MPa - 160 MPa); simultaneously ductility has increased from (6.8%- 21%). In order to find exact recrystallization temperature, annealing was performed at 275 °C, where fully recrystallized structures with 3.5 µm along with small fraction of sub grain boundaries were observed (Figure 4.29d). It is reasonable to infer that recrystallization is occurring between 250 °C-275 °C. From these findings, it can be concluded that 5083 Al alloy processed through cryorolling followed by warm rolling at 175 °C is thermally stable up to 250 °C.

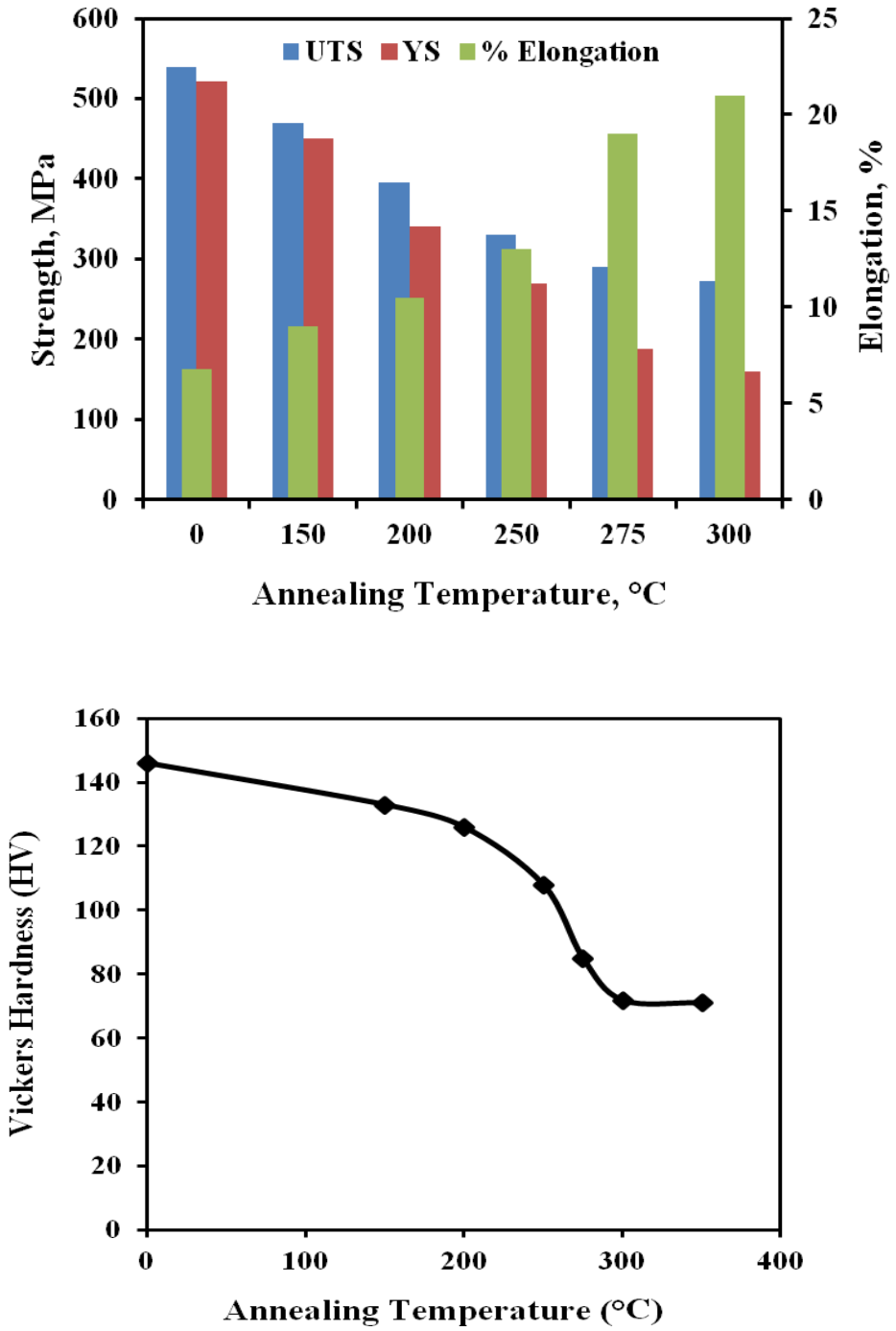

Figure 4.30: Variation in UTS, YS, elongation and hardness with respect to annealing temperature for 1 hr; (a) UTS, YS and elongation values, (b) Vickers hardness values.

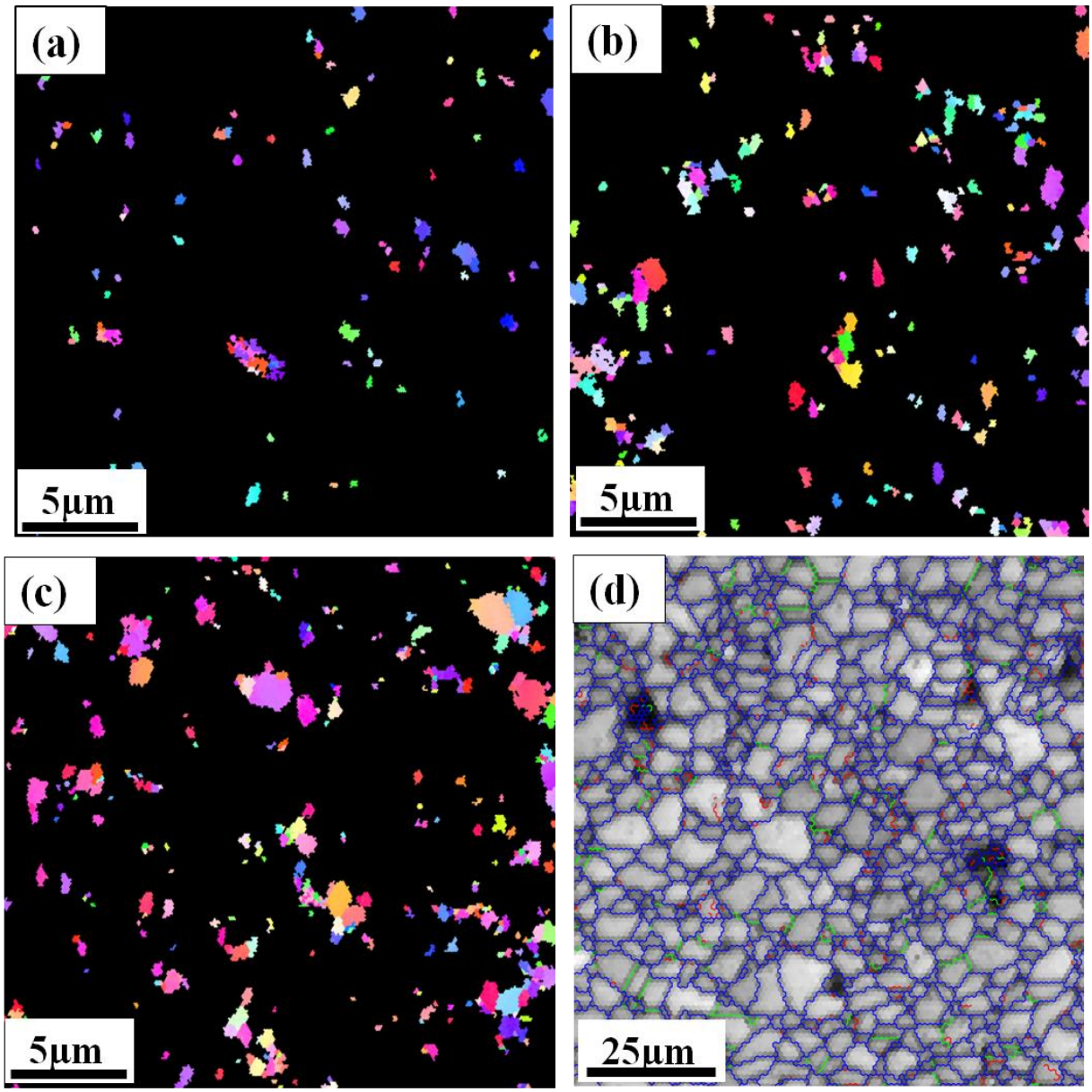

Figure 4.31: Recrystallized area micrographs of WR at 175 °C samples with various annealing temperatures; (a) 150 °C, (b) 200 °C, (c) 250 °C, (d) 275 °C.

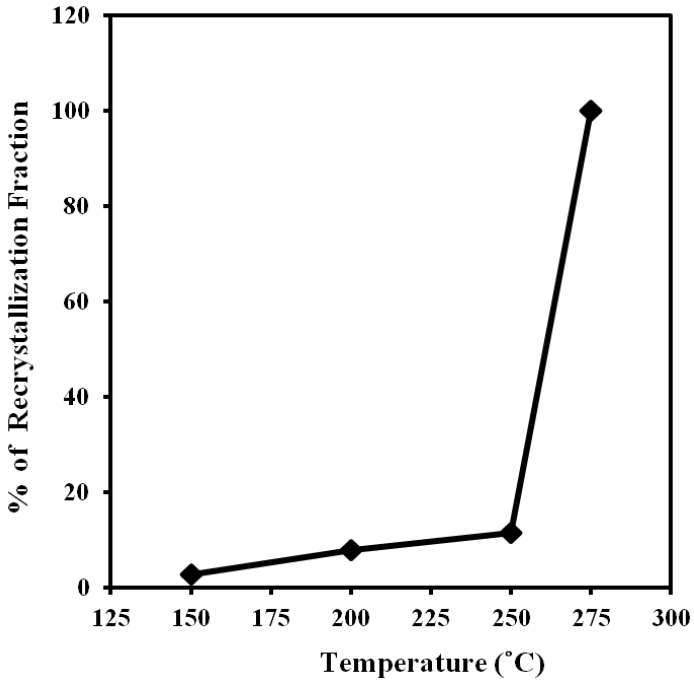

Figure 4.32: Variation in % of recrystallization fraction with various annealing temperatures.

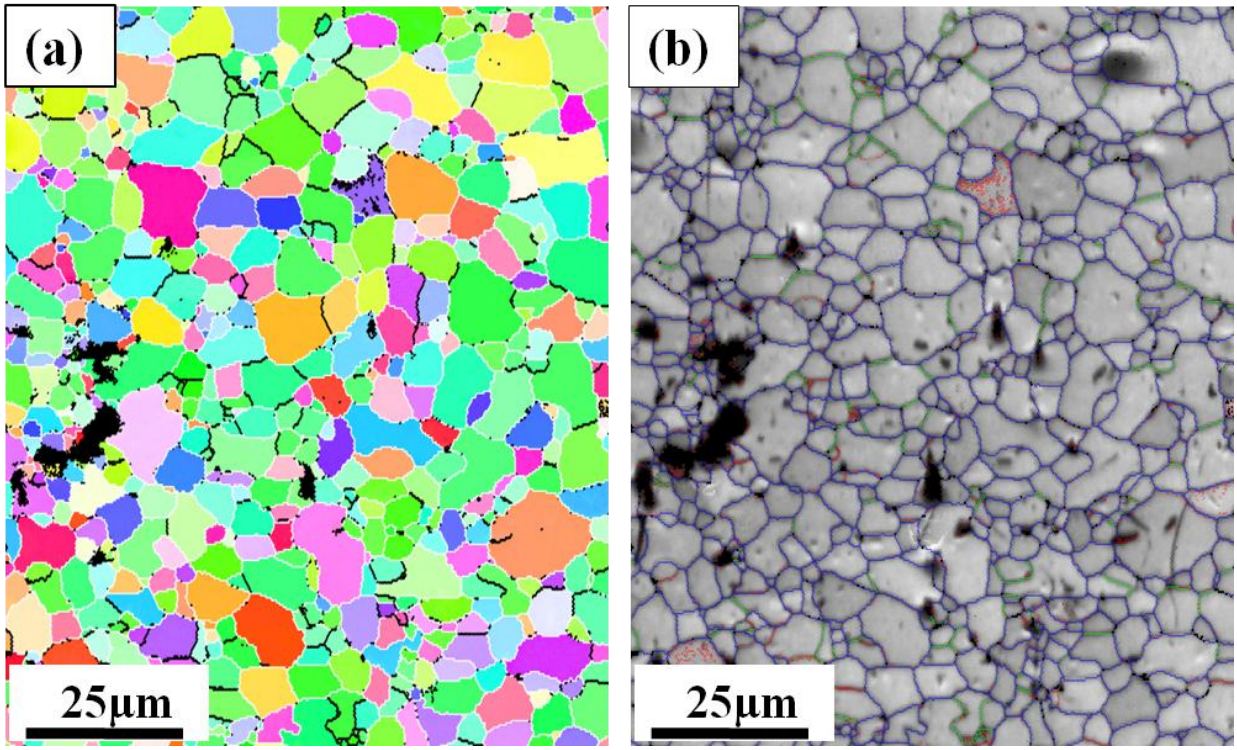

Figure 4.33: EBSD micrographs of 5083 Al alloy WR at 175 °C, annealed at 300 °C, (a) IPF map, (b) Image quality map with grain boundaries.

4.3.4 Summary

The effect of cryorolling followed by warm rolling on improving strength and ductility of 5083 Al alloy has been investigated in the present work. Detailed studies of microstructure and mechanical properties, using EBSD, TEM, Vickers hardness test and Tensile test on 5083 Al alloy were carried out in the present work and the following observations are drawn:

- Cryorolling followed by warm rolling was performed at different temperatures and optimized warm rolling condition was found to be 175 °C for obtaining higher hardness values (Hv-146).
- From TEM and EBSD micrographs, it is observed that CR and CR followed byWR samples exhibit high density of dislocations and substructures. The fraction of low angle grain boundaries has reduced and high angle grain boundaries have increased in CR followed by WR sample due to dynamic recovery effect after cryorolling followed by warm rolling at 175 °C.
- The significant improvement in strength (UTS-539 MPa, YTS-522 MPa, and ductility 6.8%) is observed in the samples obtained through the process with combination of cryorolling followed by warm rolling at 175 °C compared to cryorolled samples alone (UTS- 478 MPa, YTS-460 MPa, and ductility-3%). The increase in strength and ductility can be attributed to formation of fine precipitates and dynamic recovery effect, respectively.
- Cryorolling followed by warm rolling at high temperatures (> 175 °C) leads to a drop in tensile strength due to dominant dynamic recovery effect.
- Significant difference in the microstructure was observed in the alloy subjected to cryorolling followed by warm rolling compared to cryorolling alone.
- Two DSC peaks were observed in both the conditions, but smaller peak intensity observed in WR sample is due to already formed precipitates. It leads to suppression of exothermic peak and are in accordance with the mechanical behaviour.
- With increase in annealing temperature, the fraction of low and high angle grain boundaries has changed significantly and % fraction of recrystallized grains has increased.

- A significant improvement in ductility (6.8% to 19%) of WR (175 °C) after annealing at 275 °C for 1 hr was observed due to the formation of fully recrystallized equiaxed fine grain structure with an average grain size of 3.5 μm. The microstructure was found to be thermally stable up to 250 °C.

4.4 High cycle fatigue behaviour of ultrafine grained 5083 Al Alloy

4.4.1 Introduction

Ultrafine grained/nanostructured materials have received significant importance in last decade due to their improved mechanical properties. Metals and their alloys with improved strength and higher strength to weight ratio are essential for structural applications. The demand for lighter and stronger materials is ever growing due to its applications in aerospace, automobile, transportation, food and chemical processing industries. Production of bulk ultrafine grained (UFG) structure in 5083 Al alloys through cryorolling and cryorolling followed by warm rolling has been studied in detail in previous sections. It is observed that microstructural changes occurred during processing is reflected on mechanical behaviour of material (hardness, tensile strength, impact toughness). In addition to excellent monotonic excellent strength, these materials also possess better fatigue strength. Most of the structures and components of machinery are not subjected to constant load or stress during its service. In fact these loads and stresses are changing constantly. The change in stress causes fatigue failure in the material which is of utmost importance for developing high fatigue strength materials. Therefore, mechanisms governing fatigue life of the materials requires thorough investigation.

It is well known from literature on fatigue properties of UFG aluminium alloys that refining microstructure to submicron or nanoscale range enhances the high cyclic fatigue strength of the material (Estrin et al. 2013). Strength and ductility are influenced by grain size, whereas fatigue strength and fracture toughness are properties of a material, which can be tailored through strength and ductility (Lee et al. 2005). UFG Al-7.5 Mg alloys developed through cryomilling have shown high resistance to stress controlled fatigue compared to conventional microcrystalline material (Hanlon et al. 2003).

Interesting behaviour was observed in Al 6061 alloy processed through ECAP, that the material after single pass has shown better fatigue performance in high cyclic as well as in low cyclic regime, than the multi passed material (Chung et al. 2002). Patlan et al. (2011) have observed poor fatigue performance during plastic strain controlled tests at low cyclic regime in ECAPed Al 5056 alloy. It was mentioned that post ECAP annealing for short times enhanced the fatigue behaviour by increasing tensile elongation (Vinogradov et al. 1999). The low cyclic fatigue behaviour of UFG materials is not better than its conventional alloy. To analyze the fatigue life of a UFG material in low cyclic and high cyclic regimes, it is necessary to substantiate the influence

of micro structural characteristics for achieving better fatigue life. Mugrabhi et al. (2000, 2004) have divided the total strain amplitude in to two components, i.e., elastic and plastic components. The elastic component refers to high cycle fatigue, where strength of the material is determining factor and the plastic component refers to the low cycle fatigue, where ductility of the material is critical factor. UFG materials possess high strength compared to its coarse grained counterpart with limited ductility. Therefore, the high cycle fatigue life of UFG metal is more, and the low cycle fatigue life is less. Therefore, it is necessary to develop material with balanced strength and ductility in order to have better fatigue performance. May et al. (2007) have investigated the effect of variation in weight % of magnesium on the microstructure and mechanical properties of Al-Mg alloy processed through ECAP technique. It was observed that the microstructure after ECAP becomes finer with increase in amounts of alloying elements. An improvement in the fatigue behaviour was observed due to UFG microstructure observed after ECAP.

Along with the smaller grain size, presence of second phase as impurities and precipitates leads to higher dislocation density and improved fatigue behaviour of the material. Recent study by Wong et al. (2010) in commercial pure Al has shown shorter fatigue life for UFG Al than its coarse grain counterpart and this reduced fatigue life is attributed to strain localization by the formation of shear bands. It was observed that annealing, adding alloying elements and the presence of impurities in pure metals would enhance stability of the microstructure and reduces the cyclic softening effect during low cyclic fatigue (Vinogradov et al. 2002, Niendorf et al. 2008, Hoppel et al. 2006). Malekjani et al. (2011) have reported a reduced fatigue life of cryorolled Al 2014 alloy under strain controlled fatigue test. It was also reported that cryorolled material has shown stability under cyclic loading and it is attributed to presence of precipitates and impurities, which prevents microstructure instability through grain boundary pinning. Still, the mechanisms governing fatigue behaviour of UFG aluminium alloys are not well understood.

The behaviour of UFG 5083 Al alloys, produced by cryorolling, under cyclic loading is scarce in literature. Also the various reporting on fatigue behaviour of aluminium alloys are focused mainly on ECAP based studies. Therefore, an attempt has been made to investigate the fatigue behaviour of ultrafine grained 5083 Al alloy produced by cryorolling and cryorolling followed by warm rolling in the present work. The effect of microstructure on fatigue life of the material in the high cycle regime was investigated. Fractography studies based on SEM and TEM were used to explain the improvement in fatigue life of the UFG Al alloy as compared to its bulk counterpart.

4.4.2 Experimental procedure

5083 Al alloy plate after solution treatment was subjected to cryorolling upto thickness reduction of 50% and 85%, is referred as cryorolling CR. CR up to 50% reduction was deformed further at 175 °C up to 85% thickness reduction using oil bath furnace to obtain a good combination of strength and ductility, which is referred as WR. 85% thickness reduction of samples was selected to avoid buckling of sample during loading. The stress- life (S-N) fatigue test of ST, CR, WR conditions were performed under high-cycle fatigue (HCF) experiments carried out on 25 kN servo hydraulic universal testing machine in a laboratory air environment. The specimens were axially loaded under stress control mode keeping stress ratio 0.1 and frequency of 20 Hz using a sinusoidal waveform in all cases. The surface of all samples were polished using abrasive grit emery papers upto 1200 to eliminate irregularities after machining and notches that may act as stress risers during tests.

The procedure for cryorolling and cryorolling followed by warm rolling, samples for tensile and fatigue testing, characterization techniques are explained in detail in Chapter 3.

4.4.3 Results and discussion

4.4.3.1 Microstructure and mechanical properties

Microstructural evolution, distribution of second phase particles, and mechanical properties of starting material, cryorolled and cryorolled followed by warm rolled samples are discussed in detail in previous sections. Even though 5xxx series comes under non-heat treatable alloys, precipitation of Al_6Mn (Mn-rich) and Al_3Mg_2 (Mg-rich, β phase) was observed (Huskin et al. 2010, Goswami et al. 2010). Huskin et al. (2010) investigated the influence of rod like Mn precipitates on the strength of 5083 Al alloy. Toroghinejad et al. (2013) reported the improvement in mechanical behaviour of 5083 Al alloy after ARB process, where recovery due to static and dynamic restoration phenomena leads to annihilation of dislocation and hence improvement in ductility was observed. Superior properties of WR samples over CR samples could be due to the formation of fine precipitates and dynamic ageing effect during warm rolling.

4.4.3.2 High cycle fatigue properties

Figure 4.34 shows the stress amplitude (σ_a) versus number of cycles to failure (S-N) curve for ST, CR 50%, CR 85% and WR conditions. It is observed from this figure that there is no apparent knee observed and fatigue limit is not well defined in aluminium alloys unlike other

metals with BCC and HCP crystal structures. Therefore, in the present investigation, fatigue limit based on an arbitrary cut off value of 10^6 cycles is choosen as a measure to predict high cycle fatigue life (Srivatsan et al. 2000). The fatigue strength of ST sample has been observed as 50 MPa. After cryorolling up to 50% and 85% reduction, fatigue strength has increased to 100 MPa, 165 MPa, respectively. The observed improvement in fatigue strength of CR 85% reduction material is approximately 3.3 times more than ST material. The combination of cryorolling followed by warm rolling (WR) resulted in increase in fatigue strength to 180 MPa. This indicates that the trend in improvement of fatigue strength under HCF of CR 50% and CR 85% material is in accordance with the improvement in static strength discussed in the previous section.

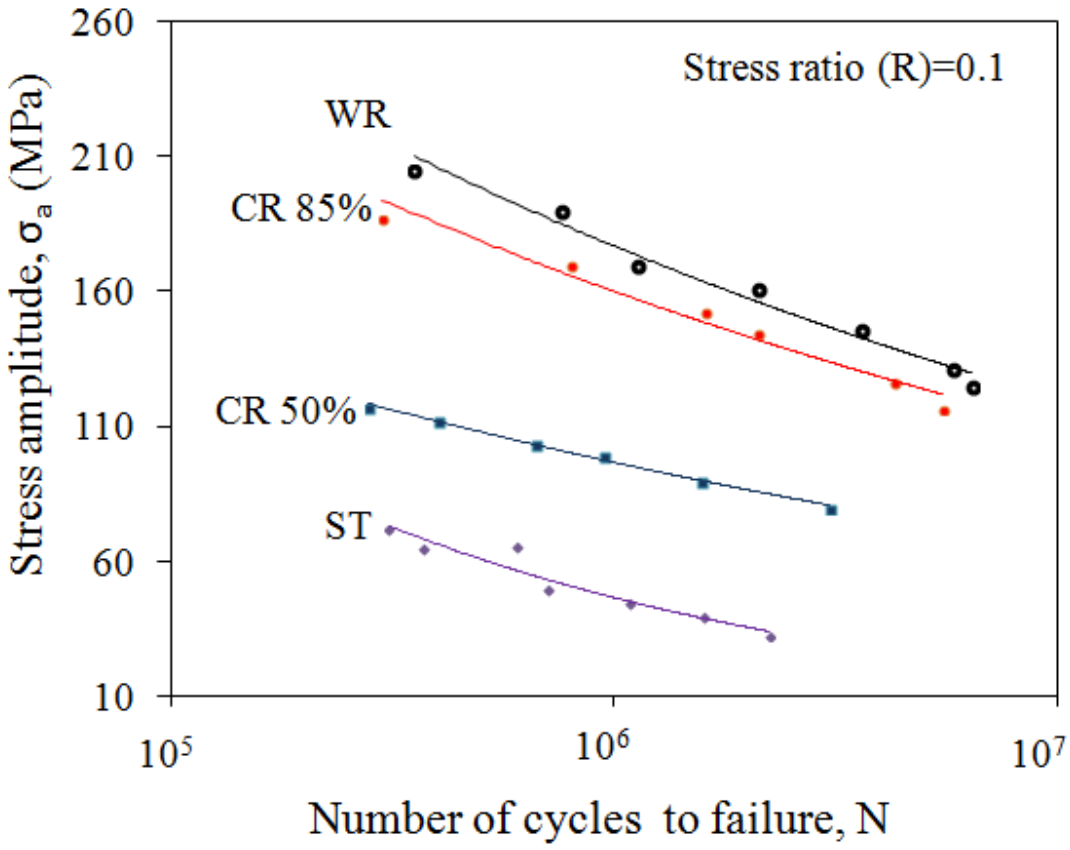

Figure 4.34: S-N cure of 5083 Al alloy; (a) ST, (b) CR 50% reduction, (c) CR, 85% reduction, (d) WR upto 85% reduction.

With increasing yield strength and ultimate tensile strength, fatigue strength under HCF has increased. The similar behaviour was also observed by Mughrabi et al. (2004) in UFG Cu tested for HCF. It can be understood that, out of total strain amplitude, elastic component refers to high

cycle fatigue that is basically governed by strength of the material. Based on the mechanical properties observed in present study, it is obvious that the WR sample would show better HCF life compared to other conditions. However, Chung et al. (2002) have observed in ECAPed AA 6061, with increasing number of ECAP passes from 1 to 4, the yield strength and ultimate strength have increased but it is not true in HCF behaviour. This could be due to nature of the grain boundaries. The resistance to crack nucleation increases significantly at low angle grain boundaries, where the dislocations can be transported easily to adjacent grains by shear bands, but it is difficult for slip bands to pass through high angle grain boundaries. Therefore, intergranular cracking by piling up of dislocations at grain boundaries is more likely to occur at high angle grain boundaries (Chung et al. 2002, Zhang et al. 2000). The same behaviour was reported in review made by Suresh et al. (1998). Whereas, in Al 1050 alloy processed through ECAP, material deformed up to 4 passes through Bc route has shown higher fatigue strength in HCF region than material deformed through 2 passes. But, the average grain boundary misorientation achieved after 4 ECAP passes was 15°, which is the lower limit angle for high angle grain boundaries. In the present study, SAED map of warm rolled material shown in Figure 4.26, indicated existence of sub grains with high angle grain boundaries. It is mixture of low angle and high angle grain boundaries. As well as, the grain size achieved in warm rolled material is very small (100-200 nm), which contributes for increasing HCF life of the material. In WR material, the simultaneous increase in strength and ductility may be observed due to combined effect of precipitation strengthening in addition to the strengthening mechanisms affecting cryorolling strength.

Another factor which improves fatigue strength of CR and WR samples is due to size and distribution of second phase particles. The random distribution of coarse second phase intermetallic particles (Fe rich phase) as shown in optical micro graph (Figure 4.1) of starting material causes rapid nucleation of secondary cracks during cyclic loading due to stress concentration effect that merges with main crack, thus reducing crack initiation resistance (Yeglin et al. 2002). After cryorolling and warm rolling, these particles got fragmented and aligned homogeneously in rolling direction into matrix resulted in reducing rate of fatigue crack growth, promoting zigzag crack growth and tip deflection (Malekjani et al. 2011). Singh et al. (2005) have showed that the main features that improve the fatigue properties are; fine distribution of second phase particles, and uniform distribution of network of precipitation and dislocation tangles that inhibit dynamic recovery thereby hindering formation of primary shear bands and intense cell walls, which provides the path for crack propagation. In our previous work, we have observed that

Al 6061 alloy deformed through cryorolling followed by warm rolling resulted fine distribution of precipitates after peak ageing treatment. Warm rolling caused dislocation induced precipitation. Goswami et al. (2010) have observed formation of β phase (Al_3Mg_2) preferentially at the grain boundaries in annealed 5083 Al alloy. Therefore, it can be concluded that the high fatigue strength of WR material over CR material in HCF could be due to formation of very fine subgrains along with dislocation cell networks and fine distribution of precipitates in the matrix.

4.4.3.3 Microstructure after fatigue test

TEM microstructures of ST, CR and WR material after fatigue fracture test and location of TEM samples cut after test are shown in Figure 4.35. In ST samples (Figure 4.35a), there is considerable increase in dislocation density inside the grains through interaction between second phase particles (Al_6Mn) and dislocation lines during cyclic deformation. Formation of shear bands (Figure 4.35b) and pile up of dislocation at the high angle grain boundary can be seen in Figure 4.35c.

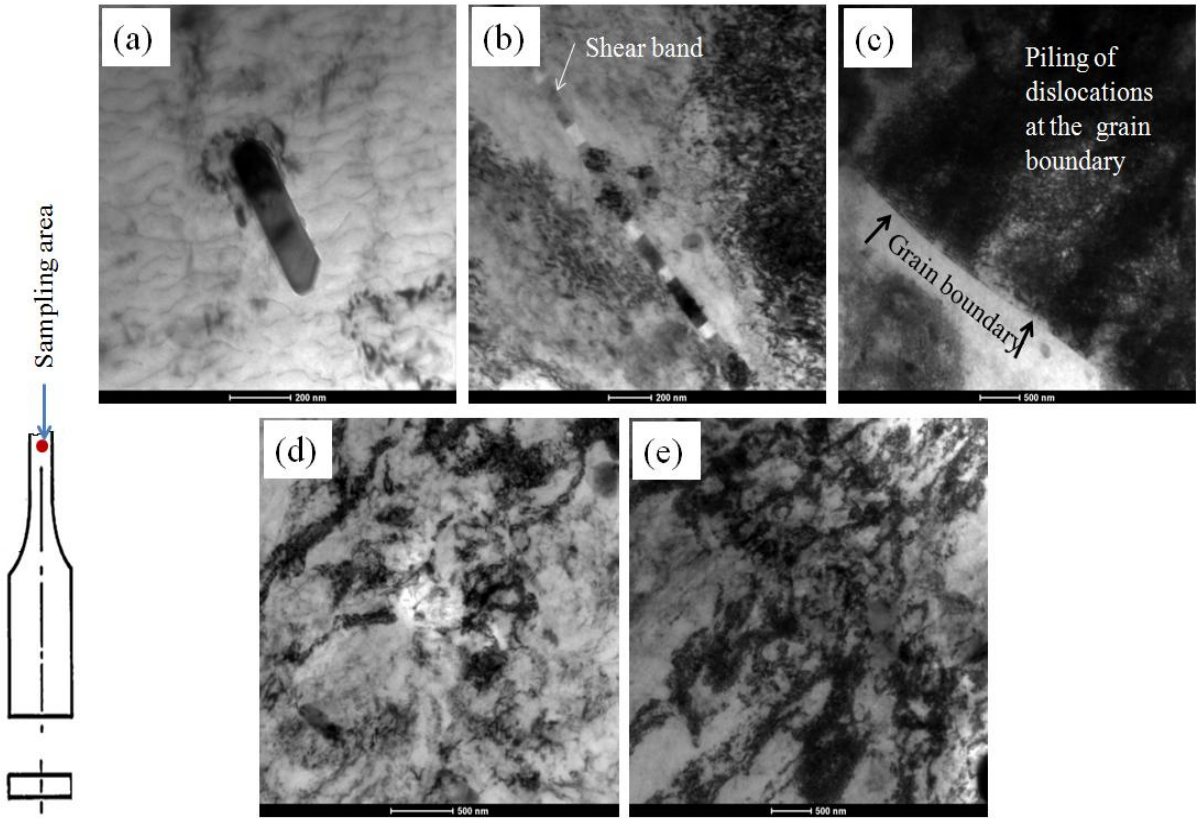

Figure 4.35: TEM micrographs of 5083 Al alloy after fatigue testing; (a) ST, (b) CR 50% reduction, (c) CR 85% reduction, (d) WR upto 85% reduction.

Chung et al. (2002) have observed increase in hardness with increasing number of cycles in ST Al 6061 alloy. Figure 4.35d,e shows microstructure of CR 85% and WR samples subjected to fatigue studies. CR 85% material after fatigue did not reveal any significant changes in microstructure; it is almost similar to features observed before fatigue testing. Where as in WR material (Figure 4.35e), increase in dislocation density and formation of fine cell structure can be observed. This could be due to the formation of fine precipitates during warm rolling impedes dynamic recovery and provides microstructural stability under cyclic loading. These WR samples with good strength and ductility with improved toughness may have better fatigue performance in low cycle fatigue regime, which requires detailed investigation. Mechanical properties of different conditions of samples are listed in Table 4.2.

Table 4.2: Mechanical properties of different processing conditions of 5083 Al alloy

5083 Al alloy	Hardness (HV)	σ_{UTS} (MPa)	σ_{YS} (MPa)	σ_f (MPa)	Elongation (%)
ST	58	278	160	50	22
CR 50%	104	390	370	100	9
CR 85%	124	470	455	165	4
WR	140	530	514	180	7.5

4.4.3.4 Fractography

The fractured surfaces of fatigue tested samples are examined under SEM and the fractographs are presented in Figure 4.36, 4.37, and 4.38 respectively. Figure 4.36 corresponds to fractured surface of ST material tested at stress amplitude of 65 MPa. It shows shallower dimples and cleavage planes along with micro cracks. The observations of multi micro cracks in Al 6061 alloy ECAPed upto 4 passes, are due to low resistance to the crack nucleation of the material (Chung et al. 2002). The another reason for low fatigue life of ST material could be due to structural heterogeneities like coarse second phase Fe rich particles, which might act as potential sites for crack nucleation (Chawla et al. 1998).

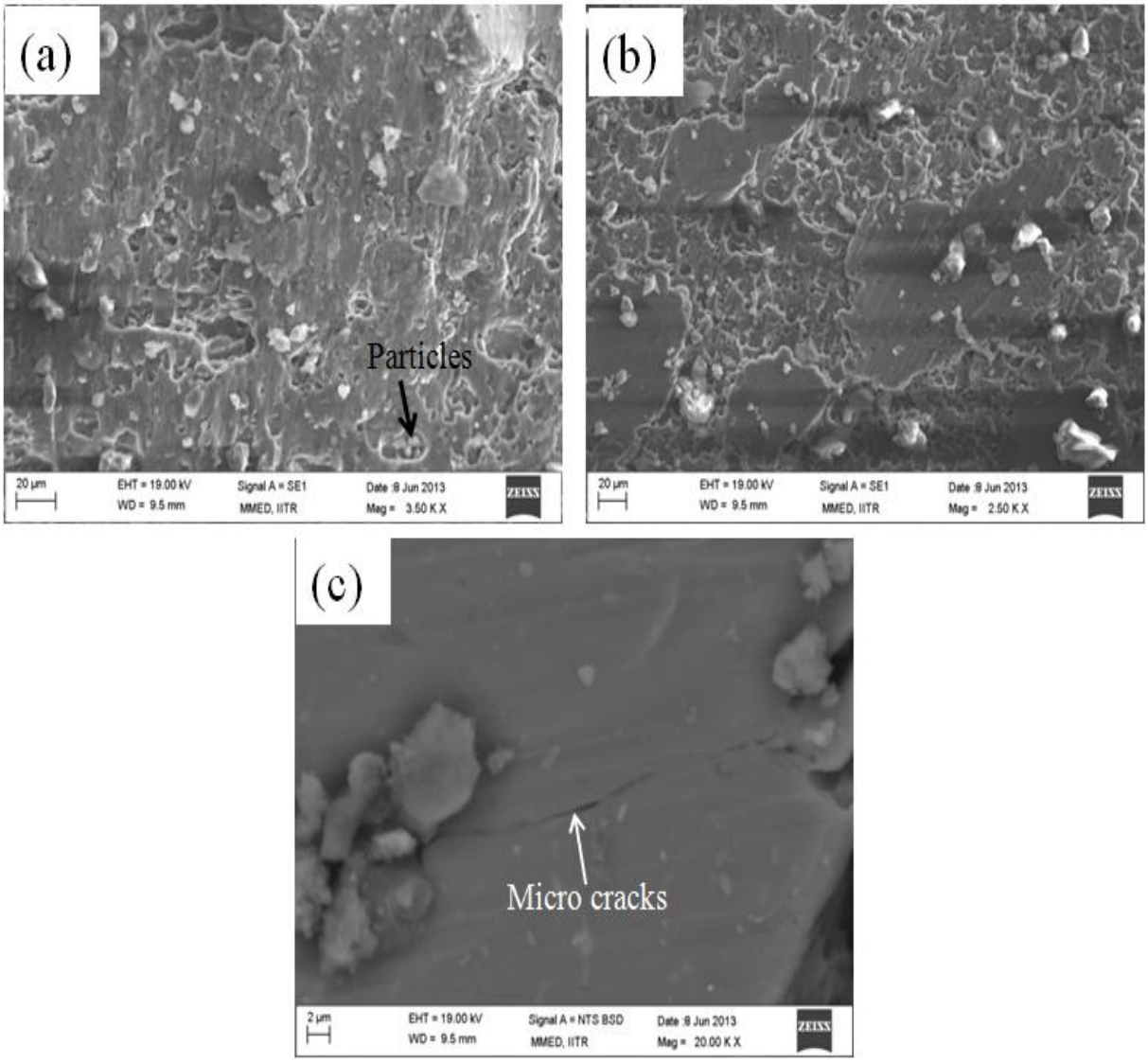

Figure 4.36: Fractured surfaces of 5083 Al alloy after subjecting to fatigue testing of solution treated sample (ST).

Fractured surface of CR 85% material tested under HCF regime with stress amplitude of 187 MPa is shown in Figure 4.37. Figure 4.37a, b shows several dimples and ductile striations, which are representation of positions during movement of crack front (Singh et al. 2005). These striations were observed ahead of crack tip, and it was reported that during fatigue, dislocation bands are produced, which leads to decohesion of band- matrix due to high stress concentration (Singh et al. 2005). It is evident from the figure 4.37d that formation of the cracks occurs at the dense striation walls.

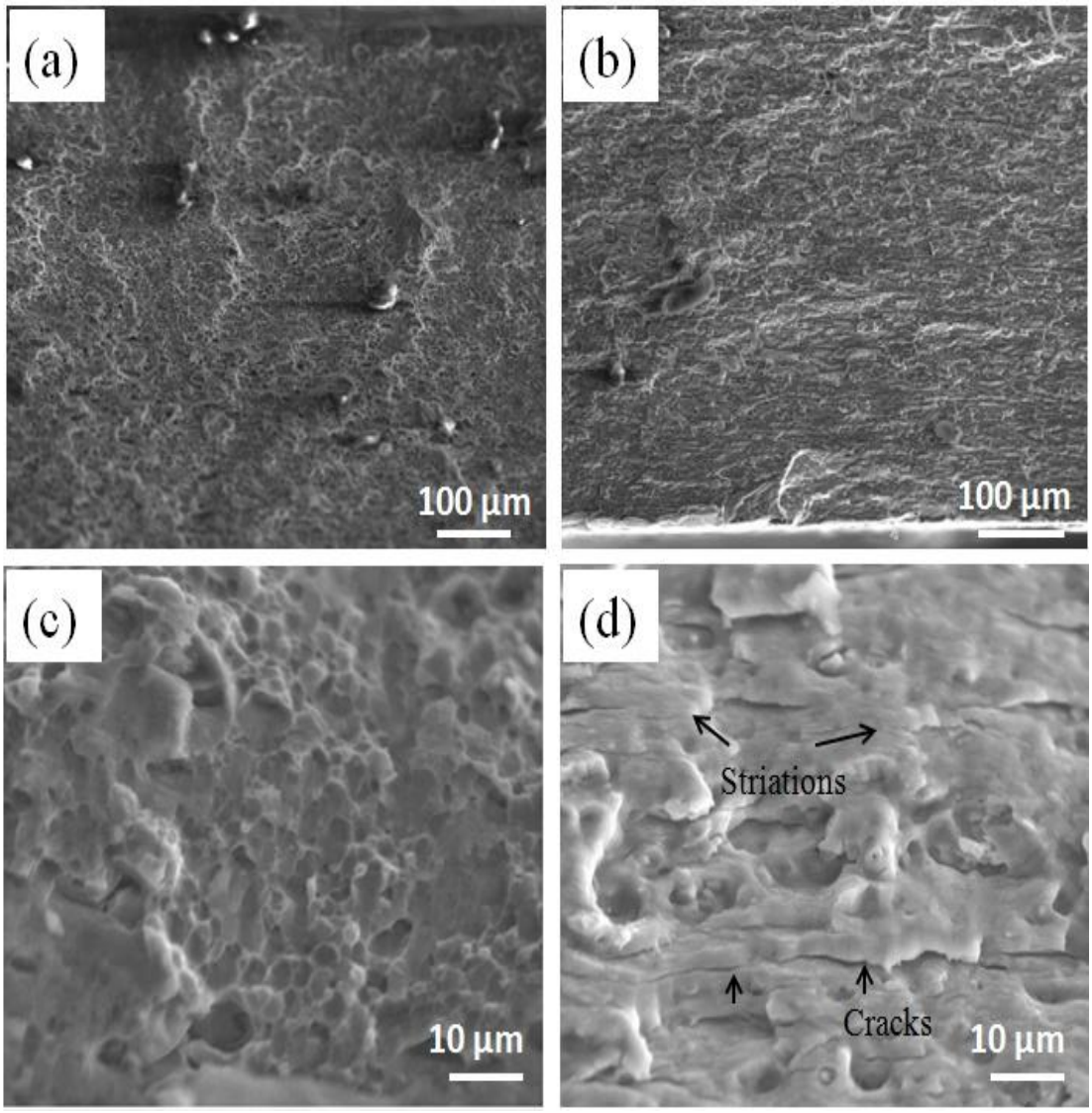

Figure 4.37: Fractured surfaces of 5083 Al alloy after subjecting to fatigue testing of cryorolled sample (CR 85%).

Figure 4.38 shows fractured surface of WR material tested under maximum stress amplitude 205 MPa. Micro cracks are not seen in the fractured surface rather formation of fine and coarse ductile dimples is observed. Formation of fine striations is evident from the figure 4.38b. Fine precipitates formed during warm rolling interact with dislocations leads to the formation of precipitate-dislocation tangled zones, which inhibits the fatigue crack propagation. High fatigue life WR material can be attributed to the formation of fine and coarse ductile dimples as shown in Figure 4.38c.

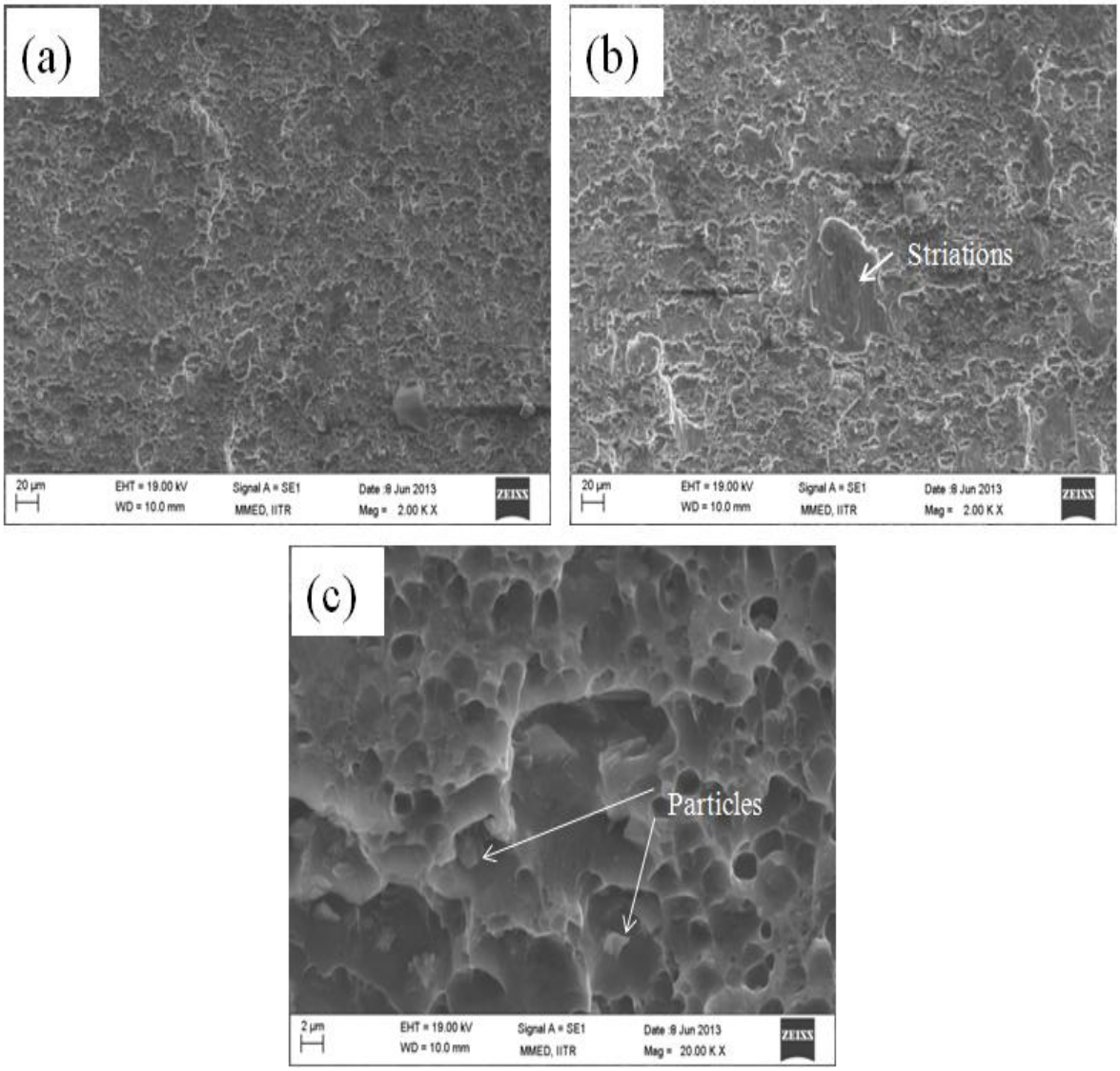

Figure 4.38: Fractured surfaces of 5083 Al alloy after subjecting to fatigue testing of cryorolling followed by warm rolling sample (WR).

4.4.4. Summary

In the present study, microstructure, and fatigue behaviour of 5083 Al alloy processed through CR and WR were evaluated and the following observations were drawn:

- 5083 Al alloy was successfully processed through CR and WR up to total thickness reduction of 85%.
- Upon increasing CR deformation, fine dislocation cell structures with high density dislocation tangled zones were observed.

- Combination of cryorolling followed by warm rolling (WR) resulted in very fine sub grain structure in the order of 100-150 nm in the processed alloy.
- Yield strength, Ultimate tensile strength, and % elongation of 5083 Al alloy processed through WR was considerably higher than alloy processed through CR.
- With increasing cryorolling deformation, the enhancement in fatigue strength under HCF is in accordance with static strength improvement.
- The warm rolled samples has shown existence of subgrains with high angle grain boundaries. The grains with 100-200 nm sizes contribute to the increased fatigue life.
- The improvement in fatigue strength of WR material over CR material is attributed to enhancement in yield strength through solid solution strengthening, dislocation strengthening, grain boundary strengthening and precipitation strengthening.
- SEM observations of fractured surface of WR material reveal fine striations along with fine dimple formation, which accounts for the better fatigue properties.

4.5 Corrosion behaviour of ultrafine grained 5083 Al alloy developed by cryorolling

4.5.1 Introduction

Al 5083 series are the most popular aluminium alloys used in marine applications because of its excellent corrosion resistance with balanced mechanical properties, good weldability, formability, and low maintenance cost (Romanji et al.). Due to the formation of tightly adhered oxide film on the surface when it is exposed to air or water render good corrosion resistance to the material. 5083 Al alloy is a non-heat treatable alloy with magnesium (> 4%) as the major alloying element that imparts solid solution strengthening to the material (Ryen et al. 2006). Along with solid solution strengthening, dispersion hardening renders from fine intermetallic particles of Al-Fe-Si-Mn, to the matrix. In the corrosion perspective the role of Mg as a solute and intermetallic particles of Al-Fe-Si-Mn are very important. The particles rich in Fe and Mn are more cathodic to the matrix (Davis et al. 1999, Tan et al. 2010). Due to the variation in potential between different intermetallic particles with Al matrix, the alloys are susceptible to localized corrosion, mainly pitting corrosion (Aballe et al. 2004). Along with inhomogenities in the alloy, presence of heterogeneities in the medium or exposure conditions can also cause localized corrosion (Aballe et al. 2001). Several researchers have investigated the effect of presence of iron rich inert-metallic particles on the corrosion behaviour, and reported that presence of iron rich inter-metallic particles increase the susceptibility to the pitting corrosion by micro galvanic coupling with the Al matrix (Murray et al. 1967, Aziz et al. 1954, Yasakau et al. 2007).

Another serious issue in Al-Mg alloys is intergranular corrosion (IGC) due to sensitization. When the material is subjected to elevated temperatures (50 - 200 °C) in service Mg presented as a solute in Al-Mg supersaturated solid solution will segregate as a β-phase (Al_3Mg_2) precipitate to the grain boundaries. This phenomenon is called sensitization. The high electrochemical activity (anodic in nature) of β-phase (anodic in nature) caused to susceptible of grain boundaries to IGC when the material exposed to corrosive environments. Due to this, the application of the material limited to low temperatures. In the present study the as received material (Al 5083-H111) was subjected to solution treatment at 510 °C for 2 hr and water quenched to room temperature to obtain Al 5083-O state where the Mg is in supersaturated solid solution state. Al 5083-O was used as a beginning material for the present study. So it was expected that the alloy will show more resistance to IGC. However it was reported that the degree of IGC susceptibility is depends on

corrodent, material chemistry, and fabrication process (Jones 1992). In the present study UFG high strength AA 5083 alloy was developed through cryorolling followed by warm rolling at 175 °C. So it was expected that the fabrication process used in the present study would affect the resistance to IGC of parent material. Several researchers have studied IGC susceptibility of 5XXX alloys and the common observation was, IGC is caused by preferential precipitation of magnesium- rich particle, the β phase (Al_2Mg_3), along the grain boundaries (Chang et al. 1999, Searles et al. 2001, Jones et al. 2001). Davenport et al. (2006) has reported that the crystallographic orientation of the grain boundary has a great influence on the degree of susceptibility for an attack and low angle grain boundaries were more resistance to IGC than high angle grain boundaries.

There is a great demand for materials with improved mechanical properties and higher corrosion resistance. Grain size of the material plays a key role to control its physical, chemical and mechanical properties of polycrystalline material (Estrin et al. 2013). Severe plastic deformation (SPD) is considered as potential technique for microstructure refinement by imposing severe strain in the material. In the race for better materials, based on grain size alteration, numerous SPD techniques were evolved in the recent two decades, as already discussed in detail in Chapter 2. Cryorolling is another approach where the processing temperature effect is used to refine the microstructure to sub micrometer or nanometer range even by imposing lower strain than SPD techniques. Lee et al. (2004) have studied the effect cryorolling followed by annealing on microstructure evolution and mechanical properties of 5083 Al alloy and suggested the optimized annealing condition to have good combination of uniform elongation and strength. The improved strength and ductility, impact toughness studies, high cycle fatigue behaviour and microstructural evolution of cryorolled 5083 alloy and cryorolling followed by warm rolling of 5083 alloy are reported in previous sections.

It is also very essential to understand corrosion behaviour of the material in addition to ensuring superior mechanical properties of the materials for its structural applications. It is expected that during the process of improving mechanical properties, its corrosion behaviour will change with respect to its base material (Gopal Krishna et al. 2012). High hardness and strength of UFG material attributes from presence of large number of grain boundaries and high dislocation density (Kapoor et al. 2013, Zao et al. 2006, Kamikawa et al. 2009). It is expected that these structural defects due to dislocations and highly reactive grain boundaries would reduce the corrosion resistance of UFG Aluminium alloys. Rangaraju et al. (2005) have reported in commercial pure aluminium that UFG structured sample has shown more dissolution rate with

increased pitting corrosion resistance as compared to base material due to large volume fraction of grain boundaries and lattice defects. Zhang et al. (2007) have reported similar findings in microcrystalline aluminium coatings fabricated through magnetron sputtering technique. The poor corrosion resistance of microcrystalline Al coating as compared with cast pure Al in Na_2SO_4 acidic solution has been reported. However, higher resistance to pitting corrosion was observed in NaCl solution (Zhang et al. 2007). Son et al. (2006) have reported that the pitting corrosion resistance of UFG Aluminium and Al-Mg alloys processed through ECAP have increased and reported that the increased pitting corrosion resistance is attributed to decrease in size of precipitates during ECAP and increased rate of Al oxide film formation. UFG Ti, Al 1050 fabricated through ECAP has shown increased corrosion resistance than its counterpart (Balyanov et al. 2004, Chung et al. 2004).

In precipitation hardenable alloys, AA 6082 processed through ECAP followed by ageing have shown better corrosion resistance than its counterpart (Hockauf et al. 2008). Recent studies by Gopal Krishna et al. (2012) in UFG structured Al-4Zn-2Mg alloy processed through cryorolling followed by short annealing and ageing, the alloys has shown better corrosion resistance than its coarse grain peak aged material. Whereas, samples with cryorolling alone has shown decreased potential. It may be mentioned that there is no consensus view on the corrosion behaviour of material with decreasing grain size and presence of dislocations. But, it is clear that the size and distribution of impurities like second phase intermetallic particles present in material are greatly influencing the pitting corrosion behaviour of the material along with structural defects like dislocations and large fraction of grain boundaries. The corrosion behaviour of coarse grained material Al 5083 has been well studied (Jafarzadeh et al. 2009). There is no reported literature so far on corrosion behaviour of UFG 5083 Al alloy processed through cryorolling. Therefore, the present investigation has been focused to understand the corrosion behaviour of UFG 5083 Al alloy in chloride environment. Salt immersion test and electrochemical tests were carried out in 3.5% NaCl solution. Nitric acid mass loss test was also performed to observe intergranular corrosion in 5083 Al alloy. Morphological characterstics of the alloys were carried out through SEM with EDS before and after the corrosion tests.

4.5.2 Experimental Procedures

4.5.2.1 Specimens

Commercially available rolled plate of 5083 Al alloy with chemical composition (wt %) as given in Table 3.1 is used in the present study. Samples with 10 × 30 × 40 mm^3 dimensions were machined from the as received (AR) material and solution treated (ST) at 510 ºC for 2 h, quenched in water. Cryorolling (CR) and cryorolling followed by warm rolling (WR) was performed on ST samples up to 90% thickness reduction. Immersion tests and NAMLT were conducted for ST, CR, WR and AR samples to estimate corrosion rate and resistance to intergranular corrosion (IGC). For nitric acid mass loss (NAML) test samples of 50 mm length and 6 mm width and specific thickness (depends on sample condition) (shown in Figure 4.39)were prepared and polished up to 1000 grid emery paper as per ASTM-G 67-13 standards. For salt immersion tests, ST samples with 10×10×3 mm^3 and CR and WR samples with 10×10×1 mm^3 were used.

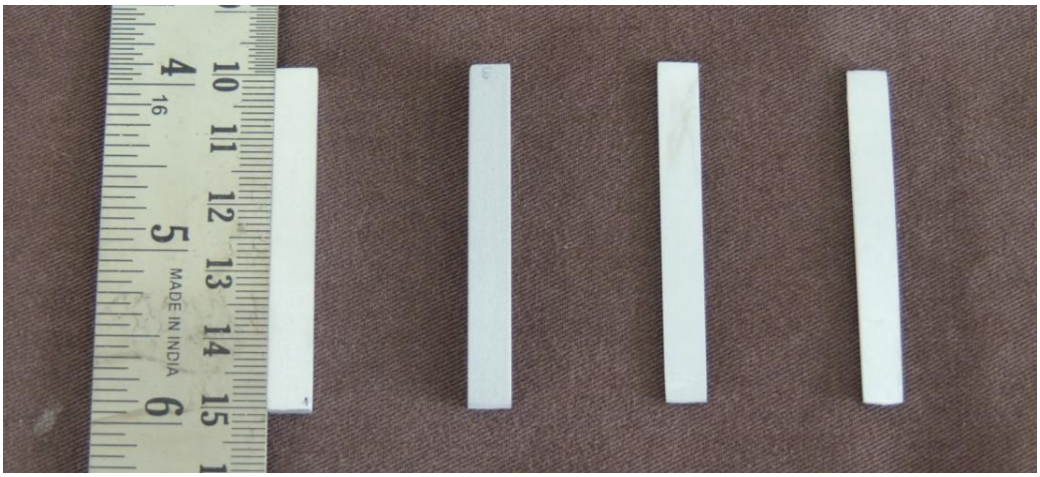

Figure 4.39: The photographs of the 5083 Al alloy samples after nitric acid mass loss test.

4.5.2.2 Corrosion test

Electrochemical polarization test was used to investigate the corrosion behaviour of 10 x 10 mm^2 dimension samples in 3.5% NaCl solution at a scan rate of 1 mV/s using Voltamaster 4 software of electrochemical laboratory voltalab PGZ301. Samples were prepared by placing a copper wire on one face of the sample and then cold mounted in resin. Measurements were made in a conventional three-electrode cell using a saturated calomel electrode (SCE) as the reference electrode and a graphite rod as a counter electrode.

Immersion test and Nitric acid mass loss (NAML) tests were carried out in accordance with the ASTM G-31 and ASTM G-67 standards. Sample preparation and testing procedure with schematics are well explained in chapter 3.

4.5.2.3 Investigation of the microstructure

Microstructural characterization of ST, CR and WR samples was performed by using optical microscopy, transmission electron microscopy (TEM- FEI Technai 20) and the scanning electron microscopy (SEM/EDS-Carl Zeiss,). The surface morphology after the corrosion damage of immersion test and NAML test samples were evaluated using SEM. Sample preparation techniques for SEM and TEM characterization are discussed in chapter 3.

4.5.3 Experimental Results

4.4.3.1 Microstructure

Figure shows the typical optical micrographs of ST, CR and WR samples. The average grain size of ST material is about 85 μm. The black spots appearing in Figure are second phase intermetallic particles. With CR and WR the initial microstructure got perturbed and band structure along the rolling direction can be observed in Figure 4.40. The SEM micrograph of ST material in back scattered diffraction (BSD) mode is shown in Figure 4.41 The micrograph in Figure 4.41a reveals the coarse second phase particles aligned in a particular direction. Figure 4.41b shows presence of second phase intermetallic particles with varying contrast in solution treated material. In order to find the type of intermetallic particles, energy dispersive X-ray was used at various spots of the particle. The corresponding chemical composition is listed in Figure 4.41c. From the elemental analysis, it was found that the coarse particle in white color (marked as 1) corresponds to Al-Fe-Mn-Si particles, which are rich in Fe and Mn. Whereas, black color particles (marked as 2) corresponds to oxide phase (Al-Si-Mg-O) rich in oxygen and having effective atomic number lower than the aluminium matrix. Along with these two, ultrafine grey color particles (marked as 3) evenly distributed throughout the matrix are Al_6Mn precipitates.

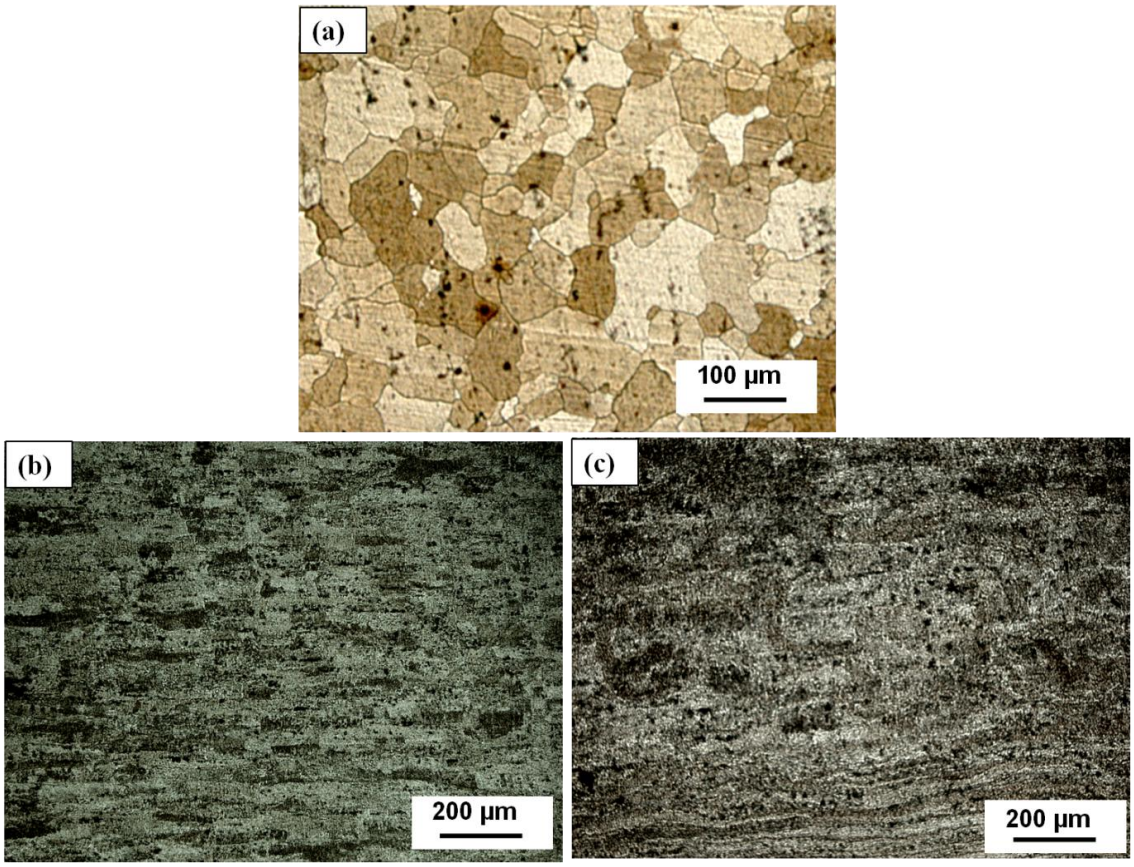

Figure 4.40: Optical micrographs of 5083 Al alloy samples after etching; (a) ST, (b) CR, (c) WR.

Line scan was performed on big black sized particles (shown in Figure 4.42), and the corresponding elemental distribution profiles are shown. Tan et al. (2010) have reported in 5083 Al alloy that the black color particles corresponds to Mg_2Si precipitates, whereas in current study, percentage of oxygen corresponding to the spot on the black color particle is significantly high along with magnesium and silicon. These particles are expected to be oxides of Mg and Si. There is no color contrast between β phase precipitates and oxides of Mg and Si which indicates that they are having effective atomic number nearby each other. The only difference is in size distribution. β phase precipitates appears to be very fine and oxides of Mg and Si are coarse.

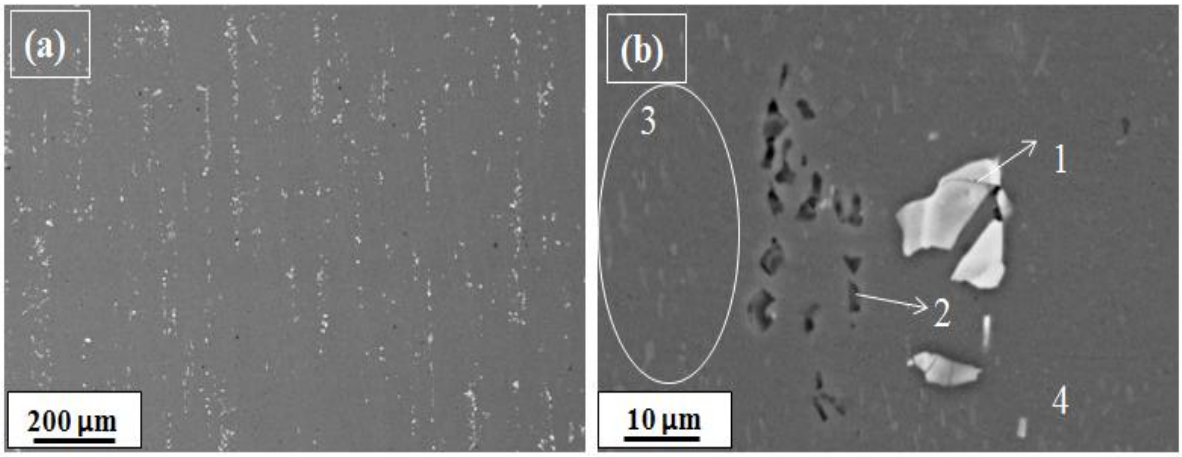

	Mg	Fe	Mn	Si	O	Al
1	2.05	10.44	5.03	1.75	-	80.7
2	6.05	0.04	0.44	3.71	7.22	82.62
3	4.08	0.06	1.54	0.11	2.25	92.08
4	4.00	0.08	0.55	0.23	1.28	93.86

Figure 4.41: SEM micrographs of ST sample before immersion testing; (a) SEM micrograph taken in BSD mode showing distribution of coarse second phase particles without etching, (b) Magnified view of Figure (a).

TEM micrographs of ST, CR and WR are discussed in previous sections 4.1 and 4.3 in detail. With increasing percentage of reduction, the dislocation density accumulated has increased. The presence of undissolved second phase particles enhances the accumulation of dislocation density. These microstructural features significantly affect the corrosion behaviour of material as reported by many researchers.

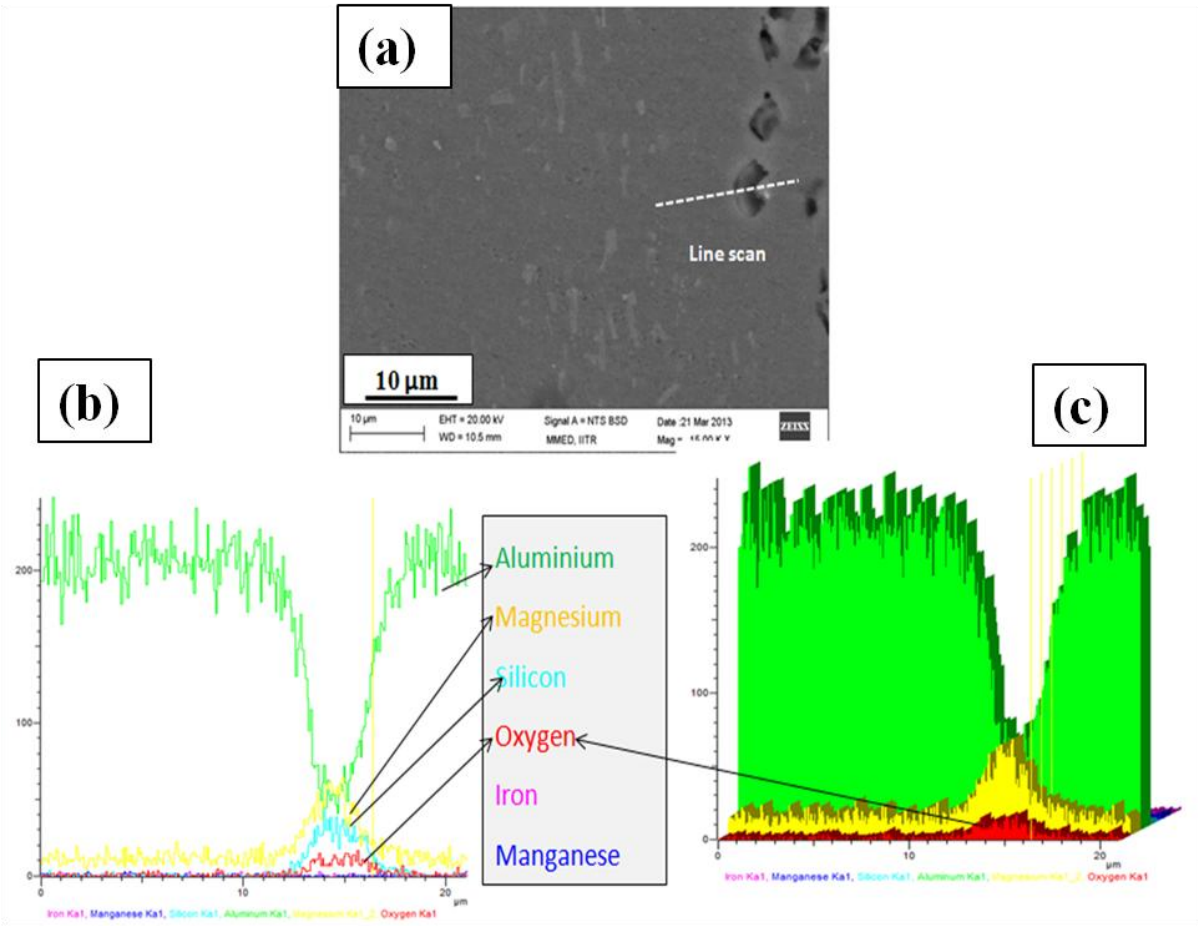

Figure 4.42: (a) SEM micrographs of ST sample with the line scan, (b) Elemental distribution obtained from characterstic X-ray along the line marked in Figure (a), (c) 3D view of the plot shown in Figure (b).

4.4.3.2 Electrochemical characteristics

a. Open circuit Potential (OCP)

Variation in open circuit potential (OCP) as a function of time for ST, CR and WR of 5083 Al alloy in 3.5% NaCl solution is shown in Figure 4.43. For the first 400 s OCP has increased towards positive direction in all the samples. After 400 s it has dropped slightly and further increased to achieve steady state. After 2250 s steady state is achieved in all the samples.

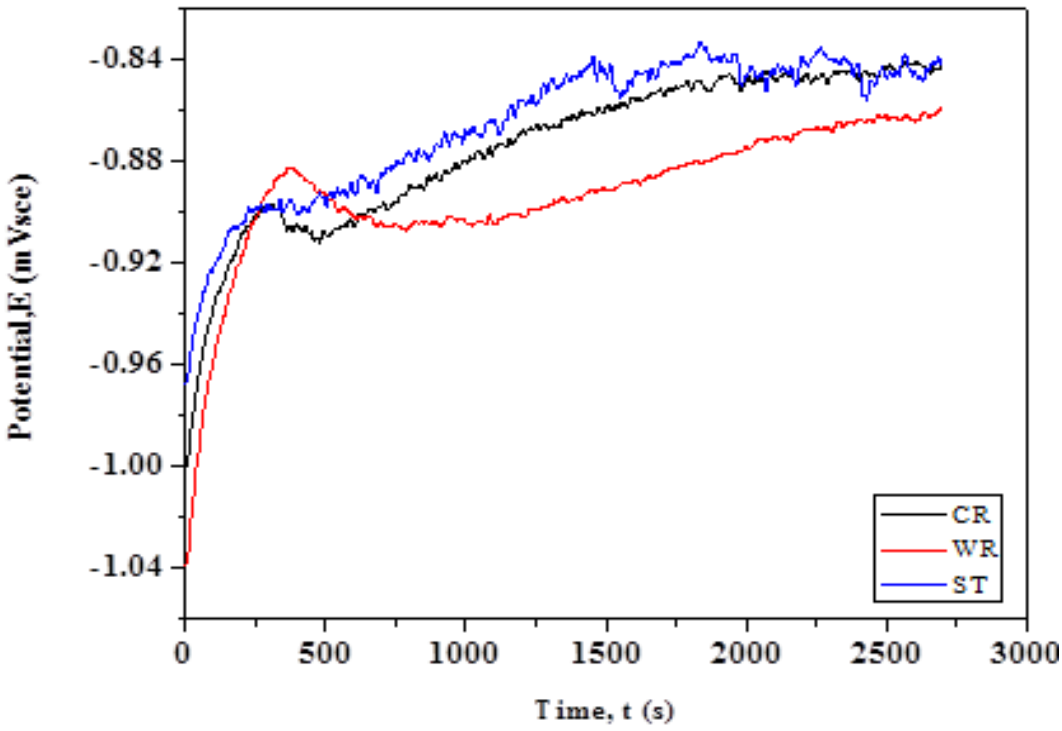

Figure 4.43: Variation in open circuit potential of ST, CR and WR conditions in 3.5 wt. % NaCl for 1800 sec.

ST sample has shown more positive potential as compared to CR and WR, but the noise level of OCP in ST sample has increased with increasing time signaling that pitting is taking place. The potential difference between ST and CR is nearly same. The observations in ST sample are in agreement with reported literature (Gopal Krishna et al. 2012, Ambat et al. 2006). The noise level in CR, WR sample with increasing time is very low as compared to the ST condition but the OCP value of WR sample was slightly lower than the ST sample. The behaviour of CR sample in the present study is in agreement with the findings reported by Gopal Krishna et al. (2012), for CR Al-4Zn-2Mg alloy.

b. Potentiodynamic polarization

Figure 4.44 shows typical E-logI polarization plots for ST, CR and WR samples, obtained from potentiodynamic polarization tests performed in deaerated 3.5% NaCl solution. Before running the test, 1800 s were given to stabilize the OCP. Tafel extrapolation method is used to obtain E_{corr} and i_{corr} values. E_{corr} is a measure of corrosion resistance of a material in a corrosive environment, and i_{corr} (corrosion current density) is rate of corrosion at the corrosion potential in a

given environment (Hadzima et al. 2007). Minimum five experiments were conducted in each condition and the mean values with standard deviation of $E_{corr,}$ $E_{pit,}$ i_{corr} values for ST, CR and WR samples are listed in a Table 4.3 along with E_{pit} - E_{corr} values.

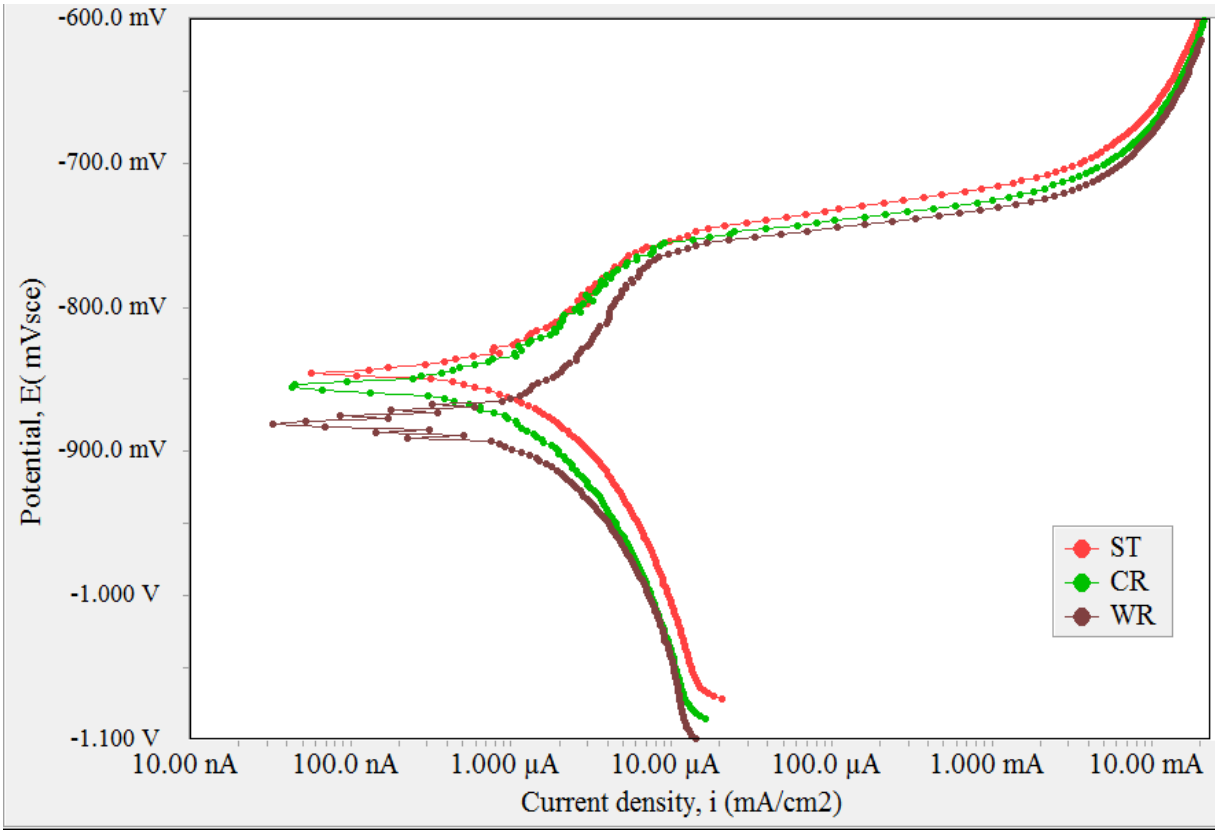

Figure 4.44: Polarization curves for ST, CR and WR of Al 5083 alloy in 3.5 wt. % NaCl solution.

Table 4.3: Electrochemical parameters of 5083 Al alloy obtained from potentiodynamic polarization test.

Sample condition	**E_{corr} (mV_{SCE})**	**E_{pit} (mV_{SCE})**	**E_{pit} - E_{corr} (mV_{SCE})**	**I_{Corr} ($\mu A/cm^2$)**
ST	-845±9	-759±8	86	1.82 ±0.8397
CR	-856±4	-760±4	96	2.05± 0.65
WR	-883±5	-764±5	119	2.33± 0.639

The i_{corr} values of ST, CR and WR are 1.82 ±0.8397, 2.05± 0.65 and 2.33± 0.639 μA/cm^2 respectively. The current density of CR and WR samples is slightly increased. But the increment is not significant. The corrosion potential of CR sample is slightly more negative (-856 mV) than ST sample (-845 mV). After WR the corrosion potential has further moved towards negative potential direction (-883 mV). Pitting potentials of ST and CR are nearly same. Whereas in WR sample pitting potential is slightly lower to the ST and CR conditions. The difference between E_{pit} and E_{corr} values indicates the pitting resistance of WR samples is better than CR and ST. From the Table 4.3, E_{pit} - E_{corr} values are increased in the order of ST < CR < WR.

4.5.3.3 Susceptibility to Intergranular corrosion (IGC)

To estimate the susceptibility of the alloy to intergranular corrosion, the ST, CR, and WR samples were immersed in HNO_3 at 30 °C for 24 hr. The weight loss measurements were made after cleaning of samples and compared to standards, to investigate their susceptibility to ICG. The observed mass loss after testing are listed in Table 4.4. According to ASTM -G66 if the weight loss after NAMLT is equal or more than 15 mg/cm^2 then the material is considered to be more prone to IGC.

Table 4.4: Weight loss measurements of 5083 Al alloy obtained from nitric acid mass loss test.

Sample Condition	Initial weight (gm)	Final weight (gm)	Weight loss (mg)	Surface area (cm^2)	Weight loss in (mg/cm2)	Average
ST1	2.7893	2.7592	30.1	10.15	2.96	2.56
ST2	2.7112	2.6895	21.7	10.05	2.15	
AR1	2.6865	2.521	165.5	9.99	16.55	16.31
AR2	2.7313	2.5696	161.7	10.05	16.07	
CR1	0.8843	0.864	20.3	7.68	2.64	2.89
CR2	0.8405	0.8175	23.0	7.33	3.13	
WR1	0.8107	0.7844	26.3	7.22	3.63	3.91
WR2	0.8444	0.8139	30.5	7.27	4.19	

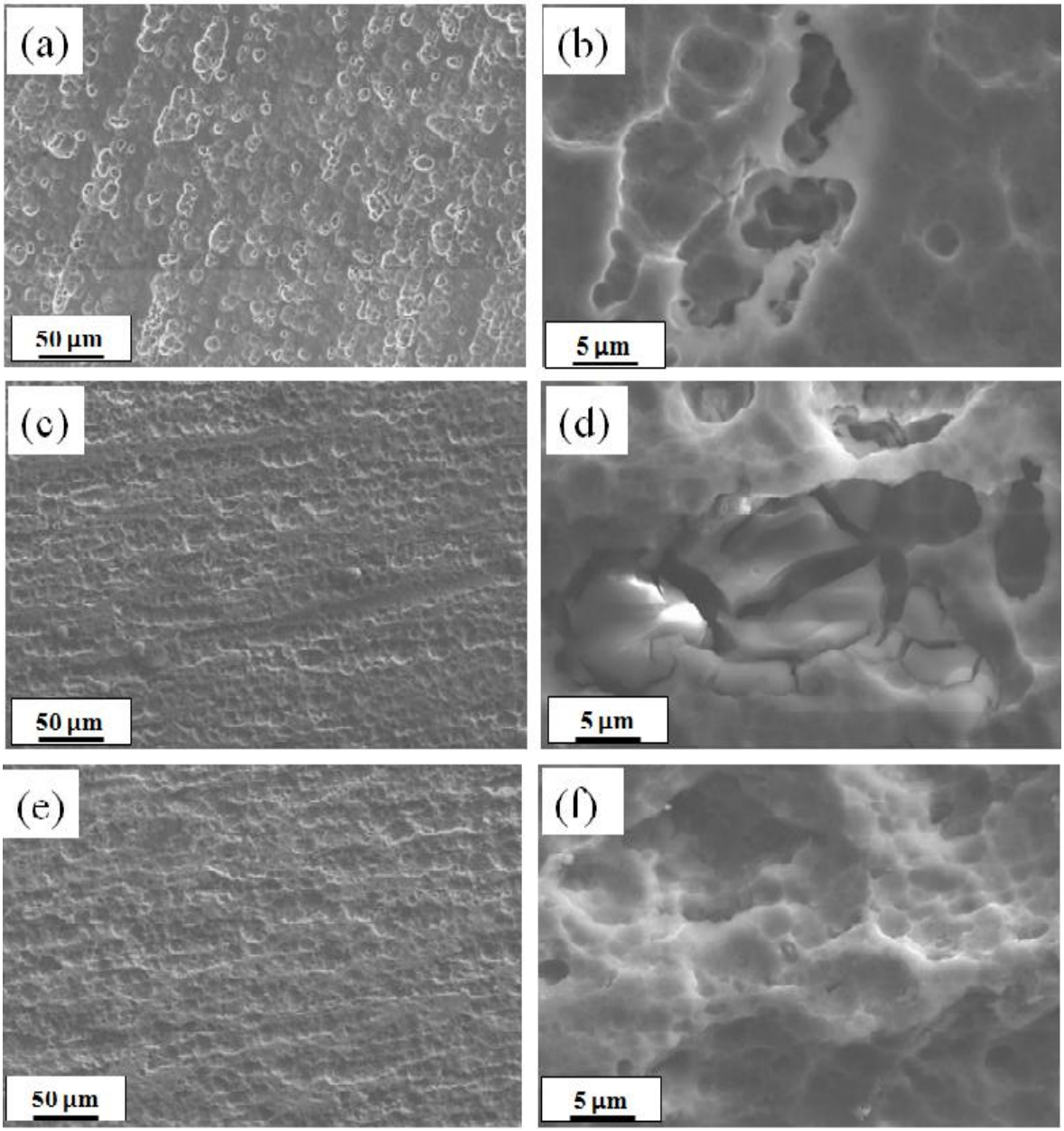

Figure 4.45: SEM micrographs of 5083 Al alloy after subjecting to NAMLT; (a) ST, (c) CR, (e) WR and magnified view of (a), (c), (e) are shown in (b), (d), (f).

In the present study the average values weight loss obtained for ST, CR and WR indicates that the above three materials possess good resistance to IGC. Individual comparison of weight loss with ST sample indicates by performing CR and WR the resistance to IGC slightly decreased. In the present study the sate of as received material was H111 condition. For comparison purpose as received material also subjected to NAMLT and the obtained weight loss is listed in Table 4.4. Considerable weight loss was observed in AR material which indicates less resistance to IGC.

Compared to ST, CR and WR, AR material is more susceptible to IGC. After NAMLT of AR, ST, CR and WR samples the sample surface was investigated through SEM and the results were shown in Figure 4.45. Shallow pit morphology was commonly observed in all three conditions in Figure 4.45a, c&e. This could be due to surface cleaning and etching process through NaOH, HNO_3 solutions respectively involved in the sample preparation process. Figure 4.45b, d&f shows magnified view of deep pits observed rarely on the surface due to IGC. The BSD micrograph of AR in Figure 4.46b (inset) shows fine black particles (β phase) along the grain boundaries and at triple junctions. The SEM micrograph of AR sample surface after NAMLT is shown in Figure 4.46 c, d.

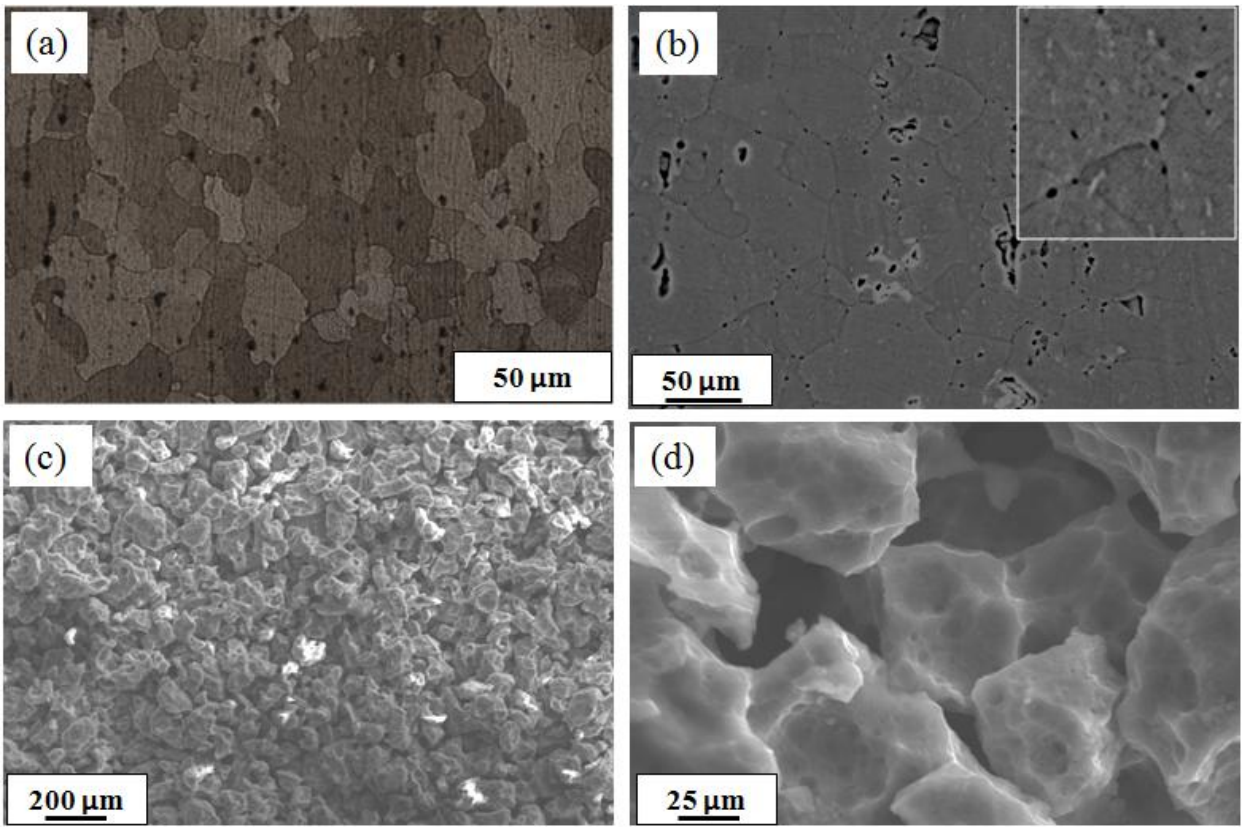

Figure 4.46: (a) Optical micrograph of AR, (b) SEM micrograph of AR in BSD mode, (c), (d) SEM micrographs at different magnifications of AR sample after NAMLT.

4.5.3.4 Corrosion behavior study through Immersion test

a. Weight loss measurements

To estimate the corrosion resistance of ST, CR and WR material directly, samples were immersed in 3.5% NaCl solution for 15 days. Weight loss measurements were taken after immersion period; corrosion rate was calculated and compared with corrosion rate obtained from polarization technique. The observed weight loss and corrosion rate of the ST, CR and WR material after immersion tests are listed in Table 4.5. ST sample has shown highest corrosion rate and CR material has shown lowest corrosion rate unlike corrosion rates obtained from polarization technique. The corrosion rate observed in WR sample is slightly higher than CR sample but much lower than ST sample. To understand the corrosion behaviour, samples immersed for 15 days were subjected to surface morphology study through SEM.

Table 4.5: Weight loss measurements and corrosion rates of 5083 Al alloy obtained from immersion test.

S. No.	Condition	Wt. loss (gm)	corrosion Rate (mill inches per year)	Corrosion rate (From tafel) (mill inches per year)
1	ST	0.0009	0.71925	0.799
2	CR	0.0001	0.379	0.90
3	WR	0.0003	0.44869	1.02

b. Surface observations before immersion test

Figure 4.47 shows the BSD micrograph of ST, CR and WR material at various magnifications. The white coarse second phase intermetallic particles observed in starting material (ST) are found to be fragmented during CR. Significant difference in size and distribution of second phase intermetallic particles can be observed between ST and CR samples. The microstructural features observed through BSD in WR sample are similar to CR sample. Elemental analysis through EDS of various constituent particles observed in ST material is discussed in section.

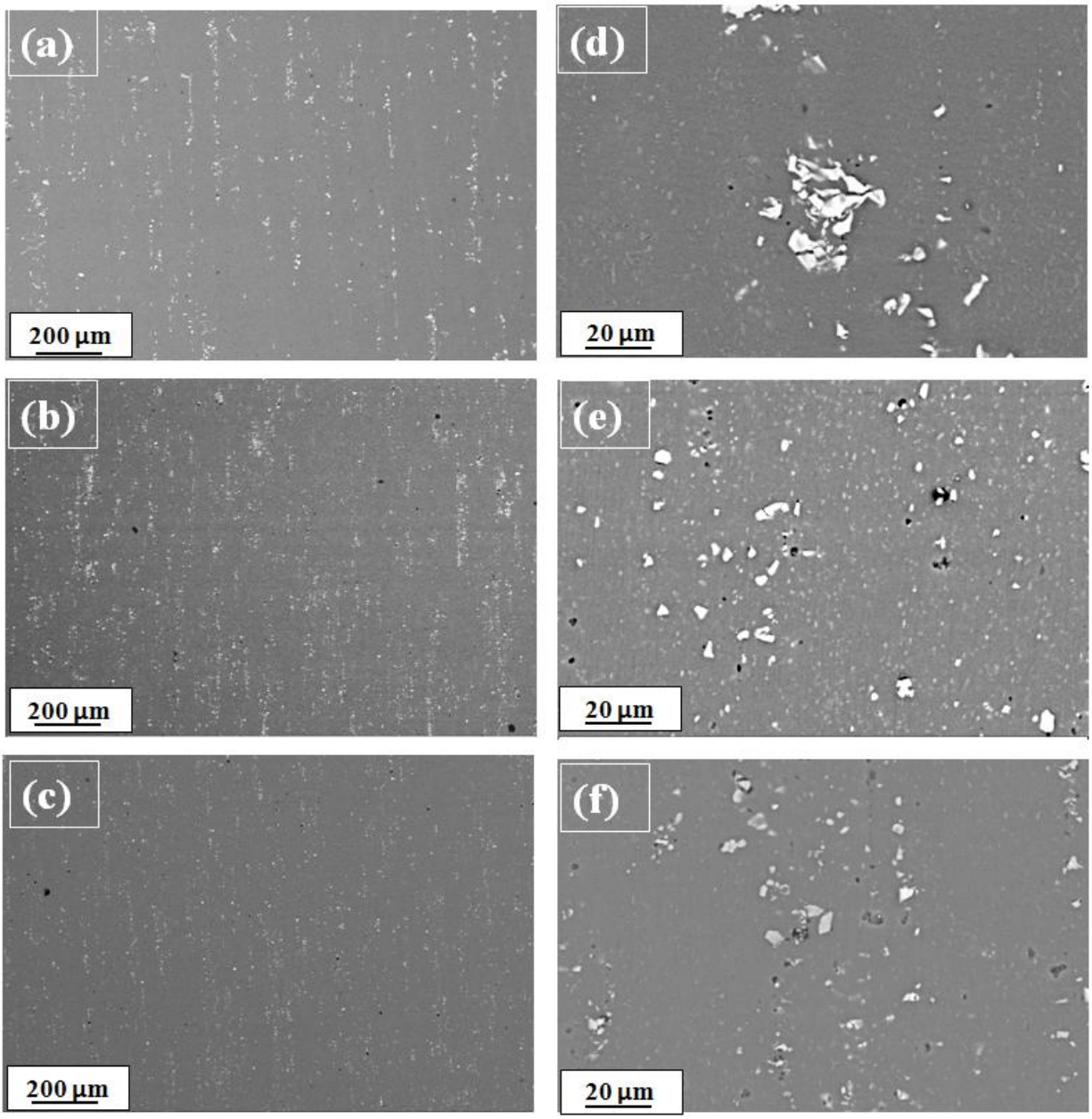

Figure 4.47: SEM micrographs of 5083 Al alloy before immersion test; (a) and (d) ST, (b) and (e) CR, (c) and (f) WR**.**

4.5.3.5 Surface characterizations after immersion test

Figure 4.48 shows the BSD micrograph with elemental area mappings of corroded surface in ST 5083 Al alloy. Figure 4.48a shows existence of two types of second phase particles, which are in white and black color. From the characteristic X-ray images (4.48 c-f), it can be assumed that white particles are Al (Fe, Mn) rich and black particles are Mg and Si rich phases.

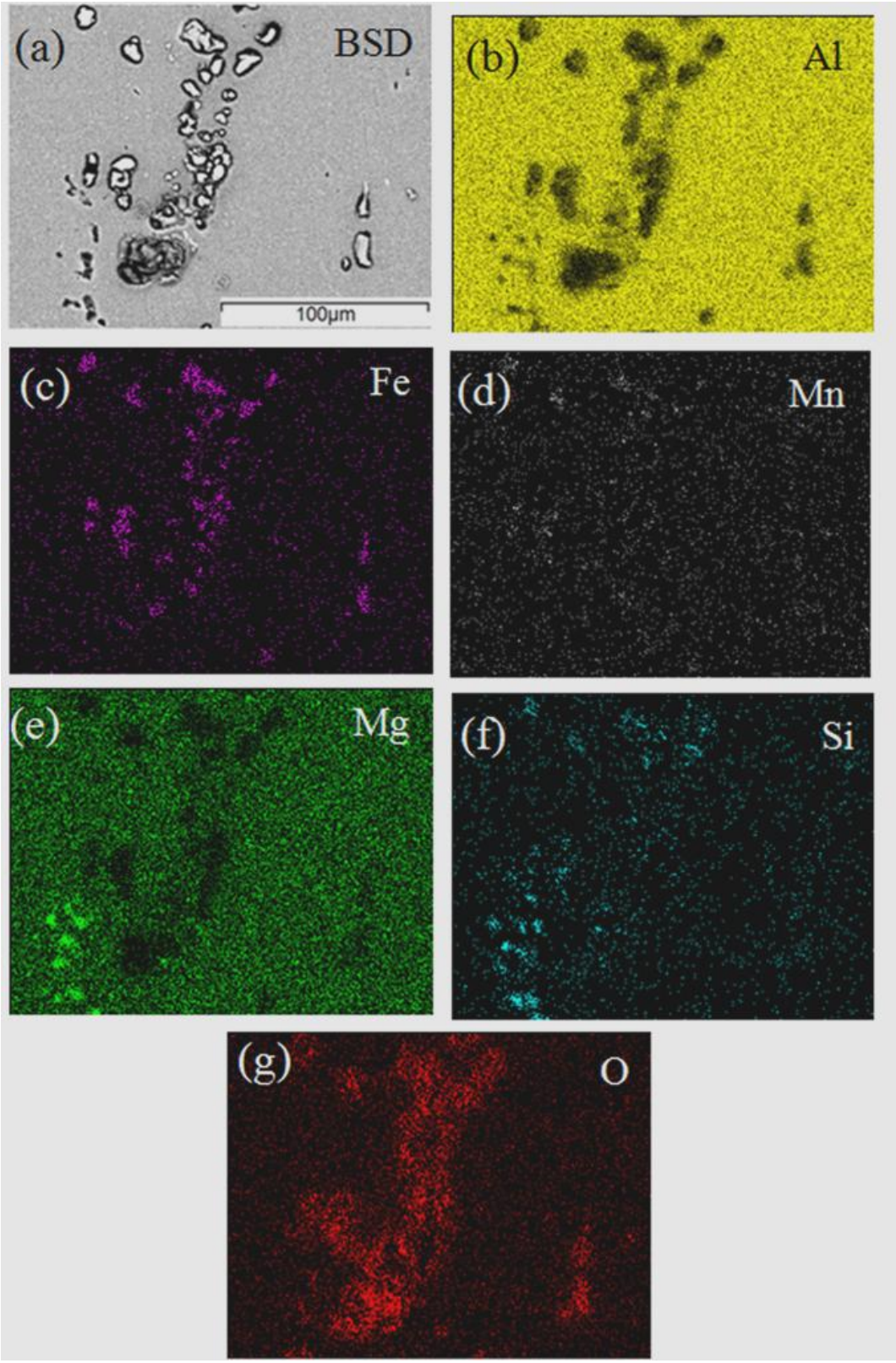

Figure 4.48: Surface morphology obtained from SEM analysis of ST sample after immersion with characteristic X-Ray area maps of elements.

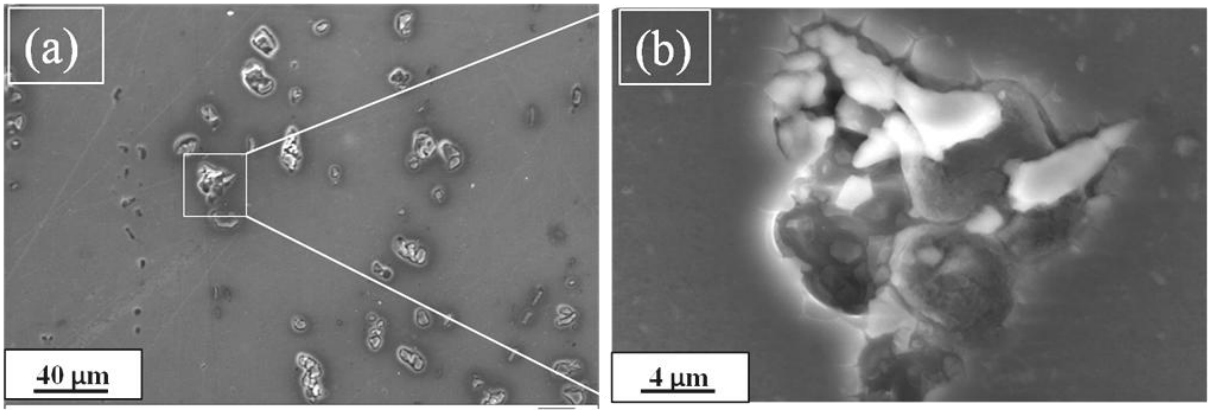

Figure 4.49: SEM micrograph of ST sample after immersion test; (a) Formation of pits around the second phase intermetallic particles, (b) Magnified view of marked area in Figure (a).

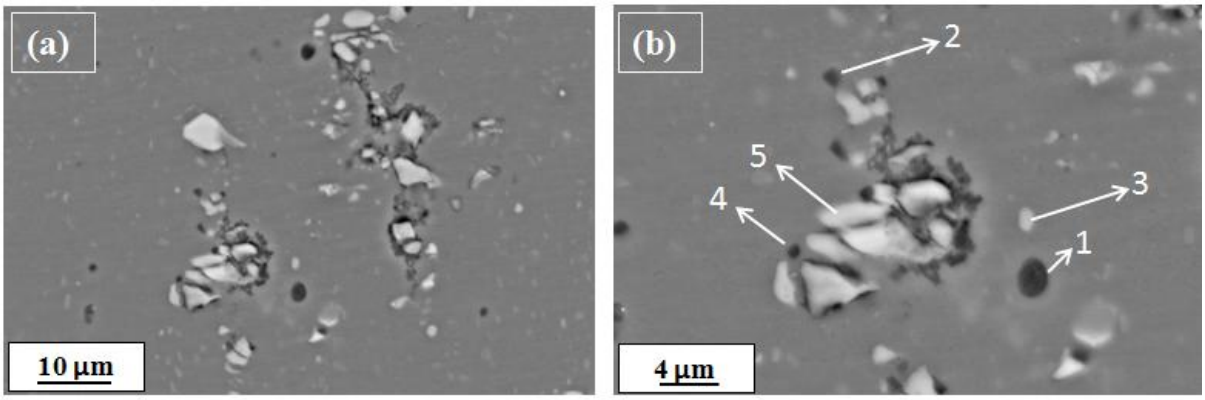

	Mg	Fe	Mn	Si	O	Al
1	3.15	0.13	0.31	12.64	22.48	61.06
2	3.27	0.57	1.35	5.95	14	74.76
3	2.95	5.94	3.74	0.01	7.48	78.82
4	3.60	0.09	0.63	1.77	11.29	82.62
5	0.51	17.24	7.37	1.33	2.51	71.04

Figure 4.50: SEM micrograph of CR sample after immersion test; (a) Observation of pit morphology around the second phase intermetallic particles, (b) Magnified view of marked area in Figure (a), Table shows elemental distribution of the spots from Figure (b).

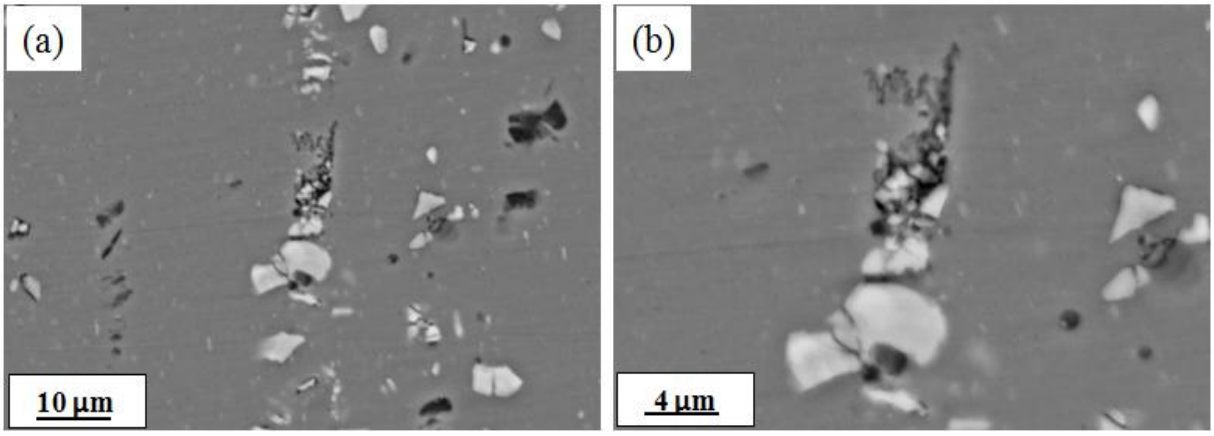

Figure 4.51: SEM micrograph of WR sample after immersion test; (a) Observation of pit morphology around the second phase intermetallic particles, (b) Magnified view of pits shown in Figure (a).

Figure 4.48g shows presence of oxygen associated with corroded product at the second phase particles. From the Figure 4.48a, g, it is reasonable to conclude that the corroded product is very low around Mg-Si rich phase particles. It shows that coarse Fe and Mn rich second phase particles are more prone to corrosion with Aluminium matrix. Figure 4.49 shows SEM micrograph of corroded area in ST sample. The magnified view of marked area in Figure 4.49a is shown in Figure 4.49b. It is evident from the Figure 4.49a, that big pits in several micrometers were formed around the precipitate particles. From EDS, it is confirmed that these particles are Al (Fe, Mn) complexes. Since Al (Fe, Mn) rich particles are noble than Al matrix, these big particles will act as cathodes in a micro galvanic cell formed between Aluminium matrix and these particles. Figure 4.50 shows corroded surface of CR material. The magnified view of marked area in Figure 4.50a shown in Figure 4.50b reveals that the damage of Aluminium matrix surrounded to the inter-metallic particles is very low as compared to the ST sample. The pitting morphology has changed as compared to ST sample. From Figure 4.50, it is clear that CR sample has undergone crystallographic pit formation along the lateral direction. Whereas, in case of WR, the pit morphology is similar to CR sample but few number of pits were observed in WR sample compared to ST and CR samples which resembles high pitting corrosion resistance (Figure 4.51).

4.5.4 Discussion

UFG material has received an extensive attention since last two decades due to its unique physical, chemical and mechanical properties (Sikora et al. 2004). The superior mechanical

properties of UFG material renders from high volume fraction of grain boundaries and high defect densities which will be the primary distinction with its polycrystalline coarse grain counterpart. In corrosion perspective, it is assumed that, due to high defect densities and large volume fraction of grain boundaries, corrosion resistance of the UFG material will get will worsen (Brunner et al. 2010). In 5083 Al alloys, the primary strengthening mechanism is through solid solution strengthening due to the presence of magnesium as a solid solution in the matrix. By the formation of β- phase through excess magnesium with aluminium, and presence of intermetallic particles (Al-Fe-Mn) and oxides of Mg-Si contribute to the dispersion strengthening. In the present study UFG 5083 Al alloy with improved mechanical properties was developed through cryorolling followed by warm rolling (WR) which can be possible replacements in marine applications. The improvement in mechanical properties after WR can be attributed to solid solution strengthening, dislocation strengthening, grain boundary strengthening and precipitation hardening. To estimate the corrosion behavior of UFG 5083 Al alloy which will be the potential material for marine applications, polarization tests, salt immersion tests were conducted in 3.5% NaCl simulated sea water conditions. NAMLT was performed to estimate the susceptibility to the IGC. The obtained results were compared with its conventional coarse grained counterpart (ST) and CR material. From the polarization experiments, it was observed that the OCP of CR material is nearly same to the OCP of ST material. OCP of WR material was lower to the CR and ST material. The lower OCP of WR material can be attributed to decreased grain size effect. Further, clear information of corrosion behaviour can be obtained from the polarization curves shown in Figure 4.44. The corrosion current density of the material was not greatly affected by the CR and WR. The obtained current density values of ST material were slightly lower than CR and WR. But the standard deviation in ST material was more. Over all the current density values were nearly same. Gopal Krishna et al. (2012) has observed lower corrosion density in Al-4Zn-2Mg after CR and it was reported that lowest current density of CR is due to the sluggish cathodic reactions due to cryorolling. The similar observations were found in industrial pure Al, Cu and Ti processed through ECAP (Balyanov et al. 2004, Chung et al. 2004, Vinagradov et al. 1999), where the corrosion resistance has increased in deformed microstructures as compared to its undeformed counterparts. Superior corrosion resistance of samples with deformed microstructure is due to rapid formation of passive films facilitated by higher density of dislocations and grain boundaries (Balyanov et al. 2004, Wei et al. 2007).

The difference between E_{pit} -E_{corr} of CR and WR material is more than ST material, indicates CR and WR resulted increase in pitting corrosion resistance of the material. The increase in pitting corrosion resistance can be evidenced from SEM observation of immersion test samples. The trend in estimated corrosion rate through immersion test was quite different than polarization test results. CR and WR material has shown lower corrosion rate than ST material. SEM results of immersed surfaces of ST, CR and WR reveals that ST material has undergone pitting corrosion unlike uniform corrosion in CR and WR material. The pits are located at the coarse intermetallic particles. Due to the formation of micro galvanic cells between intermetallic particles (cathodic) and the matrix (anodic), matrix material around the particles got dissolved, resulted deep hemispherical pits in ST material. The degree of the material damage through pitting corrosion depends on particle size, distribution and type of particle and environment (Chen et al. 1996). Through CR and WR, significant changes have occurred in the size and distribution of second phase particles of solution treated material. The particles got fragmented and finely distributed in the matrix of cryorolled sample as shown in Figure 4.47 b, e. Microstructural changes are reflected through increase in hardness from 58HV to 127 HV in CR and 58 HV to 146 HV in WR by increase in dislocation density and volume fraction low angle grain boundaries. Uniform corrosion observed in deformed material rather than localized corrosion is due to decrease in micro galvanic current between intermetallic particles and Al matrix (Chung et al. 2004). The increased difference between E_{pit} - E_{corr} values of CR and WR sample indicates increase in resistance to susceptibility for pitting corrosion. Superior corrosion resistance of samples with deformed microstructure is due to rapid formation of passive films facilitated by higher density of dislocations and grain boundaries (Balyanov et al. 2004, Wei et al. 2007).

According to ASTM-G67-13 if the mass loss of an alloy is about 1 to 15 mg/cm^2 then the alloy considered to be IGC resistant alloy. So in the present study from the NAMLT results it can be concluded that ST, CR and WR are more resistant to IGC. The mass loss of CR material was 0.33 more than ST material. The reported mass loss values are average of outcome of at least three samples in each condition. This minor difference is within the range of experimental scatter. As reported in the ASTM-G67-13 the standard deviation for test results of various laboratories for resistant materials ranged from 0.2 to 3.9 mg/cm^2. In ST material, Mg got dissolved in the matrix and it will be present in supersaturated solid solution after water quenching to room temperature. So it is obvious that absence of β phase along the grain boundaries would reduce the susceptibility to IGC of ST material. But the resistance to IGC diminishes with the precipitation of Mg as β

phase and the rate of work hardening. In CR material the deformation is achieved at very lower temperatures. This would suppress the precipitation of β phase. Besides CR resulted high fraction of low angle grain boundaries along with high dislocation densities. It was reported that low angle grain boundaries are more resistant to IGC (Davenport et al. 2006). Whereas in WR material the observed mass loss indicates the resistance to IGC has slightly decreased compared to ST and CR. The mass loss in WR material is 1.35 mg/cm^2 and 1.02 mg/cm^2 more than ST and CR respectively. This increment in mass loss is not significant as we discussed earlier about the standard deviation in experimental results. However the slight increase in mass loss could be also due to precipitation of β phase during warm rolling process at 175 °C. From TEM micrographs of WR material in the previous sections indicates mixed nature of high angle and low angle grain boundaries. Presence of high angle grain boundaries would acts as preferential sites for precipitation for β phase. This can be caused to increase in mass loss in WR material compared to ST and CR. Over all the proper control of thermo mechanical processing during the manufacturing process resulted pitting corrosion and IGC resistant material with improved mechanical properties.

4.5.5. Summary

The effect of cryorolling (CR) and cryorolling followed by warm rolling (WR) on corrosion resistance of 5083 Al alloy was investigated and the following conclusions were drawn:

- From the polarization measurements, it was observed that, WR material has shown higher corrosion current density (Icorr- 2.37 μA/cm^2) compared to CR material (I_{corr}-2.05 μA/cm^2) and ST material (I_{corr}-1.82 μA/cm^2). But this increment is not very significant compared to experimental error. But the E_{pit} - E_{corr} value (119 mV) of WR material is significantly more than ST material, which indicates more resistances to pitting corrosion.
- From the weight loss measurements and SEM characterization of samples surfaces after salt immersion tests confirmed that, ST material has undergone pitting corrosion. Presence of coarse intermetallic second phase particles leads to formation of micro galvanic cells with matrix resulted pitting corrosion in ST material. Whereas, CR and WR materials has shown resistance to pitting corrosion. The recorded material dissolution rate of CR and WR samples are low as compared to ST material.
- CR and WR did not create any adverse affect on the resistance to IGC. The high resistance to IGC after CR and WR can be attributed to the combination of various effects, which

reduced the presence of active precipitates at the grain boundaries. In WR material processing temperature did not sensitize the material and formation of low angle grain boundaries which are less prone to IGC imparted, increased IGC resistance.

CHAPTER 5
Conclusions and Suggestions for Future Work

This chapter presents the summary of major findings of the research work and directions for future work. The present work provides fundamental understanding of the influence of rolling temperature (cryorolling, room temperature rolling and cryorolling followed by warm rolling) and various thickness reductions (strains), post process annealing treatments, on evolution of microstructure and mechanical properties (hardness, tensile and impact toughness). In addition, the high cycle fatigue behaviour and corrosion behaviour of Al-Mg (5083Al) alloy processed under different deformation processing conditions are investigated

5.1 Conclusions

- 5083 Al alloy with high strength and good ductility was produced by cryorolling (CR). It has been observed that cryorolling has a great impact on improving yield strength of the alloy.
- The coarse grains have got fragmented and high dislocation density is generated with subgrain structure. After severe deformation, microstructural features indicate formation of fine dislocation cells and sub-grains along with dislocation tangle zones. This behaviour is attributed to suppression of dynamic recovery during rolling at liquid nitrogen temperature.
- CR has shown significant effect on increasing yield strength, but the ductility has reduced. Post CR short annealing at 300 °C for 6 minutes has resulted in UFG structure (300 nm), which is due to combined effect of static recovery and recrystallization.
- The Charpy impact test has shown reduced impact toughness of the alloy with increasing % of cryorolling as compared to starting solution treated material (ST - 32 J to CR 50% -7.5 J). This is attributed to lack of plastic deformation in the sample due to increase in yield strength, and brittle fracture of CR samples observed through SEM investigation.
- The loss in impact toughness has been compensated by occurrence of recrystallization after annealing treatments at 350 °C (7.5 J to 28 J) in CR 50% samples. The difference observed in grain size of CR 30% and CR 50% after annealing is due to more nuclei generated during CR 50%, leading to the formation of smaller grain size.

- Cryorolling followed by warm rolling (WR) performed at 175 °C was found to be optimum due to higher hardness and strength values (UTS-539 MPa, YTS-522 MPa, and ductility 6.8%). This improvement in strength and ductility can be attributed to formation of fine precipitates and dynamic recovery effect.
- The microstructure developed through cryorolling followed by warm rolling was observed to be thermally stable up to 250 °C. Significant improvement in ductility of WR sample (6.8% to 19%) after annealing was observed due to fully recrystallized equiaxed fine grain structure with an average grain size of 3.5 μm at 275 °C.
- Cryorolling and cryorolling followed by warm rolling has shown improved fatigue strength (180 MPa) compared to solution treated material (50 MPa) due to increase in yield strength. WR material has more fatigue strength than CR alone (165 MPa) is owing to combined effect of solid solution strengthening, precipitation hardening, dislocation strengthening and grain boundary strengthening. The resistance to crack nucleation increases significantly at low angle grain boundaries. Also, after rolling, particles got fragmented and aligned homogeneously in rolling direction into matrix resulted in reducing rate of fatigue crack growth.
- WR material has shown higher corrosion current density (Icorr- 2.37 $\mu A/cm^2$) compared to CR material (I_{corr}-2.05 $\mu A/cm^2$) and ST material (I_{corr}-1.82 $\mu A/cm^2$) during polarization test. But, this increment is not very significant compared to experimental error. The E_{pit} - E_{corr} value (119 mV) of WR material is significantly more than ST material, which indicates more resistances to pitting corrosion.
- Weight loss measurements and SEM characterization of samples surfaces after salt immersion tests confirmed that, ST material has undergone pitting corrosion. Coarse intermetallic second phase particles leads to formation of micro galvanic cells with matrix, causing pitting corrosion in ST material. Whereas, CR and WR materials has shown resistance to pitting corrosion. The recorded material dissolution rate of CR and WR samples are low as compared to ST material.
- CR and WR have shown high resistance to IGC. The high resistance to IGC after CR and WR can be attributed to the combination of various effects, which reduced the presence of active precipitates at the grain boundaries. In WR material, processing temperature did not

sensitize the material and formation of low angle grain boundaries imparted IGC resistance to the material.

5.2 Suggestions for future work

The outcomes of the present work have provided fundamental understanding on the effect of processing (cryorolling and cryorolling followed by warm rolling) on microstructural evolution and mechanical properties of 5083 Al alloy. Further, influence of processed conditions on the fatigue and corrosion characteristics was elucidated. The following suggestions are proposed for future work as an extension of current work:

- The effect of rolling on mechanical properties and microstructural behaviour performed at temperatures such as -50 °C, -100 °C, and -269 °C (Liquid Helium) can be studied.
- A comprehensive study on the influence of asymmetric rolling and cross rolling at different temperatures can be performed to investigate the changes in microstructural features and its effect on mechanical properties.
- Precipitation in the alloy subjected to cryorolling followed by warm rolling occurs as observed in the present work. However, it requires detailed investigation of the precipitation kinetics of ultrafine grained 5083 Al alloy, using DSC and TEM, for quantifying the improvement in mechanical properties realizable through precipitates. Studies related to fatigue crack growth, fracture toughness, and wear characteristics of ultrafine grained 5083 Al alloy produced under different thermo mechanical conditions could be investigated.
- The corrosion studies on ultrafine grained 5083 Al alloy subjected to different annealing conditions can be carried out for understanding its degradation behavior

References

1 **Aballe A.,** Bethencourt M., Botana F. J., Cano M.J., Marcos M., (2001), "Localized alkaline corrosion of alloy AA5083 in neutral 3.5% NaCl solution", Corrosion Science, 43, 1657-1674.

2 **Aballe A.,** Bethencourt M., Botana M.J., Marcos M., Sanchez-Amaya J.M., (2004), "Influence of the degree of polishing of alloy AA 5083 on its behaviour against localised alkaline corrosion", Corrosion Science., 46, 1909-1920.

3 **Ambat R.,** Davenport A.J., Scamans G.V.M., Afseth A., (2006), "Effect of Iron containing intermetallic particles on the corrosion behaviour of aluminium", Corrosion Science, 48, 3455-3471.

4 **Apps P.J.,** Bowen J.R., Prangnell P.B., (2003), "The effect of coarse second-phase particles on the rate of grain refinement during severe deformation processing", Acta Materialia, 51, 2811-2822.

5 **Ashby M.F.**, (1992), "Physical modeling of materials problems", Material science and Technology", 8, 102-111.

6 ASM International Hand Book, Vol. 2.

7 **Attallah Moataz M.,** (2007), **"**Microstructure-property development in friction stir welds of aluminium-based alloys [dissertation]": Metallurgy and Materials, School of Engineering, University of Birmingham.

8 **Aziz P.M.,** Godard H.P., (1954), "Pitting corrosion characteristics of aluminium: Influence of iron and silicon", Corrosion Science, 10, 269-272.

9 **Azushima A.,** (2000), "Materials development by extrusion process", Journal of Japan Society for Technology of Plasticity 47, 456-459.

10 **Azushima A.,** Kopp R., Korhonen A., Yang D.Y., Micari F., Lahoti G.D., Groche P., Yanagimoto J., Tsuji N., Rosochowski A., Yanagida A., (2008), "Severe plastic deformation (SPD) processes for metals", CIRP Annals - Manufacturing Technology, 57, 716–735.

11 **Balyanov A.,** Kutnyakova J, Amirkhanova N.A., Stolyarov V.V., Valiev R.Z., Liao X.Z., Zhao Y.H., Jiang Y.B., Xu H.F., Lowe T.C., Zhu Y.T., (2004), "Corrosion resistance of ultra fine-grained Ti", Scripta Materialia.,51, 225-229.

12 **Bay B.,** Hansen N., Hughes D.A., Wilsdorf D.K., (1992), “Evolution of FCC deformation structures in polyslip”, Acta Metallurgica Materialia, 40, 205-219.

13 **Blanc C.,** Mankowski G., (1997), “Susceptibility to pitting corrosion of 6056 aluminium alloy”, Corrosion Science, 39, 949-959.

14 **Bridgman P.W.,** (1935**), “**Effects of high shearing stress combined with high hydrostatic pressure”, Physical Review, 48, 825-847.

15 **Bridgman P.W.,** (1937) “Flow phenomena in heavily stressed metals”, Journal of Applied Physics, 8, 328-336.

16 **Brown S.,** (1999), “Feasibility of replacing structural steel with aluminum alloys in the ship building industry”, University of Wisconsin-Madison, April 29.

17 **Brunner J.G,** May J., Hoppel H.W., Goken M., Virtanen S., (2010), "Localised corrosion of ultrafine grained Al-Mg model alloys", Electrochimica Acta, 55, 1966-1970.

18 **Callister W.D.,** (2007), “Jr. Material Science and Engineering: An Introduction”, John Wiley & Sons, Inc., 7th Ed.

19 **Carrol W.,** Breslin C., (1991), "Stability of passive films formed on aluminium in acqueous halide solutions", British Corrosion Journal, 26, 255-259.

20 **Chang H.,** Zheng M.Y., Wu K., Gan W.M., Tong L.B., Brokmeier H.G., (2012), Microstructure and mechanical properties of the Mg/Al multilayer fabricated by accumulative roll bonding (ARB) at ambient temperature”, Material Science and Engineering A, 543, 249-256.

21 **Chang J.C.,** Chuang T.H., (1999), "Stress-Corrosion Cracking Susceptibility of the Superplastically formed 5083 Aluminium Alloy in 3.5 % NaCl solution", Metallurgical and Materials Transcations, 37A, 1391-1399

22 **Chatterjee A**., Sharma G., Sarkar A, Singh J.B., Chakravartty J.K., (2012), "Study on cryogenic temperature ECAP on the microstructure and mechanical properties of Al-Mg alloy, Material Science and Engineering A, 556, 653-657.

23 **Chawla N.,** Andres C., Jones J.W., Allison J.E., (1998), "Effect of SiC volume fraction and particle size on the fatigue resistance of a 2080 Al/SiC p composite", Metallurgical and Material Transaction A, 29, 2843- 2849.

24 **Chen G.S.,** Gao M., Wei R.P., (1996), “Micro constituent-Induced Pitting Corrosion in Aluminum Alloy 2024-T3”, NACE International, Corrosion Science, 52, 8-15.

25 **Chen Y.,** Li Y., Lu C., Ding H., Li Q., (2008), “Influence of cryo ECAP on microstructure and property of commercial pure aluminium”, Materials Letters, 62, 17-18, 2821-2824.

26 **Chen Y.J.,** Roven H.J., Gireesh S.S., Skaret P.C., Hjelen J., (2011), “Quantitative study of grain refinement in Al-Mg alloy processed by equal channel angular pressing at cryogenic temperature”, Materials Letters, 65, 3472-3475.

27 **Cheng S.,** Zao Y.H., Zhu Y.T., Ma E., (2007), “Optimizing the strength and ductility of fine structured 2024 Al alloy by nano-precipitation”, Acta Materialia, 55, 5822-5832.

28 **Choy K.,** (2003), “Chemical vapour deposition of coatings”, Progress in Material Science, 48, 57-70.

29 **Chun Y.B.,** Ahn S.H., Shin D.H., Hwang S.K., (2009), “Combined effects of grain size and recrystallization on the tensile properties of cryorolled pure vanadium”, Material Science and Engineering A, 508, 253-258.

30 **Chung C.S.,** Kim J.K., Kim H.K., Kim W.J., (2002), "Improvement of high-cycle fatigue life in a 6061 Al alloy produced by equal channel angular pressing", Material Science and Engineering A, 337, 39-44.

31 **Das J.,** (2011), “Evolution of nanostructure in α brass upon cryorolling”, Material Science and Engineering A, 530, 675-679.

32 **Das P.,** Jayaganthan R., Chowdhury T., Singh I.V., (2011), “Fatigue behaviour and crack growth rate of cryorolled Al 7075 alloy”, Material Science and Engineering A, 528, 7124-7132.

33 **Das P.,** Jayaganthan R., Singh I.V., (2011), “Tensile and impact-toughness behaviour of cryorolled Al 7075 alloy”, Materials and Design, 32, 1298-1305.

34 **Davenport A.L.,** Yuan Y., Ambat R., Connolly B.J., Strangwood M., Afseth A., Scamans G., (2006), "Intergranular corrosion and stress corrosion cracking of sensitised AA5182", Material Science Forum, 519-521, 641-647.

35 **Davis J.R.,** (1999), Corrosion of Aluminum and Aluminum Alloys, ed. by J.R.Davis & Associates, ASM Int., Metals Park OH, USA.

36 **Dean R.,** (1995), “Aluminum-large aluminum extrusion in marine applications”, Materials World, 3, 65-67.

37 **Defeng G.,** Li M., Shi Y., Zhang Z., Zhang H., Liu X., Wei B., Zhang X., (2012), “High strength and ductility in multimodal-structured Zr”, Materials and Design, 34, 275-278.

38 **Dybiec H.,** (2007), “Plastic consolidation of metallic powders”, Archieves of Metallury and Materials, 52, 61-170.

39 **Erb U.,** (1995), “Electrodeposited nanocrystals: Synthesis, properties and industrial applications”, Nanostructured Materials, 6, 533-538.

40 **Erbel S.,** (1979), "Mechanical properties and structure of extremely strain hardened copper", Metals Technology, 6, 482-486.

41 **Estrin Y.,** Gottstein G., Shvindlerman L.S., (2004), "Diffusion controlled creep in nanocrystalline materials under grain growth", Scripta Materialia, 50, 993-997.

42 **Estrin Y.,** Vinogradov A., (2013), "Extreme grain refinement by severe plastic deformation: A wealth of challenging science", Acta Materialia, 61, 782-817.

43 **Fang D.R.,** Tian Y.Z., Duan Q.Q., Wu S.D., Zhang Z.F., Zhao N.Q., Li J.J, (2011), “Effect of equal channel angular pressing on the strength and toughness of Al-Cu alloys”, Journal of Material Science, 46, 5002-5008.

44 **Fomenko L.S.,** Rusakova A.V., Lubenets S.V., Moskalenko V.A., (2012), “Micromechanical properties of nanocrystalline titanium obtained by cryorolling”, Low Temperature Physics, 36, 1042-1046.

45 **Gang U.G.,** Lee S.H., Nam W.J., (2009), “The evolution of microstructure and mechanical properties of a 5052 aluminium alloy by the application of cryogenic rolling and warm rolling”, Materials Transaction, 50, 82-86.

46 **George E. Totten.,** MacKenzie D. Scott, (2003), “Hand Book of Aluminium alloys, Physical Metallurgy and Processes”, 7, Marcel Dekker, Inc., NewYork, Basel.

47 **Ghali E.,** (2010), Corrosion Resistance of Aluminum and Magnesium Alloys, Published by John Wiley & Sons, Inc., Hoboken, New Jersey

48 **Gleiter H.,** (1981), "Materials with ultrafine grain size. In:N.Hansen, editor, deformation of polycrystals: mechanism and microstructures, Riso National Laboratory, Roskilde, 15.

49 **Gleiter H.,** (1989), "Nanocrystalline materials", Progress in Material Science", 33, 223-315.

50 **Gopala Krishna K.,** Sivaprasad K., Sankara Narayanan T.S.N., Hari Kumar K.C., (2012), “Localized corrosion of an ultrafine grained Al-4Zn-2Mg alloy produced by cryorolling”, Corrosion Science, 60, 82-89.

51 **Gopala Krishna K.,** Sivaprasad K., Venkateswarlu K., Hari Kumar K.C., (2012), “Microstructural evolution and aging behavior of cryorolled Al-4Zn-2Mg alloy”, Material

Science and Engineering A, 535, 129-135.

52 **Goswami R.,** Spanos G., Pao P.S., Holtza R.L., (2010), "Precipitation behavior of the phase in Al-5083", Material Science and Engineering A, 527, 1089-1095.

53 **Grimes R.,** Dashwood R.J., Durban A., Jackson M., Katsas S., Pong I., Todd G., (2007), "Development of superplastic properties in quasi single phase alloys", Material Science Forum, 551-552, 357-364.

54 **Gubicza J.,** Schiller I., Chinh N.Q., Illy J., Horita Z., Langdon T.G., (2007), " The effect of severe plastic deformation on precipitation in supersaturated Al-Zn-mg alloy", Material Science and Emgineering A., 460, 77-85.

55 **Hadzima B.,** Janecek M., Estrin Y., Kim H.S., (2007), "Microstructure and corrosion properties of ultrafine-grained interstitial free steel", Material Science and Engineering A, 462, 243-247.

56 **Hailiang Y.U.,** Cheng L.U., Tiet K., Liu X., Sun Y., Yu Q., Kong C., (2012), "Asymmetric cryorolling for fabrication of nanostructural aluminum sheets", Scientific Reports, 2, 772-777.

57 **Hall E.O.,** (1951), "The Deformation and Ageing of Mild Steel: III Discussion of Results", Proceedings of Physical Society, London, 64, 747-753.

58 **Han B.Q.,** Lee Z., Witkin D., Nutt S., Lavernia E.J., (2005), "Deformation behaviour of bimodal nanostructured 5083 Al alloy", Metallurgical and Materials Transactions A, 36, 957-965.

59 **Hanlon T.,** Kwon Y.N., Suresh S., (2003), "Grain size effects on the fatigue response of nanocrystalline metals", Scripta Materialia, 49, 675-680.

60 **Hansen N.,** (1992), "Deformation microstructures", Scripta Metallurgica Materialia, 27, 1447- 1452.

61 **Hatch J.E.,** (1984), "Aluminium: Properties and Physical Metallurgy", ASM Metals, Park Ohio, 26.

62 **Hecht R.L.,** (1995), K. Kannan: In superplasticity and superplastic forming, A.K. Gosh and T.R. Bieler, eds., TMS, Warrendale, PA, 259

63 **Hefti L.D.,** (2007), "Commercial airplane applications of superplastically formed AA 5083 Aluminum Sheet", Journal of Materials Engineering and Performance, 16, 136-141.

64 **Hirsch J.,** (2011), Aluminium in innovative light weight car design, Materials Transactions, 52, 818-824.

65 **Hirth J.P.,** (1982), “Lothe J., Theory of Dislocation”, 2nd Ed. Wiley, New York.

66 **Hockauf M.,** Meyer L.W., Nickel D., Alisch G., Lampke T., Wielage B., Kruger L., (2008), “Mechanical properties and corrosion behaviour of ultrafine-grained AA6082 produced by equal-channel angular pressing”, Journal of Materials Science, 43, 7409-7417.

67 **Hoeven J.,** (2002), “A New 5xxx Series Alloy Developed for Automotive Applications” SAE International, Doc. 2002-01-2128.

68 **Hoppel H.W.,** Kautz M., Xu C., Murashkin M., Langdon T.G., Valiev R.Z., (2006), "An overview: Fatigue behaviour of ultrafine-grained metals and alloys", International Journal of Fatigue, 28, 1001-1010.

69 **Horita Z.,** Smith D.J., Furukawa M., Nemoto M., Valiev R.Z., Langdon T.G., (1996), “An investigation of grain boundaries in submicrometer-grained Al-Mg solid solution alloys using high-resolution electron microscopy”, Journal of Materials Research, 11, 1880-1890.

70 **Hu C.M.,** Lai C.M., Kao P.W., Ho N.J., Huang J.C., (2009), "Solute-enhanced tensile ductility of ultrafine grained Al-Zn alloy fabricated by friction stir processing", Scripta Materialia, 60, 639-642.

71 **Huang J.Y.**, Zhu Y.T., Jiang H., Lowe T.C., (2001), “Microstructure and dislocation configurations in nanostructured Cu processed by repetitive corrugation and straightening”, Acta Materialia, 49, 1497-1505.

72 **Humphreys F.J.,** Hatherly M., (2004), Recrystalization and Related Annealing Phenomena, 2nd ed. Elsevier Pub.

73 **Huskins E.L.,** Cao B., Ramesh K.T., (2010), “Strengthening mechanisms in an Al-Mg alloy”, Materials Science and Engineering A., 527, 1292-1298.

74 **Iwahashi Y.,** Horita Z., Nemoto M., Langdon T.G., (1998), The process of grain refinement in equal channel angula pressing, Acta Materialia, 46, 3317-3331.

75 **Jaeger R.C.,** (2002). "Film Deposition: Introduction to Microelectronic Fabrication”, Upper Saddle River: Prentice Hall., ed. 2nd, ISBN 0-201-44494-1.

76 **Jafarzadeh K.,** Shahrabi T., Oskouei A.A., (2009), “Novel approach using EIS to study flow accelerated pitting corrosion of AA 5083-H321 aluminium - magnesium alloy in NaCl solution”, Journal of Applied Electrochemistry, 39, 1725-1731.

77 **Jayaganthan R.,** Brokmeier H.G., Schwebke B., Panigrahi S.K., (2010), “Microstructure and texture evolution in cryorolled Al 7075 alloy”, Journal of Alloys and Compounds”, 496, 183-188.

78 **Jayatilaka,** (1979), A Fracture of Engineering Brittle Materials", Applied Science Publishers Ltd., London, 378.

79 **Jiang D.,** Ning J., Sun J., Hu Z., Hou Y., (2008), "Annealing behavior of Al-Mg-Mn alloy processed by ECAP at elevated temperature", 18, 248-254.

80 **Jones R.H.,** (1992), "In: Stress corrosion cracking", ASM International, Materials Park, Ohio.

81 **Jones R.H.,** Baer D.A., Daneielson M.J., Vetrano J.S., (2001), "Role of Mg in the Stress Corrosion Cracking of an Al-Mg Alloy", Metallurgical and Materials Transcations, 37A, 1699-1705.

82 **Kaibyshev O.A.,** (2001), "Grain refinement in commercial alloys due to high plastic deformations and phase transformations", Journal of materials processing technology, 117, 300-306.

83 **Kaibyshev R.O.,** Mazurina I.A., Gromov D.A., (2006), **"**Mechanisms of grain refinement in aluminum alloys in the process of severe plastic deformation", Material Science and Heat Treatment, 48, 57-62.

84 **Kamikawa N.,** Huang X., Tsuji N., Hansen N., (2009), "Strengthening mechanisms in nanostructured high-purity aluminium deformed to high strain and annealed", Acta Materialia, 57, 4198-4208.

85 **Kang U.G.,** Lee H.J., Nam W.J., (2012), "The achievement of high strength in an Al 6061 alloy by the application of cryogenic and warm rolling", Journal of Material Science, 47, 7883-7887.

86 **Kang U.G.,** Lee J.C., Jeong S.W., Nam W.J. (2010), "The improvement of strength and ductility in ultra-fine grained 5052 Al alloy by cryogenic- and warm-rolling", Journal of Material Science, 45, 4739-4744.

87 **Kapoor R**., Sarkar A., Yogi R., Shekhawat S.K., Samajdar I., Chakravartty J.K., (2006), "Softening of Al during multi-axial forging in a channel die", Material Science and Engineering A, 560, 404-412.

88 **Kauffmann A.,** Freudenberger J., Geissler D., Yina S., Schillinger W., Sarma V.S., Bahmanpour H., Scattergood R., Khoshkhoo M.S., Wendrock H., Koch C.C., Eckert J., Schultz L., (2011), "Severe deformation twinning in pure copper by cryogenic wire drawing" Scripta Materialia, 59, 7816–7823.

89 **Kawano K.,** (2005), Wakita M., Fukushima S., Eto M., Sasaki T., Shibahara T., “Super short interval multi-pass rolling technology for manufacturing ultrafine grained steel”, Material Science and Technology, 55-64.

90 **Kawasaki M.,** Figueiredo R.B., Xu C., Langdon T.G., (2007), "Developing Superplastic Ductilities in Ultrafine-Grained Metals", Metallurgical and Materials Transactions A, 38, 1891-1898.

91 **Kim H.S.,** Estrin Y., (2005), “Microstructural modelling of equal channel angular pressing for producing ultrafine grained materials”, Materials Science and Engineering A, 410-411, 285-289

92 **Kim K.H.,** Chun Y.B., Hwang S.K., (2011), “Deformation heterogeneity of Ti under cryogenic channel-die compression”, International, 21, 277-285

93 **Koch C.G.,** (1997), Synthesis of nanostructured materials by mechanical milling: problems and opportunities", Nanostructured materials, 9, 13-22.

94 **Konkova T.N.,** Mironov S.Y., Korznikov A.V., (2012), “grain refinement in copper via cryogenic deformation”, Reviews of Advanced Materials Science, 31, 31-35.

95 **Krishnaiah A.,** Chakkingal U., Kim H.S., “Mechanical properties of commercially pure aluminium subjected to repetitive bending and straightening process", (2008), Transactions of the Indian Institute of Metals, 61,165-167.

96 **Kumar S.,** Sarma V.S., Murty B.S., **(**2009), “The influence of room temperature and cryogenic temperature rolling on the aging and wear behaviour of Al-4Cu-5TiB2 in situ composites”, Journal of Alloys and Compounds, 479, 268-273.

97 **Lee J.C.,** Lee S.H., Kim S.W., Hwang D.Y., (2012), “The thermal behavior of aluminum 5083 alloys deformed by equal channel angular pressing”, Thermochimica Acta, 499, 100-105.

98 **Lee J.C.,** Suh J.Y., Ahn J.P., (2003), “Work-softening behavior of the Ultrafine grained Al Alloy processed by high-strain-rate, dissimilar-channel angular pressing”, Metallurgical and Materials Transaction, 34, 625-632.

99 **Lee S.H.,** Kim W.J., Utsunomiya H., (2011), “Fabrication and evaluation of nano-structure Al SiCp composite by accumulative roll-bonding”, Journal of Nanoscience and Nanotechnology, 11, 7451-7455.

100 **Lee S.H.,** Sakai T., Saito Y., Utsunomiya H., Tsuji N., (1999), “Strengthening of seath-rolled aluminum based MMC by the ARB process”, Materials Transactions, JIM, 40,

1422-1428.

101 **Lee S.W.,** Yeh J.W., (2007) "Superplasticity of 5083 alloys with Zr and Mn additions produced by reciprocating extrusion", Materials Science and Engineering A, 460-461, 409–419

102 **Lee T.R.,** Chang C.P., Kao P.W., (2005), "The tensile behavior and deformation microstructure of cryo-rolled and annealed pure nickel", Material Science Engineering A, 408, 131-135.

103 **Lee Y.B.,** Shin D.H., Park K.T., Nam W.J., (2004), "Effect of annealing temperature on microstructure and mechanical properties of a 5083 Al alloy deformed at cryogenic temperature." Scripta Materialia, 51, 355-359.

104 **Liddicoat P.V.,** Liao X.Z., Zhao Y.H., Zhu Y.T., Murashkin M.Y., Lavernia E.J., Valiev R.Z., Ringer S.P., (2010), " Nanostructural hierarchy increases the strength of aluminium alloys", Nature Communication,63, 1-7.

105 **Liu C.Y.,** Jing R., Wang Q., Zhang B., Jia Y.Z., Ma M.Z., Liu R.P., (2012), "Fabrication of Al/Al_3Mg_2 composite by vacuum annealing and accumulative roll-bonding process", Materials Science and Engineering A., 558, 510-516.

106 **Liu M.,** Roven H.J., Liu X., Murashkin M., Valiev R.Z., Ungar T., Balogh L., (2010), "Grain refinement in nanostructured Al-Mg alloys subjected to high pressure torsion", Journal of Materials Science, 45, 4659-4664.

107 **Liu X.D.,** Wang J.T., Ding B.Z., (1993), "Preparation and properties of nanocrystalline $(Fe_{0.99}Mo_{0.01})_{78}Si_9B_{13}$ alloys", Scripta Metallurgica Materialia, 28, 59-64.

108 **Lu L.,** Shwaiger R., Shan Z.W., Dao M., Lu K., Suresh S., (2005), "Nano-sized twins induce high rate sensitivity of flow stress in pure copper", Acta Materialia, 53, 2169-2179.

109 **Ma A.,** Suzuki K., Nishida Y., Saito N., Shigematsu I., Takagi M., Iwata H., Watazu A., Imura T., (2005), "Impact toughness of an ultrafine-grained Al-11mass % Si alloy processed by rotary- die equal-channel angular pressing", Acta Materialia, 53, 211-220.

110 **Malekjani S.,** Hodgson P.D., Cizek P., Sabirov I., Hilditch T.B., (2011), "Cyclic deformation response of UFG 2024 Al alloy", International Journal of Fatigue, 33, 700-709.

111 **Mani Krishna K.V.,** Sahoo S.K., Samajdar I., Neogy S., Tewari R., Srivastava D., Dey G.K., Das G.H., Saibaba N., Banarjee S., (2008), "Microstructural and textural

developments during Zircaloy-4 fuel tube fabrication", Journal of Nuclear Materials, 383, 78-85.

112 **May J.,** M. Dinkel, D. Amberger, H. W. Hoppel, M. Goken, (2007), "Mechanical Properties, Dislocation Density and Grain Structure of Ultrafine-Grained Aluminum and Aluminum-Magnesium Alloys", Metallurgical and Material Transaction A, 38, 1941-1945.

113 **Mecking H.,** Kocks U.F., "Kinetics of flow and strain hardening", (1981), Acta Materialia, 29, 1865-1875.

114 **Meyers M.A.,** Mishra A., Benson D.J., (2006), B212"Mechanical properties of nano crystalline materials", Progress in Material Science, 51, 427-556.

115 **Mishra R.S.,** Ma Z.Y.,(2005), "Friction stir welding and processing", Materials Science and Engineering R: Reports, 50,1-78

116 **Miyamoto H.,** Ota K., Mimaki T., (2006), "Viscous nature of deformation of ultra-fine grain aluminum processed by equal-channel angular pressing", Scripta Materialia, 54, 1721–1725.

117 **Morris M.A.,** Oca C.G., Morris D.G., (2003), Mechanical behaviour of dilute Al-Mg alloy processed by equal channel angular pressing", Scripte Materialia, 48, 213-218.

118 **Mughrabi H.,** Lowe T.C., Valiev R.Z., (2000), Investigations and Applications of Severe Plastic Deformation,NATO Science, 241-253.

119 **Mughrabi H.,** Hoppel H.W., Kautz M., (2004), "Fatigue and microstructure of ultrafine-grained metals produced by severe plastic deformation", Scripta Materialia, 51, 807-815.

120 **Murray G.A.W.,** Lamb H.J., Godard H.J., (1967), "Role of iron in aluminum on the initiation of pitting in water", British Corrosion Journal, 2, 216-223.

121 **Nakamura K.,** Neishi K., Kaneko K., Nakagaki M., Horita Z., (2004), "Development of severe torsion straining process for rapid continuous grain refinement", Materials Transactions, 45, 3338- 3342.

122 **Nieh T.G.,** Wadsworth J., Sherby O.D., (1997), Superplasticity in Metals and Ceramics, B138 Cambridge University, Cambridge, 181-183.

123 **Niendorf T.,** Canadinc D., Maier H.J., Karaman I., (2008), "The role of heat treatment on the cyclic stress-strain response B136of ultrafine- grained interstitial-free steel", International Journal of Fatigue, 30, 426-436.

124 **Nikulin I.,** Kipelova K., Malopheyev S., Kaibyshev R., (2012), "Effect of second phase particles on grain refinement during equal-channel angular pressing of an Al-Mg-Mn alloy", Acta Materialia, 60, 487-497.

125 **Niranjani V.L.,** Hari Kumar K.C., Sarma V.S, (2009), "Development of high strength Al-Mg-Si AA6061 alloy through cold rolling and ageing", Materials Science and Engineering A, 515, 169-174.

126 **Nishida Y.,** Arima H., Kim J.C., Ando T., (2001), "Rotary-die Equal-channel Angular Pressing of an Al-7 mass% Si-0.35 mass%-Mg alloy", Scripta Materialia, 45, 261-266.

127 **Nisida Y**., Arima H., Kim J.C., Ando T., (2000), "Superplasticity of SiCw/7075 composites processed by Rotary-Die Equal-channel Angular Pressing", The Japan Institute of Metals, 64, 1224-1229.

128 **Noda M.,** Funam K., Suwahara Y., (2005), "Effects of constraint and strain path on evolution of ultrafine grained microstructure by multi-axial alternative forging", Materials Science Forum, 475 -479, 3471-3474.

129 **Orowan E.,** (1948), "Symposium on internal stresses", Institution of Metals, London, 415

130 **Osmura K.,** (1984), Tetsuzo O., "Metastable phasees in early stages of precipitation in Al-Mg alloy", Metallurgical Transaction, 15, 838-842.

131 **Ozden S.,** Ekici R., Nair F., (2007), "Investigation of impact behavior of aluminium based SiC particle reinforced metal-matrix composites", Composites: Part A, 38, 484-494.

132 **Panigrahi S.K.,** (2009), "Processing mechanical and microstructural studies of ultrafine grained Al alloys [dissertation]": Metallurgical and Materials Engineering, Indian Institute of Technology, Roorkee, India.

133 **Panigrahi S.K.,** Devanand D., Jayaganthan R., (2010), "Effect of ageing on strength and ductility of ultrafine grained al 6061 alloy", Materials Science Forum, 633-6340, 303-309.

134 **Panigrahi S.K.,** Jayaganthan ., (2008), "Effect of rolling temperature on microstructure and mechanical properties of 6063 Al alloy", Material Science and Engineering A, 492, 300-305.

135 **Panigrahi S.K.,** Jayaganthan R., (2008), "A study on the mechanical properties of cryorolled Al-Mg-Si alloy", Material Science and Engineering A, 480, 299-305.

136 **Panigrahi S.K.,** Jayaganthan R., (2010), "Effect of annealing on precipitation, microstructural stability, and mechanical properties of cryorolled Al 6063 alloy", Journal of Materials Science, 45, 5624-5636.

137 **Panigrahi S.K.,** Jayaganthan R., (2011), "Development of ultrafine-grained Al 6063 alloy by cryorolling with the optimized initial heat treatment conditions", Materials and Design, 32, 2172-2180.

138 **Panigrahi S.K.,** Jayaganthan R., Pancholi V., Gupta M., (2010), "A DSC study on the precipitation kinetics of cryorolled Al 6063 alloy", Materials Chemistry and Physics, 122, 188-193.

139 **Park K.T.,** Park J.H., Lee Y.S., Nam W.J., (2005), " Microstructures developed by compressive deformation of coarse grained and ultrafine grained 5083 Al alloys at 77 K and 298 K", Materials Science and Engineering A, 408, 102-109.

140 **Patlan V.,** Vinogradov A., Higashi K., Kitagawa K., (2001), "Cyclic response of fine grain 5056 Al-Mg alloy processed by equal-channel angular pressing", Material Science and Engineering A, 300, 171-182.

141 **Petch N.J.,** (1953), "The cleavage strength of polycrystals", Journal of the Iron and Steel Institute, 174, 25.

142 **Polmear I.J.,** (1995),"Light Metals: Metallurgy of Light Metals", Arnold, London.

143 **Prangnell P.B.,** Bowen J.R., Apps P.J., (2004), "Ultra-Fine Grain Structures in Aluminium Alloys by Severe Deformation Processing", Materials Science and Engineering A, 375-377, 178-185.

144 **Raju S.S.,** Krishna M.G., Padmanbhan K.A., Sarma V.S., Gurao N.P., Wilde G., (2011), "Microstructure evolution and hardness variation during annealing of equal channel angular pressed ultra-fine grained nickel subjected to 12 passes", Journal of material Science, 46, 2662-2671.

145 **Rangaraju N.,** Raghuram T., Krishna B.V., Rao K.P., Venugopal P., (2005), "Effect of cryorolling and annealing on microstructure and properties of commercially pure aluminium", Materials Science and Engineering A, 398, 246-251.

146 **Rao P.N.,** Jayaganthan R., (2012), "Effects of warm rolling and ageing after cryogenic rolling on mechanical properties and microstructure of Al 6061 alloy", Materials and Design, 39, 226-233.

147 **Rao P.N.,** Panigrahi S. K., Jayaganthan R., (2010), "Effect of annealing and aging treatment on mechanical properties of ultrafine grained Al 6061 alloy", Materials Science and Technology, 26, 371- 374.

148 **Rao P.N.,** Singh D., Jayaganthan R., (2013), “Effect of annealing on microstructure and mechanical properties of Al 6061 alloy processed by cryorolling”, Materials Science and Technology, 29, 76-82.

149 **Richert J.,** Richert M., (1986), “A new method for unlimited deformation of metals and alloys”, Aluminium, 62, 604-607.

150 **Romhanji E.**, Popovic M., “Problems and prospect of Al-Mg alloys application in marine constructions”, Association of Metallurgical Engineers of Serbia, 297-307.

151 **Ryen O.,** Nijs O., Lander E.S, Holmedal B., (2006), "Strengthening Mechanisms in Solid Solution", Metallurgical and Materials Transcations, 37A, 1999-2006.

152 **Sabirov I.,** Yu M., Murashkin, Valiev R.Z., (2013), “Nanostructured aluminium alloys produced by severe plastic deformation: New horizons in development”, Materials Science and Engineering A, 560, 1-24

153 **Saito Y.,** Utsunomiya H., Tsuji N., Sakai T., (1999), “Novel ultra-high straining process for bulk material development of the accumulative roll bonding (ARB) process”, Acta Materialia, 47, 579-583.

154 **Sanders Jr. R. E.,** Hollinshead P. A., Simielli E. A., (2004), “Industrial development of non heat treatable aluminum alloys”, Materials Forum, 28, 53-64.

155 **Sarma V.S.,** Sivaprasad K., Sturm D. Heilmaier M., (2008), “Microstructure and mechanical properties of ultra fine grained Cu-Zn and Cu-Al alloys produced by cryorolling and annealing”, Materials Science and Engineering A, 489, 253-258.

156 **Sarma V.S.,** WanG J., Jian W.W., Kauffmann A., Conrad H., Fredenbergerd J., Zhu Y.T., (2010), "Role of stacking fault energy in strengthening due to cryo-deformation of FCC metals", Materials Science and Engineering A, 527, 7624–7630.

157 **Sauvage X.,** Ganeev A., Ivanisenko Y., Enikeev N., Murashkin M., Valiev R., (2012), “Grain boundary segregation in UFG alloys processed by severe plastic deformation”, Advanced Engineering Materials, 68, 968-974.

158 **Searles J.L.,** Gouma P.I., Buchheit R.G., "Stress Corrosion Cracking of Sensitized AA5083 (Al-4.5Mg-1.0Mn)", Metallurgical and Materials Transcations, 37A, 1999-2006.

159 **Segal V.M.,** Hartong K.T., Gofortz R.E., (1997), In situ composites prepared by simple shear", Material Science Engineering A, 224, 107-115.

160 **Shimizu K.,** Furneaux R., Thompson G., Wood G., Gotoh A., Kobayashi, (1991), "On the nature of easy path for the diffusion of oxygen in thermal oxide films, on aluminium", Oxidation of Metals, 35, 427-439

161 **Singh D., Rao P.N.,** Jayaganthan R., (2013), "Effect of deformation temperature on mechanical properties of ultrafine grained Al-Mg alloys processed by rolling", Materials and Design, 50, 646-655.

162 **Singh S.,** Goel D.B., (2005), "Influence of thermomechanical aging on fatigue behaviour of 2014 Al-alloy", Bulletin of Material Science, 28, 91-96.

163 **Sklenicka V.,** Dvorak J., Svoboda M., Kral P., Kvapilova M., (2013), "Equal-Channel Angular Pressing and Creep in Ultrafine Grained Aluminium and Its Alloys"Intech Open Science, 1-46.

164 **Son I.J.,** Nakano H., Oue S., Kobayashi S., Fukushima H., Horita Z., (2006), "Pitting corrosion resistance of ultrafine-grained aluminum processed by severe plastic deformation", Materials Transactions, JIM, 47, 1163-1169.

165 **Srivatsan T.S.**, Anand S., Sriram S., Vasudevan V.K., (2000), "The high-cycle fatigue and fracture behavior of aluminum alloy 7055", Material Science and Engineering A, 281, 292-304.

166 **Starnik M.J.,** Zahra M., (1998), "β' and β precipitation in an Al-Mg alloy studied by DSC and TEM", Acta Materialia, 46, 3381-3397.

167 **Stolyarov V.V.,**Valiev R.Z., (2006), "Enhanced low temperature impact toughness of nano- structured Ti", Applied Physics Letters, 88, 041905-3.

168 **Suresh S.,** Fatigue of Metals", (1998), Cambridge University Press, Cambridge, UK, 2nd Ed.

169 **Suwas S.,** Toth I.S., Fundenberger J.J., Eberhardt A., (2005), "Texture evolution in commercially pure Al during equal channel angular extrusion as a function of processing routes", Solid State Phenomena, 105, 357-362.

170 **Suzuki T.,**Takeuchi S., Yoshinaga H., (1990), "Dislocation dynamics and plasticity", In: U. Gonser (Ed.), Springer Series in Materials Science, Springer-Verlag, New York, 12, 32-44.

171 **Tajally M.,** Huda Z., Masjuki H.H., (2010), "A comparative analysis of tensile and impact toughness behavior of cold worked and annealed 7075 Aluminium alloy", International Journal of Impact Engineering, 37, 425-432.

172 **Takayama Y.,**Jerzy A. Szpunar, Kato H., (2005), “Analysis of intragranular misorientation related to deformation in an Al-Mg-Mn alloy”, Materials Science Forum, 495-497, 1049-1054.

173 **Tan L.,** Allen T. R., (2010), “Effect of thermomechanical treatment on the corrosion of AA5083”, Corrosion Science, 52, 548-554.

174 **Taylor A.S.,** Weiss M., Hilditch T., Stanford N., (2012), "Formability of cryo-rolled aluminium in uniaxial and biaxial tension", Materials Science and Engineering A, 55, 148-153.

175 **Tellkamp V.L.,** Melmed A., Lavernia E.J., (2001), “Mechanical behaviour and microstructure of a thermally stable bulk nanostructured Al alloy", Metallurgical and Materials Transactions A, 32, 2335-2343.

176 **Tokita M.,** (1993) , “Trends in advanced SPS spark plasma sintering systems and technology”, Journal of the Society of Powder Technology, Jayat,. 30, 790-804.

177 **Tong H.Y.,** Wang J.T., Ding B.Z., Jiang H.G., Lu K.J., (1992), “The structure and properties of nanocrystalline $Fe_{78}B_{13}Si_9$ alloy”, Journal of Non-Crystalline Solids, 150, 444-447.

178 **Toroghinejad M.R.,** Ashrafizadeha F., Jamaati R., (2013), "On the use of accumulative roll bonding process to develop nanostructured aluminum alloy 5083", Material Science and Engineering A, 561, 145-151.

179 **Ulrich K.,** Katharina M., Alexander G., Gerd K., Ulrich B.H., Henning Z., (2012), “Development of ultrafine-grained zinc-ferrite-strengthened aluminum alloys by high-energy milling”, Reviews on Advanced Materials Science, 3, 19-24.

180 **Urrutia I.G.,** Morris M.A., Morris D.G., (2005), "The effect of coarse second phase particles and fine precipitates on microstructure and mechanical properties of severely deformed Al alloy", Material Science and engineering A, 1-2, 339-410.

181 **V. Yelagin,** (2002), Metal Science and Heat Treatment, 9, 10-16.

182 **Valiev R. Z.,** Islamgaliev R. K., Alexandrov I. V., (2000), “Bulk nanostructured materials from severe plastic deformation”, Progress in Material Science, 45, 103-189.

183 **Valiev R. Z.,** Korznikov A.V., Mulyukov R.R., (1993), “Structure and properties of ultrafine-grained materials produced by severe plastic deformation”, Material Science and Engineering A, 168, 141-148.

184 **Valiev R. Z.,** Krasilnikov N. A., Tsenev N. K., (1991), " Plastic deformation of alloys with submicron-grained structure", Material Science Engineering A, 137, 35-40.

185 **Valiev R.,** (2004), "Nanostructuring of metals by severe plastic deformation for advanced properties", Nature Materials, 3, 511-516.

186 **Valiev R.,** Yu.V. I., Rauch E.F., Baudelet B., (1996), "Structure and deformaton behaviour of Armco iron subjected to severe plastic deformation", Acta Materialia, 44, 12, 4705-4712.

187 **Valiev R.Z.,** Estrin Y., Horita Z., Langdon T.g., Zehetbauer M.J., Zhu Y.T., (2006), "Producing Bulk Ultrafine grained materials by severe plastic deformation", Nanostructured Materials, 33-39

188 **Valiev R.Z.,** Gertsman V.Yu., Kaibyshev O.A., (1986), "Grain boundary structure and properties under external influences", Physica Status Solidi (a), 97, 11-56.

189 **Valiev R.Z.,** Kozlov E.V., Ivanov Yu.F., Lian J., Nazarov A.A., Baudelet B., (1994), "Deformation behaviour of ultra-fine-grained copper", Acta Metallurgica Materialia, 42, 2467-2475.

190 **Valiev R.Z.,** Langdon T. G., (2006), "Principles of equal-channel angular pressing as a processing tool for grain refinement", Progress in Material Science, 51, 881-981.

191 **Valiev R.Z.,** Nazarov A.A., (2009), "Bulk Nanostructured Materials", In: M.J. Zehetbauer, Y.T. Zhu (Eds.), WILEY-VCH Verlag, Weinheim, Germany, 21.

192 **Vargel C.,** (2004), Corrosion of Aluminium, Published by Elsevier

193 **Verlindin B.,** (2002), "Severe plastic deformation of metals", Metallurgija- Journal of Metallurgy,165-181.

194 **Vinogradov A.,** Mimaki T., Hashimoto S., Valiev R., (1999), "On the corrosion behaviour of ultra-fine grain copper", Scripta Materialia, 41, 319-326.

195 **Vinogradov A.,** Patlan V., Hashimoto S., Kitagawa K., (2002), "Acoustic emission during cyclic deformation of ultrafine-grain copper processed by severe plastic deformation", Philosophical Magazines A, 82, 317-335.

196 **Vinogradov A.,** S. Nagasaki, V. Patlan, K. Kitagawa, M. Kawazoe, (1999), "Fatigue properties of 5056 Al-Mg alloy produced by equal-channel angular pressing", Nanostructured Materials, 11, 925-934.

197 **Wang C.P.,** Li F.G., Wang L., Quao H.J., (2012), "Review on modified and novel techniques of severe plastic deformation", Science China- Technological Sciences, 9,

2377-2390.

198 **Wang J.T.,** Roberto B.F., Langdon T.G., (2010), "Nanomaterials by severe plastic deformation: Nano SPD5", Material Science Forum,

199 **Wang Y.,** Chen M., Zhou F., Ma E., (2002), "High tensile ductility in a nanostructured metal", Nature, 419, 912-915.

200 **Wang Y.,** Jiao T., Ma. E., (2003), **"**Dynamic processes for nanostructure development in Cu after severe cryogenic rolling deformation", Materials Transactions, 44,1926-1934.

201 **Warmuzeka M.,** Mrowkab G., Sieniawskib J., (2004), "Influence of heat treatment on the precipitation of the intermetallic phases in commercial AlMn1FeSi alloy", Journal of Material Processing and Technology, 157, 624-632.

202 **Wei W.,** Wei K.X., Du Q. Bo, (2007), "Corrosion and tensile behaviors of ultra-fine grained Al-Mn alloy produced by accumulative roll bonding", Material Science and Engineering A, 454-455, 536-541.

203 **Weitkin D.B.,** Lavernia E.J., (2005), "Synthesis and mechanical behavior of nanostructured materials via cryomilling", Progress in Material Science, 51, 1-60.

204 **Wong M.K.,** Kao W.P., Lui J.T., Chang C.P., Kao P.W., "Cyclic deformation of ultrafine-grained aluminum", (2010), Acta Mater. 55, 715-725.

205 **Wu X.X.,** San X.Y., Liang X.G., Gong Y.L., Zhu X.K., (2013), "Effect of stacking fault energy on mechanical behavior of cold-forging Cu and Cu alloys", Material and Design, 47, 372-376.

206 www.keytometals.com

207 www.world-aluminium.org

208 **Xu L.,** Ma Y., Li X., Wang H., (2010), NACE International, Corrosion Conference and EXPO, 10397, 1-8

209 **Yang D.K.,** Hodgson P.D., Wen C.E., (2010), "Simultaneously enhanced strength and ductility of titanium via multimodal grain structure", Scripta Materialia, 63, 941-944.

210 **Yasakau K.A.,** Zheludkevich M.L., Lamaka S.V., Ferreira, (2007), "Role of intermetallic phases in localized corrosion of AA5083", Electrochimica Acta, 52, 7651-7659.

211 **Yelagin V.,** (2002), Metal Science and Heat Treatment, 9,10-15.

212 **Youssef K.M.,** Scattergood R.O., Murty K.L., Koch C.C., (2006), "Nanocrystalline Al-Mg alloy with ultrahigh strength and good ductility", Scripta Materialia, 54, 251-256.

213 **Zao Y.H.,** Lio X.Z., Cheng S., Ma E., Zhu Y.T., (2006), "Simultaneously increasing the ductility and strength of nanostructured alloys", Advanced Materials, 18, 2280-2283.

214 **Zhang B.,** Li Y., Wang F., (2007), "Electrochemical corrosion behaviour of micro-crystalline aluminium in acidic solutions", Corrosion Science, 49, 2071-2082.

215 **Zhang Z.F.,** Wang Z.G., (2000), "Comparison of fatigue cracking possibility along large- and low-angle grain boundaries", Material Science and Engineering A, 284, 285-292.

216 **Zhao Y.H.,** Liao X. Z., Jin Z., Valiev R.Z., Zhu Y.T., (2001), "Microstructures and mechanical properties of ultrafine grained 7075 Al alloy processed by ECAP and their evolutions during annealing", Acta Materialia, 52, 4589-4599.

217 **Zhilyaev A.P.,** Langdon T.G., (2008), "Using high-pressure torsion for metal processing: Fundamentals and applications", Progress in Material Science, 53, 893-979.

218 **Zhilyaev A.P.,** Nurislamova G.V., Kim B.K., Baro M.D., Szpunar J.A., Langdon T.G., (2003), "Experimental parameters influencing grain refinement and microstructural evolution during high-pressure torsion", Acta Materialia, 51, 753-765.

219 **Zhou F.,** Liao X.Z., Zhu Y.T., Dallek S., Lavernia S.J., (2003), "Microstructural evolution during recovery and recrystallization of a nanocrystalline Al-Mg alloy prepared by cryogenic ball milling", Acta Materialia, 51, 2777-2791.

220 **Zhu Y.T,** Jiang H., Huang J., Lowe T., (2001), "A new route to bulk nanostructured metals", Metallurgical and Materials Transaction A, 32, 1559-1562.

221 **Zhu Y.T.,** Langdon T.G., (2005), "Influence of Grain Size on Deformation Mechanisms: an extension to nanocrystalline materials, Material Science and Engineering A, 409, 234-242.

222 **Zrnik J.,** Dobatkin S.V., Mamuzi I., (2008), "Processing of metals by severe plastic deformation (SPD)- Structure and mechanical properties respond", Metalurgija, 47, 211-216